MBL-mobile: Many-body-localized engine

Nicole Yunger Halpern,[1] Christopher David White,[1] Sarang Gopalakrishnan,[1, 2, 3, 4] and Gil Refael[1, 2, 3]

[1] *Institute for Quantum Information and Matter, California Institute of Technology, Pasadena, CA 91125, USA*
[2] *Department of Physics, California Institute of Technology, Pasadena, CA 91125, USA*
[3] *Walter Burke Institute, California Institute of Technology, Pasadena, CA 91125, USA*
[4] *College of Staten Island, City University of New York, Staten Island, NY 10314, USA*

(Dated: July 25, 2017)

Many-body-localized (MBL) systems do not thermalize under their intrinsic dynamics. The athermality of MBL, we propose, can be harnessed for thermodynamic tasks. We illustrate by formulating an Otto engine cycle for a quantum many-body system. The system is ramped between a strongly localized MBL regime and a thermal (or weakly localized) regime. MBL systems' energy-level correlations differ from thermal systems'. This discrepancy enhances the engine's reliability, suppresses worst-case trials, and enables mesoscale engines to run in parallel in the thermodynamic limit. We estimate analytically and calculate numerically the engine's efficiency and per-cycle power. The efficiency mirrors the efficiency of the conventional thermodynamic Otto engine. The per-cycle power scales linearly with the system size and inverse-exponentially with a localization length. This work introduces a thermodynamic lens onto MBL, which, having been studied much recently, can now be applied in thermodynamic tasks.

Many-body localization (MBL) is a phase in which isolated quantum systems do not internally thermalize. MBL systems are sometimes regarded as integrable: They have nearly spatially local integrals of motion. These conserved quantities retain information about initial conditions for long times. For example, initially nonuniform density profiles remain nonuniform indefinitely [1]. This retention of information has been realized experimentally [2]. Applications include quantum memories [3].

Under the dynamics of "thermalizing" isolated quantum systems, in contrast, particles and quantum information spread out. Such systems obey the Eigenstate Thermalization Hypothesis (ETH) [4–6]. Local operators' expectation values quickly approach equilibrium expectation values. Local subsystems occupy states represented by equilibrium density matrices.

So far, MBL has been described with quantum statistical mechanics. But MBL systems behave athermally, and athermality facilitates thermodynamic tasks. Consider a cold bath in a hot environment. The cold bath is athermal with respect to the ambient temperature. An agent can connect the baths and extract work from the heat flow. This work can be stored in a battery[1] or applied in useful tasks, like the lifting of weights or the powering of cars. More generally, athermal systems serve as thermodynamic resources [7–18]. Since MBL systems behave athermally, one might expect MBL to have thermodynamic applications.

We illustrate a thermodynamic use of MBL: We formulate, analyze, and numerically simulate an Otto engine cycle for a quantum many-body system that has an MBL phase. The main idea is sketched in Fig. 1. This application unites the growing fields of quantum thermal machines [19–30] and MBL [3, 31–35]. Evidence of MBL, much firm and some tentative, has been observed recently [2, 36–42]. We suggest how such realizations may be harnessed in technologies. The MBL Otto cycle poses a near-term challenge for cold-atom [2, 36, 38, 39, 42]; nitrogen-vacancy-center [40]; trapped-ion [41]; and doped-semiconductor [43] experiments.

Our engine benefits from spectral-correlation properties that distinguish MBL from thermal systems [35, 44]. We illustrate this distinction with the energies of a mesoscopic interacting quantum system. Consider, for example, a chain of 15 spins. Such a system has many degrees of freedom. The energies' discreteness remains resolvable, though. Consider the gaps between neighboring energies that lie far from the energy band's edges. A gap distribution $P(\delta)$ encodes the frequency with which size-δ gaps appear (equivalently, encodes the probability that any given gap has size δ). The MBL gap distribution differs from an ETH system's gap distribution: Small and large gaps appear more in MBL spectra [45].

Let us introduce the MBL and ETH distributions in greater detail. Let $\langle\delta\rangle_E$ denote the average gap at the energy E. MBL gaps approximately obey Poisson statistics [32]: $P^{(E)}_{\rm MBL}(\delta) \approx \frac{1}{\langle\delta\rangle_E} e^{-\delta/\langle\delta\rangle_E}$. (Though the right-hand side is not a Poisson distribution, it is derived from a Poisson distribution.) Any given gap has a decent chance of being small: As $\delta \to 0$, $P^{(E)}_{\rm MBL}(\delta) \to \frac{1}{\langle\delta\rangle_E} > 0$. Neighboring energies have finite probabilities of lying close together. MBL systems' energies do not "repel" each other.

Thermal systems' energies repel. The energies obey level statistics like those of random matrices drawn from the Gaussian Orthogonal Ensemble (GOE): $P^{(E)}_{\rm GOE}(\delta) \approx$

[1] More precisely, one can store energy that can be reliably retrieved and converted into work. We abbreviate "the capacity to perform work" as "work," for conciseness.

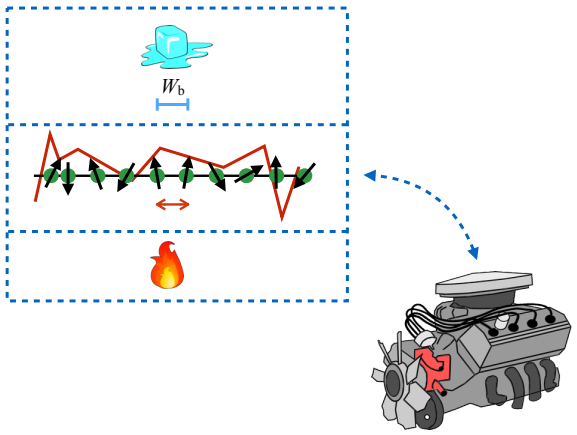

FIG. 1: Schematic of many-body-localized (MBL) engine: We formulate an Otto engine cycle for a many-body quantum system that exhibits an MBL phase. Platforms that exhibit MBL include spin chains (illustrated by the green dots and black arrows). A random disorder potential (the jagged red line) localizes the particles. Particles interact and hop between sites (as suggested by the horizontal red arrows). Strengthening the interactions and the hopping transitions the system from strong localization to a reference "thermal" phase (or to weak localization). The engine thermalizes with a hot bath (represented by the flames) and with a cold bath (represented by an ice cube). The cold bath has a small bandwidth W_b, to take advantage of small energy gaps' greater prevalence in the highly localized regime.

$\frac{\pi}{2}\frac{\delta}{\langle\delta\rangle_E^2}e^{-\frac{\pi}{4}\delta^2/\langle\delta\rangle_E^2}$ [32]. Unlike in MBL spectra, small gaps rarely appear: As $\delta \to 0$, $P^{(E)}_{\rm GOE}(\delta) \to 0$.

This discrepancy between thermal level repulsion and MBL gap statistics enhances our quantum many-body engine. Until now, thermal density matrices have been regarded as thermodynamic resources [7–18]. Also athermal energy-gap statistics, we show, offer thermodynamic advantages. Athermal gap statistics improve our engine's reliability: The amount W of work extracted by our engine fluctuates relatively little from successful trial to successful trial. Athermal statistics also lower the probability of worst-case trials, in which the engine outputs net negative work, $W_{\rm tot} < 0$.

Furthermore, our engine scales robustly due to two properties of MBL systems. First, information and energy remain frozen, or propagate slowly, in the MBL phase. Even in the thermodynamic limit, an MBL system behaves like an ensemble of mesoscale quantum systems. Mesoscale "subengines" can run in parallel in different regions of our MBL system, interacting little.

Second, consider the local operators that act nontrivially on a mesoscale subengine. Consider probing such an operator's spectrum in a finite amount of time. The spectrum retains sharp lines, as in small systems, rather than forming a broad continuum, as in large thermal systems. This *local* notion of level statistics imbues subengines with the gap statistics of mesoscale MBL systems. Even in the thermodynamic limit, subengines can take advantage of the athermality of mesoscale MBL systems' gap distributions.

The paper is organized as follows. Section I contains background about the thermodynamic Otto cycle, the quantum Otto cycle, and quantum work and heat. We construct the MBL Otto engine in three steps in Sec. II. In Sec. II A, we introduce the basic idea via a qubit (two-level quantum system). In Sec. II B, we scale up to a mesoscopic engine. This engine has many energy levels but remains outside the thermodynamic limit. We calculate the mesoscopic engine's per-cycle power and efficiency. In Sec. II C, we divide a macroscopic MBL system into regions effectively isolated from each other. The regions form subengines run in parallel. Our estimates are tested, in Sec. III, against numerical simulations on disordered spin chains. In Sec. IV, we estimate the order of magnitude of a localized semiconductor engine's power and power density, applying data from experimental literature. We compare the localized engine with competitors in Sections IV and V. The Supplemental Material contains background information, intuitive examples, and calculations.

I. THERMODYNAMIC BACKGROUND

First, we briefly review the thermodynamic and quantum Otto cycles. Details appear in App. A. Next, we review definitions of quantum work and heat. Appendix B and [46] contain elaborations.

The conventional thermodynamic Otto engine consists of a classical ideal gas [47]. Let $\gamma := \frac{C_{\rm P}}{C_{\rm v}}$ denote a ratio of the gas's constant-pressure and constant-volume specific heats. The Otto cycle consists of four strokes, two isentropic (constant-entropy) and two isochoric (constant-volume). During each isentropic stroke, the gas's volume is tuned between values V_1 and V_2. If $V_1 > V_2$, the fraction $r := \frac{V_1}{V_2}$ is called the *compression ratio*. During each isochoric stroke, the gas's temperature changes between values T_1 and T_2.

Thermodynamic engines' efficiencies are defined as

$$\eta := \frac{W_{\rm tot}}{Q_{\rm in}} \, . \tag{1}$$

The net work extracted per cycle is denoted by $W_{\rm tot}$. $Q_{\rm in}$ denotes the heat absorbed during the stroke during which the engine absorbs a positive amount of heat, $Q_{\rm in} > 0$. The Otto engine operates at the efficiency [47]

$$\eta_{\rm Otto} = 1 - r^{1-\gamma} < \eta_{\rm Carnot} \, . \tag{2}$$

The Carnot efficiency—the upper bound on the efficiency of every thermodynamic engine that involves just two heat baths—is denoted by $\eta_{\rm Carnot}$.

Otto cycles have been formulated for quantum systems such as oscillators [20, 28, 46, 48–52]. The quantum har-

monic oscillator's (QHO's) gap plays the role of the classical engine's volume. Let ω and $\Omega > \omega$ denote the values between which the natural frequency is tuned. The ideal QHO Otto cycle operates at the efficiency

$$\eta_{\rm QHO} = 1 - \frac{\omega}{\Omega} \, . \tag{3}$$

This oscillator informs the qubit toy model for our MBL Otto cycle.

We define work and heat as in many quantum-thermodynamics settings [46]:

$$W := \int_0^\tau dt \, {\rm Tr} \left(\rho \, \frac{dH}{dt} \right) , \quad \text{and} \tag{4}$$

$$Q := \int_0^\tau dt \, {\rm Tr} \left(\frac{d\rho}{dt} \, H \right) . \tag{5}$$

This Q definition is narrower than the definition prevalent in the MBL literature [53–55]: According to Eq. (4), all energy exchanged during unitary evolution counts as work.

II. INTRODUCING THE MBL OTTO CYCLE

We introduce the MBL Otto cycle in three steps: A qubit toy model illustrates the basic physics. A mesoscale engine is tuned between ETH and MBL phases. Parallelizing mesoscale subengines enables the cycle to operate in the thermodynamic limit. Figure 2 illustrates how the mesoscale engine outputs work. Table I summarizes parameters that characterize the mesoscale and macroscopic MBL engines.

II A. Qubit toy model

A qubit illustrates the MBL Otto engine's basic physics. We overview a simplified model here. Generalizations to more levels and to finite-temperature baths appear in App. C.

The system evolves under a time-varying Hamiltonian

$$H_{\rm qubit}(t) := (1 - \alpha_t) \mathbf{h} \cdot \boldsymbol{\sigma} + \alpha_t \mathbf{h}' \cdot \boldsymbol{\sigma} \, . \tag{6}$$

The three-dimensional vectors $\mathbf{h}$ and $\mathbf{h}'$ represent external fields. The components of $\boldsymbol{\sigma} = \sigma^x \, \hat{\mathbf{x}} + \sigma^y \, \hat{\mathbf{y}} + \sigma^z \, \hat{\mathbf{z}}$ are the Pauli matrices. α_t denotes a parameter tuned between 0 and 1.

The engine undergoes the following cycle. The engine begins in thermal equilibrium with a heat bath at temperature $T_{\rm H} \equiv \frac{1}{\beta_{\rm H}}$. (We set Boltzmann's constant to one.) During stroke 1, the engine is thermally isolated, and α_t is tuned from 0 to 1. Unless $\mathbf{h}$ and $\mathbf{h}'$ are parallel, $H_{\rm qubit}(t)$ remains nondegenerate, and the energy eigenstates' forms change. That is, let $\{|z+\rangle, |z-\rangle\}$ denote the σ^z eigenbasis. Let $|E_t^{(j)}\rangle = c_+^{(j)}(t)|z+\rangle + c_-^{(j)}(t)|z-\rangle$ denote the $j^{\rm th}$ energy eigenstate at time t, for $j = 1, 2$.

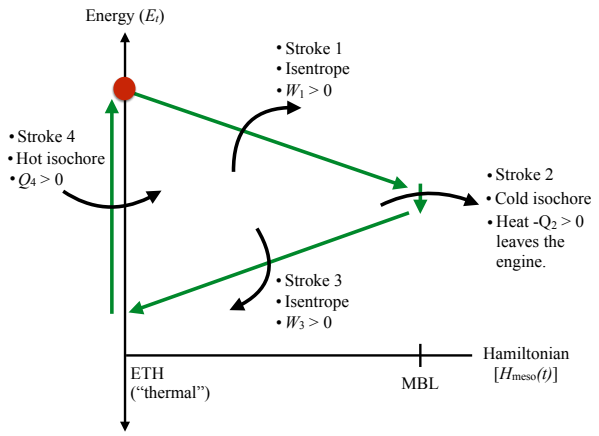

FIG. 2: Otto engine cycle for a mesoscale many-body-localized (MBL) system: Two energies in the many-body spectrum capture the cycle's basic physics. The engine can be regarded as beginning each trial in an energy eigenstate drawn from a Gibbs distribution. Let the red dot denote the engine's starting state in some trial of interest. The cycle consists of four strokes: During stroke 1, the Hamiltonian $H_{\rm meso}(t)$ is tuned from "thermal" (obeying the Eigenstate Thermalization Hypothesis, or ETH) to MBL. During stroke 2, the engine thermalizes with a cold bath. $H_{\rm meso}(t)$ returns from MBL to thermal during stroke 3. Stroke 4 resets the engine, which thermalizes with a hot bath. The tunings (strokes 1 and 3) map onto the thermodynamic Otto cycle's isentropes. The thermalizations (strokes 2 and 4) map onto isochores. The engine outputs work W_1 and W_3 during the tunings and absorbs heat Q_2 and Q_4 during thermalizations. The engine benefits from the discrepancy between MBL and thermal gap statistics: Energies have a greater probability of lying close together in the MBL phase than in the thermal phase. This discrepancy leads the engine to "slide down" the lines that represent tunings. During downward slides, the engine loses energy outputted as work.

The complex coefficients $c_\pm^{(j)}(t)$ change with time. This change distinguishes our qubit Otto engine from conventional qubit Otto engines, whose energy eigenbases remain constant [28]. During stroke 2, the engine thermalizes with a cold bath at a temperature $\frac{1}{\beta_{\rm C}} \equiv T_{\rm C} < T_{\rm H}$. During stroke 3, the engine is thermally isolated, and α_t is returned from 1 to 0. During stroke 4, the engine thermalizes with the temperature-$T_{\rm H}$ hot bath. This thermalization returns the engine to its initial state.

To supply intuition, we make three simplifying assumptions. First, we specialize to $T_{\rm H} = \infty$ and $T_{\rm C} = 0$. (We lift this assumption in App. C.) Second, we assume that the stroke-1 and stroke-3 evolutions satisfy the quantum adiabatic theorem. $H_{\rm qubit}(t)$ is tuned slowly enough that the state's form remains constant as a function of the instantaneous energy eigenstates $|E_t^{(j)}\rangle$. Third, we suppose that $\mathbf{h} = \frac{\delta_{\rm GOE}}{2} \, \hat{\mathbf{x}}$, $\mathbf{h}' = \frac{\delta_{\rm MBL}}{2} \, \hat{\mathbf{z}}$, and $\delta_{\rm GOE} \gg \delta_{\rm MBL}$.

The Hamiltonian assumes the form

$$H_{\rm qubit}(t) = (1-\alpha_t)\,\frac{\delta_{\rm GOE}}{2}\,\sigma^x + \alpha_t\,\frac{\delta_{\rm MBL}}{2}\,\sigma^z\,. \quad (7)$$

The gaps' labels are suggestive: A qubit, having only one gap, obeys neither GOE nor MBL gap statistics. But, when large, the qubit gap apes a typical GOE gap; and, when small, the qubit gap apes a useful MBL gap. This mimicry illustrates how the mesoscopic engine benefits from the greater prevalence of small gaps in MBL spectra than in GOE spectra.

We define as work the energy exchanged during the adiabatic strokes (1 and 3). We define as heat the energy exchanged during the thermalizations (strokes 2 and 4). These definitions are consistent with the quantum-thermodynamics definitions for W and Q in Eqs. (4) and (5).

Let us analyze the simplified cycle more quantitatively. The system begins at $T_{\rm H} = \infty$, with zero average energy. Stroke 1 preserves the distribution of the engine's weights across the levels. Stroke 2 cools the engine to its ground state. Heat dissipates into the cold bath, dropping the engine's energy to $-\frac{\delta_{\rm MBL}}{2}$. The energy drops to $-\frac{\delta_{\rm GOE}}{2}$ during stroke 3. During stroke 4, the engine's average energy is reset to 0. The engine absorbs an amount $\langle Q_4\rangle = \frac{\delta_{\rm GOE}}{2}$ of heat, on average.

This model's efficiency and per-cycle power can be calculated easily. The per-cycle power (the average work outputted per cycle) is $\langle W_{\rm tot}\rangle = \frac{1}{2}(\delta_{\rm GOE} - \delta_{\rm MBL})$. The efficiency is $\eta_{\rm qubit} := \frac{\langle W_{\rm tot}\rangle}{\langle Q_4\rangle} = 1 - \frac{\delta_{\rm MBL}}{\delta_{\rm GOE}}$. This efficiency is essentially equivalent to the efficiency $\eta_{\rm Otto}$ of a thermodynamic Otto engine, Eq. (2). An agent operating the qubit engine chooses a gap ratio $\frac{\delta_{\rm MBL}}{\delta_{\rm GOE}}$. An agent operating the thermodynamic engine chooses a compression ratio $r := \frac{V_1}{V_2}$. For the MBL agent's chosen $\frac{\delta_{\rm MBL}}{\delta_{\rm GOE}}$, and for a fixed specific-heat ratio γ, there exists a compression ratio $r = \left(\frac{\delta_{\rm MBL}}{\delta_{\rm GOE}}\right)^{\frac{1}{1-\gamma}}$ such that $\eta_{\rm Otto} \approx \eta_{\rm qubit}$. The toy-MBL qubit engine shares its efficiency also with a QHO Otto engine tuned between frequencies $\omega = \delta_{\rm MBL}$ and $\Omega = \delta_{\rm GOE}$ [Eq. (3)]: $\eta_{\rm qubit} = \eta_{\rm QHO}$. The toy-MBL qubit engine, however, scales to large system sizes, as explained in the following two sections.

II B. Level-statistics engine for a mesoscale system

The qubit engine encapsulates the basic physics of a mesoscale Otto engine tuned between MBL and ETH phases. The mesoscale engine is a one-dimensional (1D) system of N sites, wherein N is on the order of 10. We detail the set-up and cycle, then analyze the engine qualitatively and quantitatively. This engine will model one region in a thermodynamically large MBL engine.

This section is organized as follows. We introduce the set-up in Sec. II B 1. Section II B 2 overviews the cycle qualitatively; and Sec. II B 3, quantitatively. We present the per-trial power $\langle W_{\rm tot}\rangle$, the efficiency $\eta_{\rm MBL}$, and work costs $\langle W_{\rm diab}\rangle$ of undesirable diabatic transitions.

II B 1. Set-up for the mesoscale MBL engine

The mesoscopic engine evolves under the Hamiltonian

$$H_{\rm meso}(t) := \frac{\mathcal{E}}{Q(\alpha_t)}\left[(1-\alpha_t)H_{\rm GOE} + \alpha_t\,H_{\rm MBL}\right]\,. \quad (8)$$

The unit of energy, or average energy density per site, is denoted by $\mathcal{E}$. $H_{\rm GOE}$ denotes a random Hamiltonian whose gaps δ are distributed according to GOE statistics, $P^{(E)}_{\rm GOE}(\delta)$. $H_{\rm MBL}$ denotes a Hamiltonian whose gaps are distributed according to $P^{(E)}_{\rm MBL}(\delta)$. We illustrate $H_{\rm GOE}$ and $H_{\rm MBL}$ with a disordered Heisenberg model in Sec. III. There, $H_{\rm GOE}$ and $H_{\rm MBL}$ differ only in the ratio $\frac{\mathcal{E}}{\mathcal{E}h}$ of the hopping frequency to the disorder strength. Whether the results extend to more-general $H_{\rm GOE}$'s and $H_{\rm MBL}$'s, we leave as an open question.

The initialization, tunings, and thermalizations proceed as in the qubit cycle. However, the cold bath's bandwidth is now restricted, as detailed below. Tuning the parameter α_t between 0 and 1 tunes the engine between ETH and MBL phases.

Let $\langle\delta\rangle$ denote the average gap. (See App. D 2 for a technical definition.) $Q(\alpha_t)$ denotes a normalization factor that keeps $\langle\delta\rangle$ constant. $\langle\delta\rangle$ need not remain constant for our engine to work. Rather, the constancy of $\langle\delta\rangle$ serves as a bookkeeping device used to highlight the role of level statistics. Imagine removing $Q(\alpha_t)$ from Eq. (8). One could increase α_t—could tune the Hamiltonian from ETH to MBL [35]—by strengthening a disorder potential. This strengthening would expand the energy band. Tuning from MBL to ETH would compress the band. Expanding and compressing would generate an accordion-like motion. By interspersing the accordion motion with thermalizations, one could extract work. Such an engine would benefit little from properties of MBL, whose thermodynamic benefits we wish to highlight. Hence we "zero out" the accordion-like motion, by fixing $\langle\delta\rangle$ through $Q(\alpha_t)$. Section III details how we define $Q(\alpha_t)$ in numerical simulations. We compare the MBL engine with the accordion-bandwidth engine in Sec. V.

The key distinction between GOE and Poisson (MBL) level statistics is that anomalously small gaps (and anomalously large gaps) have higher probabilities of appearing in Poisson spectra. Level statistics are reviewed in App. D. A toy model, introduced here and detailed in App. E, illuminates the level statistics' physical origin: An MBL system can be modeled as a set of noninteracting qubits [34]. Let g_j denote the $j^{\rm th}$ qubit's gap. Two qubits, j and j', may have nearly equal gaps: $g_j \approx g_{j'}$. The difference $|g_j - g_{j'}|$ equals a gap in the many-body energy spectrum. Consider tuning the Hamiltonian from MBL to ETH. Qubits come to interact. Interactions widen gaps. The GOE spectrum therefore has fewer small gaps than the MBL spectrum has.

Symbol	Significance
N	Number of sites per mesoscale engine (in Sec. II B) or per mesoscale subengine (in the macroscopic engine, in Sec. II C). Chosen, in the latter case, to equal $\xi_>$.
$\mathcal{N}$	Dimensionality of one mesoscale (sub)engine's Hilbert space.
$\mathcal{E}$	Unit of energy, average energy density per site.
α_t	Hamiltonian parameter tuned from 0 (at which point the engine obeys the ETH, if mesoscopic, or is shallowly localized, if macroscopic) to 1 (at which point the engine is MBL, if mesoscopic, or deeply localized, if macroscopic).
$\langle\delta\rangle$	Average gap in the energy spectrum of a length-N MBL system.
$W_{\rm b}$	Bandwidth of the cold bath. Is small: $W_{\rm b} \ll \langle\delta\rangle$.
$\beta_{\rm H} = 1/T_{\rm H}$	Inverse temperature of the hot bath.
$\beta_{\rm C} = 1/T_{\rm C}$	Inverse temperature of the cold bath.
δ_-	Level-repulsion scale of a length-N MBL system. Minimal size reasonably attributable to any energy gap. Smallest gap size at which a Poissonian approximates the MBL gap distribution well.
v	Speed at which the Hamiltonian is tuned. Has dimensions of $1/\text{Time}^2$.
$\xi_>$	Localization length of the macroscopic MBL engine in its shallowly localized phase.
$\xi_<$	Localization length of the macroscopic MBL engine in its deeply localized phase. Satisfies $\xi_< < \xi_>$.
$X_{\rm macro}$	Characteristic X of the macroscopic MBL engine (e.g., $X = N, \langle\delta\rangle$).
g	Strength of coupling between engine and cold bath.
$\tau_{\rm cycle}$	Time required to implement one cycle.
$\langle\delta\rangle^{(L)}$	Average energy gap of a length-L MBL system.

TABLE I: Often-used parameters that characterize the mesoscopic and macroscopic MBL engines: Introduced in Sections II B and II C. Boltzmann's constant is set to one: $k_{\rm B} = 1$.

We take advantage of the phases' distinct level statistics using a small-bandwidth cold bath. Recall the qubit engine of Sec. II A: The qubit engine outputs net positive work because $\delta_{\rm MBL}$, the gap down which cold thermalization drops the engine, is smaller than $\delta_{\rm GOE}$, the gap up which hot thermalization raises the engine: $\delta_{\rm MBL} < \delta_{\rm GOE}$. Like the qubit engine, the mesoscopic engine must cold-thermalize across just small gaps. The average gap must upper-bound the cold bath's bandwidth, $W_{\rm b}$: $W_{\rm b} \ll \langle\delta\rangle$. This bath can thermalize only energy levels separated by anomalously small gaps [56–58]. Such gaps appear more in MBL spectra than in GOE spectra.

Applying level statistics requires one more subtlety: Suppose that the Hamiltonian $H_{\rm meso}(t)$ conserves particle number. The engine state $\rho(t)$ must occupy one particle-number sector and must remain in that sector throughout the cycle. The reason is a lack of repulsion between GOE energies not in the same particle-number sector (App. F). $\rho(t)$ occupies a Hilbert space of dimensionality $\mathcal{N} \sim 2^N$. Our numerical simulations take place at half-filling.

II B 2. Qualitative analysis of the mesoscale engine

Figure 2 illustrates a "successful," or positive-work-outputting, trial. The engine begins in the thermal state $\rho(0) = e^{-\beta_{\rm H} H_{\rm GOE}}/Z$. The partition function $Z := \text{Tr}\left(e^{-\beta_{\rm H} H_{\rm GOE}}\right)$ normalizes the state. $\rho(0)$ admits of an ensemble interpretation: We can regard the engine as beginning each trial in one energy level. The engine's probability of beginning any given trial with energy E_j equals $e^{-\beta_{\rm H} E_j}/Z$. Averaging over trials involves an average with respect to $\rho(0)$.

During stroke 1, $H_{\rm meso}(t)$ is tuned from $H_{\rm GOE}$ to $H_{\rm MBL}$. We approximate the tuning as quantum-adiabatic. (Later, we calculate diabatic corrections to adiabatic results.) Stroke 2—cold thermalization—depends on the gap δ'_j between the $j^{\rm th}$ and $(j-1)^{\rm th}$ MBL levels. This gap typically exceeds $W_{\rm b}$. If it does, the cold bath does not change the engine's energy. Zero net work is extracted during the cycle: $W_{\rm tot} = 0$. With some small probability $\sim \frac{W_{\rm b}}{\langle\delta\rangle}$,[2] the gap is small enough to thermalize: $\delta'_j < W_{\rm b}$. In these cases, the cold bath drops the engine to level $j-1$. Stroke 3 brings the engine to level $j-1$ of $H_{\rm GOE}$. The gap δ_j between the $(j-1)^{\rm th}$ and $j^{\rm th}$ $H_{\rm GOE}$ levels is typically $\langle\delta\rangle \gg W_{\rm b}$. The engine therefore outputs net positive work: $W_{\rm tot} > 0$. Hot thermalization (stroke 4) returns the engine to $\rho(0)$.

[2] This expression is derived in Sec. II B 3.

II B 3. Quantitative analysis of the mesoscale engine

We focus on the regime in which $T_{\rm C} \ll W_{\rm b} \ll \langle\delta\rangle$ and $\sqrt{N}\,\beta_{\rm H}\mathcal{E} \ll 1$. The mesoscale engine resembles a qubit engine whose state and gaps are averaged over. The gaps, δ_j and δ'_j, obey the distributions $P^{(E)}_{\rm GOE}(\delta_j)$ and $P^{(E)}_{\rm MBL}(\delta'_j)$. Correlations between the $H_{\rm GOE}$ and $H_{\rm MBL}$ spectra can be neglected. Therefore, the gap distributions can be averaged over independently. The calculations are detailed in App. G. We initially assume, for simplicity, that the tunings proceed quantum-adiabatically. Diabatic corrections are calculated in App. G 8. The calculational appendix may interest readers not only as a means to the end of assessing the engine. Appendix G also introduces and illustrates techniques for many-body calculations of quantities, such as thermodynamic work, not calculated for MBL before, to our knowledge. The present section highlights results: the average per-cycle power $\langle W_{\rm tot}\rangle$ and the efficiency $\eta_{\rm MBL}$.

On average, the mesoscopic MBL engine outputs an amount

$$\boxed{\langle W_{\rm tot}\rangle \approx W_{\rm b} - \frac{2\ln 2}{\beta_{\rm C}}} \tag{9}$$

of work per trial. This per-cycle power scales with the system size N as $W_{\rm b} \ll \langle\delta\rangle \sim \frac{\text{effective bandwidth}}{\#\text{ energy eigenstates}} \sim \frac{\mathcal{E}\sqrt{N}}{\mathcal{N}} \sim \frac{\mathcal{E}\sqrt{N}}{2^N}$. (Why $\langle\delta\rangle$ scales as $\frac{\mathcal{E}\sqrt{N}}{\mathcal{N}}$ is explained in App. D.)

We can understand physically why $W_{\rm b}$ dominates Eq. (9). Suppose, for simplicity, that $T_{\rm C} = 0$ and $T_{\rm H} = \infty$. In successful trials, the engine traverses a trapezoid clockwise, as in Fig. 2. In each such trial, the engine outputs $W_{\rm tot} \approx$ (length of trapezoid's left-hand leg) $-$ (length of right-hand leg) $\approx$ (length of left-hand leg) $\approx \langle\delta\rangle$. Which fraction of the trials is successful? The engine has a probability $\int_0^{W_{\rm b}} d\delta'\, P_{\rm MBL}(\delta') \approx \frac{1}{\langle\delta\rangle}\int_0^{W_{\rm b}} d\delta'\, e^{-\delta'/\langle\delta\rangle} \approx \frac{1}{\langle\delta\rangle}\int_0^{W_{\rm b}} d\delta' \approx \frac{W_{\rm b}}{\langle\delta\rangle}$ of occupying a trapezoid whose MBL-side gap is smaller than $W_{\rm b}$. The average work extracted is $\approx \langle\delta\rangle \cdot \frac{W_{\rm b}}{\langle\delta\rangle} = W_{\rm b}$.

The leading temperature-dependent correction in Eq. (9), $-\frac{2\ln 2}{\beta_{\rm C}}$, penalizes an agent who uses a suboptimal cold bath. The warmer an engine's cold bath, the less work one expects the engine to output. Indeed, the greater $T_{\rm C} = \frac{1}{\beta_{\rm C}}$, the more $-\frac{2\ln 2}{\beta_{\rm C}}$ detracts from $\langle W_{\rm tot}\rangle$. The penalty is smaller than the leading-order $\langle W_{\rm tot}\rangle$ term, since $T_{\rm C} \ll W_{\rm b}$.

Like a warm cold bath ($T_{\rm C} > 0$), a lukewarm hot bath ($T_{\rm H} < \infty$) limits the per-cycle power. The $\beta_{\rm H}$ correction is smaller than the terms in Eq. (9)—smaller even than the next-biggest $\beta_{\rm H}$-independent corrections, whose calculation and inclusion would be impractical. We therefore omitted the $\beta_{\rm H}$ correction from Eq. (9) to maintain order-of-magnitude consistency. The $\beta_{\rm H}$ correction depends on the density of states. The leading-order term has the form $-$(positive constant)$N(\beta_{\rm H}\mathcal{E})^2$. The cooler the hot bath, the lower $T_{\rm H}$ is, the greater $\beta_{\rm H}$ is, and the more work the correction shaves off from $\langle W_{\rm tot}\rangle$.

Like power, efficiency quantifies an engine's performance. The mesoscale engine operates at the efficiency

$$\boxed{\eta_{\rm MBL} \approx 1 - \frac{W_{\rm b}}{2\,\langle\delta\rangle}}. \tag{10}$$

The imperfection is small, $\frac{W_{\rm b}}{2\langle\delta\rangle} \ll 1$, because the cold bath has a small bandwidth. Like the qubit-engine efficiency $\eta_{\rm qubit}$, $\eta_{\rm MBL}$ is essentially equivalent to $\eta_{\rm Otto}$, a thermodynamic Otto engine's efficiency. For every choice of $W_{\rm b}$ and $\langle\delta\rangle \gg W_{\rm b}$, and for every ideal-gas heat-capacity ratio $\gamma = \frac{C_{\rm P}}{C_{\rm v}}$, there exists a compression ratio $r = \frac{V_1}{V_2}$ such that an ideal-gas Otto engine, compressed between V_1 and V_2, operates at the efficiency $\eta_{\rm Otto} = 1 - r^{1-\gamma} \approx \eta_{\rm MBL}$.

$\eta_{\rm MBL}$ is comparable not only to $\eta_{\rm Otto}$, but also to $\eta_{\rm QHO}$. The quantum-harmonic-oscillator Otto engine's efficiency was introduced in Eq. (3): $\eta_{\rm QHO} = 1 - \frac{\omega}{\Omega}$. Imagine operating an ensemble of QHO engines indexed by j. Suppose that the $j^{\rm th}$ QHO's gap is tuned between Ω_j and ω_j. [Planck's reduced constant equals one throughout this paper, $\hbar = 1$, except in order-of-magnitude estimates (Sec. IV).] Let the ETH-like gap Ω_j be distributed according to $P_{\rm GOE}(\Omega_j) = \frac{\pi}{2}\,\frac{\Omega_j}{\langle\delta\rangle^2}\,\exp\left(-\frac{\pi}{4}\,[\Omega_j]^2\right)$. (We approximate the gap distributions as independent of the energy E for simplicity.) The average large gap is $\langle\Omega_j\rangle = \langle\delta\rangle$, by design. Let the MBL-like gap ω_j be distributed according to $P_{\rm MBL}(\omega_j) = \frac{1}{\langle\delta\rangle}\,e^{-\omega_j/\langle\delta\rangle}$. This gap has a probability $\int_0^{W_{\rm b}} d\omega_j\, P_{\rm MBL}(\omega_j) \approx \int_0^{W_{\rm b}} d\omega_j\,\frac{1}{\langle\delta\rangle} = \frac{W_{\rm b}}{\langle\delta\rangle}$ of being small, i.e., of lying between 0 and $W_{\rm b}$. The average MBL-like gap ω_j, conditioned on ω_j's being small, is $\langle\omega_j\rangle \sim \frac{1}{W_{\rm b}/\langle\delta\rangle}\int_0^{W_{\rm b}} d\omega_j\,\omega_j\,P_{\rm MBL}(\omega_j) \approx \frac{1}{W_{\rm b}}\int_0^{W_{\rm b}} d\omega_j\,\omega_j = \frac{W_{\rm b}}{2}$. The efficiency, averaged over the ensemble of QHOs, is

$$\langle\eta_{\rm QHO}\rangle := 1 - \frac{\langle\omega\rangle}{\langle\Omega\rangle} \approx 1 - \frac{W_{\rm b}}{2\,\langle\delta\rangle} \approx \eta_{\rm MBL}\,. \tag{11}$$

(This definition of "average efficiency" is justified in App. C 2.) The mesoscale MBL engine operates at the ideal average efficiency of an ensemble of QHO engines. However, the MBL engine scales up to larger system sizes, i.e., to more "harmonic oscillators" (Sec. II B 4).

II B 4. Diabatic corrections to the per-cycle power

Like suboptimal baths, quick Hamiltonian tunings detract from the power. We have modeled the Hamiltonian $H_{\rm meso}(t)$ as being tuned quantum-adiabatically. Realistic tuning speeds $v := \mathcal{E}\left|\frac{d\alpha_t}{dt}\right|$ are finite. Finite speeds cause the engine to "hop" diabatically: Suppose that the engine begins some trial in the $j^{\rm th}$ energy eigenstate, with energy E_j. Suppose that $H_{\rm meso}(t)$ is measured at the end

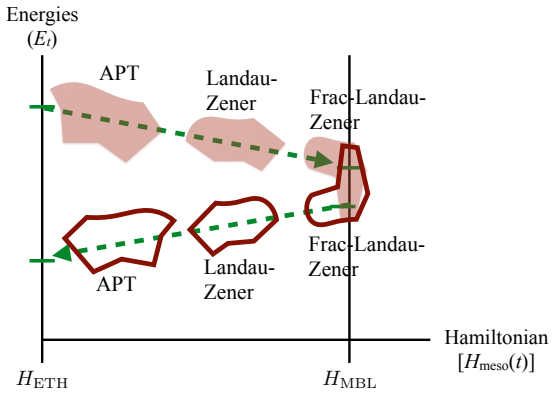

FIG. 3: Three (times two) classes of diabatic transitions: In an initial approximation, we model the engine Hamiltonian $H_{\rm meso}(t)$ as being tuned quantum-adiabatically. Realistic tuning speeds v induce diabatic transitions between energy levels. We model three classes of diabatic transitions. Each class can plague stroke 1 and stroke 3. First, consider tuning $H_{\rm meso}(t)$ within the ETH phase. The system can hop from its initial energy level to any other level. We model these hops with general adiabatic perturbation theory (APT). Second, consider tuning within the MBL phase. Energy levels wiggle toward and away from each other. Such an approach and divergence of two energies is modeled with a Landau-Zener transition. Third, consider the end of stroke 1 (or the start of stroke 3). Each "working gap" narrows (or expands), as in a fraction of a Landau-Zener transition.

of stroke 1 (e.g., by the cold bath[3]). The measurement's outcome may be the energy $E'_{j-\ell} \neq E'_j$ of the $(j-\ell)^{\rm th}$ MBL energy level, for some $\ell \neq 0$. If the outcome is so, the engine is said to have undergone a diabatic transition.

We model diabatic transitions probabilistically in App. G 8. Transitions of three types may occur during stroke 1. Transitions of the same types may occur during stroke 3. The transitions are sketched in Fig. 3.

If the engine jumps diabatically, its energy changes. The energy change does not consist of heat, as the engine interacts with no bath during tuning. The energy change must come from the battery used to tune the Hamiltonian, e.g., to strengthen a magnetic field. The energy change consists of work. In addition to depleting the battery during jumps, diabatic transitions can derail trials that would otherwise have outputted $W_{\rm tot} > 0$. We estimate, to lowest order in small parameters, the average per-cycle work costs $\langle W_{\rm diab} \rangle$ of diabatic jumps:

[3] The engine thermalizes with the cold bath, exchanging information and energy. Granted, the bath has a narrow bandwidth $W_{\rm b}$. The bath can exchange only small quanta of energy. Nonetheless, the information exchange (entanglement) decoheres the engine's state relative to the energy eigenbasis.

1. *Transitions modeled by general adiabatic perturbation theory (APT transitions):* Consider tuning $H_{\rm meso}(t)$ within the ETH phase. A perturbation is turned on or off. Consider the matrix $\mathcal{M}$ that represents the perturbation relative to the original energy eigenbasis. Off-diagonal elements of $\mathcal{M}$ may couple the engine's state to arbitrary eigenstates of the original Hamiltonian. We model such couplings with general adiabatic perturbation theory (APT) [59]. We call the corresponding transitions "APT transitions" (App. G 8 i).

   APT transitions cost an amount

$$\langle W_{\rm APT} \rangle \sim \frac{1}{\sqrt{N}} \frac{v^2 \beta_{\rm H}}{\mathcal{E} \langle \delta \rangle} \log \left(\frac{\langle \delta \rangle^2}{v} \right) e^{-N(\beta_{\rm H} \mathcal{E})^2/4} \quad (12)$$

   of work per trial, on average. Equation (12) encodes APT transitions' resemblance to an infinite-temperature bath: An APT transition can hop the engine from any energy level to any other. The probability of transitioning across a gap δ does not depend on whether δ lies above or below the engine's initial state. More levels exist above the initial state than below, if the engine begins stroke 1 at $T_{\rm H} < \infty$. Hence APT transitions tend to hop the engine upward, toward the $T = \infty$ state above and below which exist equal numbers of levels. If the engine starts at $T_{\rm H} = \infty$, APT transitions have no work to do during stroke 1, on average. As $\beta_{\rm H} = \frac{1}{T_{\rm H}} \to 0$, therefore, the right-hand side of Eq. (12) vanishes.

   The logarithm in Eq. (12) is a regulated divergence. Let $P_{\rm APT}(n|m)$ denote the probability of the engine's hopping from level m to level n. The probability diverges as the difference $|E_n - E_m|$ between the levels' energies shrinks: $P_{\rm APT}(n|m) \to \infty$ as $|E_n - E_m| \to 0$. The consequent divergence in $\langle W_{\rm APT} \rangle$ is logarithmic. We cut off the $\langle W_{\rm APT} \rangle$ integral at the greatest energy difference that contributes significantly to the integral, $|E_n - E_m| \sim \langle \delta \rangle$. The logarithm diverges in the adiabatic limit, as $v \to 0$. Yet the v^2 in Eq. (12) vanishes more quickly, sending $\langle W_{\rm APT} \rangle$ to zero, as expected. The exponential in Eq. (12) results from averaging with respect to the initial state, $e^{-\beta_{\rm H} H_{\rm GOE}}/Z$.

   Let us assess the size of $\langle W_{\rm APT} \rangle$. Since the hot bath is hot, $\sqrt{N}\, \beta_{\rm H} \mathcal{E} \ll 1$, the exponential ~ 1. The $\frac{1}{\sqrt{N}}$ and the logarithm scale subdominantly in the system size. Let us recast the dominant factors in terms of small parameters: $\langle W_{\rm APT} \rangle \sim \left(\frac{\sqrt{v}}{\langle \delta \rangle} \right)^4 (\sqrt{N}\, \beta_{\rm H} \mathcal{E}) \langle \delta \rangle$. The average work cost is suppressed fourfold in $\frac{\sqrt{v}}{\langle \delta \rangle} \ll 1$ and linearly in $\sqrt{N}\, \beta_{\rm H} \mathcal{E} \ll 1$. The $\langle \delta \rangle$ serves as the unit of work.

2. *Landau-Zener transitions:* Landau-Zener-type transitions overshadow APT transitions in the

MBL phase. Consider tuning the Hamiltonian parameter α_t within the MBL regime but at some distance from the extreme value 1. Energies drift close together and separate. When the energies are close together, the engine can undergo a Landau-Zener transition [60] (App. G 8 ii). Landau-Zener transitions hop the engine from one energy level to a nearby level. (General APT transitions hop the engine to arbitrary levels.)

Landau-Zener transitions cost zero average work, due to symmetries: $\langle W_{\rm LZ} \rangle = 0$. The $j^{\rm th}$ level as likely wiggles upward, toward the $(j+1)^{\rm th}$ level, as it wiggles downward, toward the $(j-1)^{\rm th}$ level. The engine as likely consumes work $W > 0$, during a Landau-Zener transition, as it outputs work $W > 0$. The consumption cancels the output, on average.

3. *Fractional-Landau-Zener transitions:* Consider the start of stroke 3. Ideally, the engine occupies the lower of two levels that separate. This separation constitutes a fraction of the Landau-Zener problem [59]. The engine might jump from the lower level to the upper (App. G 8 iii). A similar transition can occur at the end of stroke 1.

Fractional-Landau-Zener transitions cost an amount

$$\langle W_{\text{frac-LZ}} \rangle \sim \frac{1}{80\epsilon^5} \frac{v^2 (\delta_-)^2}{(W_{\rm b})^5} + \epsilon W_{\rm b} \tag{13}$$

of work, on average. δ_- denotes the MBL level-repulsion scale, the minimum width reasonably attributable to any MBL gap. The dimensionless parameter $\epsilon < 1$. We often assume $\epsilon \approx \frac{1}{3}$, for convenience.

The second term in Eq. (13), $\epsilon W_{\rm b}$, forms a crude upper bound that could be improved. Since $\epsilon < 1$, $\epsilon W_{\rm b} < \langle W_{\rm tot} \rangle \sim W_{\rm b}$ [Eq. (9)]: $\epsilon W_{\rm b}$ signifies a small work cost. From now on, we assume $\epsilon \approx \frac{1}{3}$. The prefactor in the first term in Eq. (13) can be neglected.

The first term has, in terms of small parameters, the form $\left(\frac{\sqrt{v}}{\langle \delta \rangle} \right)^4 \left(\frac{\delta_-}{\langle \delta \rangle} \right)^2 \left(\frac{\langle \delta \rangle}{W_{\rm b}} \right)^5 \langle \delta \rangle$. The average work cost is suppressed fourfold in $\frac{\sqrt{v}}{\langle \delta \rangle} \ll 1$ and twofold in $\frac{\delta_-}{\langle \delta \rangle} \ll 1$. The cost is fivefold large in $\frac{\langle \delta \rangle}{W_{\rm b}}$, which, though $\gg 1$, is $\ll \frac{\langle \delta \rangle}{\delta_-}$.

II C. From the mesoscale MBL Otto engine to the thermodynamic limit

The mesoscale engine has two drawbacks. Consider increasing the system size N. The average work extracted per trial declines exponentially: $\langle W_{\rm tot} \rangle \sim W_{\rm b} \ll \langle \delta \rangle \sim \frac{\mathcal{E}\sqrt{N}}{2^N}$. Additionally, the tuning speed v must shrink exponentially: $H_{\rm meso}(t)$ is ideally tuned quantum-adiabatically. The time per tuning stroke must far exceed the inverse of the average gap. Since $\langle \delta \rangle^{-1} \sim \frac{2^N}{\mathcal{E}\sqrt{N}}$, the stroke time grows exponentially. The mesoscale engine scales poorly. Properties of MBL offer a solution.

We introduce a thermodynamically large, or macroscopic, MBL Otto engine. The engine consists of mesoscale subengines that operate mostly independently. This independence hinges on *local level correlations* of the MBL phase, introduced in Sec. II C 1: Energy eigenstates localized near each other spatially tend to correspond to far-apart energies and vice versa. Local level correlations inform the engine introduced in Sec. II C 2. The engine cycle lasts for a time $\tau_{\rm cycle}$ that obeys three constraints, introduced in Sec. II C 3. We focus on exponential scaling behaviors, deemphasizing numerical prefactors, logarithms, and polynomials.

II C 1. Local level correlations

Consider subsystems, separated by a distance L, of an MBL system. The subsystems evolve roughly independently until times exponential in L, due to the localization of the MBL phase [3]. We apply this independence to parallelize mesoscale engines in different regions of a large MBL system. This application requires us to shift focus from whole-system energy-level statistics to *local level correlations* [61, 62].

Recall that an MBL system has a complete set of quasilocal integrals of motion [3]. In this context, "quasilocal" means that each integral of motion can be related to a local operator via a finite-depth unitary transformation that consists only of local unitaries, up to exponentially small corrections. (In this discussion, "local" refers to spatial locality.) Thus, each integral of motion can be associated with a lattice site. This association is unique except for a small fraction of the integrals of motion.

Let $|\psi_1\rangle$ and $|\psi_2\rangle$ denote many-body energy eigenfunctions. Let E_1 and E_2 denote the corresponding energies. $|\psi_1\rangle$ and $|\psi_2\rangle$ are eigenstates also of every integral of motion [3]. However, $|\psi_1\rangle$ and $|\psi_2\rangle$ correspond to different eigenvalues of at least some of the integrals of motion (if the eigenstates are distinct). Local level correlations concern the matrix elements O_{21} of generic strictly local operators O between pairs of many-body eigenstates. Specifically, they are correlations between (1) the matrix-element size $|O_{21}|$ and (2) the difference $|E_1 - E_2|$ between the states' energies.

Let us expand upon this definition. Heuristically, in the MBL phase, $|\psi_1\rangle$ and $|\psi_2\rangle$ are "close together" spatially if they correspond to the same configuration of the integrals of motion (and of, e.g., energy and particle density) everywhere except in some region of size L. We say that such pairs of eigenstates are a distance L apart. Let ξ denote the system's localization length. When $L \gg \xi$, the matrix element scales as $|O_{21}| \sim e^{-L/\zeta}$,

wherein $\zeta \sim \frac{1}{\frac{1}{\xi}+\ln 2}$ is discussed in App. H. All lengths appear in units of the lattice spacing, which is set to one. If the eigenfunctions lie close together, $L \lesssim \xi$, the matrix-element size scales as $|O_{21}| \sim 2^{-L}$.

Having related the matrix-element size $|O_{21}|$ to the spatial separation L, we relate L to the energy difference $|E_1 - E_2|$. Spatially close-together eigenstates, connected by $|O_{21}| \sim e^{-L/\zeta}$, are unlikely to have energies within $\mathcal{E}e^{-L/\zeta}$ of one another [3, 31, 44, 63]. The reason is the hybridization of wave functions, detailed in App. H. Therefore, small energy differences $|E_1 - E_2|$ are correlated with small matrix-element sizes $|O_{21}|$, which rearrange particles across large spatial distances.[4]

II C 2. Application of local level correlations in the macroscopic MBL engine

Let us apply local level correlations to construct a scalable generalization of the mesoscale Otto engine. We modify strokes 1 and 3: The Hamiltonian $H_{\rm macro}(t)$ is tuned within the MBL phase, between a point analogous to $H_{\rm GOE}$ and a point analogous to $H_{\rm MBL}$. The $H_{\rm GOE}$-like Hamiltonian has a localization length $\xi_>$. The $H_{\rm MBL}$-like Hamiltonian has a localization length $\xi_< \ll \xi_>$. Particles mostly remain in regions of, at most, length $\xi_>$. Such regions function as "subengines," as independent instances of the mesoscale engine. What happens in a subengine stays in a subengine.

This subdivision boosts the engine's power. We presented the average per-cycle power $\langle W_{\rm tot}\rangle$ of one length-N mesoscale engine in Sec. II B 3: $\langle W_{\rm tot}\rangle \sim W_{\rm b} \ll \langle\delta\rangle \sim \frac{\mathcal{E}\sqrt{N}}{2^N}$. Let the subscript "macro" denote properties of the macroscopic, composite engine. The composite engine consists of length-$\xi_>$ mesoscale subengines. Each subengine's per-cycle power is suppressed exponentially not in $N_{\rm macro}$, but in $N = \xi_>$: $\langle W_{\rm tot}\rangle \sim \frac{\mathcal{E}\sqrt{\xi_>}}{2^{\xi_>}}$. The reason is local level correlations: The cold bath only locally couples to subengines during stroke 2 (App. I). Local operators O typically rearrange particles across just short distances. Short-distance rearrangements tend to change an MBL system's energy by substantial amounts. Hence a locally manipulated MBL system effectively has just substantially sized energy gaps. We denoted by δ_- the level-repulsion scale, the minimum width reasonably attributable to any gap of an MBL system of length $N = \xi_>$. This δ_- scales as $\mathcal{E}e^{-\xi_>/\xi_<}\, 2^{-\xi_>}$ (App. I).

Any given gap δ in a subengine's effective energy spectrum has a high probability of being $\delta \geq \delta_-$. Hence $\delta > \langle\delta\rangle_{\rm macro} \sim \frac{\mathcal{E}\sqrt{N_{\rm macro}}}{2^{N_{\rm macro}}}$, the composite engine's average gap, with high probability. In the thermodynamic limit, $\langle\delta\rangle_{\rm macro} \to 0$: The composite engine's average gap "closes." If each subengine traversed just size-$\langle\delta\rangle_{\rm macro}$ gaps during stroke 2, the subengine's per-cycle power would vanish: $\langle W_{\rm tot}\rangle \to 0$. Localization "wedges open" the gaps in a subengine's effective energy spectrum, preventing these gaps from closing in the thermodynamic limit, keeping $\langle W_{\rm tot}\rangle$ positive. The number of subengines scales linearly with $N_{\rm macro}$. So, therefore, does the composite engine's per-cycle power:

$$\langle W_{\rm tot}\rangle_{\rm macro} \sim N_{\rm macro} \frac{\sqrt{\xi_>}}{2^{\xi_>}}\, \mathcal{E}\,. \tag{14}$$

II C 3. Time scales of the macroscopic MBL engine

Three requirements constrain the time for which a cycle is implemented: (1) Subengines must operate mostly independently. Information propagates through an MBL system, though, albeit slowly. $H_{\rm macro}(t)$ must be tuned too quickly for much information to leak between subengines (App. J). (2) Tuning at a finite speed $v > 0$ induces diabatic transitions between energy levels (Sec. II B 4). v must be small enough to suppress the average work cost, $\langle W_{\rm diab}\rangle$, of undesirable diabatic transitions (App. J). (3) The cold bath has a small bandwidth, $W_{\rm b} \ll \langle\delta\rangle$; interacts with a small coupling strength g; and interacts locally, to avoid coupling subengines together. Stroke 2 must last long enough to thermalize the engine nonetheless (App. I). We detail these requirements below. Requirement (3) determines the cycle time, $\tau_{\rm cycle}$.

II C 3 i. Lower bound on the tuning speed v from the subengines' (near) independence: The price paid for scalability is the impossibility of adiabaticity. Suppose that $H_{\rm macro}(t)$ were tuned infinitely slowly. Information would have time to propagate across the composite engine. Subengines would interact. The slow spread of information through MBL [64] lower-bounds the tuning speed:

$$v \gg (\mathcal{J}_{1.5\xi_>})^2\, \frac{\langle\delta\rangle}{\langle\delta\rangle^{(1.5\xi_>)}} \tag{15}$$

$$\sim \mathcal{E}^2\, e^{-3\xi_>/\xi(t)}\, 2^{-2.5\xi_>} \tag{16}$$

(App. J). The level-repulsion scale—the least width reasonably attributable to any gap—of a length-L MBL system is denoted by $\mathcal{J}_L$. The δ_- introduced earlier equals $\mathcal{J}_N = \mathcal{J}_{\xi_>}$. The time-$t$ localization length is denoted by $\xi(t)$. A length-L MBL system's average gap is denoted by $\langle\delta\rangle^{(L)}$. (The average subengine gap $\langle\delta\rangle$, introduced earlier, equals $\langle\delta\rangle^{(\xi_>)}$.)

Inequality (15) prevents the engine from losing much work to undesirable adiabatic transitions. During tuning, energy levels approach each other. Typically, if such a "close encounter" results in an adiabatic transition, many particles shift across the engine. Subengines effectively

[4] These features are consistent with globally Poisson level statistics: Suppose that E_1 and E_2 denote large nearest-neighbor energies. $|\psi_1\rangle$ and $|\psi_2\rangle$ typically represent configurations that differ at extensively many sites. Hence $|O_{21}| \sim e^{-L/\zeta}$. This matrix element is exponentially smaller, in L, than the average gap 2^{-L} implied by Poisson statistics.

interact, consuming a total amount $\sim N_{\rm macro} \langle W^{\rm cost}_{\rm adiab} \rangle$ of work, on average. Undesirable adiabatic transitions must cost less than the average work (14) outputted by ideal (independent) subengines. $H_{\rm macro}(t)$ must be tuned quickly enough that

$$\left\langle W^{\rm cost}_{\rm adiab} \right\rangle \ll \langle W_{\rm tot} \rangle \ . \tag{17}$$

We approximate the left-hand side as

$$\begin{aligned} \left\langle W^{\rm cost}_{\rm adiab} \right\rangle \approx & \left(\frac{\text{Work cost}}{\text{1 undesirable adiab. transition}} \right) \\ & \times \left(\frac{\text{Prob. of undesirable adiab. transition}}{\text{1 close encounter}} \right) \\ & \times \left(\frac{\text{\# close encounters}}{\text{1 tuning stroke}} \right) \\ & \times \left(\frac{\text{Avg. \# strokes during which can lose work}}{\text{1 cycle}} \right) . \end{aligned} \tag{18}$$

The first factor $\sim \langle \delta \rangle$. The second factor follows from the Landau-Zener probability $P_{\rm LZ} = e^{-2\pi \mathcal{J}^2 / v} \sim 1 - \frac{\mathcal{J}^2}{v}$ that any given close encounter induces a diabatic transition. The Hamiltonian-matrix element that couples the approaching states has the size $\mathcal{J} \sim \mathcal{J}_{1.5\xi_>}$. The $1.5\xi_>$ encodes nearest-neighbor subengines' isolation: Information should not propagate from the left-hand side of one subengine rightward, across a distance $1.5\xi_>$, to the neighbor's center. We estimate the third factor in Eq. (18) as $\frac{\langle \delta \rangle}{\langle \delta \rangle^{(1.5)}}$. This 1.5 has the same origin as the 1.5 in the $\mathcal{J}_{1.5\xi_>}$. The final factor in Eq. (18) $\sim \frac{W_{\rm b}}{\langle \delta \rangle}$, the fraction of the cycles that would, in the absence of undesirable transitions, output $W_{\rm tot} > 0$. Upon substituting into Eq. (18), we substitute into Ineq. (17). The right-hand side $\sim W_{\rm b}$ [Eq. (9)]. Solving for v yields Ineq. (15).

II C 3 ii. Upper bound on v from the work cost of undesirable diabatic transitions: Tuning at a finite speed $v > 0$ induces diabatic transitions, introduced in Sec. II B 4. Diabatic hops cost a subengine an amount $\langle W_{\rm diab} \rangle$ of work per cycle, on average. For clarity, we relabel as $\left\langle W^{\rm adiab}_{\rm tot} \right\rangle$ the average work outputted by one ideal subengine, tuned adiabatically, per cycle. The requirement $\langle W_{\rm diab} \rangle \ll \left\langle W^{\rm adiab}_{\rm tot} \right\rangle$ upper-bounds v (App. J).

When the engine is shallowly localized, APT transitions dominate $\langle W_{\rm diab} \rangle$ [Eq. (12)]. They bound the speed as

$$v \ll \langle \delta \rangle^2 \sim \frac{\mathcal{E}^2}{\mathcal{N}^2} \sim 2^{-2\xi_>} \, \mathcal{E}^2 \, . \tag{19}$$

When the engine is very localized, fractional-Landau-Zener transitions dominate $\langle W_{\rm diab} \rangle$ [Eq. (13)], and

$$v \ll \frac{(W_{\rm b})^3}{\delta_-} \sim \frac{1}{10^3} \, e^{\xi_>/\xi_<} \, 2^{-2\xi_>} \mathcal{E}^2 \, . \tag{20}$$

The final expression follows if $W_{\rm b} \sim \frac{\langle \delta \rangle}{10}$. Both upper bounds, (19) and (20), lie above the lower bound (16).

II C 3 iii. Lower bound on the cycle time $\tau_{\rm cycle}$ from cold thermalization: The upper bounds elongate the cycle for at least a time $\sim \frac{\mathcal{E}}{v}$. Thermalization with the cold bath (stroke 2) bounds $\tau_{\rm cycle}$ more stringently. The reasons are (1) the slowness with which MBL thermalizes and (2) the restriction $W_{\rm b} \ll \langle \delta \rangle$ on the cold-bath bandwidth. We elaborate after briefly introducing our cold-thermalization model. Appendix I contains details.

We envision the cold bath as a bosonic system that couples to the engine with strength g. The bath couples locally, e.g., to pairs of spins. This locality prevents subengines from interacting with each other much through the bath. The bath can, e.g., flip spin j upward while flipping spin $j+1$ downward. These flips likely change a subengine's energy by some amount E. The bath can effectively absorb only energy quanta of size $\leq W_{\rm b}$ from any subengine. The cap is set by the bath's speed of sound [65], which follows from microscopic parameters in the bath's Hamiltonian [66]. The rest of the energy emitted during the spin flips, $|E - W_{\rm b}|$, is distributed across the subengine as the intrinsic subengine Hamiltonian flips more spins.

Let $\tau_{\rm th}$ denote the time required for stroke 2. We estimate $\tau_{\rm th}$, using Fermi's Golden Rule, in App. I 3:

$$\tau_{\rm cycle} \sim \tau_{\rm th} \sim W_{\rm b} \left(\frac{\mathcal{E}}{g \delta_-} \right)^2 . \tag{21}$$

The left-hand side equals the inverse of the rate Γ_{fi} at which cold thermalization transitions the engine from an energy level $|i\rangle$ to a level $|f\rangle$: $\tau_{\rm cycle} = 1/\Gamma_{fi}$. The bath has a density of states $\mu_{\rm bath} \sim 1/W_{\rm b}$. The interaction transitions the engine via a Hamiltonian-matrix element of size $|\langle f|V|i\rangle| \sim \frac{g\delta_-}{\mathcal{E}}$. Hence Eq. (21) results from inverting Fermi's Golden Rule, $\Gamma_{fi} \sim |\langle f|V|i\rangle|^2 \, \mu_{\rm bath}$.

The interaction is assumed to be Markovian: Information leaked from the engine dissipates throughout the bath quickly. Markovianity lower-bounds $\tau_{\rm th}$ and therefore $\tau_{\rm cycle}$:

$$\tau_{\rm th} > \frac{\mathcal{E}^2}{W_{\rm b} (\delta_-)^2} \sim \frac{10}{\mathcal{E}} \, e^{2\xi_>/\xi_<} \, 2^{3\xi_>} \, . \tag{22}$$

The final expression follows if $W_{\rm b} \sim \frac{\langle \delta \rangle}{10}$.

More precisely, the cold-bath bandwidth $W_{\rm b}$ is bounded as follows. $W_{\rm b}$ must be large enough to thermalize tiny gaps δ_-. $W_{\rm b}$ must be too small to thermalize gaps comparable to $\langle \delta \rangle$. Hence

$$\delta_- < W_{\rm b} \ll \langle \delta \rangle \ . \tag{23}$$

The bounds are expressed in terms of localization lengths ξ in App. J.

III. NUMERICAL SIMULATIONS

The engine can be implemented with a disordered Heisenberg model. A similar model's MBL phase has

been realized with cold atoms [2]. We numerically simulated a 1D mesoscale chain of $N = 12$ spin-$\frac{1}{2}$ degrees of freedom, neglecting dynamical effects during strokes 1 and 3 (the Hamiltonian tunings). The chain evolves under the Hamiltonian

$$H_{\rm sim}(t) = \frac{\mathcal{E}}{Q(h(\alpha_t))}\left[\sum_{j=1}^{N-1} \boldsymbol{\sigma}_j \cdot \boldsymbol{\sigma}_{j+1} + h(\alpha_t)\sum_{j=1}^{N} h_j \sigma_j^z\right]. \tag{24}$$

Equation (24) describes spins equivalent to interacting spinless fermions. Energies are expressed in units of $\mathcal{E}$, the average per-site energy density. For $\gamma = x, y, z$, the $\gamma^{\rm th}$ Pauli operator that operates nontrivially on the $j^{\rm th}$ site is denoted by σ_j^γ. The $\boldsymbol{\sigma}_j \cdot \boldsymbol{\sigma}_{j+1}$ encodes nearest-neighbor hopping and repulsion.

The tuning parameter $\alpha_t \in [0, 1]$ determines the phase occupied by $H_{\rm sim}(t)$. The site-j disorder potential depends on a random variable h_j distributed uniformly across $[-1, 1]$. The disorder strength $h(\alpha_t)$ varies as $h(\alpha_t) = \alpha_t\, h_{\rm GOE} + (1 - \alpha_t) h_{\rm MBL}$. When $\alpha_t = 0$, the disorder is weak, $h = h_{\rm GOE}$, and the engine occupies the ETH phase. When $\alpha_t = 1$, the disorder is strong, $h = h_{\rm MBL} \gg h_{\rm GOE}$, and the engine occupies the MBL phase.

The normalization factor $Q(h(\alpha_t))$ preserves the width of the density of states (DOS). Preserving the DOS preserves the average level spacing $\langle\delta\rangle$ as a function of the time t. $Q(h(\alpha_t))$ prevents the work extracted from changing the bandwidth from polluting the work extracted with help from level statistics, as discussed in Sec. II B 1. $Q(h(\alpha_t))$ is defined and calculated in App. K 1.

We simulated the spin chain using exact diagonalization, detailed in App. K. The main results appear in Fig. 4. Figure 4a shows the average work extracted per cycle, $\langle W_{\rm tot}\rangle$; and Fig. 4b shows the efficiency, $\eta_{\rm MBL}$. The slanting lines represent analytical predictions, Eqs. (9) and (10). Each red dot represents an average over $1,000$ disorder realizations.

The error bars are smaller than the numerical-data points. Each error bar represents the error in the estimate of a mean (of $\langle W_{\rm tot}\rangle$ or of $\eta_{\rm MBL} := 1 - \frac{\langle W_{\rm tot}\rangle}{\langle Q_{\rm in}\rangle}$) over 1,000 disorder realizations. Each error bar extends a distance (sample standard deviation)$/\sqrt{\#\text{ realizations}}$ above and below that mean.

In these simulations, the baths had the extreme temperatures $T_{\rm H} = \infty$ and $T_{\rm C} = 0$. This limiting case elucidates the $W_{\rm b}$-dependence of $\langle W_{\rm tot}\rangle$ and of $\eta_{\rm MBL}$. Disregarding finite-temperature corrections, on a first pass, builds intuition. Finite-temperature numerics appear alongside finite-temperature analytical calculations in App. G. The simulations' ETH-side field had a magnitude $h(0) = 2.0$, and the MBL-side field had a magnitude $h(1) = 20.0$. These $h(\alpha_t)$ values fall squarely on opposite sides of the MBL transition at $h \approx 7$.

During strokes 1 and 3, the state was evolved as though the Hamiltonian were tuned adiabatically. Suppose, for example, that the engine began stroke 1 with weight ρ_j on eigenstate j of the pre-tuning Hamiltonian $H(\alpha_t = 0)$. The engine would end the stroke with weight ρ_j on eigenstate j of the post-tuning Hamiltonian $H(1)$. Diabatic corrections can be incorporated in future work.

Figure 4 shows how the per-cycle power and the efficiency depend on the cold-bath bandwidth $W_{\rm b}$. As expected, $\langle W_{\rm tot}\rangle \approx W_{\rm b}$. The dependence's linearity, and

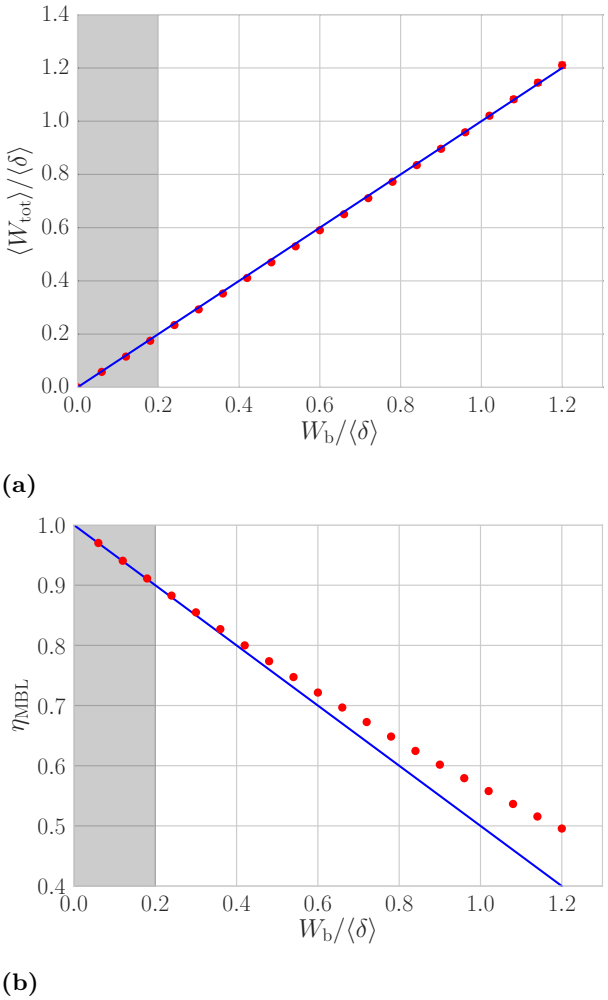

FIG. 4: Average per-cycle power $\langle W_{\rm tot}\rangle$ (top) and efficiency $\eta_{\rm MBL}$ (bottom) as functions of the cold-bath bandwidth $W_{\rm b}$, calculated from numerical simulations of an adiabatically tuned mesoscale MBL engine thermalized at $T_{\rm C} = 0$ and at $T_{\rm H} = \infty$: We numerically simulated a mesoscale engine of $N = 12$ sites. Each red dot represents an average over 1,000 disorder realizations of the random-field Heisenberg Hamiltonian (24). The disorder strength $h(\alpha_t)$ was tuned between $h(0) = 2.0$ (in the "thermal" regime governed by the Eigenstate Thermalization Hypothesis) and $h(1) = 20.0$ (in the MBL regime). The slanted blue lines represent the analytical predictions (9) and (10). When $W_{\rm b} \ll \langle\delta\rangle$ (in the gray shaded region), $\langle W_{\rm tot}\rangle$ and $\eta_{\rm MBL}$ vary linearly with $W_{\rm b}$, as in the analytical predictions. As $W_{\rm b}$ grows, $\eta_{\rm MBL}$ exceeds the analytical predictions, due to high-order corrections.

the unit proportionality factor, agree with Eq. (9). Also as expected, the efficiency declines as the cold-bath bandwidth rises: $\eta_{\rm MBL} \approx 1 - \frac{W_{\rm b}}{2\langle\delta\rangle}$. The linear dependence and the proportionality factor agree with Eq. (10).

The gray columns in Fig. 4 highlight the regime in which the analytics were performed, where $\frac{W_{\rm b}}{\langle\delta\rangle} \ll 1$. If the cold-bath bandwidth is small, $W_{\rm b} \lesssim \langle\delta\rangle$, the analytics-numerics agreement is close. But the numerics agree with the analytics even outside this regime. If $W_{\rm b} \gtrsim \langle\delta\rangle$, the analytics slightly underestimate $\eta_{\rm MBL}$: The simulated engine operates more efficiently than predicted. To predict the numerics' overachievement, one would calculate higher-order corrections in App. G: One would Taylor-approximate to higher powers, modeling subleading physical processes. Such processes include the engine's dropping across a chain of three small gaps $\delta_1', \delta_2', \delta_3' < W_{\rm b}$ during cold thermalization.

IV. ORDER-OF-MAGNITUDE ESTIMATES

How well does the localized engine perform, compared with competitors? Estimating relevant engines' power outputs will prove entertaining.

Localization has been achieved in solid-state systems.[5] Consider silicon doped with phosphorus [43]. A distance of ~ 10 nm may separate phosphorus impurities. Let our engine cycle's shallowly localized regime have a localization length of $\xi_> \sim 10$ sites, or 100 nm. Let the work-outputting degrees of freedom be electronic. The localized states will correspond to energies $\mathcal{E} \sim 1$ eV. Each subengine's half-filling Hilbert space has dimensionality[6] $\mathcal{N} = \binom{10}{5} \sim 10^2$. Each subengine therefore experiences the effective average gap $\langle\delta\rangle \sim \frac{\mathcal{E}\sqrt{N}}{\mathcal{N}} \sim \frac{1 \text{ eV}}{10^2} \sim 10$ meV. The cold-bath bandwidth must satisfy $\langle\delta\rangle \gg W_{\rm b}$. We set $W_{\rm b}$ to be an order of magnitude down from $\langle\delta\rangle$: $W_{\rm b} \sim 1$ meV ~ 10 K. The cold-bath bandwidth approximates the work outputted by one subengine per cycle:[7] $\langle W_{\rm tot}\rangle \sim W_{\rm b} \sim 1$ meV [Eq. (9)].

What volume does a localized subengine fill? Suppose that the engine is three-dimensional (3D).[8] A little room should separate the subengines. Classical-control equipment requires more room. Also, the subengine needs space to connect to the baths. We therefore associate each subengine with a volume of $V \approx (100 \text{ nm})^3$.

The last element needed for our quantitative fantasy is the cycle time, $\tau_{\rm cycle}$. We choose for δ_- to be a little smaller than $W_{\rm b}$—of the same order: $\delta_- \sim W_{\rm b} \sim 1$ meV. In the extreme case allowed by Ineq. (22), $\tau_{\rm cycle} \sim \frac{\hbar\mathcal{E}^2}{W_{\rm b}(\delta_-)^2} \sim \frac{\hbar\mathcal{E}^2}{(W_{\rm b})^3} \sim \frac{(10^{-15} \text{ eV s})(1 \text{ eV})^2}{(1 \text{ meV})^3} \sim 1$ μs.

The localized engine therefore operates with a power $\mathscr{P} \sim \frac{W_{\rm b}}{\tau_{\rm cycle}} \sim \frac{1 \text{ meV}}{1 \ \mu\text{s}} \approx 10^{-16}$ W. Interestingly, this $\mathscr{P}$ is one order of magnitude greater than a flagellar motor's [67] power, according to our estimates.

We can assess the engine by calculating not only its power, but also its power density. The localized engine packs a punch at $\frac{\mathscr{P}}{V} \sim \frac{10^{-16} \text{ W}}{(10^{-7} \text{ m})^3} = 100 \text{ kW/m}^3$.

Let us compare with a car engine, a more conventional Otto engine. A typical car engine outputs $\mathscr{P} \sim 100$ horsepower ~ 100 kW. A car's power density is $\frac{\mathscr{P}}{V} \sim \frac{100 \text{ kW}}{100 \text{ L}} = 1 \text{ MW/ m}^3$ (wherein L represents liters). The car engine's $\frac{\mathscr{P}}{V}$ exceeds the MBL engine's by only an order of magnitude, according to these rough estimates.

We can compare the MBL Otto engine not only to car engines and molecular motors, but also to an array of ideally independent bits or qubits. The qubits' gaps are shrunk and widened independently. Many papers have been written about qubit Otto engines [68–72]. A possible realization could consist of double quantum dots [73, 74]. The scales in [73, 74] suggest that a quantum-dot engine could output an amount $W_{\rm tot} \sim 10$ meV of work per cycle. We approximate the cycle time $\tau_{\rm cycle}$ with the spin relaxation time: $\tau_{\rm cycle} \sim 1$ μs. The power would be $\mathscr{P} \sim \frac{W_{\rm tot}}{\tau_{\rm cycle}} \sim \frac{10 \text{ meV}}{1 \ \mu\text{s}} \sim 10^{-15}$ W. The quantum-dot engine's power exceeds the MBL engine's by an order of magnitude. However, the quantum dots must be separated widely, so that they do not interact. In contrast, interactions feature in the definition of MBL. We attribute a volume $V \sim (1 \ \mu\text{m})^3$ to each dot. The power density would be $\frac{\mathscr{P}}{V} \sim 1 \text{ kW/m}^3$, two orders of magnitude less than the localized engine's.

V. COMPARISONS WITH COMPETITOR ENGINES

The Otto cycle can be implemented with many media. Why use MBL? Also, how does the "athermality" of

---

[5] This localization is single-particle, or Anderson, rather than many-body. See App. H for a review of Anderson localization. See App. L 4 for an extension of the MBL Otto engine to an Anderson-localized Otto engine.

[6] A larger subengine, e.g., of $\xi_> \sim 20$ sites, has an $\mathcal{N} = \binom{\xi_>}{\xi_>/2}$ of the order of magnitude of $2^{-\xi_>}$. The former scales as the latter. Therefore, we often approximate the former with the latter. The subengine under consideration is smaller: $\xi_> = 10$. Its $\mathcal{N}$ is an order of magnitude less than its $2^{-\xi_>}$. We therefore use the more precise $\mathcal{N} = \binom{\xi_>}{\xi_>/2}$.

[7] The use of semiconductors would require corrections to our results. Dipolar interactions would couple the impurities' spins. Wave functions would decay as power laws, rather than as the exponentials in App. H. However, we aim for just a rough estimate.

[8] Until now, we have supposed that the engine is 1D. Anderson localization, which has been realized in semiconductors, exists in all dimensions. Yet whether MBL exists in dimensions $D > 1$ remains an open question. Some evidence suggests that MBL exists in $D \geq 2$ [38, 40, 42]. But attributing a 3D volume to the engine facilitates comparisons with competitors. We imagine 10-nm-long 1D strings of sites. Strings are arrayed in a plane, separated by 10 nm. Planes are stacked atop each other, separated by another 10 nm.

MBL level correlations advantage our engine? We compare our engine with four competitors: an ideal thermodynamic gas, a set of ideally noninteracting qubits (e.g., quantum dots), a many-body system whose bandwidth is compressed and expanded, and an MBL engine tuned between equal-disorder-strength disorder realizations. Details appear in App. L. So do comparisons with two more engines that result from relaxing restrictions on our protocol: an MBL Otto engine whose cold bath has an ordinary bandwidth $W_{\rm b} > \langle\delta\rangle$ and an Anderson-localized Otto engine.

V A. Ideal-gas Otto engine

The conventional thermodynamic Otto engine consists of an ideal gas. Its efficiency, $\eta_{\rm Otto}$, approximately equals the efficiency $\eta_{\rm MBL}$ of an ideal mesoscopic MBL engine: $\eta_{\rm Otto} \approx \eta_{\rm MBL}$. More precisely, for every MBL parameter ratio $\frac{W_{\rm b}}{\langle\delta\rangle}$, and for every ideal-gas heat-capacity ratio $\gamma = \frac{C_{\rm P}}{C_{\rm v}}$, there exists a compression ratio $r := \frac{V_1}{V_2}$ such that $\eta_{\rm Otto} = 1 - r^{1-\gamma} = 1 - \frac{W_{\rm b}}{2\langle\delta\rangle} \approx \eta_{\rm MBL}$. However, scaling up the mesoscopic MBL engine to the thermodynamic limit requires a lower bound on the tuning speed v (App. II C). The lower bound induces diabatic jumps that cost work $\langle W_{\rm diab}\rangle$, detracting from $\eta_{\rm MBL}$ by an amount $\sim \frac{v^2(\delta_-)^2}{(W_{\rm b})^5} + \frac{W_{\rm b}}{\langle\delta\rangle}$ (App. G 8 iv). (For simplicity, we have assumed that $T_{\rm C} = 0$ and $T_{\rm H} = \infty$.) The ideal-gas engine suffers no such diabatic jumps. However, the MBL engine's $\langle W_{\rm diab}\rangle$ is suppressed in small parameters. Hence the thermodynamically large MBL engine's efficiency lies close to the ideal-gas engine's efficiency: $\eta^{\rm true}_{\rm MBL} \approx \eta_{\rm Otto}$.

Moreover, the thermodynamically large MBL engine may be tuned more quickly than the ideal-gas engine. The MBL engine is tuned nearly quantum-adiabatically. The ideal-gas engine is tuned quasistatically. The physics behind the quantum adiabatic theorem differs from the physics behind the quasistatic condition. Hence the engines' speeds v are bounded with different functions of the total system size $N_{\rm macro}$. The lower bound on the MBL engine's v remains constant as $N_{\rm macro}$ grows: $v \gg \mathcal{E}^2\, e^{-3\xi_>/\xi(t)}\, 2^{-2.5\xi_>}$ [Ineq. (15)]. Rather than $N_{\rm macro}$, the fixed localization length $\xi_>$ governs the bound on v. In contrast, we expect an ideal-gas engine's speed to shrink: $v \sim \frac{1}{N_{\rm macro}}$. The quasistatic condition requires that the engine remain in equilibrium. The agent changes the tuning parameter α by a tiny amount $\Delta\alpha$, waits for the change's influence to ripple through the gas such that the gas calms, then changes α by $\Delta\alpha$. The influence is expected to propagate as a wave with some speed c. The wave reaches the engine's far edge in a time $\sim \frac{N_{\rm macro}}{c}$. Hence the tuning speed $v < \mathcal{E}\frac{c}{N_{\rm macro}}$. The system size $N_{\rm macro}$ suppresses the ideal-gas engine's v but not the MBL engine's.[9]

However, the ideal-gas engine is expected to output more work per unit volume than the MBL engine. According to our order-of-magnitude estimates (Sec. IV), the ideal-gas engine operates at a power density of $\frac{\mathscr{P}}{V} \sim 1\ {\rm MW/m^3}$; and the localized engine, at $\frac{\mathscr{P}}{V} \sim 100\ {\rm kW/m^3}$. An order of magnitude separates the estimates.

V B. Quantum-dot engine

MBL spin chains are modeled as strings of *localized bits*, or *l-bits*. An l-bit's real-space wave function decays exponentially with distance. The l-bits' tails overlap negligibly (see App. E, App. H, and [34, 75]). We compare the MBL chain with an array of ideally independent bits or qubits, such as quantum dots. Each bit's gap is shrunk and widened during each cycle. The energy eigenbasis's form need not change: Let $\{|z_\gamma\rangle\}$ denote some unchanging basis, such as the $(\sigma^z)^{\otimes N_{\rm macro}}$ eigenbasis. Each energy eigenstate $|E_t^{(j)}\rangle = \sum_\gamma c_\gamma^{(j)}(t)|z_\gamma\rangle$ remains constant in time: $c_\gamma^{(j)}(t) = c_\gamma^{(j)}$. In contrast, the MBL engine's energy eigenbasis changes. The eigenbasis change can induce diabatic hops that detract from $\langle W_{\rm tot}\rangle$. In contrast, the ideal quantum-dot engine loses no work to diabatic hops. Hence the ideal quantum-dot engine operates at a higher power than the MBL engine: $\mathscr{P}_{\rm q.dots} > \mathscr{P}_{\rm MBL}$. According to the estimates in Sec. IV, $\mathscr{P}_{\rm q.dots} \sim 10^{-15}$ W, whereas a localized engine outputs $\mathscr{P}_{\rm localized} \sim 10^{-16}$ W. The quantum-dot estimate exceeds the localized-engine estimate by an order of magnitude.

But qubits are difficult to isolate. Consider packing quantum dots together with the density of the MBL l-bits. The quantum dots will interact, as an ETH system. The bits will decohere each others' states over some time scale T_2. The time per cycle must be much less than the decoherence time, so $v \gg \frac{\mathcal{E}}{T_2}$. This bound induces diabatic jumps that cost work $\langle W_{\rm diab}\rangle$, lowering the realistic bit-array power $\mathscr{P}$.

To compensate, we could separate the dots such that $T_2 =$ MBL l-bit lifetime. The bit array would fill a greater volume V, outputting a lower power density $\frac{\mathscr{P}}{V}$. According to our estimates in Sec. IV, $\frac{\mathscr{P}_{\rm q.dots}}{V} \sim 1\ {\rm kW/m^3}$, whereas $\frac{\mathscr{P}_{\rm localized}}{V} \sim 100\ {\rm kW/m^3}$. For the bits, power density trades off with isolation. In contrast, substantial isolation of l-bits is a built-in feature of MBL.

Like the l-bits' isolation, the MBL potential's generic nature offers an advantage. MBL requires a random disorder potential $\{h(\alpha_t)h_j\}$, e.g., a "dirty sample," a defect-riddled crystal. This "generic" potential contrasts

[9] Cold thermalization of the MBL engine lasts longer than one tuning stroke: $\tau_{\rm th} \gg \frac{\mathcal{E}}{v}$ (Sec. II C). However, even $\tau_{\rm th}$ does not depend on $N_{\rm macro}$.

with the pristine background required by quantum dots. Imposing random MBL disorder is expected to be simpler. On the other hand, a quantum-dot engine does not necessarily need a small-bandwidth cold bath, $W_{\rm b} \ll \langle \delta \rangle$. Small-bandwidth baths may be difficult to implement with certain platforms.

V C. Bandwidth engine

Imagine eliminating the scaling factor $Q\big(h(\alpha_t)\big)$ from the Hamiltonian (24). The energy band is compressed and expanded as the disorder strength $h(\alpha_t)$ is ramped down and up. The whole band, rather than a gap, contracts and widens as in Fig. 2, between a size $\sim \mathcal{E} N_{\rm macro}\, h(\alpha_0)$ and a size $\sim \mathcal{E} N_{\rm macro}\, h(\alpha_1) \gg \mathcal{E} N_{\rm macro}\, h(\alpha_0)$. The engine can remain in one phase throughout the cycle. The cycle does not benefit from the "athermality" of local level correlations.

Furthermore, this accordion-like motion requires no change of the energy eigenbasis's form. The engine therefore does not "jump" diabatically, $\langle W_{\rm diab} \rangle_{\rm macro} = 0$, if the tuning proceeds quantum-adiabatically, $v \approx 0$.

But this engine is impractical: Consider any perturbation V that fails to commute with the ideal Hamiltonian $H(t)$: $[V, H(t)] \neq 0$. Stray fields, for example, can taint an environment. As another example, consider cold atoms in an optical lattice. One can raise the disorder strength [ideally $\mathcal{E} h(\alpha_t)$] by strengthening the lattice potential $U_{\rm lattice}$. One can raise the hopping frequency (ideally $\mathcal{E}$) by raising the pressure p. Strengthening $U_{\rm lattice}$ and the pressure p while achieving the ideal disorder-to-hopping ratio $\frac{\mathcal{E} h(\alpha_t)}{\mathcal{E}} = h(\alpha_t)$ requires fine control. If the ratio changes from $h(\alpha_t)$, the Hamiltonian $H(t)$ acquires a perturbation V that fails to commute with other terms. This V can cause diabatic jumps that cost work $\langle W_{\rm diab} \rangle_{\rm macro}$. Jumps suppress the scaling of the average work outputted per cycle by a factor of $\sqrt{N_{\rm macro}}$, we estimate in App. L 1. The MBL Otto engine may scale more robustly: The net work extracted scales as $N_{\rm macro}$ [Eq. (14)]. Furthermore, diabatic jumps cost work $\langle W_{\rm diab} \rangle_{\rm macro}$ suppressed small parameters such as $\frac{\sqrt{v}}{\langle \delta \rangle}$.

V D. Engine tuned between equally localizing disorder realizations

Consider tuning a quantum many-body system not between shallowly and deeply localized MBL regimes, but between equal-disorder-strength disorder realizations. The disorder strength $h(\alpha_t)$ in Eq. (24) would remain $\gg 1$ and constant in t, while the random variables h_j would change. Let $\tilde{S}$ denote this constant-$h(\alpha_t)$ engine, and let S denote the MBL engine. $\tilde{S}$ takes less advantage of MBL's "athermality," as $\tilde{S}$ is not tuned between level-repelling and level-repulsion-free regimes.

Yet $\tilde{S}$ outputs the amount $\langle W_{\rm tot} \rangle$ of work outputted by S per cycle, on average. Because $W_{\rm b}$ is small, cold thermalization drops $\tilde{S}$ across only small gaps $\delta' \ll \langle \delta \rangle$. $\tilde{S}$ traverses a trapezoid, as in Fig. 2, in each trial. However, the MBL engine has two advantages: greater reliability and fewer worst-case (negative-work-outputted) trials.

The work $W_{\rm tot}$ outputted by $\tilde{S}$ fluctuates more, from trial to trial, than the $W_{\rm tot}$ outputted by S. Both the left-hand gap δ and the right-hand gap δ' traversed by $\tilde{S}$ are Poisson-distributed. Poisson-distributed gaps more likely assume extreme values than GOE-distributed gaps: $P^{(E)}_{\rm MBL}(\delta) > P^{(E)}_{\rm GOE}(\delta)$ if $\delta \sim 0$ or $\delta \gg \langle \delta \rangle$ [45]. The left-hand gap δ traversed by S is GOE-distributed. Hence the $W_{\rm tot}$ outputted by $\tilde{S}$ more likely assumes extreme values than the $W_{\rm tot}$ outputted by S. The greater reliability of S may suit S better to "one-shot statistical mechanics" [8, 9, 11, 12, 14, 15, 76–81]. In one-shot theory, predictability of the work $W_{\rm tot}$ extractable in any given trial serves as a resource.

In addition to operating more reliably, the MBL engine suffers fewer worst-case trials. We define as *worst-case* a trial in which the engine outputs net negative work, $W_{\rm tot} < 0$. Consider again Fig. 2. Consider a similar figure that depicts the trapezoid traversed by $\tilde{S}$ in some trial. The left-hand gap, δ, is distributed as the right-hand gap, δ', is, according to $P^{(E)}_{\rm MBL}(\delta)$. Hence δ has a decent chance of being smaller than δ': $\delta < \delta'$. $\tilde{S}$ would output $W_{\rm tot} < 0$ in such a trial.

We estimate worst-case trials' probabilities in App. L 2. Each trial undergone by one constant-$h(\alpha_t)$ subengine has a probability $\sim \left(\frac{W_{\rm b}}{\langle \delta \rangle} \right)^2$ of yielding $W_{\rm tot} < 0$. An MBL subengine has a worst-case probability one order of magnitude lower: $\sim \left(\frac{W_{\rm b}}{\langle \delta \rangle} \right)^3$. Hence the constant-$h(\alpha_t)$ engine illustrates that local MBL level correlations' athermality suppresses worst-case trials and enhances reliability.

VI. OUTLOOK

The realization of thermodynamic cycles with quantum many-body systems was proposed recently [27, 29, 30, 82–84]. MBL offers a natural platform, due to its "athermality" and to athermality's resourcefulness in thermodynamics. We have formulated an Otto engine that benefits from the discrepancy between many-body-localized and "thermal" level statistics. The engine illustrates how MBL can be used for thermodynamic advantage.

Realizing the engine may provide a near-term challenge for existing experimental set-ups. Possible platforms include cold atoms [2, 36, 38, 39, 42]; nitrogen-vacancy centers [40]; ion traps [41]; and doped semiconductors [43], for which we provided order-of-magnitude estimates. Realizations will require platform-dependent corrections due to, e.g., variable-range hopping induced by particle-phonon interactions. As another example,

semiconductors' impurities suffer from dipolar interactions. The interactions extend particles' wave functions from decaying exponentially across space to decaying as power laws.

Reversing the engine may pump heat from the cold bath to the hot, lowering the cold bath's temperature. Low temperatures facilitate quantum computation and low-temperature experiments. An MBL engine cycle might facilitate state preparation and coherence preservation in quantum many-body experiments.

Experiments motivate explicit modeling of the battery. We have defined as work the energy outputted during Hamiltonian tunings. Some work-storage device, or battery, must store this energy. We have refrained from specifying the battery's physical form, using an *implicit battery model*. An equivalent *explicit battery model* could depend on the experimental platform. Quantum-thermodynamics batteries have been modeled abstractly with ladder-like Hamiltonians [85]. An oscillator battery for our engine could manifest as a cavity mode.

MBL is expected to have thermodynamic applications beyond this Otto engine. A localized ratchet, which leverages information to transform heat into work, is under investigation. The paucity of transport in MBL may have technological applications beyond thermodynamics. Dielectrics, for example, prevent particles from flowing in certain directions. Dielectrics break down in strong fields. To survive, a dielectric must insulate well—as does MBL.

In addition to suggesting applications of MBL, this work identifies an opportunity within quantum thermodynamics. Nonequilibrium quantum states (e.g., $\rho \neq e^{-H/T}/Z$) are usually regarded as resources in quantum thermodynamics [7, 8, 10, 11, 13–18, 86–89]. Not only states, we have argued, but also energy-level statistics, offer thermodynamic advantages. Generalizing the quantum-thermodynamics definition of "thermodynamic resource" may expand the set of goals that thermodynamic agents can achieve.

Shortcuts to adiabaticity (STA) [20, 50, 90–92] offer another theoretical opportunity. The engine's Hamiltonian must be tuned slowly, to preclude diabatic transitions that cost work. Exponentially slow tuning has been avoided, outside of MBL contexts, with shortcuts to adiabaticity (STA) [20, 50, 90–92]. STA reduce the tuning time but reproduce the final state's populations (and, in some cases, coherences). STA have been used to reduce other quantum engines' cycle times [20, 50, 92]. STA might be applied to the many-body Otto cycle. To assess how, one must first incorporate STA into the field of MBL in general.

ACKNOWLEDGEMENTS

This research was supported by NSF grant PHY-0803371. The Institute for Quantum Information and Matter (IQIM) is an NSF Physics Frontiers Center supported by the Gordon and Betty Moore Foundation. NYH is grateful for partial support from the Walter Burke Institute for Theoretical Physics at Caltech. This material is based on work supported by the National Science Foundation Graduate Research Fellowship under Grant No. DGE-1144469. SG acknowledges support from the Walter Burke Foundation and from the NSF under Grant No. DMR-1653271.. GR acknowledges support from the Packard Foundation. NYH thanks Nana Liu for discussing entropy and heat and Álvaro Martín Alhambra for discussing probabilistic SWAPs.

Supplemental Material

CONTENTS

I. Thermodynamic background 2

II. Introducing the MBL Otto cycle 3
II A. Qubit toy model 3
II B. Level-statistics engine for a mesoscale system 4
II B 1. Set-up for the mesoscale MBL engine 4
II B 2. Qualitative analysis of the mesoscale engine 5
II B 3. Quantitative analysis of the mesoscale engine 6
II B 4. Diabatic corrections to the per-cycle power 6
II C. From the mesoscale MBL Otto engine to the thermodynamic limit 8
II C 1. Local level correlations 8
II C 2. Application of local level correlations in the macroscopic MBL engine 9
II C 3. Time scales of the macroscopic MBL engine 9

III. Numerical simulations 10

IV. Order-of-magnitude estimates 12

V. Comparisons with competitor engines 12
V A. Ideal-gas Otto engine 13
V B. Quantum-dot engine 13
V C. Bandwidth engine 14
V D. Engine tuned between equally localizing disorder realizations 14

VI. Outlook 14

Acknowledgements 15

Appendix A. Review of the thermodynamic and quantum Otto cycles 18
A 1. Form of the Otto cycle 18
A 2. Ideal efficiency η_{Otto} of the thermodynamic Otto cycle 19
A 3. Upper bound on the Otto efficiency by the Carnot efficiency: $\eta_{\text{Otto}} < \eta_{\text{Carnot}}$ 19

Appendix B. Work and heat in quantum thermodynamics 20

Appendix C. Qubit toy model for the MBL Otto engine 20
C 1. Formulation of the qubit model for the MBL Otto engine 20
C 2. Efficiency of the qubit model for the MBL Otto engine 22
C 2 i. Analysis of the efficiency η_{qubit} of the qubit model for the MBL Otto engine 22
C 2 ii. Calculation of the efficiency η_{qubit} of the qubit model for the MBL Otto engine 22
C 2 iii. The qubit model for the MBL Otto engine shares an ideal-gas Otto engine's efficiency: $\eta_{\text{qubit}} = \eta_{\text{Otto}}$. 25
C 2 iv. Upper bound on the qubit model's ideal efficiency by the Carnot efficiency: $\eta_{\text{qubit}} < \eta_{\text{Carnot}}$ 25
C 3. Numerical simulations of the qubit model for the MBL Otto engine 26

Appendix D. Statistical properties of MBL and GOE energy spectra 27
D 1. Density of states 27
D 2. Average gaps 27
D 3. Gaussian statistics of ETH energy spectra 28
D 4. Poisson statistics of MBL energy spectra 28

Appendix E. Two-qubit model for a "working gap" of the MBL Otto engine 29

Appendix F. Conservation of particle number 29

Appendix G. Quantitative assessment of the mesoscopic MBL Otto engine 30
G 1. Notation 30
G 2. Small parameters 31
G 3. Partial-swap model of thermalization 31
G 4. Average heat $\langle Q_2 \rangle$ absorbed during stroke 2 32
G 4 i. Heat absorbed during one trial 32
G 4 ii. Averages with respect to cold-thermalization probabilities and gap distributions 32
G 4 iii. Thermal average with respect to the initial density operator 35
G 5. Average heat $\langle Q_4 \rangle$ absorbed during stroke 4 36
G 5 i. Exact expression for $\langle Q_4 \rangle$ 37
G 5 ii. Contribution to $\langle Q_4 \rangle$ from chains of exactly $n = 1$ small gap 39
G 5 iii. Contribution $\langle Q_4^{n=2} \rangle$ to $\langle Q_4 \rangle$ from chains of exactly $n = 2$ small gaps 42
G 5 iv. Assembling the leading-order ($n = 1, 2$) contributions to $\langle Q_4 \rangle$ 46
G 6. Per-cycle power $\langle W_{\rm tot} \rangle$ 46
G 7. Efficiency $\eta_{\rm MBL}$ in the adiabatic approximation 47
G 8. Diabatic corrections 48
G 8 i. Average work costs of APT transitions in the ETH phase: $\langle W_{\rm APT,1} \rangle$ and $\langle W_{\rm APT,3} \rangle$ 49
G 8 ii. Average work costs of Landau-Zener diabatic jumps: $\langle W_{\rm LZ,1} \rangle$ and $\langle W_{\rm LZ,3} \rangle$ 53
G 8 iii. Average work costs of fractional-Landau-Zener diabatic jumps: $\langle W_{\rm frac-LZ,1} \rangle$ and $\langle W_{\rm frac-LZ,3} \rangle$ 53
G 8 iv. Diabatic correction to the efficiency $\eta_{\rm MBL}$ 56

Appendix H. Phenomenological model for the MBL Otto engine 57
H 1. Anderson-localized Hamiltonians 58
H 2. Single-particle localization length $\xi_{\rm And}$ 58
H 3. Local level repulsion in Anderson insulators 59
H 4. Generalization to many-body localization 59
H 5. Application of local level repulsion to the MBL Otto engine in the thermodynamic limit 60

Appendix I. Model for cold thermalization 61
I 1. Parameterization of cold thermalization 61
I 2. Example form for the interaction between the engine and the cold bath 61
I 3. Deriving an expression for the thermalization time $\tau_{\rm th}$ 62
I 4. Constraint 1 on cold thermalization: Markovianity 62
I 5. Constraint 2 on cold thermalization: Suppression of high-order-in-the-coupling energy exchanges 63

Appendix J. Optimization of the MBL Otto engine 64
J 1. Bounds on the Hamiltonian-tuning speed v 64
J 2. Time $\tau_{\rm cycle}$ required to implement a cycle 69
J 3. Bounds on the cold-bath bandwidth $W_{\rm b}$ 70

Appendix K. Numerical simulations of the MBL Otto engine 70
K 1. Scaling factor 71
K 2. Representing states and Hamiltonians 73
K 3. Strokes 1 and 3: Adiabatic evolution 73
K 4. Stroke 2: Thermalization with the cold bath 74

Appendix L. Comparison with competitor Otto engines: Details and extensions 75
L 1. Details: Comparison with a bandwidth engine 75
L 2. Details: Comparison with an MBL engine tuned between same-strength disorder realizations 75
L 3. Comparison with an MBL Otto engine whose cold bath has an ordinary bandwidth 76
L 4. Comparison with an Anderson-localized engine 77

References 77

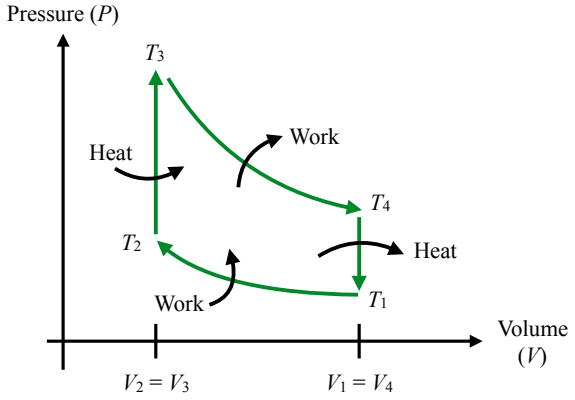

FIG. 5: Thermodynamic Otto cycle: The thermodynamic cycle's four main strokes, paralleled by strokes in the MBL Otto cycle, are sketched in green. The left-hand and right-hand green vertical lines represent isochores. The curved lines represent isentropes. Labels are as in, e.g., [47].

Appendix A REVIEW OF THE THERMODYNAMIC AND QUANTUM OTTO CYCLES

The classical thermodynamic Otto engine consists of a gas whose volume V and temperature T are varied [47]. A simple quantum Otto engine consists of a qubit (a two-level quantum system) whose gap Δ and temperature T are varied [46]. The Otto cycle involves two isentropic strokes and two isochoric strokes. We review the cycle's steps and efficiency.

A 1 Form of the Otto cycle

The Otto cycle involves two isentropes and two isochores. "Isentropic" means "constant-entropy," and "isochoric" means "constant-volume." In the quantum cycle, the gap Δ plays the role of the classical engine's volume. Figure 5 depicts the strokes, detailed below. The description begins with the lower right-hand corner of the shape formed from the green arrows.

1. *Isentropic compression*: The engine begins in thermal equilibrium with a heat bath at a temperature $T_1 \equiv T_{\rm C}$. The engine is thermally isolated at the start of stroke 1. If the engine is classical, its pressure p is increased. Its temperature T rises from T_1 to T_2. If the engine is quantum, its gap Δ is widened. The (classical or quantum) engine performs a negative amount of work: $W_{\rm compress} < 0$.

2. *Hot isochore ("combustion")*: The engine equilibrates with a hot bath at temperature $T_3 \equiv T_{\rm H} > T_{\rm C} \equiv T_1$. Net positive heat enters the engine: $Q_{\rm in} > 0$.

3. *Isentropic expansion*: The engine is thermally isolated. If the engine is classical, its pressure p is lowered. Its temperature T drops from T_3 to T_4. If the engine is quantum, its gap Δ is shrunk. The (classical or quantum) engine performs a positive amount of work: $W_{\rm expand} > 0$.

4. *Cold isochore (heat rejection)*: The engine equilibrates with a cold bath at temperature T_1. Net negative heat enters the system.

A 2 Ideal efficiency $\eta_{\rm Otto}$ of the thermodynamic Otto cycle

We follow the derivation in [47]. By definition, the ideal efficiency is

$$\eta_{\rm Otto} = \frac{\text{Net work out}}{\text{Positive heat in}} = \frac{\text{Net heat in}}{\text{Positive heat in}} \tag{A1}$$

$$= \frac{(Q \text{ absorbed during heating}) + (Q \text{ absorbed during cooling})}{Q \text{ absorbed during heating}} \tag{A2}$$

$$= 1 - \frac{Q \text{ expelled during cooling}}{Q \text{ absorbed during heating}} = 1 - \frac{C_{\rm v}(T_4 - T_1)}{C_{\rm v}(T_3 - T_2)} \tag{A3}$$

$$= 1 - \frac{T_4 - T_1}{T_3 - T_2} \, . \tag{A4}$$

The second equality follows from the first law of thermodynamics. The Q's denote heat quantities. $C_{\rm v}$ denotes the specific heat at constant volume.

Let us replace the temperatures with the compression ratio $r := \frac{V_1}{V_2}$. An isentrope connects the point (T_4, $V_4 = V_1$) with (T_3, $V_3 = V_2$), and an isentrope connects (T_1, V_1) with (T_2, V_2). Along every isentrope, $TV^{\gamma - 1} = \text{const}$. The $\gamma := \frac{C_{\rm P}}{C_{\rm v}}$ denotes a ratio of the constant-pressure and constant-volume specific heats. Hence $T_4 (V_1)^{\gamma - 1} = T_3 (V_2)^{\gamma - 1}$, and $T_1 (V_1)^{\gamma - 1} = T_2 (V_2)^{\gamma - 1}$. Subtracting the second equation from the first yields $(T_4 - T_1)(V_1)^{\gamma - 1} = (T_3 - T_2)(V_2)^{\gamma - 1}$. We solve for $T_3 - T_2$, substitute into Eq. (A4), and simplify. Invoking $r := \frac{V_1}{V_2}$ yields

$$\eta_{\rm Otto} = 1 - r^{1 - \gamma} \, . \tag{A5}$$

This expression behaves as expected. According to Fig. 5, $r > 1$. The specific heats are related by $C_{\rm P} = C_{\rm v} + R > C_{\rm v}$, wherein R denotes the universal gas constant. Hence $1 - \gamma < 0$. The correction $r^{1 - \gamma} < 1$: The efficiency lies between 0 and 1.

A 3 Upper bound on the Otto efficiency by the Carnot efficiency: $\eta_{\rm Otto} < \eta_{\rm Carnot}$

The Carnot efficiency upper-bounds the Otto efficiency strictly [47]:

$$\eta_{\rm Otto} < \eta_{\rm Carnot} = 1 - \frac{T_{\rm C}}{T_{\rm H}} \equiv 1 - \frac{T_1}{T_3} \, . \tag{A6}$$

Let us prove (A6).

We return to Eq. (A4). We factor T_1 out of the numerator and T_2 out of the denominator:

$$\eta_{\rm Otto} = 1 - \frac{\left(\frac{T_4}{T_1} - 1 \right) T_1}{\left(\frac{T_3}{T_2} - 1 \right) T_2} \, . \tag{A7}$$

Let us prove that the parenthesized factors cancel.

A thermodynamic Otto engine consists of an ideal gas. Let T and V denote the gas's temperature and volume. The T's and V's associated with different points in the cycle appear in Fig. 5. An isochore connects T_4 with T_1, and an isochore connects T_2 with T_3. Hence $V_4 = V_1$, and $V_2 = V_3$. Let us multiply the $\frac{T_4}{T_1}$ in Eq. (A7) by $1 = \frac{V_1^a}{V_1^a} = \frac{V_4^a}{V_1^a}$, wherein $a \in \mathbb{R}$. Multiplying the $\frac{T_3}{T_2}$ by $\frac{V_3^a}{V_2^a}$ yields

$$\eta_{\rm Otto} = 1 - \frac{\left(\frac{T_4 \, V_4^a}{T_1 \, V_1^a} - 1 \right) T_1}{\left(\frac{T_3 \, V_3^a}{T_2 \, V_2^a} - 1 \right) T_2} \, . \tag{A8}$$

An isentrope links T_3 with T_4, and an isentrope links T_1 with T_2. Each isentrope satisfies $T \, V^{\Gamma - 1} = b \in \mathbb{R}$, wherein Γ denotes a constant dictated by the gas's constituents (e.g., monoatomic or diatomic molecules). The relation derives from the first law of thermodynamics, the ideal gas law, and the classical equipartition theorem. Substituting into Eq. (A8) yields

$$\eta_{\rm Otto} = 1 - \frac{\left(\frac{b_{34}}{b_{12}} - 1 \right) T_1}{\left(\frac{b_{34}}{b_{12}} - 1 \right) T_2} = 1 - \frac{T_1}{T_2} \, . \tag{A9}$$

We have collapsed the four-temperature dependence of $\eta_{\rm Otto}$ to a dependence on two temperatures. $\eta_{\rm Carnot}$ depends on two other temperatures, on the T_j's to which the engine equilibrates upon thermalizing with the baths. These temperatures are T_1 and T_3, according to Fig. 5. Hence $\eta_{\rm Carnot} = 1 - \frac{T_1}{T_3} > 1 - \frac{T_1}{T_2} = \eta_{\rm Otto}$.

Appendix B WORK AND HEAT IN QUANTUM THERMODYNAMICS

We define work and heat as in many quantum-thermodynamics settings [46]. Let $\rho(t)$ denote the time-t state of a quantum system governed by a Hamiltonian $H(t)$. The system's internal energy is

$$E(t) := {\rm Tr}\big(\rho(t)\, H(t)\big) \,. \tag{B1}$$

The energy changes at a rate determined by two contributions: $\frac{dE(t)}{dt} = {\rm Tr}\left(H(t)\, \frac{d\rho(t)}{dt}\right) + {\rm Tr}\left(\frac{dH(t)}{dt}\, \rho(t)\right)$. Consider integrating over a time interval τ. During the interval, the system's energy increases by an amount

$$\Delta E = \int_0^\tau dt\, {\rm Tr}\left(H(t)\, \frac{d\rho(t)}{dt}\right) + \int_0^\tau dt\, {\rm Tr}\left(\frac{dH(t)}{dt}\, \rho(t)\right) . \tag{B2}$$

The first term signifies heat. The term contains a derivative of the density operator $\rho(t)$, the quantum analog of the classical phase-space distribution. A system's phase-space distribution approaches the canonical ensemble as a system exchanges heat with a bath. Just as heat corresponds to the change of a phase-space distribution in classical statistical mechanics, heat corresponds to a change of a density operator in many quantum-thermodynamics settings.

The density operator's statistical nature, too, suggests a connection between $\frac{d\rho(t)}{dt}$ and heat. Heat is unreliable energy. We cannot harness heat to perform useful work, in the absence of information [93]. Similarly, the density operator $\rho(t)$ encodes unreliability: Measuring $H(t)$ yields one of many possible energies, whose probabilities $\rho(t)$ encodes [if $\rho(t)$ is not a pure energy eigenstate, e.g., if $\rho(t)$ is a canonical ensemble and if $H(t)$ is not totally degenerate]. The energy exchanged by the MBL Otto engine during strokes 2 and 4 is heat.

The second term in Eq. (B2) signifies work. The derivative $\frac{dH(t)}{dt}$ is nonzero if the Hamiltonian is driven. For example, a magnetic field $\mathbf{B}(t)$ may be strengthened. Driving involves drawing energy from a "clean" (low-entropy) energy-storage system, or battery. Such "pristine" energy is work. For example, suppose that the system consists of a qubit. Ramping up $\mathbf{B}(t)$ may change the spin's orientation. Wrestling the spin toward a new direction costs work.

According to this definition, the energy exchanged by the MBL Otto engine during Hamiltonian tunings is work. The physical reason is that the engine interacts with no heat bath [94, 95]. The mathematical reason stems from Schrödinger's Equation, which implies that $\frac{d\rho(t)}{dt} = i[\rho(t),\, H(t)]$ in the absence of interactions with an environment. Consider substituting into the first trace in Eq. (B2): ${\rm Tr}\big(H(t)\, \frac{d\rho(t)}{dt}\big) = i\, {\rm Tr}\big(H(t)\, [\rho(t)\, H(t) - H(t)\, \rho(t)]\big)$. The terms equal each other, by the trace's cyclicality. The heat integral in Eq. (B2) vanishes. The energy change ΔE must constitute work, according to this line of reasoning. In contrast with some quantum-thermodynamics literature, condensed-matter literature often casts as heat energy absorbed during unitary evolutions [53–55]. These two perspectives are compared in [45].

Appendix C QUBIT TOY MODEL FOR THE MBL OTTO ENGINE

A qubit model illustrates a role played by level statistics in the MBL Otto cycle. The qubit models two neighboring energy eigenstates in the MBL engine's many-body spectrum. We first introduce the qubit's Hamiltonian, $H_{\rm qubit}(t)$. We calculate the engine's efficiency, $\eta_{\rm qubit}$, assuming that $H_{\rm qubit}(t)$ is tuned adiabatically. For each choice of qubit parameters, we show, there exist ideal-gas parameters such that the ideal-gas Otto engine's efficiency equals the qubit model's: $\eta_{\rm qubit} = \eta_{\rm Otto}$. The Carnot efficiency $\eta_{\rm Carnot}$ is shown to upper-bound $\eta_{\rm qubit}$, via two arguments. Numerical simulations support the analytic results.

C 1 Formulation of the qubit model for the MBL Otto engine

Figure 6 illustrates the qubit cycle. Let $|E_t^{(1)}\rangle$ and $|E_t^{(2)}\rangle$ denote the eigenstates at time t. The energies are assumed, without loss of generality, to satisfy $E_t^{(1)} < E_t^{(2)}$. A third energy, $E_t^{(3)}$, appears at the top of the figure. This spectator, we show, can be ignored.

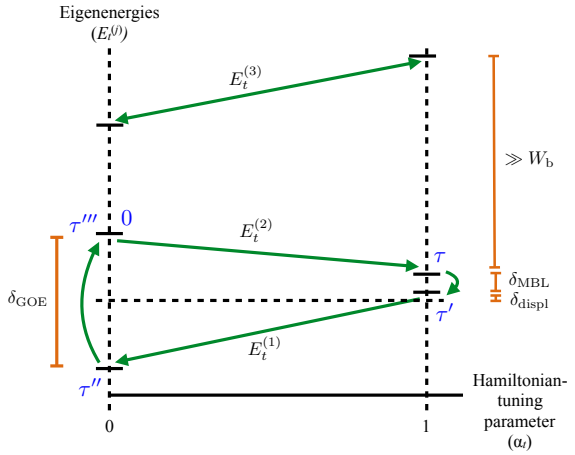

FIG. 6: Qubit toy model for the MBL Otto cycle: A qubit models two "working levels" in the MBL Otto engine's many-body spectrum. The energy eigenstates $|E_t^{(1)}\rangle$ and $|E_t^{(2)}\rangle$ span the "working subspace." The gap $E_t^{(2)} - E_t^{(1)}$ begins at size δ_GOE during a successful trial. The gap shrinks to δ_MBL, then returns to δ_GOE. In addition to changing the gap, each Hamiltonian tuning changes the eigenstates' functional forms. The displacement δ_displ is included for generality. The blue text marks the times $t = 0, \tau, \ldots, \tau'''$ at which the strokes begin and end during a work-outputting trial. The spectator level $|E_t^{(3)}\rangle$ fails to impact the engine's efficiency. The cold bath has too narrow a bandwidth W_b to couple $|E_t^{(3)}\rangle$ to any other level. If the engine begins any trial on the top green line, the engine remains on that line throughout the trial. Zero net work is outputted.

The qubit evolves under the Hamiltonian

$$H_\mathrm{qubit}(t) = (1 - \alpha_t)\frac{\delta_\mathrm{GOE}}{2}\,\sigma^x + \alpha_t\,\frac{\delta_\mathrm{MBL}}{2}\,\sigma^z + \frac{\delta_\mathrm{displ}}{2}\,f(\alpha_t)\,\mathbb{1}\,. \tag{C1}$$

The $\frac{\delta_\mathrm{MBL}}{2}\,\sigma^z$ parallels the disorder term $h(\alpha_t)\cdot h_j\sigma_j^z$ in the many-body $H_\mathrm{sim}(t)$ [Eq. (24)]. The Pauli-z eigenbasis $\{|z+\rangle, |z-\rangle\}$ plays the role of the MBL Hamiltonian's eigenbasis, which nearly coincides with the many-body position eigenbasis. The GOE-like component $\frac{\delta_\mathrm{GOE}}{2}\,\sigma^x$ has eigenstates $|x+\rangle := \frac{1}{\sqrt{2}}(|z+\rangle + |z-\rangle)$ and $|x-\rangle := \frac{1}{\sqrt{2}}(|z+\rangle - |z-\rangle)$. These states are nontrivial superpositions of σ^z eigenstates, just as the H_GOE eigenstates are nontrivial superpositions of (near-)position eigenstates.

The GOE-like gap exceeds the MBL-like gap: $\delta_\mathrm{GOE} > \delta_\mathrm{MBL}$. This condition reflects the greater frequency with which small gaps (like δ_MBL) appear in the mesoscale engine's MBL spectrum than in the GOE spectrum. δ_GOE parallels the mesoscale engine's $\langle\delta\rangle$.

The offset δ_displ is included for generality but does not affect the physics. δ_displ denotes the displacement, above zero, of the midpoint between the MBL-like energies: $\delta_\mathrm{displ} := \frac{1}{2}\left(E_\tau^{(2)} - E_\tau^{(1)}\right)$. The function

$$f(\alpha_t) = \begin{cases} 0, & \alpha_t = 0 \\ 1, & \alpha_t = 1 \\ f(\alpha_t) \in [0,\,1], & \text{otherwise} \end{cases} \tag{C2}$$

"turns on" the displacement as the system transitions from GOE-like to MBL-like. If the GOE-like-to-MBL-like tuning turns the displacement off, the δ_displ term must be negated. The δ_displ term is expected to average to zero across trials implemented with an ideal many-body system.

The tuning parameter $\alpha_t \in [0, 1]$ is defined as in Sec. II A. The qubit is tuned and thermalized as in Sec. II A. Each Hamiltonian tuning changes the gap and changes the energy eigenstates' forms. Here, similarly to in the mesoscale-engine cycle, the cold bath's bandwidth satisfies $W_\mathrm{b} \in (\delta_\mathrm{MBL}, \delta_\mathrm{GOE})$.

A spectator level $E_t^{(3)}|E_t^{(3)}\rangle\langle E_t^{(3)}|$ can be added to $H_\mathrm{qubit}(t)$, as suggested by Fig. 6. The spectator fails to influence the engine's efficiency: Consider a trial that the engine begins in $|E_t^{(3)}\rangle$. After stroke 1, a gap larger than the cold-bath bandwidth W_b separates $E_\tau^{(3)}$ from $E_\tau^{(2)}$. The cold bath cannot couple the spectator to any other level. Stroke 3 "undoes" stroke 1: $W_3 = -W_1$. The engine outputs zero net work. Subsequent hot thermalization can bump the engine to a lower level. Such a bump would cost negative heat: $Q_4 < 0$. But consider averaging Q_4 over trials. One

trial's $Q_4 < 0$ would cancel with the heat that the engine had absorbed, in an earlier trial, in rising to $|E^{(3)}_{\tau'''}\rangle$. So $|E^{(3)}_t\rangle$ contributes nothing to $\langle Q_4 \rangle$. The spectator lowers the engine's power, however.

C 2 Efficiency of the qubit model for the MBL Otto engine

We focus on the quantum-adiabatic limit in which $H_{\rm qubit}(t)$ is tuned infinitely slowly. First, we present and analyze a formula for $\eta_{\rm qubit}$. We then derive the formula. For each choice of qubit parameters, we show, there exists a choice of ideal-gas parameters such that an ideal-gas Otto engine's efficiency equals the qubit model's: $\eta_{\rm qubit} = \eta_{\rm Otto}$. This equation and a derived condition independently upper-bound $\eta_{\rm qubit}$ with the Carnot efficiency: $\eta_{\rm qubit} < \eta_{\rm Carnot}$.

C 2 i Analysis of the efficiency $\eta_{\rm qubit}$ of the qubit model for the MBL Otto engine

The qubit engine's efficiency follows from calculating the average work and heat exchanged, then substituting into $\eta_{\rm qubit} := \langle W_{\rm tot} \rangle \,/\, \langle Q_{\rm in} \rangle$ (we justify this definition in App. G 7):

$$\eta_{\rm qubit} = \begin{cases} 1 - \frac{\delta_{\rm MBL}}{\delta_{\rm GOE}} \,, & \beta_{\rm H}\, \delta_{\rm GOE} < \beta_{\rm C}\, \delta_{\rm MBL} \\ 1 - \frac{\delta_{\rm GOE}}{\delta_{\rm MBL}} \,, & \beta_{\rm H}\, \delta_{\rm GOE} > \beta_{\rm C}\, \delta_{\rm MBL} \,. \end{cases} \tag{C3}$$

The efficiency is positive in the first case and negative in the second. The condition

$$\beta_{\rm H}\, \delta_{\rm GOE} < \beta_{\rm C}\, \delta_{\rm MBL} \tag{C4}$$

ensures that the engine more likely traverses the trapezoid in Fig. 6 clockwise than counterclockwise. During a clockwise traversal, strokes 1 and 3 output net positive work: The engine slides down green solid lines. Downward sliding accompanies a decrease in energy, which leaves the engine as work. Throughout the rest of this subsection, we assume that the engine satisfies condition C4.

$\eta_{\rm qubit}$ depends on the gap ratio $\delta_{\rm MBL}/\delta_{\rm GOE}$ as $\eta_{\rm Otto}$ depends on the temperature ratio T_1/T_2 in Eq. (A9). The inverse temperatures $\beta_{\rm H}$ and $\beta_{\rm C}$ do not affect $\eta_{\rm qubit}$. They affect the power, as shown in the following two examples.

First, suppose that the hot bath is lukewarm: $T_{\rm H} \gtrsim T_{\rm C}$. Consider one trial. The temperature-$T_{\rm H}$ Gibbs distribution gives the engine a high probability of starting in the ground state, $|E^{(1)}_0\rangle$. The engine likely starts, in Fig. 6, on the left-hand side of the bottom green, sloping line. The engine slides rightward, up that line, during stroke 1. Cold thermalization likely keeps the engine in its ground state. Stroke 3 "undoes" stroke 1: $W_3 = -W_1$. The engine retraces its steps along the bottom green line. The engine outputs zero net work: $W_{\rm tot} = W_1 + W_3 = 0$. The average-over-trials power is therefore low when $T_{\rm H} \gtrsim T_{\rm C}$.

For a second example, recall that negative temperatures invert populations: If $T < 0$, the greater an energy E_j, the higher the weight $e^{-E_j/T}/Z$ of a temperature-T Gibbs state on level j. The qubit engine's power is therefore greatest when $T_{\rm H} < 0$ and $T_{\rm C} = 0$. The Gibbs distribution gives the engine a high probability of starting any given trial in the excited state $|E^{(2)}_0\rangle$. Stroke 1 outputs positive work: $W_1 > 0$. Cold thermalization likely drops the engine to its ground state. If the engine drops, stroke 3 outputs positive work: $W_3 > 0$. The work per cycle maximizes: $W_{\rm tot} > 0$. A scalding hot bath and a chilly cold bath optimize the power.

C 2 ii Calculation of the efficiency $\eta_{\rm qubit}$ of the qubit model for the MBL Otto engine

We introduce notation, then calculate the energy expectation value $E(t) := {\rm Tr}\big(H_{\rm qubit}(t)\, \rho(t)\big)$. We evaluate $E(t)$ at each endpoint of each stroke—at $t = 0, \tau, \tau', \tau''$, and τ'''. Subtracting the $E(t)$-values with which the system begins and ends a stroke yields the average work outputted, or the average heat absorbed, during the stroke. We substitute the work and heat quantities into the definition of an engine's efficiency,

$$\eta := \frac{\langle W_{\rm tot} \rangle}{\langle Q_{\rm in} \rangle} \,. \tag{C5}$$

Notation: We eigendecompose the Hamiltonian [Eq. (C1)] as

$$H_{\rm qubit}(t) = (1 - \alpha_t) \frac{\delta_{\rm GOE}}{2}\, \sigma^x + \alpha_t\, \frac{\delta_{\rm MBL}}{2}\, \sigma^z + \frac{\delta_{\rm displ}}{2}\, f(\alpha_t)\, \mathbb{1} \equiv \sum_{\ell=1}^{2} E^{(\ell)}_t |E^{(\ell)}_t\rangle\langle E^{(\ell)}_t| \,. \tag{C6}$$

The lesser the index ℓ, the lower the energy: $E_t^{(1)} < E_t^{(2)}$. The engine's state remains diagonal relative to the energy eigenbasis at all times:

$$\rho(t) = \sum_{\ell=1}^{2} \rho_t^{(\ell)} |E_t^{(\ell)}\rangle\langle E_t^{(\ell)}| \,. \tag{C7}$$

The quantum adiabatic theorem guarantees that $\rho(t)$ shares the $H_{\rm qubit}(t)$ eigenbasis throughout the tunings. $\rho(t)$ shares the $H_{\rm qubit}(t)$ eigenbasis during thermalization because thermalization changes only populations. The populations have the Gibbs form

$$\rho_t^{(\ell)} := \frac{1}{Z_{\tilde{t}}} \, e^{-\beta_{\tilde{t}} E_{\tilde{t}}^{(\ell)}} \,. \tag{C8}$$

The label $\tilde{t}$ equals t if a thermalization ends at time t. If a Hamiltonian tuning ends at t, $\tilde{t} < t$. The tuning changes the energies from $E_{\tilde{t}}^{(\ell)}$ to $E_t^{(\ell)}$ while preserving the populations. Those populations are determined by the earlier energies, $E_{\tilde{t}}^{(\ell)}$, and the inverse earlier temperature, $\beta_{\tilde{t}}$.

Calculation of the energy $E(t)$ at an arbitrary time t: Let us substitute from Eqs. (C6) and (C7) into the definition of $E(t)$, Eq. (B1):

$$E(t) = \sum_{\ell=1}^{2} \rho_t^{(\ell)} \, E_t^{(\ell)} \,. \tag{C9}$$

The eigenenergies follow from the middle expression in Eq. (C6):

$$E_t^{(1)} = \frac{1}{2} \left[\delta_{\rm displ} \, f(\alpha_t) - \Delta(t) \right] , \qquad \text{and} \qquad E_t^{(2)} = \frac{1}{2} \left[\delta_{\rm displ} \, f(\alpha_t) + \Delta(t) \right] . \tag{C10}$$

The gap has the form

$$\Delta(t) := E_t^{(2)} - E_t^{(1)} = \sqrt{(1-\alpha_t)^2 \, (\delta_{\rm GOE})^2 + (\alpha_t)^2 \, (\delta_{\rm MBL})^2} \,. \tag{C11}$$

Substituting from Eqs. (C10) and (C8) into Eq. (C9) yields

$$E(t) = \frac{\Delta(t)}{2} \, \pi(t) + \frac{\delta_{\rm displ}}{2} \, f(\alpha_t) \,. \tag{C12}$$

The imbalance between the weights $\rho_t^{(\ell)}$ is quantified with

$$\pi(t) := \rho_t^{(2)} - \rho_t^{(1)} = -\tanh\left(\beta_{\tilde{t}} \, \frac{\Delta(\tilde{t})}{2} \right) . \tag{C13}$$

The final equality follows from Eq. (C8). $\pi(t)$ is negative—the higher-energy level has less weight than the lower-energy level—if $\beta_{\tilde{t}}$ is positive.

Energy $E(t)$ at times $t = 0, \tau, \tau', \tau'', \tau'''$: Let us evaluate the internal energy $E(t)$ at each endpoint of each stroke (see Fig. 6). At $t = 0$, the Hamiltonian has the gap $\Delta(0) = \delta_{\rm GOE}$. The state is Gibbs relative to the current temperature and Hamiltonian: $\tilde{0} = 0$. Hence $\beta_{\tilde{0}} = \beta_{\rm H}$, and $\Delta(\tilde{0}) = \Delta(0) = \delta_{\rm GOE}$. The imbalance is $\pi(0) = -\tanh(\beta_{\rm H} \, \delta_{\rm GOE})$. Substituting into Eq. (C12) yields

$$E(0) = -\frac{\delta_{\rm GOE}}{2} \, \tanh\left(\frac{\beta_{\rm H} \, \delta_{\rm GOE}}{2} \right) + \frac{\delta_{\rm displ}}{2} \, f(\alpha_t) \,. \tag{C14}$$

The tuning from ETH to MBL ends at $t = \tau$. The new gap $\Delta(\tau) = \delta_{\rm MBL}$ governs the Hamiltonian. The earlier gap and temperature determine the weights: $\tilde{\tau} = 0$, $\beta_{\tilde{\tau}} = \beta_{\rm H}$, and $\Delta(\tilde{\tau}) = \Delta(0) = \delta_{\rm GOE}$. The imbalance remains $\pi(\tau) = -\tanh(\beta_{\rm H} \, \delta_{\rm GOE})$. The internal energy becomes

$$E(\tau) = -\frac{\delta_{\rm MBL}}{2} \, \tanh\left(\frac{\beta_{\rm H} \, \delta_{\rm GOE}}{2} \right) + \frac{\delta_{\rm displ}}{2} \, f(\alpha_t) \,. \tag{C15}$$

The cold thermalization ends at $t = \tau'$. Thermalization preserves the gap, $\Delta(\tau') = \delta_{\rm MBL}$, and changes the weights: $\tilde{\tau}' = \tau'$. The inverse temperature updates to $\beta_{\tilde{\tau}'} = \beta_{\rm C}$, and $\Delta(\tilde{\tau}') = \Delta(\tau') = \delta_{\rm MBL}$. The imbalance becomes $\pi(\tau') = -\tanh(\beta_{\rm C}\,\delta_{\rm MBL})$. The internal energy becomes

$$E(\tau') = -\frac{\delta_{\rm MBL}}{2}\,\tanh\left(\frac{\beta_{\rm C}\,\delta_{\rm MBL}}{2}\right) + \frac{\delta_{\rm displ}}{2}\,f(\alpha_t)\,. \tag{C16}$$

The MBL-to-ETH tuning ends at $t = \tau''$. The gap returns to $\Delta(\tau'') = \delta_{\rm GOE}$. The tuning preserves the weights: $\tilde{\tau}'' = \tau'$, $\beta_{\tilde{\tau}''} = \beta_{\rm C}$, and $\Delta(\tilde{\tau}'') = \Delta(\tau') = \delta_{\rm MBL}$. The imbalance remains $\pi(\tau'') = -\tanh(\beta_{\rm C}\,\delta_{\rm MBL})$. The internal energy is

$$E(\tau'') = -\frac{\delta_{\rm GOE}}{2}\,\tanh\left(\frac{\beta_{\rm C}\,\delta_{\rm MBL}}{2}\right) + \frac{\delta_{\rm displ}}{2}\,f(\alpha_t)\,. \tag{C17}$$

At the end of the cycle, the energy returns to its initial value:

$$E(\tau''') = E(0)\,. \tag{C18}$$

Average work, average heat, and efficiency: Subtracting the average energies with which a stroke s begins and ends yields the average work $\langle W_s\rangle$ performed, or the average heat $\langle Q_s\rangle$ absorbed, during stroke s. Work is performed during Hamiltonian tunings, and heat is absorbed during thermalizations.

During the average stroke-1 realization, the engine performs the work

$$\langle W_1\rangle = E(0) - E(\tau) = -\frac{1}{2}\,(\delta_{\rm GOE} - \delta_{\rm MBL})\,\tanh\left(\frac{\beta_{\rm H}\,\delta_{\rm GOE}}{2}\right)\,. \tag{C19}$$

The engine absorbs the heat

$$\langle Q_2\rangle = E(\tau') - E(\tau) = -\frac{\delta_{\rm MBL}}{2}\left[\tanh\left(\frac{\beta_{\rm C}\,\delta_{\rm MBL}}{2}\right) - \tanh\left(\frac{\beta_{\rm H}\,\delta_{\rm GOE}}{2}\right)\right]\,, \tag{C20}$$

on average, during stroke 2. During stroke 3, the engine extracts the work

$$\langle W_3\rangle = E(\tau') - E(\tau'') = \frac{1}{2}\,(\delta_{\rm GOE} - \delta_{\rm MBL})\,\tanh\left(\frac{\beta_{\rm C}\,\delta_{\rm MBL}}{2}\right)\,, \tag{C21}$$

on average. The final thermalization inputs the heat

$$\langle Q_4\rangle = E(0) - E(\tau'') = \frac{\delta_{\rm GOE}}{2}\left[\tanh\left(\frac{\beta_{\rm C}\,\delta_{\rm MBL}}{2}\right) - \tanh\left(\frac{\beta_{\rm H}\,\delta_{\rm GOE}}{2}\right)\right]\,, \tag{C22}$$

on average. These work and heat quantities are combined into the efficiency $\eta_{\rm qubit}$.

Suppose that $\beta_{\rm H}\,\delta_{\rm GOE} < \beta_{\rm C}\,\delta_{\rm MBL}$. The system expels net positive heat during stroke 2, and absorbs net positive heat during stroke 4, on average: $\langle Q_2\rangle < 0$, and $\langle Q_4\rangle > 0$. $\langle Q_4\rangle$ equals the $\langle Q_{\rm in}\rangle$ in Eq. (C5). Substituting into the efficiency formula from Eqs. (C19), (C21), and (C22) yields

$$\eta_{\rm qubit} = 1 - \frac{\delta_{\rm MBL}}{\delta_{\rm GOE}}\,, \qquad \beta_{\rm H}\,\delta_{\rm GOE} < \beta_{\rm C}\,\delta_{\rm MBL}\,. \tag{C23}$$

Suppose, instead, that $\beta_{\rm H}\,\delta_{\rm GOE} > \beta_{\rm C}\,\delta_{\rm MBL}$. The system absorbs net positive heat only during stroke 2, on average: $\langle Q_2\rangle = \langle Q_{\rm in}\rangle > 0$. We substitute for $\langle Q_2\rangle$, from Eq. (C20), and from Eqs. (C19) and (C21), into Eq. (C5):

$$\eta_{\rm qubit} = 1 - \frac{\delta_{\rm GOE}}{\delta_{\rm MBL}}\,, \qquad \beta_{\rm H}\,\delta_{\rm GOE} > \beta_{\rm C}\,\delta_{\rm MBL}\,. \tag{C24}$$

Since $\delta_{\rm GOE} > \delta_{\rm MBL}$, this efficiency is negative. The requirement that $\eta_{\rm qubit} > 0$ constrains the agent to choose the engine's parameters such that $\beta_{\rm H}\,\delta_{\rm GOE} < \beta_{\rm C}\,\delta_{\rm MBL}$.

C 2 iii The qubit model for the MBL Otto engine shares an ideal-gas Otto engine's efficiency: $\eta_{\rm qubit} = \eta_{\rm Otto}$.

Consider an agent who operates a qubit Otto engine and an agent who operates a thermodynamic Otto engine. The qubit agent chooses sizes $\delta_{\rm GOE}$ and $\delta_{\rm MBL}$ between which to tune the qubit's gap. The thermodynamic agent chooses a compression ratio $r := \frac{V_1}{V_2}$ of volumes between which to compress and expand the gas (Fig. 5). Let $\gamma := \frac{C_{\rm P}}{C_{\rm v}}$ denote a ratio of the gas's constant-volume and constant-pressure specific heats. Given γ, the thermodynamic agent can choose r such that the thermodynamic engine operates at the qubit engine's ideal efficiency.

Recall that $\eta_{\rm qubit} = 1 - \frac{\delta_{\rm MBL}}{\delta_{\rm GOE}}$. We equate the right-hand side with the right-hand side of Eq. (A5). Solving for the compression ratio yields

$$r := \frac{V_1}{V_2} = \left(\frac{\delta_{\rm MBL}}{\delta_{\rm GOE}} \right)^{\frac{1}{1-\gamma}} . \tag{C25}$$

The ideal-gas Otto engine operated with this r is equivalent to the qubit Otto engine.

Equation (C25) makes sense: $\frac{\delta_{\rm MBL}}{\delta_{\rm GOE}} < 1$, by Eq. (C23). Since $\gamma := \frac{C_{\rm P}}{C_{\rm v}} > 1$, $\frac{1}{1-\gamma} < 0$, and $\left| \frac{1}{1-\gamma} \right| > 1$. The right-hand side of Eq. (C25) evaluates to $\left(\frac{\delta_{\rm GOE}}{\delta_{\rm MBL}} \right)^{(\text{number}>1)} > 1$. The left-hand side, too, exceeds one. Hence Eq. (C25) is sensible.

The ideal-gas and qubit Otto cycles can operate at the same efficiency despite the discrepancy between the engines' scales: The qubit engine consists of just two levels. The thermodynamic engine achieves the ideal $\eta_{\rm Otto}$ in the thermodynamic limit of infinite system size. Such comparability characterizes many quantum engines [28, 46].

C 2 iv Upper bound on the qubit model's ideal efficiency by the Carnot efficiency: $\eta_{\rm qubit} < \eta_{Carnot}$

Two arguments imply that $\eta_{\rm qubit} < \eta_{\rm Carnot}$:

1. The Carnot efficiency is known to exceed the thermodynamic Otto engine's ideal efficiency: $\eta_{\rm Carnot} > \eta_{\rm Otto}$ (App. A 3). We showed that $\eta_{\rm Otto} = \eta_{\rm qubit}$ in App. C 2 iii. Hence $\eta_{\rm Carnot} > \eta_{\rm qubit}$.

2. Condition (C4) can be combined with the $\eta_{\rm qubit}$ formula.

Let us expound upon argument 2. Condition (C4) ensures that $\eta_{\rm qubit} > 0$, that, on average, the engine absorbs positive heat during stroke 4 ($\langle Q_4 \rangle > 0$) and negative heat during stroke 2 ($\langle Q_2 \rangle < 0$).

The qubit Otto engine ideally operates at the efficiency

$$\eta_{\rm qubit} = 1 - \frac{\delta_{\rm MBL}}{\delta_{\rm GOE}} . \tag{C26}$$

Rearranging Condition (C4) yields

$$\frac{\delta_{\rm MBL}}{\delta_{\rm GOE}} > \frac{\beta_{\rm H}}{\beta_{\rm C}} = \frac{T_{\rm C}}{T_{\rm H}} . \tag{C27}$$

$T_{\rm C}$ and $T_{\rm H}$ characterize the baths deployed in the qubit Otto cycle. Any engine cycle that involves a temperature-$T_{\rm C}$ bath, a temperature-$T_{\rm H}$ bath, and no other bath has an efficiency bounded by $\eta_{\rm Carnot} = 1 - \frac{T_{\rm C}}{T_{\rm H}}$. Equation (C26) combines with Inequality (C27) into

$$\eta_{\rm qubit} < 1 - \frac{T_{\rm C}}{T_H} = \eta_{\rm Carnot} . \tag{C28}$$

The qubit engine cannot achieve $\eta_{\rm Carnot}$ because Condition (C4) is strict. Suppose that (C4) were nonstrict and saturated: $\beta_{\rm H}\, \delta_{\rm GOE} = \beta_{\rm C}\, \delta_{\rm MBL}$. Could $\eta_{\rm qubit} = \eta_{\rm Carnot}$? Not if the engine had finite power. Throughout stroke 1, the populations form the vector $\left(\frac{e^{-\beta_{\rm H}\, \delta_{\rm GOE}/2}}{Z}, \frac{e^{\beta_{\rm H}\, \delta_{\rm GOE}/2}}{Z} \right)$. Stroke 2—cooling—is intended to drop probability weight to the ground state. The cooling ends with the probability vector $\left(\frac{e^{-\beta_{\rm C}\, \delta_{\rm MBL}/2}}{Z'}, \frac{e^{\beta_{\rm C}\, \delta_{\rm MBL}/2}}{Z'} \right)$. If $\beta_{\rm H}\, \delta_{\rm GOE}$ equaled $\beta_{\rm C}\, \delta_{\rm MBL}$, stroke 2 would fail to change the populations. Stroke 4 would undo stroke 3. $\langle W_{\rm tot} \rangle$, $\langle Q_4 \rangle$, $\langle Q_2 \rangle$, and the power would vanish. The efficiency would be ill-defined: $\eta_{\rm qubit} = \langle W_{\rm tot} \rangle \,/\, \langle Q_{\rm in} \rangle = 0/0$.

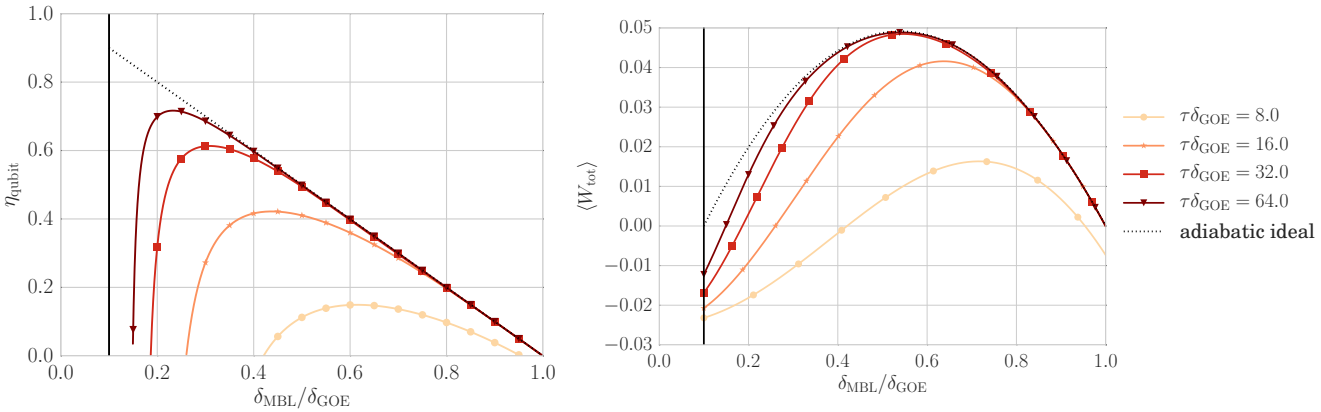

(a) **(b)**

FIG. 7: Efficiency η_{qubit} (left) and average extracted work $\langle W_{\text{tot}} \rangle$ (right) of the qubit toy model for the MBL Otto engine, as a function of the gap ratio $\delta_{\text{MBL}}/\delta_{\text{GOE}}$, at different speeds v: Different curves correspond to different tuning speeds v. The more slowly the engine is tuned, the fewer diabatic jumps the engine suffers: The more the curves approach the "adiabatic ideal" curve (the dotted black lines). The vertical black line marks $\frac{\delta_{\text{MBL}}}{\delta_{\text{GOE}}} = \frac{\beta_{\text{H}}}{\beta_{\text{C}}}$. Rightward of the vertical line, the engine obeys condition C4, so $\eta_{\text{qubit}} > 0$. Leftward of the vertical line, η_{qubit} (not shown) turns negative.

C 3 Numerical simulations of the qubit model for the MBL Otto engine

We simulated the qubit model for the MBL Otto cycle, using various sets of parameter values. Figure 7 shows how the efficiency η_{qubit} and average extracted work $\langle W_{\text{tot}} \rangle$ vary with the gap ratio $\delta_{\text{MBL}}/\delta_{\text{GOE}}$ at different tuning speeds v. In App. C 2, $H_{\text{qubit}}(t)$ was assumed to be tuned infinitely slowly, in the quantum-adiabatic limit. The simulated engine was tuned at a realistically finite speed. The engine therefore could "hop" diabatically between energy levels. In this subsection, η_{qubit} is redefined as the engine's measured, v-dependent efficiency. (η_{qubit} denoted the ideal, quantum-adiabatic efficiency in Sec. C 2.)

We simulated the qubit Otto cycle via exact diagonalization. The baths had the inverse temperatures $\beta_{\text{H}} = 0.1$ and $\beta_{\text{C}} = 1.0$. The tuning speed v and the gap ratio $\delta_{\text{MBL}}/\delta_{\text{GOE}}$ varied from trial to trial. We tuned the gap ratio by fixing $\delta_{\text{GOE}} = 1$ and varying δ_{MBL}. The vertical translation δ_{displ} in Eq. (C1) was set to zero.

In each trial, the tuning lasted for a time τ. The tuning parameter α_t was changed linearly: $\alpha_t = t/\tau$ during stroke 1, and $\alpha_t = 1 - \frac{t}{\tau}$ during stroke 3. During each time step, the time variable t was incremented by 0.001τ. In the slowest trial, $\tau\delta_{\text{GOE}} = 64.0$. In the fastest, $\tau\delta_{\text{GOE}} = 8.0$. These choices illustrate the range of performances that the engine can exhibit, from "nearly ideal" to "working poorly." Different speeds correspond to different colors and to different markers in Fig. 7.

Figure 7a shows η_{qubit}. The dotted black curve represents the adiabatic efficiency [Eq. (C3)]. The finite-speed curves increasingly hug the adiabtic curve as v decreases (as the tuning time τ grows). Consider beginning at any curve's right-hand side and scanning leftward. As the gap ratio $\delta_{\text{MBL}}/\delta_{\text{GOE}}$ decreases toward zero, the efficiency η_{qubit} rises. This rise is consistent with Eq. (C3). As the curve nears the solid black line, η_{MBL} turns over and dives. At the solid black line, $\frac{\delta_{\text{MBL}}}{\delta_{\text{GOE}}} = \frac{\beta_{\text{H}}}{\beta_{\text{C}}} = 0.1$: The parameters violate condition (C4). The engine should not be expected to operate at a positive efficiency beyond this point.

Figure 7b shows the average work extracted, $\langle W_{\text{tot}} \rangle$. [The $\langle . \rangle$ here denotes an ensemble average with respect to $\rho(t)$.] Consider any fixed-v curve. As the gap ratio $\frac{\delta_{\text{MBL}}}{\delta_{\text{GOE}}}$ increases, the curve rises, peaks, and falls. One might naïvely expect the curve only to fall: Consider the simple case in which $T_{\text{H}} = \infty$ and $T_{\text{C}} = 0$. The average work only rises as the gap ratio declines: $\langle W_{\text{tot}} \rangle = \frac{1}{2}(\delta_{\text{GOE}} - \delta_{\text{MBL}})$.

This $\langle W_{\text{tot}} \rangle$ depends on δ_{MBL} linearly because, when $T_{\text{C}} = 0$, the Boltzmann ratio $e^{-\beta_{\text{C}}\delta_{\text{MBL}}}/Z$ simplifies to a constant. Consider fixing δ_{GOE}, $T_{\text{H}} > 0$, and $T_{\text{C}} > 0$. Suppose, for simplicity, that $v = 0$. Consider the ensemble interpretation: The engine begins each trial in one energy eigenstate chosen according the Gibbs distribution $\left\{ e^{-\beta_{\text{H}} E_0^{(\ell)}}/Z_0 \right\}$. Consider one particular trial. Since $T_{\text{H}} > 0$, the engine likely begins in the lower-energy eigenstate. Stroke 1 carries the engine up the bottom green line in Fig. 6, costing work. Since $T_{\text{C}} > 0$, cold thermalization has a probability $\frac{e^{-\beta_{\text{C}}\delta_{\text{MBL}}}}{Z_{\tau'}}$ of hopping the engine to the top level. The engine will slide up the middle green line in Fig. 6 during stroke 3, consuming more work. But suppose that δ_{MBL} is large. The hopping probability $\frac{e^{-\beta_{\text{C}}\delta_{\text{MBL}}}}{Z_{\tau'}}$ is small.

The engine likely slides down the bottom green line during stroke 3. The engine outputs work, canceling the stroke-1 work consumption. A large $\delta_{\rm MBL}$ neutralizes a potentially work-costing trial.

This explanation relies on our tuning $\frac{\delta_{\rm MBL}}{\delta_{\rm GOE}}$ by fixing $\delta_{\rm GOE}$ and tuning $\delta_{\rm MBL}$. Suppose that we fixed $\delta_{\rm MBL}$ and tuned $\delta_{\rm GOE}$. An analogous explanation would concern the start-of-trial Gibbs distribution $\frac{e^{-\beta_{\rm H}\delta_{\rm GOE}\sigma^x}}{Z_0}$.

Appendix D STATISTICAL PROPERTIES OF MBL AND GOE ENERGY SPECTRA

Our quantitative analysis relies on statistical properties of quantum many-body Hamiltonians. We begin by modeling a system's density of states (DOS), $\mu(E)$. In terms of the DOS, we express the local average gap $\langle\delta\rangle_E$ at a point E in the spectrum. Averaging $\langle\delta\rangle_E$ across the spectrum yields the "average gap" $\langle\delta\rangle$. Finally, we introduce *gap distributions*: Consider a quantum many-body Hamiltonian's spectrum. What is the probability that any given energy gap is of size δ? The answer follows from the gap distribution $P(\delta)$. Poissonian gap distributions characterize MBL Hamiltonians. Gaussian gap distributions characterize Hamiltonians that obey the ETH [45].

We use the following conventions and definitions. Throughout this appendix, we focus on a general quantum many-body system of N spin-$\frac{1}{2}$ degrees of freedom. The number of accessible energy eigenstates is $\mathcal{N} \sim 2^N$. $\mathcal{E}$ denotes the unit of energy. Each gap distribution $P(\delta)$ is normalized to one. We disregard the energy band's edges: We focus on a strip of energies centered on $E = 0$. The strip has width $\sim 2\mathcal{E}\sqrt{N}$, as explained in App. D 1. Energies populate the central strip much more densely than energies populate the band's edges.

D 1 Density of states

Consider a quantum many-body Hamiltonian's density of states (DOS), far from the energy band's edges. Whether the Hamiltonian is ETH or MBL, the DOS has a Gaussian form:

$$\mu(E) \approx \frac{\mathcal{N}}{\sqrt{2\pi N}\,\mathcal{E}}\, e^{-E^2/2N\mathcal{E}^2}\,. \tag{D1}$$

The DOS is normalized to the number of accessible energy eigenstates: $\int_{-\infty}^{\infty} dE\ \mu(E) = \mathcal{N}$.

The Gaussian's variance is proportional to the square-root of the system size, N. This proportionality justifies our disregard for the band's edges: $\mu(E)$ is integrated with functions such as the Gibbs distribution $p(E) = e^{-\beta_{\rm H}E}/Z$. The Gaussian decays more quickly than the linear-in-E exponential. $\mu(E)$ effectively truncates $p(E)$ at a distance $\sim \sqrt{N}\,\mathcal{E}$ from $E = 0$. The integrand has significant weight only on a strip, centered on the band's center, of width $\sim 2\sqrt{N}\,\mathcal{E}$. The gaps near the band's edges are anomalously wide.

We checked numerically that our simulated $H_{\rm GOE}$ and $H_{\rm MBL}$ have equal densities of states (Sec. III). We assume this equality in analytical calculations (App. G).

D 2 Average gaps

The *local average gap* $\langle\delta\rangle_E$ denotes the average of the gaps about the energy E. This local average has the form

$$\langle\delta\rangle_E := \frac{1}{\mu(E)}\,. \tag{D2}$$

The function scales as $\frac{\mathcal{E}}{\mathcal{N}} \sim \frac{\mathcal{E}}{2^N}$.

Consider averaging $\langle\delta\rangle_E$ across the spectrum. This average is encapsulated by $\langle\delta\rangle$. $\langle\delta\rangle$ is defined in terms of the inverse of the average, across the spectrum, of the DOS:

$$\langle\delta\rangle := \frac{1}{\langle\mu(E)\rangle_{\rm energies}} = \frac{\mathcal{N}}{\int_{-\infty}^{\infty} dE\ \mu^2(E)} = \frac{2\sqrt{\pi N}}{\mathcal{N}}\,\mathcal{E}\,. \tag{D3}$$

We refer to $\langle\delta\rangle$ loosely as the *average gap.*

$\langle\delta\rangle$ scales as

$$\langle\delta\rangle \sim \frac{\mathcal{E}\sqrt{N}}{\mathcal{N}} \sim \frac{\mathcal{E}}{2^N}\,. \tag{D4}$$

We can understand this scaling as follows. The engine can access $\mathcal{N}$ energy levels. Most of the levels are crammed into a strip, centered around $E = 0$, of width $\sim 2\sqrt{N}\,\mathcal{E}$. The average gap roughly equals $\frac{\text{length of strip packed with energies}}{\#\text{ gaps in strip}} \approx \frac{\text{length of central strip}}{\#\text{ levels}} \sim \frac{2\mathcal{E}\sqrt{N}}{\mathcal{N}}$. The numerical prefactor is negligible.

If the engine's Hamiltonian conserves particle number, the engine state $\rho(t)$ may be restricted to a particle-number subspace associated with $\approx \frac{N}{2}$ particles. Appendix F contains details. If $\rho(t)$ is so restricted, $\mathcal{N} \sim \binom{N}{N/2} \sim \sqrt{\frac{2}{\pi N}}\,2^N$, by Stirling's approximation. Hence Eq. (D3) implies $\langle\delta\rangle \sim \frac{N}{2^N}\,\mathcal{E}$. The numerator scales as N, rather than as the $\sqrt{N}$ in (D4). This polynomial change affects our results little: The denominator's 2^N dominates the scaling of $\langle\delta\rangle$.

D 3 Gaussian statistics of ETH energy spectra

Let H denote a Hamiltonian that obeys the ETH. Consider a portion of the spectrum over which the DOS remains roughly constant. The corresponding portion of H can be represented, relative to a non-finely-tuned basis, by a random matrix $\mathcal{M}$. Each matrix entry $\mathcal{M}_{ij}$ is a random variable distributed as a Gaussian. $\mathcal{M}$ belongs to a matrix ensemble invariant under certain transformations. The transformations' natures follow from the system's physical symmetries. If H has time-reversal symmetry, M belongs to the Gaussian Orthogonal Ensemble (GOE). For background about random-matrix theory, we refer readers to [45].

The Gaussian distribution implies the probability that the gap at the point E in the spectrum is of size δ. The probability per unit energy is

$$P^{(E)}_{\text{GOE}}(\delta) \approx \frac{\pi}{2}\,\frac{\delta}{\langle\delta\rangle^2_E}\,e^{-\frac{\pi}{4}\,\delta^2/\langle\delta\rangle^2_E} \tag{D5}$$

for Hamiltonians modeled by the GOE. Equation (D5) is a realization of the *Wigner surmise*.

$P^{(E)}_{\text{GOE}}(\delta)$ encodes level repulsion. Small gaps are exponentially suppressed: $\delta \to 0$ implies $P^{(E)}_{\text{GOE}}(\delta) \to 0$. Energies tend to spread out.

D 4 Poisson statistics of MBL energy spectra

MBL Hamiltonians obey Poisson statistics. An MBL energy eigenstate $|\psi_\ell\rangle$ nearly equals a product of single-particle position eigenstates. The ℓ^{th} eigenstate's functional form can differ wildly from the $(\ell+1)^{\text{th}}$ state's functional form. Hence the levels' forms are approximately uncorrelated. So are their energies: Given the value E_ℓ of the ℓ^{th} energy, one cannot usefully update the prior with which one predicts the value $E_{\ell+1}$ of the $(\ell+1)^{\text{th}}$ energy. The Poisson distribution $P_{\text{Poisson}}(E)$ models uncorrelated energies. Let λ denote the average number of energies in a width-a interval. The probability per unit energy that n energies occupy that interval is

$$P_{\text{Poisson}}(E) = \frac{\lambda^n}{n!}\,e^{-\lambda}\,. \tag{D6}$$

Equation (D6) implies the probability $P^{(E)}_{\text{MBL}}(\delta)$ that the gap at the point E in the spectrum is of width δ:

$$P^{(E)}_{\text{MBL}}(\delta) \approx \frac{1}{\langle\delta\rangle_E}\,e^{-\delta/\langle\delta\rangle_E}\,. \tag{D7}$$

MBL energies do not repel, unlike GOE energies. As $\delta \to 0$, $P^{(E)}_{\text{MBL}}(\delta) \to 1$. Any given gap has a decent probability of being small.

Equation (D7) is an ideal approached in the thermodynamic limit. Suppose that the system size N is finite. Consider decreasing δ. Near $\delta = 0$, the gap distribution declines sharply. MBL level statistics are not strictly Poissonian. A regularized Poisson distribution can model this decline: Let ξ denote an energy eigenfunction's localization length. There exists a scale $\delta_- \sim \mathcal{E}e^{-N/\xi}$ such that energies are unlikely to lie closer together than δ_- (App. H). We can model this effect by multiplying the $e^{-\delta/\langle\delta\rangle_E}$ by $\tanh\left(\frac{\delta}{\delta_-}\right)$. The discrepancy affects just corrections to our main results.

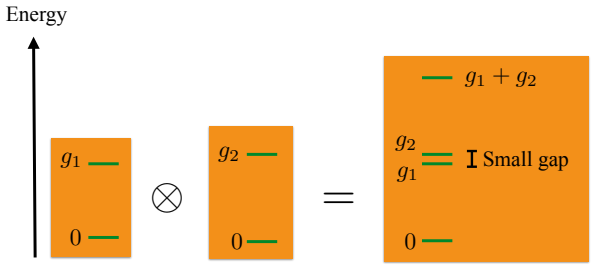

FIG. 8: Physical model for a resonance in an MBL energy spectrum: The MBL Otto engine relies on small gaps that widen as the Hamiltonian is tuned from MBL to ETH. Such gaps can be understood in terms of qubits. An MBL system consists of nearly independent pseudospins called *localized bits*, or *l-bits*. l-bits are localized far apart and interact weakly. An MBL system has a significant probability of having two l-bits whose gaps nearly equal each other: $g_1 \approx g_2$. Such g_j's imbue the MBL energy spectrum with the small gap $g_2 - g_1$. The gap widens as the Hamiltonian is tuned to ETH: Qubits increasingly interact, forcing the energies apart.

Appendix E TWO-QUBIT MODEL FOR A "WORKING GAP" OF THE MBL OTTO ENGINE

The MBL Otto engine benefits from the greater frequency with which small gaps appear in MBL spectra than in "thermal" spectra. The relative frequencies, and their roles in the cycle, are illustrated in Fig. 2. A two-qubit model illustrates how small gaps arise from localized particles' near independence.

A spin chain exemplifies an MBL system. At each site sits a spin, called a *physical bit*, or a *p-bit* [34]. An MBL Hamiltonian $H_{\rm MBL}$ can be cast in terms of p-bit Pauli operators σ_j^γ. Sites are indexed by j, and $\gamma = x, y, z$. A mathematical transformation maps the p-bits to *localized bits*, or *l-bits* [34]. l-bits are spatially localized pseudospins. An l-bit Pauli operator is denoted by $\tau_{j'}^{\gamma'}$, wherein $j' = 1, 2, \ldots, N$ and $\gamma' = x, y, z$. Each $\tau_{j'}^{\gamma'}$ equals a weighted product of σ_j^γ's. The weights' functional dependence on j is tightly peaked about one site. $H_{\rm MBL}$ conserves the $\tau_{j'}^z$'s, though not the σ_j^z's. l-bits interact weakly and are localized far apart. A similar construction appears in [75].

Let g_j denote the $j^{\rm th}$ l-bit's gap. Suppose that two l-bits have nearly equal gaps: $g_1 \approx g_2$. The MBL spectrum contains the energies $0, g_1, g_2$, and $g_1 + g_2$. (We have set each bit's ground-state energy to zero, without loss of generality.) These levels are illustrated in Fig. 8. The spectrum's probability of containing a small gap $g_2 - g_1$ is nonnegligible, by the Poisson distribution $P_{\rm MBL}^{(E)}(g_2 - g_1)$ [Eq. (D7)].

Consider a mesoscale MBL Otto engine that consists of l-bits including 1 and 2. Suppose that the engine begins the cold-thermalization stroke with energy g_2. What must happen for the cycle to output $W_{\rm tot} > 0$? Suppose that g_1 is the only energy that lies below g_2, within a distance $\leq W_{\rm b}$ of g_2. The cold bath must drop the engine's energy from g_2 to g_1. l-bit 2 must flip downward, and l-bit 1 must flip upward. l-bits whose gaps nearly equal each other tend to be localized far apart (App. H). The cold bath couples to the engine locally. Yet the bath has some nonzero probability of flipping far-apart l-bits. The cycle has a nonzero probability of outputting $W_{\rm tot} > 0$.

Consider tuning $H_{\rm meso}(t)$ from MBL to ETH during stroke 3. The interaction-strength-to-disorder-strength ratio $\frac{1}{h}$ rises. Interactions might manifest as, e.g., phononic or dipole-dipole couplings. In general, interactions split degeneracies. The near-degeneracy between g_1 and g_2 is broken increasingly drastically. The many-body gap widens. Hence the $H_{\rm MBL}$ spectrum likely has more small gaps than the $H_{\rm GOE}$ spectrum.

Appendix F CONSERVATION OF PARTICLE NUMBER

Consider the mesoscopic engine introduced in Sec. II B. Suppose that the engine's Hamiltonian [Eq. (8)] preserves particle number: $[H_{\rm meso}(t), \hat{N}] = 0$, wherein $\hat{N}$ denotes the particle-number operator. Examples include the disordered Heisenberg model simulated in Sec. III. The engine's state must occupy one $\hat{N}$ eigenspace and must remain in that eigenspace throughout the cycle. We illustrate why with the qubit toy model from App. C.

Recall the set-up: The Hamiltonian has the form $H_{\rm qubit}(t) = (1 - \alpha_t) \frac{\delta_{\rm GOE}}{2} \sigma^x + \alpha_t \frac{\delta_{\rm MBL}}{2} \sigma^z$. We have set the offset $\delta_{\rm displ}$ to zero, for simplicity. $E_t^{(1)}$ and $E_t^{(2)}$ denote the time-t energies. Let $\mathcal{M}(t)$ denote the matrix that represents $H_{\rm qubit}(t)$ relative to the eigenbasis of $\frac{\delta_{\rm MBL}}{2} \sigma^z$, the Hamiltonian's MBL-like component. When the Hamiltonian is

MBL-like, $\mathcal{M}(t)$ is diagonal. For example, when stroke 1 ends at time $t = \tau$,

$$\mathcal{M}(\tau) = \begin{bmatrix} E_\tau^{(1)} & 0 \\ 0 & E_\tau^{(2)} \end{bmatrix} . \tag{F1}$$

Consider tuning $H_{\rm qubit}(t)$ from MBL-like to GOE-like during stroke 3. The perturbation $\frac{\delta_{\rm GOE}}{2}\,\sigma^x$ is strengthened. This perturbation populates the off-diagonal elements of $\mathcal{M}(t)$. Between $t = \tau'$ and $t = \tau''$,

$$\mathcal{M}(t) = \begin{bmatrix} E_\tau^{(1)} & a_t \\ a_t^* & E_\tau^{(2)} \end{bmatrix} . \tag{F2}$$

The complex-valued $a_t \neq 0$, and the asterisk denotes complex conjugation. The off-diagonal elements widen the energy gap from $|E_\tau^{(2)} - E_\tau^{(1)}|$ to $\sqrt{|E_\tau^{(2)} - E_\tau^{(1)}|^2 + |a_t|^2}$. This widening illustrates why GOE Hamiltonians' energies "repel."

The off-diagonal elements also facilitate transitions between the MBL energy eigenstates $|E_\tau^{(1)}\rangle$ and $|E_\tau^{(2)}\rangle$ during stroke 3. Such transitions are forbidden if $|E_\tau^{(1)}\rangle$ and $|E_\tau^{(2)}\rangle$ occupy different particle-number sectors. If the states occupy different sectors, therefore, $a_t = 0$. The GOE-like gap equals the MBL-like gap.

To take advantage of level statistics, therefore, we must keep the engine's state in one $\hat{N}$ subspace. The number of particles should be close to $N/2$. Our numerics are implemented at half-filling (App. K). Half-filling changes the scaling of $\langle\delta\rangle$ negligibly, from $\sim \frac{\mathcal{E}\sqrt{N}}{2^N}$ to $\sim \frac{\mathcal{E}N}{2^N}$. The change was discussed in App. D 2.

Appendix G QUANTITATIVE ASSESSMENT OF THE MESOSCOPIC MBL OTTO ENGINE

Gauges of an engine's quality include power and efficiency. We asses the mesoscopic engine introduced in Sec. II B. This engine's Hamiltonian is tuned between the "thermal" ETH phase and the MBL phase. Mesoscopic engines operate roughly in parallel in the thermodynamically large MBL engine.

Let S denote the engine. Figure 2 illustrates one successful trial, during which a positive amount of work is extracted from S. S outputs work W_1 during stroke 1 and work W_3 during stroke 3. S absorbs heat Q_2 during stroke 2 and heat Q_4 during stroke 4. By the first law of thermodynamics, $W_{\rm tot} := W_1 + W_3 = Q_4 + Q_2$. We denote by $\langle . \rangle$ an average over trials—over Gibbs distributions and over gap distributions. The average over gap distributions parallels an average, in numerical experiments, over disorder realizations. The average work extracted per engine cycle, $\langle W_{\rm tot}\rangle$, is the per-trial power. The power—the average work extracted per unit time—equals $\frac{\langle W_{\rm tot}\rangle}{\tau_{\rm cycle}}$. The time required to implement one cycle is denoted by $\tau_{\rm cycle}$. $\tau_{\rm cycle}$ is estimated in App. J 2.

First, we review and introduce more notation. Next, we introduce the small parameters in terms of which we expand. We then review the partial swap [96, 97], with which we model cold thermalization (stroke 2). We estimate $\langle Q_2\rangle$, then $\langle Q_4\rangle$. Summing the average heat terms yields the average per-trial power: $\langle W_{\rm tot}\rangle = \langle Q_2\rangle + \langle Q_4\rangle \approx W_{\rm b} - \frac{2\eta(1)}{\beta_{\rm C}} + 4\eta(1)\,\frac{W_{\rm b}}{\beta_{\rm C}\langle\delta\rangle}$. The efficiency is defined as $\eta_{\rm MBL} := \langle W_{\rm tot}\rangle \,/\, \langle Q_{\rm in}\rangle$, wherein $\langle Q_{\rm in}\rangle = \langle Q_4\rangle$ denotes the heat absorbed during the stroke during which S absorbs, on average, a positive amount of heat. The efficiency assumes the expected form $\eta_{\rm MBL} \approx 1 - \frac{W_{\rm b}}{2\langle\delta\rangle}$. Throughout the aforementioned calculations, we assume that the Hamiltonian is tuned adiabatically. We then estimate six diabatic corrections attributable to a realistic tuning's finite speed. These analytic results largely agree with the numerics in Sec. III.

G 1 Notation

Throughout this appendix, we focus on one mesoscopic engine, S. S consists of N sites. $\mathcal{N}$ denotes the number of available energy eigenstates. If the Hamiltonian conserves particle number, the engine's state must remain in some particle-number eigensubspace associated with $\sim \frac{N}{2}$ particles. That subspace's dimensionality scales as 2^N.

To simplify notation, we drop the subscript from $H_{\rm meso}(t)$. The Hamiltonian $H(t)$ is tuned between $H_{\rm GOE}$, which obeys the ETH, and $H_{\rm MBL}$, which governs an MBL system. Several unprimed quantities denote properties of $H_{\rm GOE}$, whereas primed quantities denote properties of $H_{\rm MBL}$: We denote by E_j the $j^{\rm th}$-greatest energy of $H_{\rm GOE}$ and by E'_j the $j^{\rm th}$-greatest energy of $H_{\rm MBL}$. δ_j denotes the gap just below E_j. δ'_j denotes the gap just below E'_j. When approximating the spectra as continuous, we replace E_j with E and E'_j with E'.

Though the energies form a discrete set, they are well approximated as a continuum. ETH and MBL Hamiltonians have Gaussian densities of states (DOSs): $\mu(E) = \frac{\mathcal{N}}{\sqrt{2\pi N}\,\mathcal{E}}\,e^{-E^2/(2N\mathcal{E}^2)}$ [Eq. (D1)]. The DOS is normalized to the

number of available energy eigenstates: $\int_{-\infty}^{\infty} dE\ \mu(E) = \mathcal{N}$. When integrating a quantity with $\mu(E)$, therefore, we typically divide the integral by $\mathcal{N}$. The unit of energy is denoted by $\mathcal{E}$. We often extend energy integrals' limits to $\pm\infty$, as the Gaussian peaks sharply about $E = 0$. The local average gap $\langle\delta\rangle_E = \frac{1}{\mu(E)}$ and the average gap $\langle\delta\rangle := \frac{\mathcal{N}}{\int_{-\infty}^{\infty} dE\ \mu^2(E)} = \frac{2\sqrt{\pi N}\,\mathcal{E}}{\mathcal{N}}$ are defined as in App. D 2.

The average gap $\langle\delta\rangle$ of $H_{\rm GOE}$ equals the average gap of $H_{\rm MBL}$, by construction. $\langle\delta\rangle$ sets the scale for work and heat quantities. Therefore, we will express Q's and W's in the form (number)(function of small parameters) $\langle\delta\rangle$.

The system begins the cycle in the state $\rho(0) = e^{-\beta_{\rm H} H_{\rm GOE}}/Z$. The partition function $Z := {\rm Tr}\left(e^{-\beta_{\rm H} H_{\rm GOE}}\right)$ normalizes the state. $W_{\rm b}$ denotes the cold bath's bandwidth. We equate Planck's reduced constant and Boltzmann's constant with one: $\hbar = k_{\rm B} = 1$.

The Hamiltonian is tuned at a speed v. More precisely, $v := \mathcal{E}\left|\frac{d\alpha_t}{dt}\right|$, wherein α_t denotes the dimensionless tuning parameter. v has dimensions of $\frac{\rm energy}{\rm time} = {\rm energy}^2$. (The equality follows from our having set $\hbar$ to one.) We have chosen for v to have the dimensionality of the v in [60]. Though our v is not defined identically to the v in [60], our speed is expected to behave similarly.

G 2 Small parameters

We estimate low-order contributions to $\langle W_{\rm tot}\rangle$ and to $\eta_{\rm MBL}$ in terms of small parameters:

1. The cold bath has a small bandwidth: $\frac{W_{\rm b}}{\langle\delta\rangle} \ll 1$.
2. The cold bath is cold: $\beta_{\rm C} W_{\rm b} > 0$. In contrast, negative-temperature thermal states have considerable weight on high-energy levels, as though very hot.
3. Also because the cold bath is cold, $1 \gg e^{-\beta_{\rm C} W_{\rm b}} \approx 0$, and $\frac{1}{\beta_{\rm C}\langle\delta\rangle} \ll 1$.
4. The hot bath is hot: $\sqrt{N}\,\beta_{\rm H}\mathcal{E} \ll 1$. This inequality prevents $\beta_{\rm H}$ from contaminating leading-order contributions to heat and work quantities. ($\beta_{\rm H}$ dependence, we find, tends to manifest in factors of $e^{-N(\beta_{\rm H}\mathcal{E})^2/4}$.) Since $\beta_{\rm H}\mathcal{E} \ll \frac{1}{\sqrt{N}}$ and $\frac{\langle\delta\rangle}{\mathcal{E}} \ll 1$, $\beta_{\rm H}\langle\delta\rangle = (\beta_{\rm H}\mathcal{E})\left(\frac{\langle\delta\rangle}{\mathcal{E}}\right) \ll \frac{1}{\sqrt{N}}$.

We focus on the parameter regime in which

$$T_{\rm C} \ll W_{\rm b} \ll \langle\delta\rangle \qquad \text{and} \qquad \sqrt{N}\,\beta_{\rm H}\mathcal{E} \ll 1\,. \tag{G1}$$

The numerical simulations (Sec. III) took place in this regime. We approximate to second order in $\frac{1}{\beta_{\rm C}\langle\delta\rangle}$, $\frac{W_{\rm b}}{\langle\delta\rangle}$, and $N(\beta_{\rm H}\mathcal{E})^2$. We approximate to zeroth order in the much smaller $e^{-\beta_{\rm C} W_{\rm b}}$.

The diabatic corrections to $\langle W_{\rm tot}\rangle$ involve three more small parameters. $H(t)$ is tuned at a low speed v: $\frac{\sqrt{v}}{\langle\delta\rangle} \ll 1$. The MBL level-repulsion scale δ_- denotes the least value reasonably attributable to any gap in the $H_{\rm MBL}$ spectrum (Appendix H): $\frac{\delta_-}{\langle\delta\rangle} \ll 1$. The third parameter, $\frac{\langle\delta\rangle}{\mathcal{E}} \ll 1$, follows from $\langle\delta\rangle \sim \frac{\mathcal{E}}{\mathcal{N}}$.

G 3 Partial-swap model of thermalization

Classical thermalization can be modeled with a probabilistic swap, or partial swap, or p-SWAP [96, 97]. A column vector $\vec{v}$ represents the state. The thermalization is broken into time steps. At each step, a doubly stochastic matrix M_p operates on $\vec{v}$. The matrix's fixed point is a Gibbs state $\vec{g}$.

M_p models a probabilistic swapping out of $\vec{v}$ for $\vec{g}$: At each time step, the system's state has a probability $1 - p$ of being preserved and a probability $p \in [0,\ 1]$ of being replaced by $\vec{g}$. This algorithm gives M_p the form $M_p = (1 - p)\mathbb{1} + pG$. Every column in the matrix G equals the Gibbs state $\vec{g}$.

Let us illustrate with thermalization across two levels. If $\vec{g} = \left(\frac{e^{-\beta\Delta}}{1+e^{-\beta\Delta}}\,,\,\frac{1}{1+e^{-\beta\Delta}}\right)$,

$$M_p = \begin{bmatrix} 1 - p\,\frac{1}{1+e^{-\beta\Delta}} & p\,\frac{e^{-\beta\Delta}}{1+e^{-\beta\Delta}} \\ p\,\frac{1}{1+e^{-\beta\Delta}} & 1 - p\,\frac{e^{-\beta\Delta}}{1+e^{-\beta\Delta}} \end{bmatrix}. \tag{G2}$$

The off-diagonal elements represent the probabilities that, if the system starts in one level, it will hop to the other level during any given time step. These transition probabilities obey detailed balance [98, 99]: $\frac{P(0\to\Delta)}{P(\Delta\to 0)} = e^{-\beta\Delta}$, if the levels are labeled 0 and Δ.

The parameter p depends on the strength of the coupling between the system and the bath. Regardless of the value of p, repeated application of M_p maps every state to $\vec{g}$ [98]: $\lim_{n\to\infty} (M_p)^n \, \vec{v} = \vec{g}$. We choose $p = 1$: The system thermalizes completely at each time step. (If $p \neq 1$, a more sophisticated model may be needed to model thermalization across > 2 levels.)

G 4 Average heat $\langle Q_2 \rangle$ absorbed during stroke 2

We calculate $\langle Q_2 \rangle$ in four steps. First, we focus on one trial. The density operator's statistical interpretation enables us to suppose that the engine begins each trial in one energy eigenstate. We calculate the heat absorbed during one trial's second stroke. Next, we average over the probabilities that cold thermalization does or does not change the engine's energy. We average also with respect to the Poisson gap distribution, $P^{(E)}_{\rm MBL}(\delta)$. Finally, we average with respect to the initial density operator, $\rho(0) = e^{-\beta_{\rm H} H_{\rm GOE}}/Z$.

G 4 i Heat absorbed during one trial

Suppose that the engine begins the trial of interest on level j of $H_{\rm GOE}$. Stroke 1—adiabatic tuning—preserves the occupied level's index. Let $Q_2^{(j)}$ denote the amount of heat absorbed during cold thermalization. Suppose that the gap just above level j is smaller than the cold bath's bandwidth: $\delta'_{j+1} < W_{\rm b}$. The engine may jump upward, absorbing an amount $Q_2^{(j)} = \delta'_{j+1}$ of heat. Suppose that the gap just below level j is sufficiently small: $\delta'_j < W_{\rm b}$. The engine may drop downward, absorbing $Q_2^{(j)} = -\delta'_j$. The engine absorbs no heat if it fails to hop:

$$Q_2^{(j)} = \begin{cases} \delta'_{j+1} \, , & \text{engine jumps} \\ -\delta'_j \, , & \text{engine drops} \\ 0 \, , & \text{cold thermalization preserves engine's energy} \end{cases} . \tag{G3}$$

G 4 ii Averages with respect to cold-thermalization probabilities and gap distributions

We set up the averages, then evaluate integrals.

G 4 iia Setting up the averages with respect to cold-thermalization probabilities and gap distributions: The discrete index j becomes a continuous variable E:

$$\begin{aligned} \Big\langle \langle Q_2(E) \rangle_{\substack{\text{cold} \\ \text{therm.}}} \Big\rangle_{\text{gaps}} &= \int_0^{W_{\rm b}} d\delta'_{j+1} \, \delta'_{j+1} \, \mathcal{P}(S \text{ jumps} \,|\, \delta'_{j+1} < W_{\rm b}) \, \mathcal{P}(\delta'_{j+1} < W_{\rm b} \,;\, S \text{ does not drop}) \\ &\quad + \int_0^{W_{\rm b}} d\delta'_j \, (-\delta'_j) \, \mathcal{P}(S \text{ drops} \,|\, \delta'_j < W_{\rm b}) \, \mathcal{P}(\delta'_j < W_{\rm b} \,;\, S \text{ does not jump}) \, . \end{aligned} \tag{G4}$$

Each $\mathcal{P}(a)$ denotes the probability that an event a occurs. $\mathcal{P}(a|b)$ denotes the conditional probability that, if an event b has occurred, a will occur. $\mathcal{P}(a; b)$ denotes the joint probability that a and b will occur.

The p-SWAP model (App. G 3) provides the conditional probabilities. The Poisson distribution provides the probability that a gap is sufficiently small. Each joint probability factorizes, e.g., $\mathcal{P}(\delta'_{j+1} < W_{\rm b} \,;\, S \text{ does not drop}) = \mathcal{P}(\delta'_{j+1} < W_{\rm b}) \, \mathcal{P}(S \text{ does not drop})$.

The engine refrains from dropping if (1) the gap below level j is too large or if (2) the gap below j is small but cold thermalization fails to drop the engine's state nevertheless:

$$\mathcal{P}(S \text{ does not drop}) = \mathcal{P}(\delta'_j > W_{\rm b}) + \mathcal{P}\left(S \text{ does not drop} \,|\, \delta'_{j+1} < W_{\rm b}\right) \mathcal{P}(\delta'_{j+1} < W_{\rm b}) \, . \tag{G5}$$

The gap has a probability $\mathcal{P}(\delta'_j > W_{\rm b}) = 1 + O\left(\frac{W_{\rm b}}{\langle \delta \rangle}\right)$ of being too large. The gap has a probability $\mathcal{P}(\delta'_{j+1} < W_{\rm b}) = O\left(\frac{W_{\rm b}}{\langle \delta \rangle}\right)$ of being small enough.[10] The detailed-balance probability $\mathcal{P}\left(S \text{ does not drop} \,|\, \delta'_{j+1} < W_{\rm b}\right)$ is too small to

[10] Any given gap's probability of being small enough to thermalize

offset the $O\left(\frac{W_{\rm b}}{\langle\delta\rangle}\right)$ scaling of $\mathcal{P}(\delta'_{j+1} < W_{\rm b})$. Hence the $O\left(\frac{W_{\rm b}}{\langle\delta\rangle}\right)$ terms are negligible here: Each multiplies, in Eq. (G4), a δ'_{j+1} that will average to $\sim W_{\rm b}$ and a $\mathcal{P}(S \text{ jumps} \,|\, \delta'_{j+1} < W_{\rm b})$ that will average to $\sim \frac{W_{\rm b}}{\langle\delta\rangle}$. Each such compound term $\sim W_{\rm b}\left(\frac{W_{\rm b}}{\langle\delta\rangle}\right)^2 = \langle\delta\rangle\left(\frac{W_{\rm b}}{\langle\delta\rangle}\right)^3$. We evaluate quantities only to second order in $\frac{W_{\rm b}}{\langle\delta\rangle} \ll 1$. Hence Eq. (G5) is approximated with one. A similar argument concerns the final factor in Eq. (G4). Equation (G4) becomes

$$\left\langle \langle Q_2(E)\rangle_{\substack{\text{cold}\\ \text{therm.}}} \right\rangle_{\text{gaps}} = \int_0^{W_{\rm b}} d\delta'_{j+1}\ \delta'_{j+1}\ \frac{e^{-\beta_{\rm C}\delta'_{j+1}}}{1+e^{-\beta_{\rm C}\delta'_{j+1}}}\ P^{(E)}_{\rm MBL}(\delta'_{j+1}) - \int_0^{W_{\rm b}} d\delta'_j\ \delta'_j\ \frac{1}{1+e^{-\beta_{\rm C}\delta'_j}}\ P^{(E)}_{\rm MBL}(\delta'_j) + O\left(\left[\frac{W_{\rm b}}{\langle\delta\rangle}\right]^3\right) . \tag{G10}$$

We have neglected two possibilities. First, we assume that the cold bath cannot thermalize gaps larger than the bath's bandwidth, i.e., across $\delta'_{j+1} > W_{\rm b}$ or $\delta'_j > W_{\rm b}$. Second, multiple small gaps could lie directly below level j, e.g., $\delta'_j, \delta'_{j-1} < W_{\rm b}$. The cold bath could thermalize the engine across each gap. But the engine absorbs, on average, a negligible amount of heat from such gap chains during stroke 2: Any given gap (far from the spectrum's edges) has a probability $\sim \frac{W_{\rm b}}{\langle\delta\rangle}$ of being small enough to thermalize. Two neighboring gaps have a probability $\sim \left(\frac{W_{\rm b}}{\langle\delta\rangle}\right)^2$ of both being sufficiently small. Suppose that the engine drops across two such gaps. The engine absorbs an amount $\sim -2W_{\rm b}$ of heat. The average heat absorbed from the chain equals approximtely $-2W_{\rm b}\left(\frac{W_{\rm b}}{\langle\delta\rangle}\right)^2 = -2\langle\delta\rangle\left(\frac{W_{\rm b}}{\langle\delta\rangle}\right)^3$. This quantity is of third order in the small parameter $\frac{W_{\rm b}}{\langle\delta\rangle}$. We estimate to second order.

Let us evaluate the integrals in Eq. (G10).

G 4 iib Evaluating the downward-drop integral: We begin with the second integral in Eq. (G10). We relabel δ'_j as δ to simplify notation:

$$\mathcal{I}_2 := \int_0^{W_{\rm b}} d\delta\ \delta\ \frac{1}{1+e^{-\beta_{\rm C}\delta}}\ \left[\mu(E)\ e^{-\mu(E)\delta}\right] = \mu(E)\int_0^{W_{\rm b}} d\delta\ \frac{\delta\, e^{-\mu(E)\delta}}{1+e^{-\beta_{\rm C}\delta}} . \tag{G11}$$

We have substituted in for $P^{(E)}_{\rm MBL}(\delta)$ from Eq. (D7). This integrand echoes the Sommerfeld expansion of low-temperature statistical mechanics [100].

The detailed-balance probability decomposes as $\frac{1}{1+e^{-\beta_{\rm C}\delta}} = 1 - \frac{e^{-\beta_{\rm C}\delta}}{1+e^{-\beta_{\rm C}\delta}} = 1 - \frac{1}{1+e^{\beta_{\rm C}\delta}}$. The first equality follows from the conservation of probability. The second equality follows from multiplying the fraction's numerator and denominator by $e^{\beta_{\rm C}\delta}$. Hence

$$\mathcal{I}_2 = \mu(E)\int_0^{W_{\rm b}} d\delta\cdot\delta\, e^{-\mu(E)\delta} - \mu(E)\int_0^{W_{\rm b}} d\delta\ \frac{\delta\, e^{-\mu(E)\delta}}{1+e^{\beta_{\rm C}\delta}} . \tag{G12}$$

Let $\mathcal{I}'_2 := \mu(E)\int_0^{W_{\rm b}} d\delta\cdot\delta\, e^{-\mu(E)\delta}$ denote the first term.

We Taylor-approximate the exponential to zeroth order:

$$\mathcal{I}'_2 = \mu(E)\int_0^{W_{\rm b}} d\delta\cdot\delta\,[1 - O(\mu(E)\delta)] = \frac{1}{2}\ (W_{\rm b})^2 + O\left([\mu(E)W_{\rm b}]^3\right) . \tag{G13}$$

Substituting into Eq. (G29) yields

$$\mathcal{I}_2 = \frac{1}{2}\,\mu(E)\,(W_{\rm b})^2 - \mu(E)\int_0^{W_{\rm b}} d\delta\ \frac{\delta\, e^{-\mu(E)\delta}}{1+e^{\beta_{\rm C}\delta}} + O\left([\mu(E)\,W_{\rm b}]^3\right) . \tag{G14}$$

---

equals

$$\mathcal{P}(\delta \le W_{\rm b}) = \frac{1}{\mathcal{N}}\int_{E_{\rm min}}^{E_{\rm max}} dE\ \mu(E)\int_0^{W_{\rm b}} d\delta\ P^{(E)}_{\rm MBL}(\delta) \tag{G6}$$

$$\approx \frac{1}{\mathcal{N}}\int_{-\infty}^{\infty} dE\ \mu(E)\ \left[1 - e^{-\mu(E)W_{\rm b}}\right] . \tag{G7}$$

The first term evaluates to one, by the DOS's normalization. We Taylor-expand the exponential to first order, then integrate term by term:

$$\mathcal{P}(\delta \le W_{\rm b}) \approx 1 - \left[\frac{1}{\mathcal{N}}\int_{-\infty}^{\infty} dE\ \mu(E) - \frac{W_{\rm b}}{\mathcal{N}}\int_{-\infty}^{\infty} dE\ \mu^2(E) + O\left(\frac{(W_{\rm b})^2}{\mathcal{N}}\int_{-\infty}^{\infty} dE\ \mu^3(E)\right)\right] \tag{G8}$$

$$= \frac{W_{\rm b}}{\langle\delta\rangle} + O\left(\left[\frac{W_{\rm b}}{\langle\delta\rangle}\right]^2\right) . \tag{G9}$$

Let $\mathcal{I}_2''$ denote the second term:

$$\mathcal{I}_2'' := \mu(E) \int_0^{W_\mathrm{b}} d\delta \, \frac{\delta \, e^{-\mu(E)\delta}}{1 + e^{\beta_\mathrm{C}\delta}} \, . \tag{G15}$$

The $\frac{\delta}{1+e^{\beta_\mathrm{C}\delta}}$ echoes the integrand of the integral that evaluates to the Riemann zeta function. We magnify the resemblance in two ways.

First, we extend the integration limit from W_b to infinity. Let us bound the error incurred by the extension,

$$\epsilon := \mu(E) \int_{W_\mathrm{b}}^{\infty} d\delta \, \frac{\delta \, e^{-\mu(E)\delta}}{1 + e^{\beta_\mathrm{C}\delta}} \, . \tag{G16}$$

Since $\frac{1}{1+e^{\beta_\mathrm{C}\delta}} \leq e^{-\beta_\mathrm{C}\delta}$, $\epsilon \leq \mu(E) \int_{W_\mathrm{b}}^{\infty} d\delta \cdot \delta \, e^{-[\mu(E)+\beta_\mathrm{C}]\delta}$. Let us integrate by parts. Let $u = \delta$, $du = d\delta$, $v = -\frac{e^{-[\mu(E)+\beta_\mathrm{C}]\delta}}{\mu(E)+\beta_\mathrm{C}}$, and $dv = e^{-[\mu(E)+\beta_\mathrm{C}]\delta} \, d\delta$. Invoking $\int_a^b u \, dv = u \, v \Big|_a^b - \int_a^b v \, du$ yields

$$\epsilon \leq \mu(E) \left(- \frac{\delta}{\mu(E) + \beta_\mathrm{C}} \, e^{-[\mu(E)+\beta_\mathrm{C}]\delta} \Big|_{W_\mathrm{b}}^{\infty} + \frac{1}{\mu(E) + \beta_\mathrm{C}} \int_{W_\mathrm{b}}^{\infty} d\delta \, e^{-[\mu(E)+\beta_\mathrm{C}]\delta} \right) \tag{G17}$$

$$= \mu(E) \left(\frac{W_\mathrm{b}}{\mu(E) + \beta_\mathrm{C}} \, e^{-[\mu(E)+\beta_\mathrm{C}]W_\mathrm{b}} + \frac{1}{[\mu(E) + \beta_\mathrm{C}]^2} \, e^{-[\mu(E)+\beta_\mathrm{C}]W_\mathrm{b}} \right) \tag{G18}$$

$$= [\mu(E)W_\mathrm{b}] \, \frac{1}{\mu(E) + \beta_\mathrm{C}} \, e^{-[\mu(E)+\beta_\mathrm{C}]W_\mathrm{b}} \left(1 + \frac{1}{[\mu(E) + \beta_\mathrm{C}]W_\mathrm{b}} \right) . \tag{G19}$$

The third factor in Eq. (G19) equals $\frac{1}{\mu(E)} \, \frac{1}{1+\beta_\mathrm{C}/\mu(E)} \leq \frac{1}{\mu(E)} \, \frac{\mu(E)}{\beta_\mathrm{C}}$. The exponential in Eq. (G19) is bounded as $e^{-\mu(E)W_\mathrm{b}} \, e^{-\beta_\mathrm{C}W_\mathrm{b}} \leq e^{-\beta_\mathrm{C}W_\mathrm{b}}$, since $\mu(E)W_\mathrm{b} \geq 0$. Equation (G1) implies that $\frac{\mu(E)}{\beta_\mathrm{C}} \cdot \frac{1}{\mu(E)W_\mathrm{b}} \ll 1$. Therefore, the final factor in Eq. (G19) is $1 + \frac{1}{[\mu(E)+\beta_\mathrm{C}]W_\mathrm{b}} = 1 + \frac{1}{1+[\beta_\mathrm{C}/\mu(E)]} \cdot \frac{1}{\mu(E)W_\mathrm{b}} \leq 1 + \frac{\mu(E)}{\beta_\mathrm{C}} \cdot \frac{1}{\mu(E)W_\mathrm{b}} \leq 2$. Therefore,

$$\epsilon \leq \frac{2}{\mu(E)} \, [\mu(E)W_\mathrm{b}] \, \frac{\mu(E)}{\beta_\mathrm{C}} \, e^{-\beta_\mathrm{C}W_\mathrm{b}} = \frac{1}{\mu(E)} \, O\left([\mu(E)W_\mathrm{b}] \, \frac{\mu(E)}{\beta_\mathrm{C}} \, e^{-\beta_\mathrm{C}W_\mathrm{b}} \right) . \tag{G20}$$

Extending the upper integration limit in $\mathcal{I}_2''$ has strengthened the integral's likeness to the Riemann Zeta function. We strengthen the likeness also by decomposing $\frac{1}{1+e^{\beta_\mathrm{C}\delta}}$ into $\frac{1}{e^{\beta_\mathrm{C}\delta}-1} - \frac{2}{e^{2\beta_\mathrm{C}\delta}-1}$:

$$\mathcal{I}_2'' = \mu(E) \int_0^{\infty} d\delta \, \frac{\delta \, e^{-\mu(E)\delta}}{e^{\beta_\mathrm{C}\delta} - 1} - 2\mu(E) \int_0^{\infty} d\delta \, \frac{\delta \, e^{-\mu(E)\delta}}{e^{2\beta_\mathrm{C}\delta} - 1} + O\left([\mu(E)W_\mathrm{b}] \, \frac{\mu(E)}{\beta_\mathrm{C}} \, e^{-\beta_\mathrm{C}W_\mathrm{b}} \right) . \tag{G21}$$

We Taylor-approximate the numerators' exponentials to zeroth order. Equivalently, we approximate each integral to second order in $\frac{\mu(E)}{\beta_\mathrm{C}}$. To explain, we focus on the first integral, for simplicity. The first-order term in $e^{-\mu(E)\delta}$ has the form $-\mu(E) \, \delta$. This term appears in the whole-integral term $-\mu^2(E) \int_0^{\infty} d\delta \, \frac{\delta^2}{e^{\beta_\mathrm{C}\delta}-1}$. We multiply and divide by $\mu(E) \, (\beta_\mathrm{C})^3$. Redefining $\beta_\mathrm{C}\delta$ as x yields $-\frac{1}{\mu(E)} \left(\frac{\mu(E)}{\beta_\mathrm{C}} \right)^3 \int_0^{\infty} dx \, \frac{x^2}{e^x - 1} = \frac{1}{\mu(E)} \, O\left(\left[\frac{\mu(E)}{\beta_\mathrm{C}} \right]^3 \right)$. The lowest-order neglected term is indeed negligible. Equation (G21) approximates to

$$\mathcal{I}_2'' = \mu(E) \int_0^{\infty} d\delta \, \frac{\delta}{e^{\beta_\mathrm{C}\delta} - 1} - 2\mu(E) \int_0^{\infty} d\delta \, \frac{\delta}{e^{2\beta_\mathrm{C}\delta} - 1} + O\left([\mu(E)W_\mathrm{b}] \, \frac{\mu(E)}{\beta_\mathrm{C}} \, e^{-\beta_\mathrm{C}W_\mathrm{b}} \right) + O\left(\left[\frac{\mu(E)}{\beta_\mathrm{C}} \right]^3 \right) . \tag{G22}$$

Consider rescaling the second integral's integration variable as $\delta \mapsto \frac{1}{2} \, \delta$. We combine the two integrals and rescale $\delta \mapsto \delta/\beta_\mathrm{C}$:

$$\mathcal{I}_2'' = \frac{1}{2} \, \frac{\mu(E)}{(\beta_\mathrm{C})^2} \int_0^{\infty} d\delta \, \frac{\delta}{e^{\delta} - 1} + O\left([\mu(E)W_\mathrm{b}] \, \frac{\mu(E)}{\beta_\mathrm{C}} \, e^{-\beta_\mathrm{C}W_\mathrm{b}} \right) + O\left(\left[\frac{\mu(E)}{\beta_\mathrm{C}} \right]^3 \right) \tag{G23}$$

$$= \frac{1}{2} \, \frac{\mu(E)}{(\beta_\mathrm{C})^2} \, \Gamma(2) \, \zeta(2) + O\left([\mu(E)W_\mathrm{b}] \, \frac{\mu(E)}{\beta_\mathrm{C}} \, e^{-\beta_\mathrm{C}W_\mathrm{b}} \right) + O\left(\left[\frac{\mu(E)}{\beta_\mathrm{C}} \right]^3 \right) . \tag{G24}$$

The Gamma function evaluates, at two, to $\Gamma(2) = 1$. The Riemann zeta function evaluates, at two, to $\zeta(2) = \frac{\pi^2}{6}$. Substituting from Eq. (G24) into Eq. (G14) yields

$$\mathcal{I}_2 = \frac{1}{2}\,\mu(E)\,(W_{\rm b})^2 - \frac{\pi^2}{12}\,\frac{\mu(E)}{(\beta_{\rm C})^2} + O\left([\mu(E)\,W_{\rm b}]^3\right) + O\left([\mu(E)\,W_{\rm b}]\,\frac{\mu(E)}{\beta_{\rm C}}\,e^{-\beta_{\rm C}W_{\rm b}}\right) + O\left(\left[\frac{\mu(E)}{\beta_{\rm C}}\right]^3\right). \tag{G25}$$

We have calculated the second integral in Eq. (G10).

G 4 iic Evaluating the upward-hop integral: The first integral in Eq. (G10) has the form

$$\mathcal{I}_1 := \mu(E)\int_0^{W_{\rm b}} d\delta\cdot\delta\,\frac{e^{-\beta_{\rm C}\delta}}{1+e^{-\beta_{\rm C}\delta}}\,e^{-\mu(E)\delta} \tag{G26}$$

$$= \mu(E)\int_0^{W_{\rm b}} d\delta\,\frac{\delta\,e^{-\mu(E)\delta}}{1+e^{\beta_{\rm C}\delta}} \tag{G27}$$

$$= \frac{\pi^2}{12}\,\frac{\mu(E)}{(\beta_{\rm C})^2} + O\left([\mu(E)\,W_{\rm b}]\,\frac{\mu(E)}{\beta_{\rm C}}\,e^{-\beta_{\rm C}W_{\rm b}}\right) + O\left(\left[\frac{\mu(E)}{\beta_{\rm C}}\right]^3\right). \tag{G28}$$

The second equality follows from multiplying the numerator and the denominator by $e^{\beta_{\rm C}\delta}$. The final equality follows from recognizing (G27) as $\mathcal{I}_2''$ [Eq. (G15)]. $\mathcal{I}_2''$ is evaluated in Eq. (G24), which is copied into (G28).

G 4 iid Combining the downward-drop and upward-hop integrals: Substituting from Eqs. (G28) and (G25) into Eq. (G10) yields

$$\left\langle \left\langle Q_2(E)\right\rangle_{\substack{\rm cold\\ \rm therm.}}\right\rangle_{\rm gaps} = -\frac{1}{2}\,\mu(E)\,(W_{\rm b})^2 + \frac{\pi^2}{6}\,\frac{\mu(E)}{(\beta_{\rm C})^2} + O\left([\mu(E)\,W_{\rm b}]^3\right) + O\left([\mu(E)\,W_{\rm b}]\,\frac{\mu(E)}{\beta_{\rm C}}\,e^{-\beta_{\rm C}W_{\rm b}}\right) + O\left(\left[\frac{\mu(E)}{\beta_{\rm C}}\right]^3\right). \tag{G29}$$

G 4 iii Thermal average with respect to the initial density operator

We must integrate Eq. (G29) over energies E, weighted by the initial-state Gibbs distribution:

$$\langle Q_2\rangle := \left\langle \left\langle \left\langle Q_2(E)\right\rangle_{\substack{\rm cold\\ \rm therm.}}\right\rangle_{\rm gaps}\right\rangle_{\rho(0)} \tag{G30}$$

$$= \left(-\frac{(W_{\rm b})^2}{2} + \frac{\pi^2}{6}\,\frac{1}{(\beta_{\rm C})^2}\right)\int_{-\infty}^{\infty} dE\;\mu^2(E)\,\frac{e^{-\beta_{\rm H}E}}{Z} + O\left(\left[\frac{W_{\rm b}}{\langle\delta\rangle}\right]^3\right) + O\left(\frac{W_{\rm b}}{\langle\delta\rangle}\,e^{-\beta_{\rm C}W_{\rm b}}\right) + O\left(\left[\frac{\mu(E)}{\beta_{\rm C}}\right]^3\right). \tag{G31}$$

The DOS's sharp peaking about $E = 0$ justifies our approximation of the energy integral as extending between $\pm\infty$. We substitute in for the DOS from Eq. (D1):

$$\langle Q_2\rangle = \frac{\mathcal{N}^2}{2\pi N\mathcal{E}^2}\,\frac{1}{Z}\left(-\frac{(W_{\rm b})^2}{2} + \frac{\pi^2}{6}\,\frac{1}{(\beta_{\rm C})^2}\right)\int_{-\infty}^{\infty} dE\;e^{-E^2/N\mathcal{E}^2}\;e^{-\beta_{\rm H}E} + O(.)\,. \tag{G32}$$

We have abbreviated the correction terms as $O(.)$. The integral evaluates to $\sqrt{\pi N}\,\mathcal{E}\,e^{N(\beta_{\rm H}\mathcal{E})^2/4}$. The partition function is

$$Z = \int_{-\infty}^{\infty} dE\;\mu(E)e^{-\beta_{\rm H}E} = \mathcal{N}e^{N(\beta_{\rm H}\mathcal{E})^2/2}\,. \tag{G33}$$

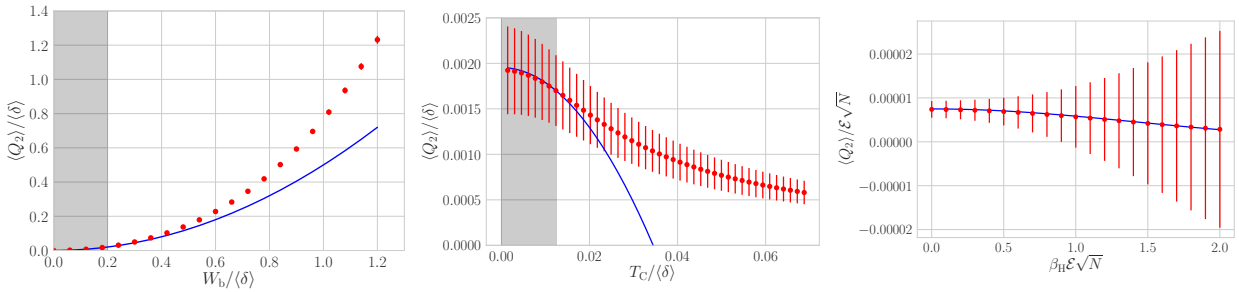

(a) $\langle Q_2\rangle$ vs. W_b at $T_C = 0$ and $T_H = \infty$

(b) $\langle Q_2\rangle$ vs. T_C at $T_H = \infty$ and $W_b = 2^{-4}\langle\delta\rangle$

(c) $\langle Q_2\rangle$ vs. β_H at $T_C = 0$ and $W_b = 2^{-4}\langle\delta\rangle$

FIG. 9: Absolute value $|\langle Q_2\rangle|$ of the average heat absorbed during cold thermalization (stroke 2) as a function of the cold-bath bandwidth W_b, the cold-bath temperature T_C, and the hot-bath temperature $T_H = 1/\beta_H$: We numerically simulated a mesoscale engine of $N = 12$ sites governed by the random-field Heisenberg Hamiltonian (24). Each red dot represents numerical simulations of 1,000 disorder realizations. The blue lines represent the absolute value of the analytical prediction (G34). The disorder strengths and error bars are discussed in Sec. III. The analytics match the numerics' shapes, and the agreement is fairly close, in the appropriate limits (where $\frac{W_b}{\langle\delta\rangle} \ll 1$ and $T_C/\langle\delta\rangle \ll 1$, in the gray shaded regions). The analytics systematically underestimate $\langle Q_2\rangle$ at fixed W_b. This underestimation stems from the small level repulsion that persists at finite N. The analytical prediction (G34) substantially underestimates $\langle Q_2\rangle$ when the cold-bath bandwidth is large, $W_b \gtrsim \langle\delta\rangle$. Such disagreement is expected: $\frac{W_b}{\langle\delta\rangle} \ll 1$ is assumed in the analytical calculation. Hence chains of small gaps $\delta'_j, \delta'_{j+1} \cdots < W_b$ are neglected in the analytics. Such chains proliferate as W_b grows. A similar reason accounts for the curve's crossing the origin in Fig. 9b: We analytically compute $\langle Q_2\rangle$ only to second order in $T_C/\langle\delta\rangle$.

Substituting into Eq. (G32) yields

$$\langle Q_2\rangle = \frac{\mathcal{N}}{2\sqrt{\pi N}\,\mathcal{E}}\left(-\frac{(W_b)^2}{2} + \frac{\pi^2}{6}\,\frac{1}{(\beta_C)^2}\right) e^{-N(\beta_H\mathcal{E})^2/4} + O(.) \tag{G34}$$

$$= \left(-\frac{(W_b)^2}{2\langle\delta\rangle} + \frac{\pi^2}{6}\,\frac{1}{(\beta_C)^2\langle\delta\rangle}\right) e^{-N(\beta_H\mathcal{E})^2/4} + O\left(\left[\frac{W_b}{\langle\delta\rangle}\right]^3\right) + O\left([\mu(E)\,W_b]\,\frac{\mu(E)}{\beta_C}\,e^{-\beta_C W_b}\right)$$
$$+ O\left(\left[\frac{\mu(E)}{\beta_C}\right]^3\right) + O\left(\left[\sqrt{N}\,\beta_H\mathcal{E}\right]^4\right). \tag{G35}$$

The prefactor was replaced with $\frac{1}{\langle\delta\rangle}$ via Eq. (D3).

Equation (G34) is compared with numerical simulations in Fig. 9. In the appropriate regime (wherein $W_b \ll \langle\delta\rangle$ and $T_C \ll W_b$), the analytics agree well with the numerics, to within finite-size effects.

In terms of small dimensionless parameters,

$$\langle Q_2\rangle = \langle\delta\rangle\left[\frac{1}{2}\left(-\frac{W_b}{\langle\delta\rangle}\right)^2 + \frac{\pi^2}{6}\,\frac{1}{(\beta_C\langle\delta\rangle)^2}\right]\left[1 - \frac{N}{4}\,(\beta_H\mathcal{E})^2\right] + O(.)\,. \tag{G36}$$

The leading-order term is second-order. So is the β_C correction; but the correction is much smaller than the leading-order term, by assumption [Eq. (G1)]. The β_H correction is fourth-order—too small to include. To lowest order, therefore,

$$\boxed{\langle Q_2\rangle \approx -\frac{(W_b)^2}{2\langle\delta\rangle}}\,. \tag{G37}$$

G 5 Average heat $\langle Q_4\rangle$ absorbed during stroke 4

The $\langle Q_4\rangle$ calculation proceeds similarly to the $\langle Q_2\rangle$ calculation: We initially focus on one trial. We suppose that the engine begins the trial in level j. We model the heat absorbed during that trial, then average over cold-thermalization

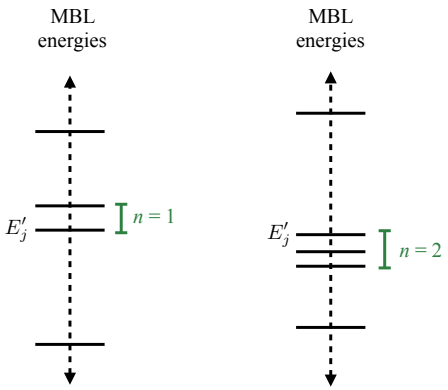

FIG. 10: Dominant chains of small MBL-Hamiltonian gaps: The engine thermalizes with a cold bath, while in the MBL phase, during stroke 2. The thermalization can transfer the engine's state across gaps no larger than the bath bandwidth, $W_{\rm b}$. A chain of $n = 0, 1, 2, \ldots$ small gaps might neighbor each other in the $H_{\rm MBL}$ spectrum. The nonnegligible contributions to $\langle Q_4 \rangle$ (the average heat absorbed during stroke 4) derive from $n = 1, 2$ chains. E'_j denotes the energy of the Hamiltonian eigenstate in which the engine starts stroke 2 in some trial.

probabilities and over gap distributions (over disorder realizations). Finally, we average over initial levels j, using the thermal distribution $\left\{ e^{-\beta_{\rm H} E_j} / Z \right\}$.

However, $\langle Q_4 \rangle$ requires more calculation than $\langle Q_2 \rangle$ required. When calculating $\langle Q_2 \rangle$, we neglected contributions from the engine's dropping across a pair of neighboring small gaps during cold thermalization. Two successive gaps have a probability $\sim \left(\frac{W_{\rm b}}{\langle \delta \rangle} \right)^2$ of being small (of size $< W_{\rm b}$). Thermalizing across each gap produces an amount $\leq W_{\rm b}$ of heat. Each pair of small gaps therefore contributes negligibly to $\langle Q_2 \rangle$, as $\langle \delta \rangle \, O\left(\left[\frac{W_{\rm b}}{\langle \delta \rangle} \right]^3 \right)$

We cannot neglect pairs of small MBL gaps when calculating $\langle Q_4 \rangle$. Each typical small gap widens, during stroke 3, to become of size $\sim \langle \delta \rangle$. These larger gaps are thermalized across during stroke 4, contributing an amount $\sim \langle \delta \rangle \, O\left(\left[\frac{W_{\rm b}}{\langle \delta \rangle} \right]^2 \right)$ to $\langle Q_4 \rangle$. Second-order contributions are not negligible. Chains of ≥ 3 small MBL gaps contribute negligibly, however.

We begin by constructing a formula accurate to all orders. Then, we evaluate the one-gap and two-gap terms.

G 5 i Exact expression for $\langle Q_4 \rangle$

Suppose that the engine, S, begins on level j in the trial of interest. The final, outermost average is over j, implemented with thermal weights $e^{-\beta_{\rm H} E_j} / Z$.

Let $P(n|j)$ denote the probability that the $j^{\rm th}$ MBL level occupies a chain of exactly n small gaps. n runs from 0 (level j may neighbor two large gaps) to $\mathcal{N} - 1$ (all the MBL gaps may be small). Figure 10 illustrates the $n = 1, 2$ cases. The $n = 0$ term contributes nothing to $\langle Q_4 \rangle$: If S cannot traverse any gaps during stroke 2, S requires no heat to reset during stroke 4 (on average, as shown below).

Let $\hat{P}(\hat{j}|n, j)$ denote the probability that, if S started some trial on level j, if the $j^{\rm th}$ MBL level occupies a chain of exactly n small gaps, cold thermalization leaves S on the $\hat{j}^{\rm th}$ rung of the small-gap chain. $\hat{j}$ runs from 0 (S may end stroke 2 on the chain's bottom rung) to n (S may end stroke 2 on the top rung). Figure 11a illustrates this notation.

Let k denote the index, in the many-body spectrum, of the small-gap chain's bottom rung. If j is the chain's bottom rung, for example, $k = j$. Figure 11b illustrates this and other examples.

$P^{(E)}_{\rm GOE}(\delta)$ denotes the probability per unit energy that the gap at energy E_j in the $H_{\rm GOE}$ spectrum is of size δ . The gap size lies between 0 and the $H_{\rm GOE}$ bandwidth $E_{\rm max} - E_{\rm min}$. We approximate the bandwidth with ∞, as integrands peak sufficiently sharply at finite δ values.

We have specified four probabilities and probability densities over which to average: $e^{-\beta_{\rm H} E_j} / Z$, $P(n|j)$, $\hat{P}(\hat{j}|n, j)$, and $P^{(E)}_{\rm GOE}(\delta)$. What must we average? The energy required to reset the engine during stroke 4. S ends stroke 4 on an $H_{\rm GOE}$ level ι selected randomly according to a Gibbs distribution $\left\{ e^{-\beta_{\rm H} E_\iota} / Z \right\}$. Consider, for simplicity, fixing n,

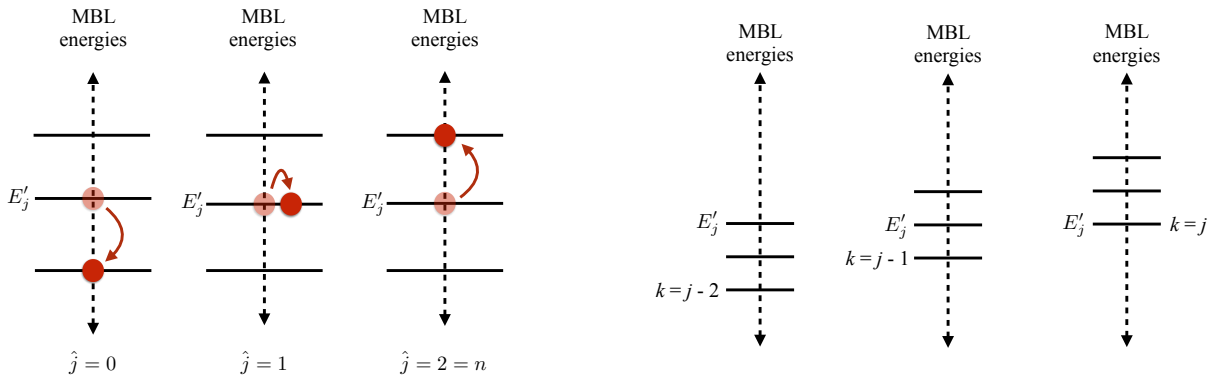

(a) **(b)**

FIG. 11: Notation for chains of small gaps in the MBL Hamiltonian's spectrum: The average heat absorbed during stroke 4, $\langle Q_4 \rangle$, depends on which gaps the engine thermalizes across during stroke 2. The engine, S, can thermalize across gaps no larger than the cold bath's bandwidth, $W_{\rm b}$. Suppose that S begins stroke 2 on energy level j, in a chain of $n = 2$ small gaps. E'_j denotes the engine's start-of-stroke-2 energy. $\hat{j}$ denotes the index, within the chain, of the level on which S ends stroke 2. $\hat{j}$ runs from 0 to n, as illustrated in Fig. 11a. k denotes the index, within the many-body spectrum, of the level on which S ends stroke 2. k runs from $j - n$ to j, as illustrated in Fig. 11b.

k, and $\hat{j}$. The average reset heat equals

$$\sum_j \frac{e^{-\beta_{\rm H} E_j}}{Z} \sum_\iota \frac{e^{-\beta_{\rm H} E_\iota}}{Z} \left(E_\iota - E_{\hat{j}+k} \right) = \sum_\iota \frac{e^{-\beta_{\rm H} E_\iota}}{Z} E_\iota - \sum_j \frac{e^{-\beta_{\rm H} E_j}}{Z} E_{\hat{j}+k} \, . \tag{G38}$$

We have invoked the probability distribution's normalization. The right-hand side's ι is a dummy index; we can relabel it as j. The first term can then be combined with the second. $\langle Q_4 \rangle$ becomes $\sum_j \frac{e^{-\beta_{\rm H} E_j}}{Z} \left(E_j - E_{\hat{j}+k} \right)$. Stroke 4 resets S to the level j on which S began the trial, on average. We can rewrite $E_j - E_{\hat{j}+k}$ as the sum of gaps $\sum_{\ell=0}^{n} \Delta_{k+\ell}$. $\Delta_{k+\ell}$ denotes the $\ell^{\rm th}$ gap from the chain's bottom. Each gap must be disorder-averaged individually, as in

$$\sum_{\ell=0}^{n} \left[\int_0^\infty d\Delta_{k+\ell} \, P_{\rm GOE}^{(E_{k+\ell})}(\Delta_{k+\ell}) \, \Delta_{k+\ell} \right] = \sum_{\ell=0}^{n} \langle \delta \rangle_{E_{k+\ell}} \, . \tag{G39}$$

The average heat absorbed during stroke 3 therefore equals

$$\langle Q_4 \rangle = \sum_j \frac{e^{-\beta_{\rm H} E_j}}{Z} \sum_{n=1}^{\mathcal{N}-1} P(n|j) \sum_{\hat{j}=0}^{n} \hat{P}(\hat{j}|n,j) \sum_{k=j-n}^{j} \sum_{\ell=1}^{n} \langle \delta \rangle_{E_{k+\ell}} \, . \tag{G40}$$

The average gap remains nearly constant throughout the chain. The correction is a factor of $\frac{1}{\mathcal{N}}$ smaller than the leading-order term.[11] We will omit the correction from our error accounting, which is intended to highlight dependence on the small parameters in App. G 2. The sum over ℓ equals the average gap times the number $(j - \hat{j} - k)$ of gaps that

[11] How does the average gap, $\langle \delta \rangle_E = \frac{1}{\mu(E)}$, change with the energy E? The relative change in the average gap is

$$\frac{\Delta \langle \delta \rangle_E}{\langle \delta \rangle_E} = \frac{1}{1/\mu(E)} \left(\frac{d}{dE} \frac{1}{\mu(E)} \cdot dE \right) . \tag{G41}$$

The $dE = \langle \delta \rangle_E$ cancels with the leftmost $\frac{1}{1/\mu(E)}$. We substitute in for $\mu(E)$ from Eq. (D1), then differentiate: $\frac{\Delta \langle \delta \rangle_E}{\langle \delta \rangle_E} = \sqrt{\frac{2\pi}{N}} \frac{E}{\mathcal{N}\mathcal{E}} e^{E^2/2N\mathcal{E}^2}$. The energies of interest occupy a band, centered at $E = 0$, of width $\sim \mathcal{E}\sqrt{N}$. In the worst case (when the relative change is largest), $E \sim \mathcal{E}\sqrt{N}$, such that $\frac{\Delta \langle \delta \rangle_E}{\langle \delta \rangle_E} \sim \frac{1}{\mathcal{N}}$.

S must climb, during stroke 4, to return to its start-of-cycle level: $\sum_{\ell=1}^{n} \langle\delta\rangle_{E_{k+\ell}} = \frac{1}{\mu(E_j)} (j - \hat{j} - k)$. Equation (G40) becomes

$$\langle Q_4 \rangle = \sum_j \frac{e^{-\beta_{\rm H} E_j}}{Z} \sum_{n=1}^{\mathcal{N}-1} P(n|j) \sum_{\hat{j}=0}^{n} P(\hat{j}|n,j) \sum_{k=j-n}^{j} \frac{1}{\mu(E_j)} (j - \hat{j} - k) . \tag{G42}$$

We can calculate $P(n|j)$ for all n. $P(n|j)$ denotes the probability that the $j^{\rm th}$ $H_{\rm MBL}$ level occupies a chain of exactly n small gaps. The density of states, $\mu(E'_j)$, remains nearly constant throughout the chain, as $\langle\delta\rangle_E$ does (see footnote 11):

$$\begin{aligned} P(n|j) &= (\text{Prob. that some particular gap is small})^n (\text{Prob. that the gap just below the chain is large}) \\ &\quad \times (\text{Prob. that the gap just above the chain is large}) \qquad \text{(G43)} \\ &\equiv (F_j)^n (G_j)^2 . \qquad \text{(G44)} \end{aligned}$$

We have defined

$$\begin{aligned} F_j &:= \int_0^{W_{\rm b}} d\delta \; P_{\rm MBL}^{(E'_j)}(\delta) \qquad \text{(G45)} \\ &= 1 - e^{-\mu(E'_j) W_{\rm b}} \qquad \text{(G46)} \\ &= \mu(E'_j) W_{\rm b} - \frac{1}{2} \left[\mu(E'_j) W_{\rm b}\right]^2 + O\left(\left[\mu(E'_j) W_{\rm b}\right]^3\right) \qquad \text{(G47)} \end{aligned}$$

as the probability that any given $H_{\rm MBL}$ gap (far from the energy band's edges) is small. We have defined

$$\begin{aligned} G_j &:= \int_{W_{\rm b}}^{\infty} d\delta \; P_{\rm MBL}^{(E'_j)}(\delta) = 1 - F_j \qquad \text{(G48)} \\ &= e^{-\mu(E'_j) W_{\rm b}} \qquad \text{(G49)} \\ &= 1 - \mu(E'_j) W_{\rm b} + \frac{1}{2} \left[\mu(E'_j) W_{\rm b}\right]^2 + O\left(\left[\mu(E'_j) W_{\rm b}\right]^3\right) \qquad \text{(G50)} \end{aligned}$$

as the probability that any given $H_{\rm MBL}$ gap (far from the energy band's edges) is large. Squaring the right-hand side of Eq. (G50) yields

$$(G_j)^2 = 1 - 2\mu(E'_j) W_{\rm b} + 2\left[\mu(E'_j) W_{\rm b}\right]^2 + O\left(\left[\mu(E'_j) W_{\rm b}\right]^3\right) . \tag{G51}$$

We substitute from Eqs. (G51) and (G47) into Eq. (G44) to evaluate $P(n|j)$ at $n = 1, 2$. Consider a chain of exactly one small gap, illustrated in the left-hand side of Fig. 10. The probability that E'_j occupies such a one-gap chain equals

$$\begin{aligned} P(1|j) &= F_j (G_j)^2 \qquad \text{(G52)} \\ &= \mu(E'_j) W_{\rm b} - \frac{5}{2} \left[\mu(E'_j) W_{\rm b}\right]^2 + O\left(\left[\mu(E'_j) W_{\rm b}\right]^3\right) . \qquad \text{(G53)} \end{aligned}$$

Consider a chain of exactly two small gaps, illustrated in the right-hand side of Fig. 10. E'_j has a probability

$$\begin{aligned} P(2|j) &= (F_j)^2 (G_j)^2 \qquad \text{(G54)} \\ &= \left[\mu(E'_j) W_{\rm b}\right]^2 + O\left(\left[\mu(E'_j) W_{\rm b}\right]^3\right) \qquad \text{(G55)} \end{aligned}$$

of occupying a two-gap chain.

Let us evaluate the $n = 1$ and $n = 2$ terms in Eq. (G42).

G 5 ii Contribution to $\langle Q_4 \rangle$ from chains of exactly $n = 1$ small gap

First, we calculate $P(\hat{j}|n{=}1, j)$. Then, we substitute into Eq. (G42) and compute the sums.

$P(\hat{j}|n{=}1,j)$ equals the probability that, if S began the trial of interest in level j, and if the MBL energy E'_j occupies a chain of exactly one small gap, cold thermalization leaves S in the chain's $\hat{j}^{\text{th}}$ level. $\hat{j}$ runs from 0 (S might end on the chain's bottom rung) to 1 (S might end on the top rung). We compute the values individually.

S has a probability

$$P(\hat{j}{=}1|n{=}1,j) = \frac{1}{F_j} \int_0^{W_{\rm b}} d\delta \, \Big[\mu(E'_j) \, e^{-\mu(E'_j)\delta} \Big] \, \frac{e^{-\beta_{\rm C}\delta}}{1+e^{-\beta_{\rm C}\delta}} \tag{G56}$$

of ending stroke 2 atop the one-small-gap chain. The $\frac{1}{F_j}$ conditions the probability on the chain's containing exactly one small gap, as in Bayes' Theorem. [The denominator implicitly contains a $(G_j)^2$ that cancelled with a $(G_j)^2$ implicit in the numerator. The complete denominator equals $P(n{=}1|j) = F_j (G_j)^2$, by Eq. (G52).] We multiply the detailed-balance probability's numerator and denominator by $e^{\beta_{\rm C}\delta}$.

Extending the upper integration limit to ∞ simplifies the integral. The extension incurs an error ϵ. We bound this ϵ as we bounded the ϵ in Eq. (G16) (we are redefining the symbol ϵ):

$$\epsilon := \frac{\mu(E'_j)}{F_j} \int_{W_{\rm b}}^{\infty} d\delta \, e^{-\mu(E'_j)\delta} \, \frac{1}{1+e^{\beta_{\rm C}\delta}} \, . \tag{G57}$$

Since $\frac{1}{1+e^{\beta_{\rm C}\delta}} \leq e^{-\beta_{\rm C}\delta}$, Therefore,

$$\epsilon \leq \frac{\mu(E'_j)}{F_j} \int_{W_{\rm b}}^{\infty} d\delta \, e^{-[\mu(E'_j)+\beta_{\rm C}]\delta} = \frac{\mu(E'_j)}{F_j} \, \frac{1}{\mu(E'_j)+\beta_{\rm C}} \, e^{-\mu(E'_j)W_{\rm b}} \, e^{-\beta_{\rm C}W_{\rm b}} \tag{G58}$$

$$\leq \frac{1}{F_j} \, \frac{1}{1+\beta_{\rm C}/\mu(E'_j)} \, e^{-\beta_{\rm C}W_{\rm b}} \, . \tag{G59}$$

The final inequality follows from $\frac{W_{\rm b}}{\langle\delta\rangle} \ll 1$. The second factor is $\leq \frac{\mu(E'_j)}{\beta_{\rm C}}$. The $\frac{1}{F_j}$ will cancel with the $P(1|j) \propto F_j$ in Eq. (G42). Inequality (G59) therefore implies that

$$\epsilon = \frac{1}{F_j} \, O\left(\frac{\mu(E'_j)}{\beta_{\rm C}} \, e^{-\beta_{\rm C}W_{\rm b}} \right) . \tag{G60}$$

The $e^{-\beta_{\rm C}W_{\rm b}}$ is negligible. Equation (G56) becomes

$$P(\hat{j}{=}1|n{=}1,j) = \frac{\mu(E'_j)}{F_j} \int_0^{\infty} d\delta \, e^{-\mu(E'_j)\delta} \, \frac{1}{1+e^{\beta_{\rm C}\delta}} + \frac{1}{F_j} \, O\left(\frac{\mu(E'_j)}{\beta_{\rm C}} \, e^{-\beta_{\rm C}W_{\rm b}} \right) . \tag{G61}$$

The first exponential has the Taylor expansion $e^{-\mu(E'_j)\delta} = \sum_{r=0}^{\infty} \frac{1}{r!} \big[-\mu(E'_j)\delta \big]^r$. After substituting into Eq. (G61), we rearrange terms. If $x := \beta_{\rm C}\delta$,

$$P(\hat{j}{=}1|n{=}1,j) = \frac{\mu(E'_j)}{F_j \, \beta_{\rm C}} \sum_{r=0}^{\infty} \left(-\frac{\mu(E'_j)}{\beta_{\rm C}} \right)^r \left(\frac{1}{r!} \int_0^{\infty} dx \, \frac{x^r}{1+e^x} \right) + \frac{1}{F_j} \, O\left(\frac{\mu(E'_j)}{\beta_{\rm C}} \, e^{-\beta_{\rm C}W_{\rm b}} \right) \tag{G62}$$

$$= \frac{\mu(E'_j)}{F_j \, \beta_{\rm C}} \sum_{r=0}^{\infty} \eta(r+1) \left(-\frac{\mu(E'_j)}{\beta_{\rm C}} \right)^r + \frac{1}{F_j} \, O\left(\frac{\mu(E'_j)}{\beta_{\rm C}} \, e^{-\beta_{\rm C}W_{\rm b}} \right) . \tag{G63}$$

The Dirichlet eta function, evaluated at $r+1$, is denoted by $\eta(r+1)$.

We have calculated the conditional probability $P(\hat{j}{=}1|n{=}1,j)$ that cold thermalization leaves S at the top of a chain of exactly one small gap. If S does not end at the top, S ends at the bottom. By the probabilities' normalization,

$$P(\hat{j}{=}0|n{=}1,j) = 1 - P(\hat{j}{=}1|n{=}1,j) \, . \tag{G64}$$

Having calculated the $P(\hat{j}|n{=}1,j)$'s, we will substitute into the contribution, to $\langle Q_4 \rangle$, of chains of exactly $n = 1$ small gap. We label that contribution $\big\langle Q_4^{n=1} \big\rangle$. By Eq. (G42),

$$\big\langle Q_4^{n=1} \big\rangle = \sum_j \frac{e^{-\beta_{\rm H}E_j}}{Z} \, \frac{P(n{=}1|j)}{\mu(E_j)} \Big[P(\hat{j}{=}0|n{=}1,j) - P(\hat{j}{=}1|n{=}1,j) \Big] \, . \tag{G65}$$

The bracketed factor equals

$$1-2P(\hat{j}{=}1|n{=}1,j)=1-2\,\frac{\mu(E'_j)}{F_j\,\beta_{\rm C}}\sum_{r=0}^{\infty}\eta(r+1)\left(-\frac{\mu(E'_j)}{\beta_{\rm C}}\right)^r+\frac{1}{F_j}\,O\left(\frac{\mu(E'_j)}{\beta_{\rm C}}\,e^{-\beta_{\rm C}W_{\rm b}}\right), \tag{G66}$$

by Eqs. (G64) and (G63). Substituting into Eq. (G65) from Eqs. (G66) and (G52) yields

$$\begin{aligned}\left\langle Q_4^{n=1}\right\rangle=&\sum_j\frac{e^{-\beta_{\rm H}E_j}}{Z}\,\frac{F_j\,(G_j)^2}{\mu(E_j)}-\frac{2}{\beta_{\rm C}}\sum_j\frac{e^{-\beta_{\rm H}E_j}}{Z}\,(G_j)^2\,\frac{\mu(E'_j)}{\mu(E_j)}\left[\sum_{r=0}^{\infty}\eta(r+1)\left(-\frac{\mu(E'_j)}{\beta_{\rm C}}\right)^r\right]\\&+\sum_j\frac{e^{-\beta_{\rm H}E_j}}{Z}\,\frac{F_j\,(G_j)^2}{\mu(E_j)}\cdot\frac{1}{F_j}\,O\left(\frac{\mu(E'_j)}{\beta_{\rm C}}\,e^{-\beta_{\rm C}W_{\rm b}}\right).\end{aligned} \tag{G67}$$

Substituting in for $F_j\,(G_j)^2$ from Eq. (G53), and for $(G_j)^2$ from Eq. (G51), yields

$$\begin{aligned}\left\langle Q_4^{n=1}\right\rangle=&\sum_j\frac{e^{-\beta_{\rm H}E_j}}{Z}\,\frac{1}{\mu(E_j)}\left\{\mu(E'_j)W_{\rm b}-\frac{5}{2}\left[\mu(E'_j)W_{\rm b}\right]^2+O\left(\left[\mu(E'_j)W_{\rm b}\right]^3\right)\right\}\\&-\frac{2}{\beta_{\rm C}}\sum_j\frac{e^{-\beta_{\rm H}E_j}}{Z}\left\{1-2\mu(E'_j)W_{\rm b}+2\left[\mu(E'_j)W_{\rm b}\right]^2+O\left(\left[\mu(E'_j)W_{\rm b}\right]^3\right)\right\}\frac{\mu(E'_j)}{\mu(E_j)}\\&\times\left[\sum_{r=0}^{\infty}\eta(r+1)\left(-\frac{\mu(E'_j)}{\beta_{\rm C}}\right)^r\right]+\sum_j\frac{e^{-\beta_{\rm H}E_j}}{Z}\,\frac{1}{\mu(E_j)}\,O\left(\frac{\mu(E'_j)}{\beta_{\rm C}}\,e^{-\beta_{\rm C}W_{\rm b}}\right).\end{aligned} \tag{G68}$$

As usual, the sums are approximated by integrals. We assume that $\mu(E_j)\approx\mu(E'_j)$:

$$\begin{aligned}\left\langle Q_4^{n=1}\right\rangle=&\int_{-\infty}^{\infty}dE\,\frac{e^{-\beta_{\rm H}E}}{Z}\left\{\mu(E)W_{\rm b}-\frac{5}{2}\left[\mu(E)W_{\rm b}\right]^2+O\left(\left[\mu(E)W_{\rm b}\right]^3\right)\right\}\\&-\frac{2}{\beta_{\rm C}}\int_{-\infty}^{\infty}dE\,\frac{e^{-\beta_{\rm H}E}}{Z}\,\mu(E)\left\{1-2\mu(E)W_{\rm b}+2\left[\mu(E)W_{\rm b}\right]^2+O\left(\left[\mu(E)W_{\rm b}\right]^3\right)\right\}\\&\times\left[\sum_{r=0}^{\infty}\eta(r+1)\left(-\frac{\mu(E)}{\beta_{\rm C}}\right)^r\right]+O\left(e^{-\beta_{\rm C}W_{\rm b}}\right).\end{aligned} \tag{G69}$$

We integrate, expressing the result in terms of $\langle\delta\rangle$. In the second integral, we keep only the two lowest-order terms in the $\{\ldots\}$ and only the two lowest-order terms in the $\sum_r$:

$$\begin{aligned}\left\langle Q_4^{n=1}\right\rangle=&\left\{W_{\rm b}-\frac{5}{2}\,\frac{(W_{\rm b})^2}{\langle\delta\rangle}\,e^{-N(\beta_{\rm H}\mathcal{E})^2/4}+O\left(\left[\frac{W_{\rm b}}{\langle\delta\rangle}\right]^3\right)\right\}+\left\{-\frac{2\eta(1)}{\beta_{\rm C}}+4\eta(1)\,\frac{W_{\rm b}}{\beta_{\rm C}\,\langle\delta\rangle}\,e^{-N(\beta_{\rm H}\mathcal{E})^2/4}\right.\\&\left.+2\eta(2)\,\frac{1}{(\beta_{\rm C})^2\,\langle\delta\rangle}\,e^{-N(\beta_{\rm H}\mathcal{E})^2/4}+O\left(\left[\frac{W_{\rm b}}{\langle\delta\rangle}\right]^2\frac{1}{\beta_{\rm C}\,\langle\delta\rangle}\right)+O\left(\left[\frac{1}{\beta_{\rm C}\,\langle\delta\rangle}\right]^3\right)+O\left(\frac{W_{\rm b}}{\langle\delta\rangle}\left[\frac{1}{\beta_{\rm C}\,\langle\delta\rangle}\right]^2\right)\right\}\\&+O\left(e^{-\beta_{\rm C}W_{\rm b}}\right).\end{aligned} \tag{G70}$$

We regroup terms, rearrange terms roughly in order from greatest to least, and express the sum in terms of small parameters:

$$\begin{aligned}\left\langle Q_4^{n=1}\right\rangle=&\langle\delta\rangle\left\{\frac{W_{\rm b}}{\langle\delta\rangle}-\frac{2\eta(1)}{\beta_{\rm C}\,\langle\delta\rangle}+\left[-\frac{5}{2}\left(\frac{W_{\rm b}}{\langle\delta\rangle}\right)^2+4\eta(1)\,\frac{W_{\rm b}}{\langle\delta\rangle}\,\frac{1}{\beta_{\rm C}\,\langle\delta\rangle}+2\eta(2)\,\frac{1}{(\beta_{\rm C}\,\langle\delta\rangle)^2}\right]\left[1-\frac{1}{4}N\,(\beta_{\rm H}\mathcal{E})^2\right]\right.\\&+O\left(\left[\frac{W_{\rm b}}{\langle\delta\rangle}\right]^3\right)+O\left(\left[\frac{W_{\rm b}}{\langle\delta\rangle}\right]^2\frac{1}{\beta_{\rm C}\,\langle\delta\rangle}\right)+O\left(\frac{W_{\rm b}}{\langle\delta\rangle}\left[\frac{1}{\beta_{\rm C}\,\langle\delta\rangle}\right]^2\right)+O\left(\left[\frac{1}{\beta_{\rm C}\,\langle\delta\rangle}\right]^3\right)\\&\left.+O\left(\left\{N\left[\beta_{\rm H}\mathcal{E}\right]^2\right\}^2\right)+O\left(e^{-\beta_{\rm C}W_{\rm b}}\right).\right\}\end{aligned} \tag{G71}$$

The lowest-order $\beta_{\rm H}$ corrections are too small to keep. So is the $O\left(\frac{1}{(\beta_{\rm C})^2\langle\delta\rangle}\right)$ term. Evaluating $\eta(1)=\ln 2$ yields

$$\boxed{\left\langle Q_4^{n=1}\right\rangle\approx W_{\rm b}-\frac{2\ln 2}{\beta_{\rm C}}-\frac{5}{2}\frac{(W_{\rm b})^2}{\langle\delta\rangle}+4\ln 2\,\frac{W_{\rm b}}{\beta_{\rm C}\,\langle\delta\rangle}}. \tag{G72}$$

G 5 iii Contribution $\left\langle Q_4^{n=2} \right\rangle$ to $\langle Q_4 \rangle$ from chains of exactly $n = 2$ small gaps

We must calculate the probabilities $P(\hat{j}|n{=}2, j)$ that, if S begins a trial in level j, and if the j^{th} MBL level occupies a chain of exactly $n = 2$ small gaps, cold thermalization leaves S on the chain's $\hat{j}^{\text{th}}$ rung. $\hat{j}$ runs from 0 to 2, as illustrated by the solid red dots in Fig. 11a. After calculating these conditional probabilities, we substitute into the $n = 2$ term of Eq. (G42).

G 5 iiia $P(\hat{j}{=}2|n{=}2, j)$: The engine may end stroke 2 on the top rung of a two-small-gap chain. The solid red dot on the right-hand side of Fig. 11a illustrates this scenario. Let δ_1 and δ_2 denote the bottom and top gaps. The conditional probability $P(\hat{j}{=}2|n{=}2, j)$ depends on the gaps' being small [on $P_{\text{MBL}}^{(E'_j)}(\delta_1)$ and on $P_{\text{MBL}}^{(E'_j)}(\delta_2)$], on the detailed-balance probability $\frac{e^{-\beta_{\text{C}}(\delta_1+\delta_2)}}{1+e^{-\beta_{\text{C}}\delta_1}+e^{-\beta_{\text{C}}(\delta_1+\delta_2)}}$, and on a Bayes normalization factor from Bayes' Theorem:

$$P(\hat{j}{=}2|n{=}2, j) = \frac{1}{(F_j)^2} \int_0^{W_{\text{b}}} d\delta_1 \left[\mu(E'_j)\, e^{-\mu(E'_j)\delta_1}\right] \int_0^{W_{\text{b}}} \left[\mu(E'_j)\, e^{-\mu(E'_j)\delta_2}\right] \frac{e^{-\beta_{\text{C}}(\delta_1+\delta_2)}}{1 + e^{-\beta_{\text{C}}\delta_1} + e^{-\beta_{\text{C}}(\delta_1+\delta_2)}} \,. \tag{G73}$$

To simplify the integral, we multiply and divide by $e^{\beta_{\text{C}}(\delta_1+\delta_2)}$. Defining

$$z \equiv z(\delta_1) := \frac{1}{1 + e^{\beta_{\text{C}}\delta_1}} \tag{G74}$$

yields

$$P(\hat{j}{=}2|n{=}2, j) = \frac{\mu^2(E'_j)}{(F_j)^2} \int_0^{W_{\text{b}}} d\delta_1\, e^{-\mu(E'_j)\delta_1} \int_0^{W_{\text{b}}} d\delta_2\, \frac{e^{-\mu(E'_j)\delta_2}}{1 + e^{\beta_{\text{C}}\delta_2}/z} \,. \tag{G75}$$

We extend the second integral to infinity, incurring an error

$$\epsilon := \frac{\mu^2(E'_j)}{(F_j)^2} \int_0^{W_{\text{b}}} d\delta_1\, e^{-\mu(E'_j)\delta_1} \int_{W_{\text{b}}}^{\infty} d\delta_2\, \frac{e^{-\mu(E'_j)\delta_2}}{1 + e^{\beta_{\text{C}}\delta_2}/z} \,. \tag{G76}$$

Let $\bar{\epsilon}$ denote the final integral. At fixed $z(\delta_1)$, the final integrand's $\frac{1}{1+e^{\beta_{\text{C}}\delta_2}/z} \leq z\, e^{-\beta_{\text{C}}\delta_2}$. Hence

$$\bar{\epsilon} \leq z \int_{W_{\text{b}}}^{\infty} d\delta_2\, e^{-[\mu(E'_j)+\beta_{\text{C}}]\delta_2} = \frac{z}{\mu(E'_j) + \beta_{\text{C}}}\, e^{-[\mu(E'_j)+\beta_{\text{C}}]W_{\text{b}}} \leq \frac{z}{\mu(E'_j)}\, \frac{\mu(E'_j)}{\beta_{\text{C}}}\, e^{-\beta_{\text{C}}W_{\text{b}}} \,. \tag{G77}$$

Inequalities (G76) and (G77), with the definition of z, imply

$$\epsilon \leq \frac{1}{(F_j)^2}\, \frac{\mu(E'_j)}{\beta_{\text{C}}}\, e^{-\beta_{\text{C}}W_{\text{b}}} \int_0^{W_{\text{b}}} d\delta_1\, \frac{e^{-\mu(E'_j)\delta_1}}{1 + e^{\beta_{\text{C}}\delta_1}} \,. \tag{G78}$$

The integral is upper-bounded by $e^{-\beta_{\text{C}}W_{\text{b}}}$. The $\frac{1}{(F_j)^2}$ will cancel with the $(F_j)^2$ in $P(n{=}2|j)$, in Eq. (G42). Hence

$$\epsilon = \frac{1}{(F_j)^2}\, O\left(\frac{\mu(E'_j)}{\beta_{\text{C}}}\, e^{-2\beta_{\text{C}}W_{\text{b}}}\right) . \tag{G79}$$

Returning to Eq. (G75), we change variables from δ_2 to $x := \beta_{\text{C}}\delta_2$:

$$P(\hat{j}{=}2|n{=}2, j) = \frac{\mu^2(E'_j)}{(F_j)^2\beta_{\text{C}}} \int_0^{W_{\text{b}}} d\delta_1\, e^{-\mu(E'_j)\delta_1} \int_0^{\infty} dx\, \frac{e^{-\mu(E'_j)x/\beta_{\text{C}}}}{1 + e^x/z} + \frac{1}{(F_j)^2}\, O\left(\frac{\mu(E'_j)}{\beta_{\text{C}}}\, e^{-2\beta_{\text{C}}W_{\text{b}}}\right) . \tag{G80}$$

Let $\mathcal{I}_2$ denote the second integral. We replace the numerator with its Taylor expansion. Pulling the sum out in front of the integral yields

$$\mathcal{I}_2 = \sum_{r=0}^{\infty} \left(-\frac{\mu(E'_j)}{\beta_{\text{C}}}\right)^r \frac{1}{r!} \int_0^{\infty} dx\, \frac{x^r}{1 + e^x/z} \,. \tag{G81}$$

Part of $\mathcal{I}_2$ forms an instance of the polylogarithm function. In the context of Fermi-Dirac distributions, the order-$(r + 1)$ polylogarithm function $\text{Li}_{r+1}(-e^{\mu})$ appears in the form [101]

$$\text{Li}_{r+1}(-e^{\mu}) = -\frac{1}{\Gamma(r+1)} \int_0^{\infty} dx\, \frac{x^r}{1 + e^{x-\mu}} \,. \tag{G82}$$

The polylogarithm has the power-series expansion

$$\mathrm{Li}_{r+1}(-z) = \sum_{\ell=1}^{\infty} \frac{(-z)^\ell}{\ell^{r+1}} \, . \tag{G83}$$

Returning to Eq. (G82), we recall that $\Gamma(r+1) = r!$ Setting $e^{-\mu} = \frac{1}{z}$ yields $\mathrm{Li}_{r+1}(-z) = -\frac{1}{r!} \int_0^\infty dx \, \frac{x^r}{1+e^x/z}$. Hence Eq. (G81) contains $-\mathrm{Li}_{r+1}(-z)$, such that $\mathcal{I}_2 = \sum_{r=0}^\infty \left(-\frac{\mu(E'_j)}{\beta_\mathrm{C}} \right)^r [-\mathrm{Li}_{r+1}(-z)]$. We substitute into Eq. (G80), then rearrange factors. Changing variables from δ_1 to $y := \beta_\mathrm{C} \delta_1$ yields

$$P(\hat{j}{=}2|n{=}2,j) = \frac{-1}{(F_j)^2 \beta_\mathrm{C}} \sum_{r=0}^\infty \left(-\frac{\mu(E'_j)}{\beta_\mathrm{C}} \right)^{r+2} \int_0^{\beta_\mathrm{C} W_\mathrm{b}} dy \, e^{-\mu(E'_j) y / \beta_\mathrm{C}} \, \mathrm{Li}_{r+1}(-z) + \frac{1}{(F_j)^2} \, O\left(\frac{\mu(E'_j)}{\beta_\mathrm{C}} \, e^{-2\beta_\mathrm{C} W_\mathrm{b}} \right) . \tag{G84}$$

Let us extend the upper integration limit to $y = \infty$. The extension incurs an error

$$\tilde{\epsilon} := \frac{-1}{(F_j)^2 \beta_\mathrm{C}} \sum_{r=0}^\infty \left(-\frac{\mu(E'_j)}{\beta_\mathrm{C}} \right)^{r+2} \int_{\beta_\mathrm{C} W_\mathrm{b}}^\infty dy \, e^{-\mu(E'_j) y / \beta_\mathrm{C}} \, \mathrm{Li}_{r+1}(-z) \, . \tag{G85}$$

Let $\tilde{\epsilon}'$ denote the integral. The $e^{-\mu(E'_j) y / \beta_\mathrm{C}} \leq 1$. We bound the final factor's magnitude using Eq. (G83):

$$|\mathrm{Li}_{r+1}(-z)| = \left| \sum_{\ell=1}^\infty \frac{(-z)^\ell}{\ell^{r+1}} \right| \leq \sum_{\ell=1}^\infty \frac{z^\ell}{\ell^{r+1}} \leq \sum_{\ell=1}^\infty z^\ell \, . \tag{G86}$$

The first inequality follows from the Triangle Inequality. Since $z = \frac{1}{1+e^y} \in [0,1)$, we can apply a geometric-series formula: $|\mathrm{Li}_{r+1}(-z)| \leq \frac{1}{1-z} - 1$. The one is subtracted off because Ineq. (G86) lacks an $\ell = 0$ term. Substituting in for z yields $|\mathrm{Li}_{r+1}(-z)| = \frac{1}{1+e^y} (e^{-y} + 1) \leq 2e^{-y}$. The integral in Eq. (G85) is upper-bounded by $2 \int_{\beta_\mathrm{C} W_\mathrm{b}}^\infty dy \, e^{-y} = 2e^{-\beta_\mathrm{C} W_\mathrm{b}}$. The largest term in Eq. (G85) is the $r = 0$ term: Incrementing r increments the power of $\frac{\mu(E'_j)}{\beta_\mathrm{C}}$ on which the r^{th} term depends. Hence

$$\tilde{\epsilon} = \frac{1}{(F_j)^2} \, O\left(\left[\frac{\mu(E'_j)}{\beta_\mathrm{C}} \right]^3 e^{-\beta_\mathrm{C} W_\mathrm{b}} \right) . \tag{G87}$$

Equation (G84) becomes

$$P(\hat{j}{=}2|n{=}2,j) = \frac{-1}{(F_j)^2 \beta_\mathrm{C}} \sum_{r=0}^\infty \left(-\frac{\mu(E'_j)}{\beta_\mathrm{C}} \right)^{r+2} \int_0^\infty dy \, e^{-\mu(E'_j) y / \beta_\mathrm{C}} \, \mathrm{Li}_{r+1}(-z) + \frac{1}{(F_j)^2} \, O\left(\frac{\mu(E'_j)}{\beta_\mathrm{C}} \, e^{-2\beta_\mathrm{C} W_\mathrm{b}} \right) . \tag{G88}$$

Let us replace the $e^{-\mu(E'_j) y / \beta_\mathrm{C}}$ with its Taylor series and z with $\frac{1}{1+e^y}$. Rearranging factors yields

$$P(\hat{j}{=}2|n{=}2,j) = \frac{1}{(F_j)^2} \sum_{r,s=0}^\infty \frac{1}{s!} \left(-\frac{\mu(E'_j)}{\beta_\mathrm{C}} \right)^{r+s+2} \int_0^\infty dy \cdot y^s \left[-\mathrm{Li}_{r+1} \left(\frac{-1}{1+e^y} \right) \right] + \frac{1}{(F_j)^2} \, O\left(\frac{\mu(E'_j)}{\beta_\mathrm{C}} \, e^{-2\beta_\mathrm{C} W_\mathrm{b}} \right) \tag{G89}$$

$$= \frac{1}{(F_j)^2} \, O\left(\left[\frac{\mu(E'_j)}{\beta_\mathrm{C}} \right]^2 \right) . \tag{G90}$$

The $\frac{1}{(F_j)^2}$ will cancel with the $(F_j)^2$ in $P(n{=}2|j)$ [Eq. (G54)]. Hence $\boxed{P(\hat{j}{=}2|n{=}2,j) \approx 0}$ is too small to include in our result.

G 5 iiib $P(\hat{j}{=}1|n{=}2,j)$*:* The red dot in the central subfigure of Fig. 11a represents an engine that has cold-thermalized to the middle rung in a chain of exactly two small gaps. S has a conditional probability $P(\hat{j}{=}1|n{=}2,j)$ of cold-thermalizing to such a middle rung, upon beginning a trial in level j (if the j^{th} MBL level occupies a chain of

exactly two small gaps). Let δ_1 and δ_2 denote the lower and upper gaps. We construct the conditional probability as in Eq. (G73):

$$P(\hat{j}{=}1|n{=}2,j) = \frac{1}{(F_j)^2}\int_0^{W_\mathrm{b}} d\delta_1 \left[\mu(E_j')\, e^{-\mu(E_j')\delta_1}\right] \int_0^{W_\mathrm{b}} d\delta_2 \left[\mu(E_j')\, e^{-\mu(E_j')\delta_2}\right] \frac{e^{-\beta_\mathrm{C}\delta_1}}{1+e^{-\beta_\mathrm{C}\delta_1}+e^{-\beta_\mathrm{C}(\delta_1+\delta_2)}}\,. \tag{G91}$$

To simplify, we multiply and divide by $e^{\beta_\mathrm{C}\delta_1}$. Then, we define

$$z \equiv z(\delta_1) := 1 + e^{\beta_\mathrm{C}\delta_1}\,. \tag{G92}$$

Pulling out the DOS factors yields

$$P(\hat{j}{=}1|n{=}2,j) = \frac{\mu^2(E_j')}{(F_j)^2}\int_0^{W_\mathrm{b}} d\delta_1\, e^{-\mu(E_j')\delta_1} \int_0^{W_\mathrm{b}} d\delta_2\, \frac{e^{-\mu(E_j')\delta_2}}{z+e^{-\beta_\mathrm{C}\delta_2}}\,. \tag{G93}$$

We approximate the numerator to zeroth order: $e^{-\mu(E_j')\delta_2} \approx 1$. The leading correction ends up smaller by a factor of $\frac{\mu(E_j')}{\beta_\mathrm{C}}$. The proof resembles the argument just after Eq. (G21).

We change variables from δ_2 to $y := e^{-\beta_\mathrm{C}\delta_2}$:

$$P(\hat{j}{=}1|n{=}2,j) = -\frac{\mu^2(E_j')}{(F_j)^2\beta_\mathrm{C}}\int_0^{W_\mathrm{b}} d\delta_1\, e^{-\mu(E_j')\delta_1} \int_1^{e^{-\beta_\mathrm{C}W_\mathrm{b}}} \frac{dy}{y(z+y)}\,. \tag{G94}$$

The right-hand integrand decomposes as $\frac{1}{y(z+y)} = \frac{1}{z}\left(\frac{1}{y} - \frac{1}{z+y}\right)$. We must integrate

$$\int_1^{e^{-\beta_\mathrm{C}W_\mathrm{b}}} dy\, \left(\frac{1}{y} - \frac{1}{z+y}\right) = -\beta_\mathrm{C}W_\mathrm{b} - \ln\left(\frac{z+e^{-\beta_\mathrm{C}W_\mathrm{b}}}{z+1}\right)\,. \tag{G95}$$

Equation (G94) evaluates to

$$P(\hat{j}{=}1|n{=}2,j) = \frac{\mu^2(E_j')}{(F_j)^2\beta_\mathrm{C}}\int_0^{W_\mathrm{b}} d\delta_1\, \frac{e^{-\mu(E_j')\delta_1}}{z}\left[\beta_\mathrm{C}W_\mathrm{b} + \ln\left(\frac{z+e^{-\beta_\mathrm{C}W_\mathrm{b}}}{z+1}\right)\right]\,. \tag{G96}$$

Only the $\beta_\mathrm{C}W_\mathrm{b}$ term, we will show later, is nonnegligible. Therefore, since $z := 1 + e^{\beta_\mathrm{C}\delta_1}$,

$$P(\hat{j}{=}1|n{=}2,j) = \frac{\mu^2(E_j')\,W_\mathrm{b}}{(F_j)^2}\int_0^{W_\mathrm{b}} d\delta_1\, \frac{e^{-\mu(E_j')\delta_1}}{1+e^{\beta_\mathrm{C}\delta_1}} + \tilde{\epsilon}\,, \tag{G97}$$

wherein

$$\tilde{\epsilon} := \frac{\mu^2(E_j')}{(F_j)^2\beta_\mathrm{C}}\int_0^{W_\mathrm{b}} d\delta_1\, \frac{e^{-\mu(E_j')\delta_1}}{z}\, \ln\left(\frac{z+e^{-\beta_\mathrm{C}W_\mathrm{b}}}{1+z}\right)\,. \tag{G98}$$

The explicit integral in Eq. (G97) equals $\frac{F_j}{\mu(E_j')}\, P(\hat{j}{=}1|n{=}1,j)$ by Eq. (G56). The latter probability is evaluated in Eq. (G63). Hence

$$P(\hat{j}{=}1|n{=}2,j) = \frac{1}{F_j}\,\frac{\mu^2(E_j')W_\mathrm{b}}{\beta_\mathrm{C}}\sum_{r=0}^{\infty}\eta(r+1)\left(-\frac{\mu(E_j')}{\beta_\mathrm{C}}\right)^r + \frac{1}{F_j}\,O\left(\frac{\mu(E_j')}{\beta_\mathrm{C}}\,e^{-\beta_\mathrm{C}W_\mathrm{b}}\right) + \tilde{\epsilon}\,. \tag{G99}$$

Again, η denotes the Dirichlet eta function.

Let us calculate $\tilde{\epsilon}$, Eq. (G98). As before, we approximate the $e^{-\mu(E_j')\delta_1}$ to zeroth order. Let us factor $\frac{z}{1+z}$ out of the log:

$$\tilde{\epsilon} = \frac{\mu^2(E_j')}{(F_j)^2\beta_\mathrm{C}}\int_0^{W_\mathrm{b}} d\delta_1\, \frac{1}{z}\,\left[\ln\left(\frac{z}{1+z}\right) + \ln\left(1+\frac{e^{-\beta_\mathrm{C}W_\mathrm{b}}}{z}\right)\right]\,. \tag{G100}$$

The final logarithm is $O\left(e^{-\beta_{\rm C} W_{\rm b}}\right)$. We prepare the initial logarithm for a Taylor approximation: $\ln\left(\frac{z}{1+z}\right) = -\ln\left(1+\frac{1}{z}\right)$. Hence

$$\tilde{\epsilon} = -\frac{\mu^2(E'_j)}{(F_j)^2 \beta_{\rm C}} \int_0^{W_{\rm b}} d\delta_1 \, \frac{1}{z} \, \ln\left(1+\frac{1}{z}\right) + O\left(e^{-\beta_{\rm C} W_{\rm b}}\right) . \tag{G101}$$

Let us change variables from δ_1 to $x := \beta_{\rm C} W_{\rm b}$, such that $z = 1+e^x$. Extending the integration limit yields a correction of order $e^{-\beta_{\rm C} W_{\rm b}}$. Hence

$$\tilde{\epsilon} = -\frac{\mu^2(E'_j)}{(F_j)^2 (\beta_{\rm C})^2} \int_0^{\infty} d\delta_1 \, \frac{1}{1+e^x} \, \ln\left(1+\frac{1}{1+e^x}\right) + O\left(e^{-\beta_{\rm C} W_{\rm b}}\right) \tag{G102}$$

$$= \frac{1}{(F_j)^2} \, O\left(\left[\frac{\mu(E'_j)}{\beta_{\rm C}}\right]^2\right) . \tag{G103}$$

The $\frac{1}{(F_j)^2}$ will cancel with the $(F_j)^2$ in $P(n{=}2|j) = (F_j)^2 (G_j)^2$ in Eq. (G42). This correction is negligible, as claimed.

Substituting into Eq. (G99) yields

$$P(\hat{j}{=}1|n{=}2,j) = \frac{1}{F_j} \, \frac{\mu^2(E'_j) W_{\rm b}}{\beta_{\rm C}} \sum_{r=0}^{\infty} \eta(r+1) \left(-\frac{\mu(E'_j)}{\beta_{\rm C}}\right)^r + \frac{1}{F_j} \, O\left(\frac{\mu(E'_j)}{\beta_{\rm C}} \, e^{-\beta_{\rm C} W_{\rm b}}\right) + \frac{1}{(F_j)^2} \, O\left(\left[\frac{\mu(E'_j)}{\beta_{\rm C}}\right]^2\right) . \tag{G104}$$

The sole nonnegligible term is the leading-order term:

$$\boxed{P(\hat{j}{=}1|n{=}2,j) \approx \frac{\eta(1)}{F_j} \, [\mu(E'_j) W_{\rm b}] \, \frac{\mu(E'_j)}{\beta_{\rm C}}} . \tag{G105}$$

G 5 iiic $P(\hat{j}{=}0|n{=}2,j)$*:* If the engine begins a trial on level j of $H_{\rm GOE}$, and if the $j^{\rm th}$ level of $H_{\rm MBL}$ occupies a chain of exactly two small gaps, cold thermalization might leave S on the chain's bottom ($\hat{j} = 0$) rung. The leftmost subfigure in Fig. 11a depicts this scenario. By the normalization of probabilities,

$$\boxed{P(\hat{j}{=}0|n{=}2,j) = 1 - P(\hat{j}{=}2|n{=}2,j) - P(\hat{j}{=}1|n{=}2,j)} . \tag{G106}$$

G 5 iiid $\left\langle Q_4^{n=2} \right\rangle$*:* Consider the $n = 2$ term in Eq. (G42). We perform the final two sums explicitly and substitute in from Eq. (G106):

$$\left\langle Q_4^{n=2} \right\rangle = \sum_j \frac{e^{-\beta_{\rm H} E_j}}{Z} \, P(n{=}2|j) \sum_{\hat{j}=0}^{2} P(\hat{j}|n{=}2,j) \sum_{k=j-2}^{j} \frac{1}{\mu(E_j)} (j - \hat{j} - k) \tag{G107}$$

$$= 3 \sum_j \frac{1}{\mu(E_j)} \, \frac{e^{-\beta_{\rm H} E_j}}{Z} \, P(n{=}2|j) [1 - P(\hat{j}{=}1|n{=}2,j) - 2P(\hat{j}{=}2|n{=}2,j)] . \tag{G108}$$

The final term is negligible, by Eq. (G90). We substitute in $P(n{=}2|j) = (F_j)^2 (G_j)^2$ from Eq. (G54) and for $P(\hat{j}{=}1|n{=}2,j)$ from Eq. (G105). We omit corrections, for conciseness:

$$\left\langle Q_4^{n=2} \right\rangle \approx 3 \sum_j \frac{1}{\mu(E_j)} \, \frac{e^{-\beta_{\rm H} E_j}}{Z} \, \left\{ (F_j)^2 (G_j)^2 - \eta(1) \, [\mu(E'_j) W_{\rm b}] \, \frac{\mu(E'_j)}{\beta_{\rm C}} \, F_j (G_j)^2 \right\} . \tag{G109}$$

We substitute in $(F_j)^2 (G_j)^2 \approx [\mu(E'_j) W_{\rm b}]^2$ and $F_j (G_j)^2 \approx \mu(E'_j) W_{\rm b}$ from Eqs. (G55) and (G53). The final term in Eq. (G109) turns out to be negligible, of order $[\mu(E'_j) W_{\rm b}]^2 \, \frac{\mu(E'_j)}{\beta_{\rm C}}$. We assume that the $H_{\rm GOE}$ and $H_{\rm MBL}$ DOS's roughly equal each other: $\mu(E_j) \approx \mu(E'_j)$. The sum is approximated as an integral:

$$\boxed{\left\langle Q_4^{n=2} \right\rangle} \approx \; 3 (W_{\rm b})^2 \int_{-\infty}^{\infty} dE \, \mu^2(E) \, \frac{e^{-\beta_{\rm H} E}}{Z} = 3 \, \frac{(W_{\rm b})^2}{\langle \delta \rangle} \, e^{-N(\beta_{\rm H} \mathcal{E})^2/4} \tag{G110}$$

$$\boxed{\approx 3 \, \frac{(W_{\rm b})^2}{\langle \delta \rangle}} . \tag{G111}$$

This heat quantity is of the order of $\langle Q_2 \rangle \approx -\frac{(W_{\rm b})^2}{\langle \delta \rangle}$, the heat absorbed during cold thermalization. $\left\langle Q_4^{n=2} \right\rangle$ contributes to the greatest correction in $\langle Q_4 \rangle$.

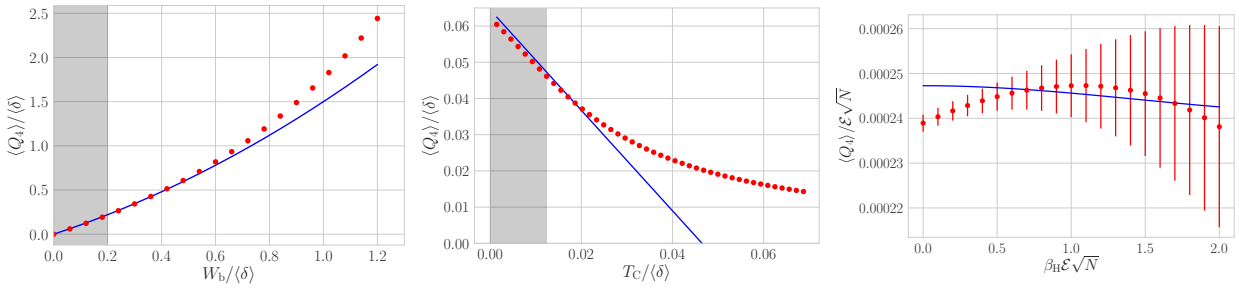

(a) $\langle Q_4 \rangle$ vs. W_b at $T_C = 0$ and $T_H = \infty$

(b) $\langle Q_4 \rangle$ vs. T_C at $T_H = \infty$ and $W_b = 2^{-4} \langle \delta \rangle$

(c) $\langle Q_4 \rangle$ vs. β_H at $T_C = 0$ and $W_b = 2^{-4} \langle \delta \rangle$

FIG. 12: Average heat $\langle Q_4 \rangle$ absorbed during hot thermalization (stroke 4) as a function of the cold-bath bandwidth W_b, the cold-bath temperature T_C, and the hot-bath temperature $T_H = 1/\beta_H$: We numerically simulated a mesoscale engine of $N = 12$ sites, governed by the random-field Heisenberg Hamiltonian (24). Each red dot represents numerical simulations of 1,000 disorder realizations. The blue lines represent the analytical prediction (G112), to lowest order in T_C, with the β_H dependence of $\langle Q_4 \rangle$ [too small a correction to include in Eq. (G112)]: $\langle Q_4 \rangle \approx W_b - \frac{2 \ln 2}{\beta_C} + \frac{(W_b)^2}{2 \langle \delta \rangle} e^{-(\beta_H \mathcal{E})^2/4}$. The disorder strengths and error bars are discussed in Sec. III. $\mathcal{E}$ represents the unit of energy. The analytics' shapes agree with the numerics', and the fit is fairly close, in the appropriate limits (where $e^{-\beta_C W_b} \ll 1$, $\frac{1}{\beta_C \langle \delta \rangle} \ll 1$, and $\frac{W_b}{\langle \delta \rangle} \ll 1$, in the gray shaded regions). The analytical predictions systematically underestimate $\langle Q_4 \rangle$ in the ways in which, and for the reasons that, the analytics underestimate $\langle Q_2 \rangle$ (Fig. 9). Figure 12c suggests that the numerics deviate significantly from the analytics: The numerics appear to depend on β_H via a linear term absent from the $\langle Q_4 \rangle$ prediction. This seeming mismatch appears to symptomatic of finite sample and system sizes.

G 5 iv Assembling the leading-order ($n = 1, 2$) contributions to $\langle Q_4 \rangle$

The average heat absorbed during stroke 4 follows from summing Eqs. (G72) and (G111), to leading order:

$$\boxed{\langle Q_4 \rangle \approx} \; \langle Q_4^{n=1} \rangle + \langle Q_4^{n=2} \rangle \approx \boxed{W_b - \frac{2 \ln 2}{\beta_C} + \frac{(W_b)^2}{2 \langle \delta \rangle} + 4 \ln 2 \, \frac{W_b}{\beta_C \langle \delta \rangle}} \, . \tag{G112}$$

The leading-order β_C correction, $-\frac{2 \ln 2}{\beta_C}$, shows that a warm cold bath lowers the heat required to reset the engine. Suppose that the cold bath is maximally cold: $T_C = 0$. Consider any trial that S begins just above a working gap (an ETH gap $\delta > W_b$ that narrows to an MBL gap $\delta' < W_b$). Cold thermalization drops S deterministically to the lower level. During stroke 4, S must absorb $Q_4 > 0$ to return to its start-of-trial state. Now, suppose that the cold bath is only cool: $T_C \gtrsim 0$. Cold thermalization might leave S in the upper level. S needs less heat, on average, to reset than if $T_C = 0$. A finite T_C detracts from $\langle Q_4 \rangle$. The $+4 \ln 2 \, \frac{W_b}{\beta_C \langle \delta \rangle}$ offsets the detracting. However, the positive correction is smaller than the negative correction, as $\frac{W_b}{\langle \delta \rangle} \ll 1$.

In a similar argument, we suppose that the hot bath is very hot: $T_H = \infty$. After cold thermalization, S needs considerable "reset" heat to return to infinite temperature. Now, suppose that the hot bath is lukewarm: $T_H < \infty$. The engine requires less reset heat. $\langle Q_4 \rangle$ shrinks as β_H grows: $\langle Q_4 \rangle \propto -(\text{positive constant}) N (\beta_H \mathcal{E})^2$. This conclusion concurs with Eq. (G110), though the β_H correction is too small to include in Eq. (G112).

Figure 12 shows Eq. (G112), to lowest order in T_C, with the β_H dependence of $\langle Q_4 \rangle$, too small a correction to include in Eq. (G112): $\langle Q_4 \rangle \approx W_b - \frac{2 \ln 2}{\beta_C} + \frac{(W_b)^2}{2 \langle \delta \rangle} e^{-(\beta_H \mathcal{E})^2/4}$. This analytical prediction is compared with numerical simulations. The agreement is close, up to finite-size effects, in the appropriate limits, $T_C \ll W_b \ll \langle \delta \rangle$.

G 6 Per-cycle power $\langle W_{tot} \rangle$

By the first law of thermodynamics, the net work outputted by the engine equals the net heat absorbed. Summing Eqs. (G112) and (G37) yields the per-trial power, or average work outputted per engine cycle:

$$\boxed{\langle W_{tot} \rangle} = \langle Q_2 \rangle + \langle Q_4 \rangle \boxed{\approx W_b - \frac{2 \ln 2}{\beta_C} + 4 \ln 2 \, \frac{W_b}{\beta_C \langle \delta \rangle}} \, . \tag{G113}$$

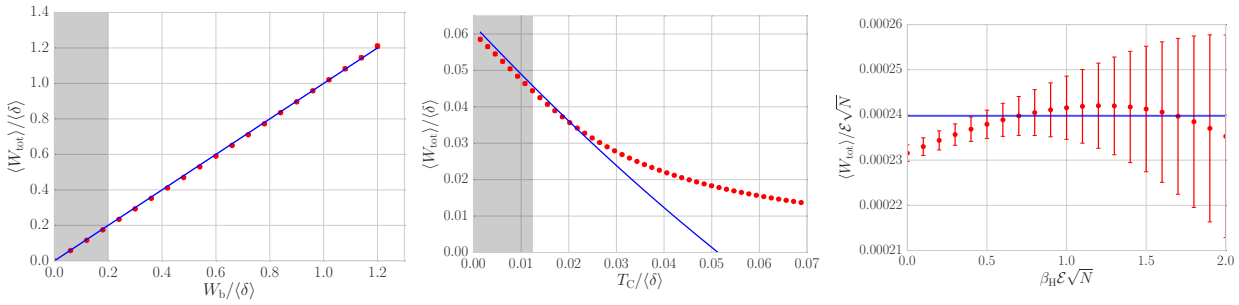

(a) $\langle W_{\rm tot}\rangle$ vs. $W_{\rm b}$ at $T_{\rm C} = 0$ and $T_{\rm H} = \infty$

(b) $\langle W_{\rm tot}\rangle$ vs. $T_{\rm C}$ at $T_{\rm H} = \infty$ and $W_{\rm b} = 2^{-4}\,\langle\delta\rangle$

(c) $\langle W_{\rm tot}\rangle$ vs. $\beta_{\rm H}$ at $T_{\rm C} = 0$ and $W_{\rm b} = 2^{-4}\,\langle\delta\rangle$

FIG. 13: Per-cycle power $\langle W_{\rm tot}\rangle$ as a function of the cold-bath bandwidth $W_{\rm b}$, the cold-bath temperature $T_{\rm C}$, and the hot-bath temperature $T_{\rm H} = 1/\beta_{\rm H}$: We numerically simulated a mesoscale engine of $N = 12$ sites governed by the random-field Heisenberg Hamiltonian (24). Each red dot represents numerical simulations of 1,000 disorder realizations. The disorder strengths and error bars are explained in Sec. III. $\mathcal{E}$ represents the unit of energy. The blue lines represent the analytical prediction $\langle W_{\rm tot}\rangle \approx W_{\rm b} - \frac{2\ln 2}{\beta_{\rm C}}$: Eq. (G113), to first order in $\frac{W_{\rm b}}{\langle\delta\rangle}$ and in $\frac{1}{\beta_{\rm C}\langle\delta\rangle}$. The analytics largely agree with the numerics in the regime in which the analytics were performed: $\frac{W_{\rm b}}{\langle\delta\rangle} \ll 1$, $\frac{T_{\rm C}}{\langle\delta\rangle} \ll 1$ (in the gray shaded region). Outside that regime, the analytics systematically underestimate $\langle W_{\rm tot}\rangle$. The trends and reasons mirror those discussed beneath Fig. 9. Figure 13c suggests that the numerics depend on $\beta_{\rm H}$ via a linear term absent from the analytical prediction. The seeming mismatch stems from the simulation practicalities highlighted below Fig. 12c.

The leading-order $\beta_{\rm H}$ correction is negative and too small to include—of order $\left(\frac{W_{\rm b}}{\langle\delta\rangle}\right)^2 N\,(\beta_{\rm H}\mathcal{E})^2$. Equation (G113) agrees well with the numerics in the appropriate limits ($T_{\rm C} \ll W_{\rm b} \ll \langle\delta\rangle$) and beyond, as shown in Fig. 13. The main text contains the primary analysis of Eq. (G113). Here, we discuss the $\langle Q_2\rangle$ correction, limiting behaviors, and scaling.

The negative $\langle Q_2\rangle = -\frac{(W_{\rm b})^2}{\langle\delta\rangle}$ detracts little from the leading term $W_{\rm b}$ of $\langle Q_4\rangle$: $\frac{(W_{\rm b})^2}{\langle\delta\rangle} \ll W_{\rm b}$, since $\frac{W_{\rm b}}{\langle\delta\rangle} \ll 1$. The $\langle Q_2\rangle$ cuts down on the per-trial power little.

The limiting behavior of Eq. (G113) makes sense: Consider the limit as $W_{\rm b} \to 0$. The cold bath has too small a bandwidth to thermalize the engine. The engine should output no work. Indeed, the first and third terms in Eq. (G113) vanish, being proportional to $W_{\rm b}$. The second term vanishes because $\beta_{\rm C} \to \infty$ more quickly than $W_{\rm b} \to 0$, by Eq. (G1): The cold bath is very cold.

Equation (G113) scales with the system size N no more quickly than $\sqrt{N}/2^N$. This scaling follows from the assumption $W_{\rm b} \ll \langle\delta\rangle \sim \sqrt{N}/2^N$. This scaling makes sense: The engine outputs work because the energy eigenvalues meander upward and downward in Fig. 2 as $H(t)$ is tuned. In the thermodynamic limit, levels squeeze together. Energy eigenvalues have little room in which to wander. The engine outputs little work. Hence our parallelization of fixed-length mesoscopic subengines in the thermodynamic limit (Sec. II C). We cap each mesoscopic subengine's size at $\xi_>$. This capping keeps each mesoscale engine's effective $\langle\delta\rangle$ constant as a function of the composite-engine length $N_{\rm macro}$. The number of subengines grows linearly with $N_{\rm macro}$. Hence the total per-cycle power grows as $\sim \frac{N_{\rm macro}}{2^{\xi_>}}$ in the thermodynamic limit.

G 7 Efficiency $\eta_{\rm MBL}$ in the adiabatic approximation

The efficiency is defined as

$$\eta_{\rm MBL} := \frac{\langle W_{\rm tot}\rangle}{\langle Q_{\rm in}\rangle}\,. \tag{G114}$$

We average the numerator and the denominator independently. Calculating the work and heat associated with one trial, then averaging $\frac{W_{\rm tot}}{Q_{\rm in}}$ over trials, might seem more natural. But two reasons motivate the separation of the averages. First, the separation facilitates the calculation. Second, averaging $W_{\rm tot}$ over runs of a mesoscopic-engine cycle is roughly equivalent to averaging over simultaneous runs of parallel mesoscopic engines in one thermodynamically large composite engine. $\frac{\langle W_{\rm tot}\rangle}{\langle Q_{\rm in}\rangle}$ may therefore be regarded as the $\frac{W_{\rm tot}}{Q_{\rm in}}$ of one self-averaged thermodynamic-engine trial.

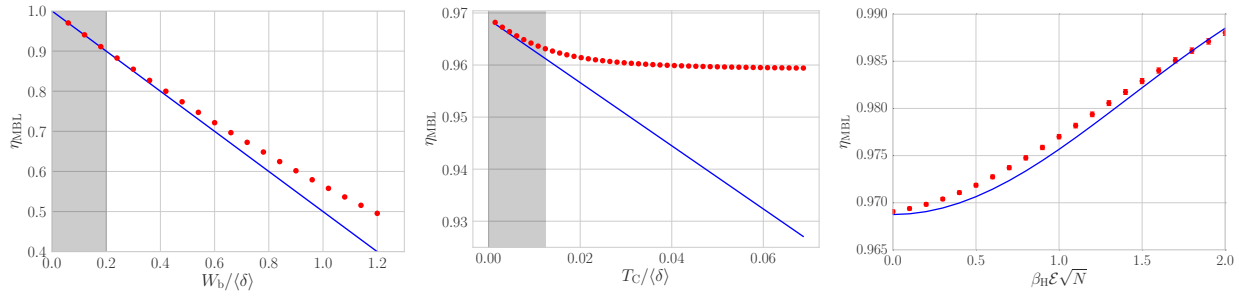

(a) $\eta_{\rm MBL}$ vs. $W_{\rm b}$ at $T_{\rm C} = 0$ and $T_{\rm H} = \infty$

(b) $\eta_{\rm MBL}$ vs. $T_{\rm C}$ at $T_{\rm H} = \infty$ and $W_{\rm b} \approx 10^{-4}\sqrt{N}\mathcal{E} \approx 0.04\,\langle\delta\rangle$

(c) $\eta_{\rm MBL}$ vs. $\beta_{\rm H}$ at $T_{\rm C} = 0$ and $W_{\rm b} = 2^{-4}\,\langle\delta\rangle$

FIG. 14: Efficiency $\eta_{\rm MBL}$ as a function of the cold-bath bandwidth $W_{\rm b}$, the cold-bath temperature $T_{\rm C}$, and the hot-bath temperature $T_{\rm H} = 1/\beta_{\rm H}$: We numerically simulated a mesoscale engine of $N = 12$ sites governed by the random-field Heisenberg Hamiltonian (24). Each red dot represents numerical simulations of 1,000 disorder realizations. The blue lines represent the analytical predictions (G117) and (G118). Figure (14c) shows the leading-order $\beta_{\rm H}$ dependence of $\eta_{\rm MBL}$, a correction too small to include in Eq. (G118): $1 - \frac{W_{\rm b}}{2\langle\delta\rangle}\, e^{-N(\beta_{\rm H}\mathcal{E})^2/4}$. The disorder strengths and error bars are discussed in Sec. III. $\mathcal{E}$ represents the unit of energy. The analytics agree with the numerics fairly well in the regime in which the analytics were performed ($\frac{W_{\rm b}}{\langle\delta\rangle} \ll 1$, $\frac{T_{\rm C}}{\langle\delta\rangle} \ll 1$, and $\sqrt{N}\,T_{\rm H}\mathcal{E} \ll 1$). The analytics systematically underestimate $\eta_{\rm MBL}$ in the ways in which, and for the reasons that, the analytics underestimate $\langle Q_2\rangle$ (Fig. 9).

Having calculated $\langle W_{\rm tot}\rangle$, we must identify $\langle Q_{\rm in}\rangle$. In most trials, the engine expels a positive amount of heat during cold thermalization and absorbs a positive amount of heat during hot thermalization: $Q_2 < 0$, and $Q_4 > 0$. The positive-heat-absorbing-stroke is stroke 4, in the average trial. Hence $\langle Q_{\rm in}\rangle = \langle Q_4\rangle$. This heat can be expressed in terms of the total work:

$$\langle Q_{\rm in}\rangle = \langle Q_4\rangle = \langle W_{\rm tot}\rangle - \langle Q_2\rangle = \langle W_{\rm tot}\rangle \left(1 - \frac{\langle Q_2\rangle}{\langle W_{\rm tot}\rangle}\right) = \langle W_{\rm tot}\rangle\,(1+\phi)\ , \tag{G115}$$

wherein

$$\phi := -\frac{\langle Q_2\rangle}{\langle W_{\rm tot}\rangle} \approx \frac{(W_{\rm b})^2}{2\,\langle\delta\rangle}\,\frac{1}{W_{\rm b}} \approx \frac{W_{\rm b}}{2\,\langle\delta\rangle}\ . \tag{G116}$$

Substituting from Eq. (G115) into Eq. (G114) yields

$$\boxed{\eta_{\rm MBL} \approx} \frac{\langle W_{\rm tot}\rangle}{\langle W_{\rm tot}\rangle\,(1+\phi)} \approx 1 - \phi = \boxed{1 - \frac{W_{\rm b}}{2\,\langle\delta\rangle}}\ . \tag{G117}$$

Using suboptimal baths diminishes the efficiency. We can see how by incorporating temperature-dependent terms into ϕ [Eq. (G116)]. We include, in the $\langle W_{\rm tot}\rangle$, the $\beta_{\rm C}$-dependent terms in Eq. (G113). ϕ becomes

$$\phi' = \frac{W_{\rm b}}{2\,\langle\delta\rangle} + \frac{\ln 2}{\beta_{\rm C}\,\langle\delta\rangle} - 2\ln 2\,\frac{W_{\rm b}}{\langle\delta\rangle}\,\frac{1}{\beta_{\rm C}\,\langle\delta\rangle}\ . \tag{G118}$$

The leading $\beta_{\rm H}$ correction is too small to include. The correction has the same sign as $\beta_{\rm H}$: A lukewarm hot bath detracts from the efficiency.

Expressions (G117) and (G118) are compared with results from numerical simulations in Fig. 14. Figure (14c) shows the leading-order $\beta_{\rm H}$ dependence of $\eta_{\rm MBL}$, a correction too small to include in Eq. (G118): $1 - \frac{W_{\rm b}}{2\langle\delta\rangle}\, e^{-N(\beta_{\rm H}\mathcal{E})^2/4}$. The analytics agree with the numerics in the appropriate limits ($T_{\rm C} \ll W_{\rm b} \ll \langle\delta\rangle$).

G 8 Diabatic corrections

We have approximated strokes 1 and 3 as quantum-adiabatic. But the strokes proceed at a finite speed $v := \mathcal{E}\left|\frac{d\alpha_t}{dt}\right|$. The engine may "hop" diabatically between energy eigenstates. Such hops cost work. We estimate the work costs from three types of diabatic transitions, depicted in Fig. 3: In the ETH phase, S may undergo transitions modeled

with general adiabatic perturbation theory (APT). In the MBL phase, S may undergo Landau-Zener (LZ) transitions. At the end of stroke 1 and the start of stroke 3, S may undergo fractional-LZ transitions. After estimating the work costs, we estimate the diabatic correction to the efficiency $\eta_{\rm MBL}$.

We neglect the variation of the local average gap $\langle\delta\rangle_E$ with energy: We approximate the GOE and Poisson distributions (App. D) with $P_{\rm GOE}(\delta) \approx \frac{\pi}{2}\,\frac{\delta}{\langle\delta\rangle^2}\,\exp\left(-\frac{\pi}{4}\left[\frac{\delta}{\langle\delta\rangle}\right]^2\right)$ and$P_{\rm MBL}(\delta) \approx \frac{1}{\langle\delta\rangle}\,e^{-\delta/\langle\delta\rangle}$. The approximations facilitate this appendix's calculations, which, in some cases, require heavier machinery than our adiabatic approximation. We aim to estimate just diabatic corrections' sizes, rather than to nail down each correction's precise form.

G 8 i Average work costs of APT transitions in the ETH phase: $\langle W_{\rm APT,1}\rangle$ and $\langle W_{\rm APT,3}\rangle$

Consider the start of stroke 1. (An analogous argument concerns the end of stroke 3.) $H(t)$ is tuned within the ETH phase. Let $|E_m(t)\rangle$ denote the instantaneous $m^{\rm th}$ eigenstate of $H(t)$. The perturbation couples together eigenstates of the initial Hamiltonian. Consider the tuning between times t_i and t_f. Suppose that S begins in some eigenstate $|E_m(t_i)\rangle$ of $H(t_i)$. The engine might transition to the $n^{\rm th}$ energy eigenstate, for some $n \neq m$. The transition probability is denoted by $P_{\rm APT}(n|m)$. These transitions cost an amount $\langle W_{\rm APT,1}\rangle$ of work during stroke 1 and an amount $\langle W_{\rm APT,3}\rangle$ of work during stroke 3, on average.

We estimate $P_{\rm APT}(n|m)$ by applying an APT calculation from [59]. We apply the $P_{\rm APT}$ estimate to approximate $\langle W_{\rm APT,1}\rangle$. Then, we argue that $\langle W_{\rm APT,3}\rangle \approx \langle W_{\rm APT,1}\rangle$.

Diabatic-hopping probability $\mathbf{P_{APT}(E_f - E_i)}$ derived from adiabatic perturbation theory: In this section, we generalize from the engine S to a closed quantum system $\tilde{S}$. Let $H(t)$ denote a time-dependent Hamiltonian. The $m^{\rm th}$ instantaneous energy eigenstate is denoted by $|E_m(t)\rangle$. Suppose that $\tilde{S}$ begins in the $|E_m(t_i)\rangle$ of an initial Hamiltonian $H(t_i)$. Let V denote the term "turned on" in the Hamiltonian. V couples together eigenstates of $H(t_i)$. The coupling may transfer $\tilde{S}$ diabatically to some eigenstate $|E_n(t_f)\rangle$. This transition has a probability $P_{\rm APT}(n|m)$ of occurring.

De Grandi and Polkovnikov calculate $P_{\rm APT}(n|m)$ using APT [59]. Equation (20) on their page 4 has the form

$$P_{\rm APT}(n|m) \approx \left(\frac{v}{\mathcal{E}}\right)^2 \left[\frac{\left|\langle E_n(t)|\partial_{\alpha_t}|E_m(t)\rangle|_{\alpha_{t_i}}\right|^2}{[E_n(t_i)-E_m(t_i)]^2} + \frac{\left|\langle E_n(t)|\partial_{\alpha_t}|E_m(t)\rangle|_{\alpha_{t_f}}\right|^2}{[E_n(t_f)-E_m(t_f)]^2} - 2\,\frac{\langle E_n(t)|\partial_{\alpha_t}|E_m(t)\rangle|_{\alpha_i}}{E_n(t_i)-E_m(t_i)}\,\frac{\langle E_n(t)|\partial_{\alpha_t}|E_m(t)\rangle|_{\alpha_f}}{E_n(t_f)-E_m(t_f)}\,\cos(\Delta\Theta_{nm})\right]. \tag{G119}$$

Equation (G119) contains a blend of our notation and de Grandi and Polkovnikov's. Their λ is our Hamiltonian-tuning parameter α_t. Their speed δ, which has dimensions of energy, equals our $\frac{v}{\mathcal{E}}$. The $\Delta\Theta_{nm}$ denotes a difference between two phase angles.

The final term in Eq. (G119) results from interference. This term often oscillates quickly and can be neglected [59]. We have further reason to neglect the term: We will integrate $P_{\rm APT}(n|m)$ over energies. The integration is expected to magnify cancellations.

The second term in Eq. (G119) shares the first term's form. The first term is evaluated at $t = t_i$; the second term, at $t = t_f$. The quantities evaluated at t_i are close their t_f counterparts: The Hamiltonian remains ETH throughout the time interval. The system is slightly less localized at t_i than at t_f. Equation (G119) is therefore approximated with

$$P_{\rm APT}(n|m) \sim 2\left(\frac{v}{\mathcal{E}}\right)^2 \frac{\left|\langle E_n(t)|\partial_{\alpha_t}|E_m(t)\rangle|_{\alpha_{t_i}}\right|^2}{[E_n(t_i)-E_m(t_i)]^2} \tag{G120}$$

Equation (G121) accounts for the greater frequency with which APT transitions occur in the ETH phase than in the MBL phase. In the ETH phase, $|\langle E_n|V|E_m\rangle|$ has a considerable size, $\sim \frac{1}{\sqrt{\mathcal{N}}}$, for most (n,m) pairs [5]. In the MBL phase, few pairs correspond to a large numerator: $|\langle E_n|V|E_m\rangle| \sim \frac{1}{\mathcal{N}}$ [33]. The corresponding energies tend to lie far apart: $|E_n - E_m| \gg |\langle E_n|V|E_m\rangle|$. Most APT transition probabilities are therefore suppressed [102].

The perturbation-matrix element comes from the Chain Rule and from the Eq. (10) in [59]:

$$\langle E_n(t)|\partial_{\alpha_t}|E_m(t)\rangle = \left\langle E_n(t)\left|\frac{\partial t}{\partial\alpha_t}\,\frac{\partial}{\partial t}\right|E_m(t)\right\rangle = \frac{\mathcal{E}}{v}\,\langle E_n(t)|\partial_t|E_m(t)\rangle = \frac{\mathcal{E}}{v}\left(-\frac{v}{\mathcal{E}}\,\frac{\langle E_n(t)|V|E_m(t)\rangle}{E_n(t)-E_m(t)}\right). \tag{G121}$$

The modulus $|\langle E_n(t)|V|E_m(t)\rangle|$ is known to scale as $1/\sqrt{\mathcal{N}}$ for ETH Hamiltonians [5].[12] We introduce an $\mathcal{E}$ for dimensionality: $|\langle E_n(t)|\partial_{\alpha_t}|E_m(t)\rangle| \sim \frac{\mathcal{E}}{\sqrt{\mathcal{N}}\,|E_n(t)-E_m(t)|}$. Substituting into Eq. (G120) yields

$$P_{\rm APT}(n|m) \sim \frac{v^2}{\mathcal{N}\left[E_n(t_i) - E_m(t_i)\right]^4} \, . \tag{G122}$$

We have dropped a two due to our focus on scaling behaviors. Greater precision would be needed to estimate numerical coefficients. This probability is an even function of the signed gap $E_n(t_i) - E_m(t_i)$. We will drop the time arguments for conciseness.

The probability $P_{\rm APT}(n|m)$ is normalized to one. Therefore, the right-hand side of Eq. (G122) makes sense only when < 1. The right-hand side diverges if E_n lies close to E_m. But energies rarely lie close together in the ETH phase, which exhibits level repulsion. Furthermore, slow tuning of $H(t)$ impedes diabatic transitions. We therefore introduce a regularization factor R into the approximation:

$$P_{\rm APT}(n|m) \sim \frac{v^2}{\mathcal{N}\left[(E_n - E_m)^2 + R^2\right]^2} \, . \tag{G123}$$

Equation (G123) reduces to Eq. (G122) when the energy difference $|E_n - E_m|$ is large.

In the worst case—when the right-hand side of Eq. (G123) is largest—$|E_n - E_m|$ is small. The right-hand side then approximates to $\frac{v^2}{\mathcal{N}R^4}$, which must < 1 for Eq. (G123) to make sense. The regularization must obey

$$R > \frac{\sqrt{v}}{\mathcal{N}^{1/4}} \, . \tag{G124}$$

How to choose a form for R is unclear. We therefore leave R unspecified temporarily. We will compute $\langle W_{\rm APT}\rangle$ in terms of R, then survey the possible forms of R. We will choose the worst-case form for R—the form that maximizes the average work cost $\langle W_{\rm APT}\rangle$—consistent with Ineq. (G124) and with the smallness of v. Even in the worst case, we will see, $\langle W_{\rm APT}\rangle$ is parametrically small.

Average work cost $\langle W_{\rm APT,1}\rangle$ of APT transitions that occur during stroke 1: The engine begins stroke 1 in a Gibbs state at temperature $T_{\rm H}$. We focus on $T_{\rm H} < \infty$. Most of the state's weight lies below the spectrum's center: $\langle E_m\rangle \equiv {\rm Tr}\left(\frac{e^{-\beta_{\rm H} H_{\rm GOE}}}{Z} H_{\rm GOE}\right) < 0$. During stroke 1, S may transition between levels. The probability of an upward jump across a magnitude-δ' gap equals the probability of a drop across a magnitude-δ' gap. More levels lie above $\langle E_m\rangle$ than below. Hence S more likely hops upward than drops downward. These diabatic hops resemble thermalization with an infinite-temperature bath, bringing the state toward maximal mixedness.

The average work cost depends on the thermal probability that S starts with energy E_m, the APT probability $P_{\rm APT}(n|m)$ of hopping, and the magnitude $E_n - E_m$ of a hop. $\langle W_{\rm APT,1}\rangle$ depends also on the density of the states to which S might hop. E_n has a negligible chance of lying a distance $< \langle\delta\rangle$ from E_m in the spectrum, due to level repulsion. We incorporate this level repulsion into a *conditional density of states*,

$$\mu(n|m) \sim \mu(E_n) \, \frac{|E_n - E_m|}{\sqrt{(E_n - E_m)^2 + \langle\delta\rangle^2}} \, . \tag{G125}$$

We approximate sums with integrals, replacing E_m with E and E_n with E':

$$\langle W_{\rm APT,1}\rangle \sim \int_{-\infty}^{\infty} dE \, \frac{e^{-\beta_{\rm H} E}}{Z} \, \mu\left(E\right) \int_{-\infty}^{\infty} dE' \, \mu(E'|E) \, P_{\rm APT}\left(E'|E\right) \cdot \left(E' - E\right) \, . \tag{G126}$$

The partition function has the form $Z = \mathcal{N} e^{(\beta_{\rm H}\mathcal{E})^2 N/2}$ [Eq. (G33)]. Equation (D1) shows the form of $\mu(E)$. The APT

---

[12] One might worry that, when this mesoscale engine functions as a component of a macroscopic engine, the Hamiltonian will not obey the ETH. Rather, $H(t)$ will be MBL at all times t. However, for the purposes of level-spacing statistics and operator expectation values on length scales of the order of the localization length, $L \sim \xi_>$, $H(t)$ can be regarded as roughly ETH. The shallowly localized Hamiltonian's key feature is some nontrivial amount of level repulsion. The ETH gap distribution, encoding level repulsion, suffices as an approximation. However, $|\langle E_n(t)|V|E_m(t)\rangle| \sim \frac{1}{\mathcal{N}}$ for a mesoscale subengine in the macroscopic engine [33].

hopping probability appears in Eq. (G123). Substituting in yields

$$\langle W_{\rm APT,1}\rangle \sim \int_{-\infty}^{\infty} dE\, \frac{e^{-\beta_{\rm H}E}}{Z}\, \left(\frac{\mathcal{N}}{\sqrt{2\pi N\mathcal{E}^2}}\, e^{-\frac{(E)^2}{2N\mathcal{E}^2}}\right) \tag{G127}$$
$$\times \int_{-\infty}^{\infty} dE'\, \left(\frac{\mathcal{N}}{\sqrt{2\pi N\mathcal{E}^2}}\, e^{-\frac{(E')^2}{2N\mathcal{E}^2}}\, \frac{|E'-E|}{\sqrt{(E'-E)^2+\langle\delta\rangle^2}}\right) \left(\frac{v^2}{\mathcal{N}\left[(E'-E)^2+R^2\right]^2}\right) (E'-E)\,.$$

Let us change variables from E and E' to $x := E - E'$ and $y := E + E'$. As $E = \frac{1}{2}(x+y)$ and $E' = \frac{1}{2}(y-x)$,

$$\langle W_{\rm APT,1}\rangle \sim -\frac{1}{8\pi}\, \frac{v^2\mathcal{N}}{N\mathcal{E}^2} \int_{-\infty}^{\infty} dy\, \frac{e^{-\beta_{\rm H}y/2}}{Z}\, e^{-y^2/4N\mathcal{E}^2} \int_{-\infty}^{\infty} dx\, e^{-\beta_{\rm H}x/2}\, e^{-x^2/4N\mathcal{E}^2}\, \frac{|x|x}{\sqrt{x^2+\langle\delta\rangle^2}\,(x^2+R^2)^2}\,. \tag{G128}$$

We focus first on the x integral, which we denote by $\mathcal{I}$. The regularization factor, R, is small. (Later, we will see that all reasonable options for $R \leq \sqrt{v}$, which $\ll \langle\delta\rangle$ by assumption.) Therefore, the integral peaks sharply around $x = 0$. We Taylor approximate the more slowly varying numerator exponentials to first order in x: $e^{-\beta_{\rm H}x/2}\, e^{-x^2/4N\mathcal{E}^2} \sim \left(1-\frac{\beta_{\rm H}}{2}\,x\right)\left(1-\frac{x^2}{4N\mathcal{E}^2}\right)$. The zeroth-order term vanishes by parity. Hence

$$\mathcal{I} \sim -\frac{\beta_{\rm H}}{\langle\delta\rangle} \int_{-\infty}^{\infty} dx\, \frac{x^2|x|}{\sqrt{x^2+\langle\delta\rangle^2}\,(x^2+R^2)^2} = -\frac{2\beta_{\rm H}}{\langle\delta\rangle} \int_0^{\infty} dx\, \frac{x^3}{\sqrt{x^2+\langle\delta\rangle^2}\,(x^2+R^2)^2}\,. \tag{G129}$$

The final equality follows from the integrand's evenness.

The square-root's behavior varies between two regimes:

$$\frac{1}{\sqrt{x^2+\langle\delta\rangle^2}} = \begin{cases} \frac{1}{\langle\delta\rangle} + O\left(\left[\frac{x}{\langle\delta\rangle}\right]^2\right), & x \ll \langle\delta\rangle \\ \frac{1}{x} + O\left(\left[\frac{\langle\delta\rangle}{x}\right]^2\right), & x \gg \langle\delta\rangle \end{cases}. \tag{G130}$$

We therefore split the integral:

$$\mathcal{I} \sim -\frac{2\beta_{\rm H}}{\langle\delta\rangle}\left(\frac{1}{\langle\delta\rangle}\int_0^{\langle\delta\rangle} dx\, \frac{x^3}{(x^2+R^2)^2} + \int_{\langle\delta\rangle}^{\infty} dx\, \frac{1}{x^2}\right). \tag{G131}$$

We have dropped the $+R^2$ from the second integral's denominator: Throughout the integration range, $x \gg \langle\delta\rangle$, which $\gg R$. Integrating yields

$$\mathcal{I} \approx -\frac{\beta_{\rm H}}{\langle\delta\rangle} \log\left(\frac{\langle\delta\rangle^2}{R^2}\right). \tag{G132}$$

We have evaluated the x integral in Eq. (G128). The y integral evaluates to $\frac{2\sqrt{\pi N}}{\mathcal{N}}\,\mathcal{E}e^{-N(\beta_{\rm H}\mathcal{E})^2/4}$. Substituting into Eq. (G128) yields

$$\langle W_{\rm APT,1}\rangle \sim \left(-\frac{1}{8\pi}\,\frac{v^2\mathcal{N}}{N\mathcal{E}^2}\right)\left[-\frac{2\beta_{\rm H}}{\langle\delta\rangle}\,\log\left(\frac{\langle\delta\rangle^2}{R^2}\right)\right]\left(\frac{2\sqrt{\pi N}}{\mathcal{N}}\,\mathcal{E}e^{-N(\beta_{\rm H}\mathcal{E})^2/4}\right) \tag{G133}$$
$$= \frac{1}{2\sqrt{\pi}}\,\frac{1}{\sqrt{N}}\,\frac{v^2\beta_{\rm H}}{\mathcal{E}\,\langle\delta\rangle}\,\log\left(\frac{\langle\delta\rangle^2}{R^2}\right) e^{-N(\beta_{\rm H}\mathcal{E})^2/4}\,. \tag{G134}$$

The regularization R appears only in the logarithm. Therefore, the form of R impacts $\langle W_{\rm APT,1}\rangle$ little. Which forms can R assume? The regularization should be small in v and should have dimensions of energy. The only other relevant energy scales are $\langle\delta\rangle$ and $\mathcal{E}$. [δ_- is irrelevant, being a property of MBL systems. This calculation concerns the ETH phase (or less localized regime).] Let us choose the "worst-case" R, which leads to the greatest work-cost estimate, consistent with Ineq. (G124) and with the smallness of v. $\langle W_{\rm APT,1}\rangle$ is large when R is small. The possible regularizations small in v are $\sqrt{v}$, $\frac{v}{\langle\delta\rangle}$, and $\frac{v}{\mathcal{E}}$. Consider substituting each value into Ineq. (G124), $R > \frac{\sqrt{v}}{\mathcal{N}^{1/4}}$,

successively. If $R \propto v$, Ineq. (G124) lower-bounds v. Diabatic transitions should upper-bound, not lower-bound, the speed. We therefore exclude $\frac{v}{\langle\delta\rangle}$ and $\frac{v}{\mathcal{E}}$ from our regularization choices. Substituting $R = \sqrt{v}$ into Ineq. (G124) yields $1 > \frac{1}{\mathcal{N}^{1/4}}$, which is true. We therefore choose

$$R = \sqrt{v} \, . \tag{G135}$$

Consequently,

$$\boxed{\langle W_{\rm APT,1} \rangle \sim \frac{1}{\sqrt{N}} \, \frac{v^2 \beta_{\rm H}}{\mathcal{E} \, \langle\delta\rangle} \, \log\left(\frac{\langle\delta\rangle^2}{v} \right) \, e^{-N(\beta_{\rm H}\mathcal{E})^2/4}} \, . \tag{G136}$$

We have dropped numerical prefactors, to maintain our focus on scaling.

We assess the work cost's magnitude by recasting (G136) in terms of small parameters: $\langle W_{\rm APT,1} \rangle \sim \frac{1}{N} \left(\frac{\sqrt{v}}{\langle\delta\rangle} \right)^4 (\sqrt{N} \, \beta_{\rm H} \mathcal{E}) \left(\frac{\langle\delta\rangle}{\mathcal{E}} \right)^2 \log\left(\left[\frac{\langle\delta\rangle}{\sqrt{v}} \right]^2 \right) e^{-N(\beta_{\rm H}\mathcal{E})^2/4} \, \langle\delta\rangle$. This work cost is suppressed in $\frac{1}{N} < 1$ linearly, in $\frac{\sqrt{v}}{\langle\delta\rangle} \ll 1$ fourfold, and in $\sqrt{N} \, \beta_{\rm H} \mathcal{E} \ll 1$ linearly. Due to the final inequality, the $e^{-N(\beta_{\rm H}\mathcal{E})^2/4} \approx 1$ affects $\langle W_{\rm APT,1} \rangle$ little. The work cost is large twofold in $\frac{\mathcal{E}}{\langle\delta\rangle} \gg 1$ and logarithmically in $\left(\frac{\langle\delta\rangle}{\sqrt{v}} \right)^2$.

Two limits of Eq. (G136) make sense: (1) If $\beta_{\rm H} = 0$, then $\langle W_{\rm APT,1} \rangle = 0$. APT transitions function as an infinite-temperature bath, as mentioned earlier. If the engine begins at infinite temperature ($\beta_{\rm H} = 0$) APT transitions have no work to do: $\langle W_{\rm APT,1} \rangle = 0$. (2) In the adiabatic limit, $v \to 0$. The v^2 approaches zero more quickly than the $\log\left(\frac{\langle\delta\rangle^2}{v} \right)$ diverges. Hence diabatic transitions cost zero average work.

Average work cost $\langle W_{\rm APT,3} \rangle$ of APT transitions that occur during stroke 3: The stroke-3 work cost depends on the engine's probability of beginning with energy E_m, the probability $P_{\rm MBL}(|\delta'|)$ that a neighboring $H_{\rm MBL}$ gap is of size δ', the engine's probability $P_\downarrow$ of dropping across a gap during cold thermalization, the engine's probability $P_\uparrow$) of hopping upward across a gap during cold thermalization, and the engine's probability $P_{\rm APT}$ of transitioning to level n during the ETH portion of stroke 3. In the lowest-order approximation, (i) the stroke-1 tuning is adiabatic (the engine remains in level m), and (ii) cold thermalization transfers S across just one gap. The average work cost is

$$\begin{aligned}
\langle W_{\rm APT,3} \rangle \approx \sum_m \frac{e^{-\beta_{\rm H} E_m}}{Z} \sum_n \Bigg\{ & \int_{-W_{\rm b}}^0 d\delta' \, P_{\rm MBL}(|\delta'|) \, P_\downarrow(|\delta'|) \, P_{\rm APT}(n|m-1)(E_n - E_{m-1}) \\
& + \int_0^{W_{\rm b}} d\delta' \, P_{\rm MBL}(\delta') \, P_\uparrow(\delta') \, P_{\rm APT}(n|m+1)(E_n - E_{m+1}) \\
& + \left[1 - \int_{-W_{\rm b}}^0 d\delta' \, P_{\rm MBL}(|\delta'|) \, P_\downarrow(|\delta'|) - \int_0^{W_{\rm b}} d\delta' \, P_{\rm MBL}(\delta') \, P_\uparrow(\delta') \right] P_{\rm APT}(n|m)(E_n - E_m) \Bigg\} \, .
\end{aligned} \tag{G137}$$

We have artificially extended the gap variable δ' to negative values: $\delta' < 0$ denotes a size-$|\delta'|$ gap that lies just below level m. The bracketed factor $[1 - \ldots]$ represents the probability that cold thermalization fails to change the engine's energy.

Let us analyze $\langle W_{\rm APT,3} \rangle$ physically. Consider the $T_{\rm C} = 0$ limit, for simplicity. On average over trials, the engine's state barely changes between strokes 1 and 3. Just tiny globules of probability weight drop across single gaps. Therefore, most stroke-3 APT transitions look identical, on average over trials, to the stroke-1 APT transitions analyzed above. Hence $\langle W_{\rm APT,3} \rangle \approx \langle W_{\rm APT,1} \rangle + (\text{correction})$.

The correction comes from the probability-weight globules that dropped during cold thermalization. APT transitions hop some globules off the bottoms of the "working gaps" depicted in Fig. 2, derailing trials that would have outputted $W_{\rm tot} \sim \langle\delta\rangle$. But other globules, which began stroke 3 elsewhere in the spectrum, hop onto the bottoms of working gaps. The globules hopping off roughly cancel with the globules hopping on. Hence $\boxed{\langle W_{\rm APT,3} \rangle \approx \langle W_{\rm APT,1} \rangle}$.

Substituting in from Eq. (G136) yields

$$\boxed{\langle W_{\rm APT} \rangle} = \langle W_{\rm APT,1} \rangle + \langle W_{\rm APT,3} \rangle \approx 2 \, \langle W_{\rm APT,1} \rangle \tag{G138}$$

$$\boxed{\sim \frac{1}{\sqrt{N}} \, \frac{v^2 \beta_{\rm H}}{\mathcal{E} \, \langle\delta\rangle} \, \log\left(\frac{\langle\delta\rangle^2}{v} \right) \, e^{-N(\beta_{\rm H}\mathcal{E})^2/4}} \, . \tag{G139}$$

We have dropped numerical prefactors, focusing on scaling behaviors.

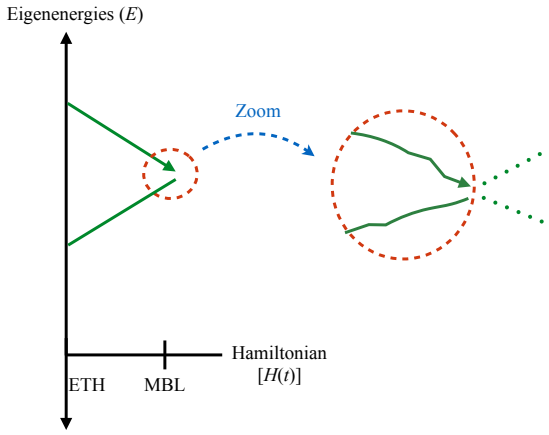

FIG. 15: Fractional-Landau-Zener transition: The straight solid green lines represent two eigenenergies. The engine ideally occupies the upper level throughout stroke 1. At the end of stroke 1, the energies approach each other. Zooming in on the approach shows that the lines are not straight, but wiggle slightly. A full Landau-Zener transition could occur if the approaching lines came very close together and then separated. The green dotted lines illustrate the hypothetical separation. Since the approaching energies do not separate, the engine may undergo an approximate fractional-Landau-Zener transition.

G 8 ii Average work costs of Landau-Zener diabatic jumps: $\langle W_{\mathrm{LZ},1} \rangle$ and $\langle W_{\mathrm{LZ},3} \rangle$

Consider the tuning near, but not quite at, the end of stroke 1 or the start of stroke 3. $H(t)$ is tuned within the MBL phase. Two energy levels can wiggle toward each other and then apart. Such wiggling can induce a Landau-Zener transition [60]. The wiggling has a probability

$$P_{\mathrm{LZ}}(\Delta) \approx e^{-2\pi(\delta_-)^2/v} \tag{G140}$$

of resulting in a diabatic hop. δ_- denotes the MBL level-repulsion scale—the least size reasonably attributable to an MBL gap. δ_- roughly equals the size of the Hamiltonian-perturbation matrix element that couples the wiggling-together states.

The average work cost, $\langle W_{\mathrm{LZ},1} \rangle$ vanishes by parity. S has as great a probability of hopping upward as of hopping downward, according to Eq. (G140). Only hops to nearest neighbors have significant probabilities. Hence the existence of more levels above the engine's average energy than below has no impact on $\langle W_{\mathrm{LZ},1} \rangle$. (The imbalance impacted the $\langle W_{\mathrm{APT}} \rangle$'s in Sec. G 8 i. There, we Taylor-approximated $e^{-\beta_{\mathrm{H}} x}$ to first order in $x := E - E'$, because S could hop across several levels. The zeroth-order term vanished by parity. The LZ calculation may be thought of as a truncation of the APT calculation at zeroth order, because S can hop only one gap. Put another way, in the APT calculation, the E integral affected the Δ integral, preventing parity from sending the Δ integral to zero. Here, the integrals decouple.) The work cost of upward hops cancels, on average, with the work cost of downward hops. Hence $\langle W_{\mathrm{LZ},1} \rangle = 0$. The same conclusions concern Landau-Zener transitions at the start of stroke 3: $\boxed{\langle W_{\mathrm{LZ},3} \rangle = \langle W_{\mathrm{LZ},1} \rangle = 0}$.

G 8 iii Average work costs of fractional-Landau-Zener diabatic jumps: $\langle W_{\mathrm{frac-LZ},1} \rangle$ and $\langle W_{\mathrm{frac-LZ},3} \rangle$

A Landau-Zener transition may occur when two energies begin far apart, come together, suffer a mixing of eigenstates, and separate. Eliminating the final step can induce a *fractional-Landau-Zener transition*. Energies begin far apart, come together, and suffer a mixing of eigenstates at the end of stroke 1. Figure 15 depicts this process. The reverse process occurs at the start of stroke 3. We apply to these strokes the model developed by De Grandi and Polkovnikov [59].

Modeling fractional-Landau-Zener transitions: De Grandi and Polkovnikov model an arbitrary portion of the Landau-Zener protocol using APT [59, Sec. II A]. Their Hamiltonian appears in their Eq. 21. We relabel their

parameters and conjugate their Hamiltonian by the unitary $\frac{1}{\sqrt{2}}(\sigma^x + \sigma^z)$:[13]

$$H_{\text{frac-LZ}} = \delta_- \, \sigma^z + vt \, \sigma^x \, . \tag{G141}$$

This Hamiltonian roughly models the result of projecting out, from the many-body Hamiltonian $H(t)$, the two levels that approach each other at the end of stroke 1.[14] De Grandi and Polkovnikov's speed δ translates into our v.[15]

De Grandi and Polkovnikov's time parameter t runs from t_i to t_f. In the ordinary Landau-Zener problem, t runs from $t_i = -\infty$ to $t_f = \infty$. We approximate t as running from $t_i = -\infty$ to $t_f = 0$ at the end of stroke 1 and from $t_i = 0$ to $t_f = \infty$ at the start of stroke 3.

Suppose that the qubit begins in one of the energy eigenstates. Consider the probability that, while the fractional-LZ protocol is implemented, the system hops to the other eigenstate. De Grandi and Polkovnikov calculate that probability using APT. Their Eq. (29) has the form

$$P_{\text{frac-LZ}} \approx \frac{v^2 \left(\delta_-\right)^2}{16} \left(\frac{1}{\left[\left(\delta_-\right)^2 + \left(vt_i\right)^2 \right]^3} + \frac{1}{\left[\left(\delta_-\right)^2 + \left(vt_f\right)^2 \right]^3} \right) \tag{G142}$$

$$= \frac{v^2 \left(\delta_-\right)^2}{16} \left(\frac{1}{\left(\text{Initial gap}\right)^6} + \frac{1}{\left(\text{Final gap}\right)^6} \right) . \tag{G143}$$

Let us focus on stroke 3, which, we will see, dominates $\langle W_{\text{frac-LZ}} \rangle$. The second fraction vanishes, according to (G142), because $t_f = \infty$. Let Δ' denote the gap with which stroke 3 starts. Our MBL spectrum's "working gaps" have been modeled as ranging from 0 to W_{b}. Integrating through $\Delta' = 0$ causes (G143) to diverge. Therefore, we must refine our model. In which trials do fractional-LZ transitions cost net positive work $W_{\text{frac-LZ}} > 0$? The trials that otherwise—in the absence of the transitions—would output $W_{\text{tot}} > 0$.[16] Most otherwise-successful trials involve MBL-spectrum gaps $\Delta' \in [\delta_-, W_{\text{b}}]$. Gaps $\Delta' \leq \delta_-$ are very rare and contribute little to $\langle W_{\text{tot}} \rangle$ (App. G 6). Most otherwise-successful trials involve gaps $\Delta' \sim W_{\text{b}}$. Therefore, we will integrate Δ' from ϵW_{b} to W_{b}, wherein ϵ is some proper fraction greater than $\frac{\delta_-}{W_{\text{b}}}$.[17]

We approximate, as follows, the average work cost of fractional-LZ transitions across MBL gaps $\Delta' < \epsilon W_{\text{b}}$. In any given trial, the engine has a probability $\sim \frac{\epsilon W_{\text{b}}}{\langle \delta \rangle}$ of neighboring an MBL gap $\Delta' < \epsilon W_{\text{b}}$. In the worst case, whenever the engine neighbors such a gap, the engine undergoes a stroke-3 fractional-LZ transition. Suppose, for simplicity, that $T_{\text{C}} = 0$. Each such diabatic transition costs work $\sim \langle \delta \rangle$ (the work that the trial would have yielded, in the absence of the diabatic transition). Hence gaps $\Delta' < \epsilon W_{\text{b}}$ cost, at most, an amount

$$\frac{\epsilon W_{\text{b}}}{\langle \delta \rangle} \cdot \langle \delta \rangle = \epsilon W_{\text{b}} \tag{G144}$$

of work, on average. This upper bound could be refined, but it suffices for showing that $\langle W_{\text{frac-LZ}} \rangle$ is small.

Approximating dominant initial gaps with $\sim W_{\text{b}}$ implies a condition on v under which Eq. (G143) is justified. The probability $P_{\text{frac-LZ}}$ must be normalized. Hence the right-hand side of (G143) must not exceed one: $P_{\text{frac-LZ}} \sim \frac{v(\delta_-)^2}{16(W_{\text{b}})^6} \leq 1$. Solving for the speed yields

$$v \leq \frac{4(W_{\text{b}})^3}{\delta_-} \, . \tag{G145}$$

---

[13] This unitary is called the *Hadamard* in quantum computation. The Hadamard represents a rotation through an angle π. The rotation axis lies midway between the $\hat{x}$- and $\hat{z}$-axes. The rotation interchanges σ^x and σ^z. Conjugation by the Hadamard is equivalent to the use of a rotating reference frame.

[14] The $H(t)$ levels may change more complicatedly than the $H_{\text{frac-LZ}}$ levels. For example, the true effective two-body Hamiltonian might contain a σ^y term, more-complicated coefficients, etc. But $H_{\text{frac-LZ}}$ captures the basic physics of growing energies and metamorphosing eigenstates.

[15] The significance of δ changes between the general APT discussion and the fractional-LZ discussion in [59]. In the latter discussion, δ has dimensions of Time^2. This conclusion follows from de Grandi and Polkovnikov's Eq. (21), $\mathcal{H} = \lambda\sigma_z + g\sigma_x$, and the $\lambda = \delta t$ below their Eq. (23).

[16] A fractional-LZ transition costs work of two types. To describe them concretely, we suppose that the transition boosts the engine upward across a gap at the start of stroke 3:

1. The engine absorbs energy from the battery while hopping.

2. After hopping, typically, the engine slides up an energy level, like the top green line in Fig. 2, during the MBL-to-ETH tuning. The engine "undoes" the work extraction performed during the ETH-to-MBL tuning.

The average type-1 work cost roughly equals W_{b}. The average type-2 work cost roughly equals $\langle \delta \rangle \gg W_{\text{b}}$. Hence we approximate the total work cost with the type-2 work.

[17] Earlier sections contain Δ' integrals that run from 0 to W_{b}. These integrals remain justified: Those integrands do not diverge as $\Delta' \to 0$. Moreover, those integrals are dominated by the region near W_{b}. Hence shifting integration limits would affect the integrals negligibly.

We can bound v alternatively by estimating $\langle W_{\text{frac-LZ}} \rangle$ and demanding that fractional-LZ transitions cost less work than the ideal engine outputs per average cycle: $\langle W_{\text{frac-LZ}} \rangle \ll \langle W_{\text{tot}} \rangle$. This inequality, we will find, implies Ineq. (G145), up to prefactors. The approximation (G143) therefore leads to a self-consistent argument.

Average work cost $\langle \mathbf{W_{frac\text{-}LZ,1}} \rangle$ of fractional-Landau-Zener diabatic transitions at the end of stroke 1: These transitions cost zero work, on average, by symmetry: $\boxed{\langle W_{\text{frac-LZ},1} \rangle = 0}$. The reason is the reason why $\langle W_{\text{LZ}} \rangle = 0$. Suppose that the engine starts stroke 1 on the j^{th} energy level. At the end of stroke 1, level j as likely approaches level $j-1$ as it approaches level $j+1$. A fractional-LZ transition as likely costs positive work as it costs negative work. The average work cost therefore vanishes. This symmetry is absent from $\langle W_{\text{frac-LZ},3} \rangle$, due to cold thermalization.

Average work cost $\langle \mathbf{W_{frac\text{-}LZ,3}} \rangle$ of fractional-Landau-Zener diabatic transitions at the start of stroke 3: We focus first on one trial. Let E denote the energy of the level in which S begins. S undergoes no diabatic transitions during stroke 1, in a lowest-order approximation. E is mapped to the MBL eigenenergy E'. E' neighbors at most one small gap, to lowest order in the gap distribution $P_{\text{MBL}}(|\Delta'|)$. (We artificially extend the distribution to negative values: $\Delta' > 0$ signifies a gap above E'. $\Delta' < 0$ signifies a gap below.) Cold thermalization has probabilities $\frac{1}{1+e^{\pm \beta_{\text{C}} |\Delta'|}}$ of transferring S upward or downward across a small gap. As stroke 3 begins, S has a probability $P_{\text{frac-LZ}}(\Delta')$ of reversing across the gap.

S has a probability $1 - \mathcal{P}_\downarrow - \mathcal{P}_\uparrow \equiv 1 - \int_{-W_{\text{b}}}^0 d\Delta' \, P_{\text{MBL}}(|\Delta'|) \, \frac{1}{1+e^{-\beta_{\text{C}} |\Delta'|}} - \int_0^{W_{\text{b}}} d\Delta' \, P_{\text{MBL}}(\Delta') \, \frac{1}{1+e^{\beta_{\text{C}} \Delta'}}$ of staying in the energy-E' level throughout the cold thermalization. If S stays in the energy-E' level, any fractional-LZ transitions at the start of stroke 3 cost an amount $\langle W_{\text{frac-LZ},1} \rangle = 0$ of work, on average. Hence

$$\langle W_{\text{frac-LZ},3} \rangle \approx \int_{-\infty}^{\infty} dE \, \frac{e^{-\beta_{\text{H}} E}}{Z} \, \mu(E) \Bigg[\int_{-W_{\text{b}}}^{-\epsilon W_{\text{b}}} d\Delta' \, P_{\text{MBL}}(|\Delta'|) \, \frac{1}{1+e^{-\beta_{\text{C}} |\Delta'|}} \, P_{\text{frac-LZ}}(\Delta') \int_0^{\infty} d\Delta \cdot \Delta \, P_{\text{GOE}}(\Delta)$$
$$+ \int_{\epsilon W_{\text{b}}}^{W_{\text{b}}} d\Delta' \, P_{\text{MBL}}(\Delta') \, \frac{e^{-\beta_{\text{C}} \Delta'}}{1+e^{-\beta_{\text{C}} \Delta'}} \, P_{\text{frac-LZ}}(\Delta') \int_{-\infty}^{0} d\Delta \cdot \Delta \, P_{\text{GOE}}(|\Delta|) \Bigg] + (1 - \mathcal{P}_\downarrow - \mathcal{P}_\uparrow) \, \langle W_{\text{frac-LZ},1} \rangle + \epsilon W_{\text{b}} \, . \tag{G146}$$

The final term, ϵW_{b}, forms a crude upper bound estimated in (G144). Substituting in for various factors yields

$$\langle W_{\text{frac-LZ},3} \rangle \approx \int_{-W_{\text{b}}}^{-\epsilon W_{\text{b}}} d\Delta' \, \frac{e^{\Delta'/\langle \delta \rangle}}{\langle \delta \rangle} \, \frac{1}{1+e^{-\beta_{\text{C}} |\Delta'|}} \left(\frac{v^2 (\delta_-)^2}{16} \frac{1}{(\Delta')^6} \right) \int_0^{\infty} d\Delta \cdot \Delta \left(\frac{\pi}{2} \, \frac{\Delta}{\langle \delta \rangle^2} \, e^{-\frac{\pi}{4} \Delta^2 / \langle \delta \rangle^2} \right)$$
$$+ \int_{\epsilon W_{\text{b}}}^{W_{\text{b}}} d\Delta' \, \frac{e^{-\Delta'/\langle \delta \rangle}}{\langle \delta \rangle} \, \frac{e^{-\beta_{\text{C}} \Delta}}{1+e^{-\beta_{\text{C}} \Delta'}} \left(\frac{v^2 (\delta_-)^2}{16} \frac{1}{(\Delta')^6} \right) \int_{-\infty}^{0} d\Delta \cdot \Delta \left(\frac{\pi}{2} \, \frac{|\Delta|}{\langle \delta \rangle^2} \, e^{-\frac{\pi}{4} \Delta^2 / \langle \delta \rangle^2} \right) + 0 + \epsilon W_{\text{b}} \, . \tag{G147}$$

The E integral has evaluated to one.

The first Δ integral evaluates to $\langle \delta \rangle$; and the second, to $-\langle \delta \rangle$. The average work cost simplifies to

$$\langle W_{\text{frac-LZ},3} \rangle \approx \frac{v^2 (\delta_-)^2}{16} \left(\int_{-W_{\text{b}}}^{-\epsilon W_{\text{b}}} d\Delta' \, e^{\Delta'/\langle \delta \rangle} \, \frac{1}{1+e^{\beta_{\text{C}} \Delta'}} \, \frac{1}{(\Delta')^6} - \int_{\epsilon W_{\text{b}}}^{W_{\text{b}}} d\Delta' \, e^{-\Delta'/\langle \delta \rangle} \, \frac{1}{1+e^{\beta_{\text{C}} \Delta'}} \, \frac{1}{(\Delta')^6} \right) + \epsilon W_{\text{b}} \, . \tag{G148}$$

We map $\Delta' \mapsto -\Delta'$ in the first integral, then combine the integrals. Then, we Taylor-approximate to first order in $e^{-\beta_{\text{C}} \Delta'} \ll 1$:

$$\langle W_{\text{frac-LZ},3} \rangle \approx \frac{v^2 (\delta_-)^2}{16} \int_{\epsilon W_{\text{b}}}^{W_{\text{b}}} d\Delta' \, e^{-\Delta'/\langle \delta \rangle} \left(\frac{1}{1+e^{-\beta_{\text{C}} \Delta'}} - \frac{1}{1+e^{\beta_{\text{C}} \Delta'}} \right) \frac{1}{(\Delta')^6} + \epsilon W_{\text{b}} \tag{G149}$$
$$\approx \frac{v^2 (\delta_-)^2}{16} \int_{\epsilon W_{\text{b}}}^{W_{\text{b}}} d\Delta' \, e^{-\Delta'/\langle \delta \rangle} \left(1 - 2 e^{-\beta_{\text{C}} \Delta'} \right) \frac{1}{(\Delta')^6} + \epsilon W_{\text{b}} \, . \tag{G150}$$

While evaluating the integrals, we invoke the small-parameter assumptions in App. G 2. We approximate the $O\left(\left[e^{-\beta_{\text{C}} \Delta'} \right]^0 \right)$ term to second-lowest order, because the biggest $O\left(e^{-\beta_{\text{C}} \Delta'} \right)$ term is one order lower (due to the

$e^{-\beta_{\rm C}\Delta'}$) than the largest $O\left(\left[e^{-\beta_{\rm C}\Delta'}\right]^0\right)$ term. The average work cost evaluates to

$$\boxed{\langle W_{\text{frac-LZ},3}\rangle \approx \frac{v^2(\delta_-)^2}{16}\left[\frac{1}{5(W_{\rm b})^5}\left(\frac{1}{\epsilon^5}-1\right)-\frac{1}{4\,\langle\delta\rangle\,(W_{\rm b})^4}\left(\frac{1}{\epsilon^4}-1\right)-\frac{e^{-\epsilon\beta_{\rm C}W_{\rm b}}}{60\epsilon}\,\frac{(\beta_{\rm C})^4}{W_{\rm b}}\right]+\epsilon W_{\rm b}} \tag{G151}$$

$$\boxed{\sim \frac{1}{80\epsilon^5}\,\frac{v^2(\delta_-)^2}{(W_{\rm b})^5}+\epsilon W_{\rm b}}\,. \tag{G152}$$

By assumption, $\epsilon < 1$. We will often assume that $\epsilon \approx \frac{1}{3}$. Hence the final term in Eq. (G152) is smaller than $\langle W_{\rm tot}\rangle \sim W_{\rm b}$.

Let us gauge the size of the first term in Eq. (G152). In terms of small parameters, $\frac{1}{80\epsilon^5}\,\frac{v^2(\delta_-)^2}{(W_{\rm b})^5} = \frac{\langle\delta\rangle}{80\epsilon^5}\left(\frac{\sqrt{v}}{\langle\delta\rangle}\right)^4\left(\frac{\delta_-}{\langle\delta\rangle}\right)^2\left(\frac{\langle\delta\rangle}{W_{\rm b}}\right)^5$. The average work cost is suppressed fourfold in $\frac{\sqrt{v}}{\langle\delta\rangle} \ll 1$ and twofold in $\frac{\delta_-}{\langle\delta\rangle} \ll 1$. The cost is fivefold large in $\frac{\langle\delta\rangle}{W_{\rm b}}$, which $\gg 1$ but which $\ll \frac{\langle\delta\rangle}{\delta_-}$, and fivefold large in $\frac{1}{\epsilon} < 1$.

Equation (G152) implies an upper bound on v of the form in Ineq. (G145). The Hamiltonian must be tuned slowly enough that fractional-LZ transitions cost less work than an ideal cycle outputs, on average: $\langle W_{\text{frac-LZ}}\rangle \ll \langle W_{\rm tot}\rangle$. The right-hand side roughly equals $W_{\rm b}$, by Eq. (9). We substitute in for the left-hand side from Eq. (G152). Solving for the speed yields $v \ll \sqrt{80\epsilon^5}\,\frac{(W_{\rm b})^3}{\delta_-}$. For every tolerance $\epsilon \in (0,1)$, there exist speeds v such that the inequality is satisfied. For simplicity, we suppose that $\epsilon \sim \frac{1}{3}$, such that the overall constant ≈ 1. The bound reduces to

$$v \ll \frac{(W_{\rm b})^3}{\delta_-}\,. \tag{G153}$$

This bound has the form of Ineq. (G145). Therefore, our approximation (G143) leads to a self-consistent argument.

The final term in Eq. (G151) constitutes a finite-temperature correction. Suppose temporarily that the cold bath is maximally cold: $\frac{1}{\beta_{\rm C}} = 0$. The final term in (G151) vanishes. If the engine energy E' lies just above an MBL gap of size $< W_{\rm b}$, cold thermalization drops the engine's energy deterministically. Any subsequent diabatic hop increases the engine's energy, costing work. Suppose, instead, that the cold bath has a "largish small" temperature: $\epsilon W_{\rm b} \ll \frac{1}{\beta_{\rm C}} < W_{\rm b}$. Even if E' lies just above a small gap, cold thermalization might fail to drop the engine's energy. A subsequent diabatic drop could compensate for the failure. The hop would turn a no-op (a $W_{\rm tot} = 0$ trial) into a successful trial. Hence the final term in Eq. (G151) is negative, detracting from the work cost of diabatic transitions.

G 8 iv Diabatic correction to the efficiency $\eta_{\rm MBL}$

Recall that

$$\eta_{\rm MBL} = \frac{\langle W_{\rm tot}\rangle}{\langle Q_{\rm in}\rangle} = \frac{\langle W_{\rm tot}\rangle}{\langle Q_4\rangle} = \frac{\langle W_{\rm tot}\rangle}{\langle W_{\rm tot}\rangle - \langle Q_2\rangle} = \frac{\langle W_{\rm tot}\rangle}{\langle W_{\rm tot}\rangle\left(1-\frac{\langle Q_2\rangle}{\langle W_{\rm tot}\rangle}\right)} \tag{G154}$$

(App. G 7). Here, $\langle W_{\rm tot}\rangle$ denotes the net work extracted per trial, on average over trials. [Earlier, $\langle W_{\rm tot}\rangle$ denoted the average net work extracted per trial in which $H(t)$ is tuned adiabatically.] Taylor-approximating to first order yields

$$\eta_{\rm MBL} \approx 1 + \frac{\langle Q_2\rangle}{\langle W_{\rm tot}\rangle} = 1 + \frac{\langle Q_2\rangle}{\left\langle W_{\rm tot}^{\rm adiab}\right\rangle - \langle W_{\rm diab}\rangle}\,. \tag{G155}$$

For clarity, we have relabeled as $\left\langle W_{\rm tot}^{\rm adiab}\right\rangle$ the adiabatic approximation (G113) to the per-cycle power. The average total per-cycle diabatic work cost is denoted by $\langle W_{\rm diab}\rangle$.

Since $\left\langle W_{\rm tot}^{\rm adiab}\right\rangle \gg \langle W_{\rm diab}\rangle$,

$$\eta_{\rm MBL} \approx 1 + \frac{\langle Q_2\rangle}{\left\langle W_{\rm tot}^{\rm adiab}\right\rangle\left(1-\frac{\langle W_{\rm diab}\rangle}{\left\langle W_{\rm tot}^{\rm adiab}\right\rangle}\right)} \approx 1 + \frac{\langle Q_2\rangle}{\left\langle W_{\rm tot}^{\rm adiab}\right\rangle}\left(1+\frac{\langle W_{\rm diab}\rangle}{\left\langle W_{\rm tot}^{\rm adiab}\right\rangle}\right)\,. \tag{G156}$$

We relabel as $\eta_{\rm MBL}^{\rm adiab}$ the adiabatic estimate (G117) of the efficiency:

$$\eta_{\rm MBL} \approx \eta_{\rm MBL}^{\rm adiab} + \langle W_{\rm diab} \rangle \frac{\langle Q_2 \rangle}{\left\langle W_{\rm tot}^{\rm adiab} \right\rangle^2} \, . \tag{G157}$$

Substituting in from Eq. (G37), and substituting in the leading-order term from Eq. (G113), yields

$$\eta_{\rm MBL} \approx \eta_{\rm MBL}^{\rm adiab} - \frac{\langle W_{\rm diab} \rangle}{2 \langle \delta \rangle} \equiv \eta_{\rm MBL}^{\rm adiab} - \phi_{\rm diab} \, . \tag{G158}$$

For simplicity, we specialize to $T_{\rm H} = \infty$ and $T_{\rm C} = 0$. The diabatic correction becomes

$$\boxed{\phi_{\rm diab}} = \frac{\langle W_{\rm diab} \rangle}{2 \langle \delta \rangle} \Bigg|_{\substack{T_{\rm C}=0, \\ T_{\rm H}=\infty}} \tag{G159}$$

$$= \frac{1}{2 \langle \delta \rangle} \left(\langle W_{\rm APT}, 3 \rangle + \langle W_{\text{frac-LZ},3} \rangle \right) \Big|_{\substack{T_{\rm C}=0, \\ T_{\rm H}=\infty}} \tag{G160}$$

$$\boxed{\approx \frac{v^2 W_{\rm b}}{2 \langle \delta \rangle^5} + \frac{1}{160 \epsilon^5} \frac{v^2 (\delta_-)^2}{(W_{\rm b})^5 \langle \delta \rangle} + \frac{\epsilon}{2} \frac{W_{\rm b}}{\langle \delta \rangle}} \, . \tag{G161}$$

We have substituted in from Eqs. (G139) and (G152).

Work-costing diabatic jumps detract from the efficiency, as expected. The detraction is small in $\frac{\sqrt{v}}{\langle \delta \rangle} \ll 1$, among other small parameters. In contrast, the leading-order correction in $\eta_{\rm MBL}^{\rm adiab}$ is suppressed linearly in the greatest of the small parameters, $\frac{W_{\rm b}}{\langle \delta \rangle}$.

Appendix H PHENOMENOLOGICAL MODEL FOR THE MBL OTTO ENGINE

We introduced the thermodynamically large MBL Otto engine in Sec. II C: Mesoscale subengines operate in parallel. We parallelized subengines because the per-cycle power $\langle W_{\rm tot} \rangle_L$ outputted by a length-L MBL subengine decays as 2^{-L}. Suppose that L equaled the whole-system size $N_{\rm macro}$—that we did not decompose the engine into subengines. In the thermodynamic limit as $L = N_{\rm macro} \to \infty$, $\langle W_{\rm tot} \rangle_{\rm macro} \sim 2^{-N_{\rm macro}}$ would vanish. Parallelization fixes L as a constant function of $N_{\rm macro}$. The parallelization relies on local level repulsion, described below.

We extend local level repulsion to MBL from Anderson insulators. Anderson localization was discovered before many-body localization [63]. Like MBL systems, Anderson insulators experience disorder and hopping. The disorder localizes particles, preventing them from flowing, as in an insulator. In Anderson insulators, particles interact negligibly. Anderson Hamiltonians lack the $\sigma_j^z \sigma_{j+1}^z$ repulsion term in $H_{\rm sim}(t)$. Each whole-system eigenstate of an Anderson Hamiltonian equals a Slater determinant of single-particle states. Eigenfunctions localized near each other spatially tend to have far-apart energies. This tendency is called *local level repulsion* [61, 62]. We review local level repulsion in Anderson insulators and extend the concept to MBL. Local level repulsion helps mesoscale Otto subengines to operate in parallel in the thermodynamically large MBL engine. Also, the slowness with which information spreads through MBL impedes interactions between subengines.

We begin by reviewing Anderson Hamiltonians, their energy eigenfunctions, and their localization lengths $\xi_{\rm And}$ [44, 63]. We discuss local level repulsion in Anderson insulators [44] in the strong-disorder limit. We extend local level repulsion to MBL, then apply the repulsion to scale the MBL Otto engine. We also estimate the MBL level repulsion's energy scale. This estimate informs our optimization of the cycle in Apps. I and J.

Throughout the rest of this appendix, we denote by N the length of the whole system of interest, be it an Anderson insulator or an MBL system.

H 1 Anderson-localized Hamiltonians

Consider a 1D spin chain or, equivalently, lattice of spinless fermions. Lengths will be expressed in units of the lattice spacing, set to one. The Hamiltonian

$$H_{\rm And} = \mathcal{E}\left[h \sum_{j=1}^{N} h_j \sigma_j^z + \sum_{j=1}^{N-1} \left(\sigma_j^+ \, \sigma_{j+1}^- + \sigma_j^- \, \sigma_{j+1}^+ \right) \right] \tag{H1}$$

$$= \mathcal{E}\left[2h \sum_{j=1}^{N} h_j n_j + \sum_{j=1}^{N-1} \left(c_j^\dagger \, c_{j+1} + c_j \, c_{j+1}^\dagger \right) + \text{const.} \right] \tag{H2}$$

exhibits Anderson localization. The disorder strength h and the on-site potential h_j are defined as in the main text. $H_{\rm And}$ has the disorder and hopping terms of Eq. (24) but lacks the interaction $\sigma_j^z \sigma_{j+1}^z$. The unit of energy—the average energy density per site—is $\mathcal{E}$. $\mathcal{E}$ equals also the hopping frequency.

In Eq. (H1), the site-j raising and lowering operators are denoted by $\sigma_j^+ := \frac{1}{2}\left(\sigma_j^x + i\sigma_j^y\right)$ and $\sigma_j^- := \frac{1}{2}\left(\sigma_j^x - i\sigma_j^y\right)$. Equation (H2) is cast in fermionic language, to facilitate later discussion. $c_j^\dagger$ and c_j represent the creation and the annihilation of a fermion at site j. The number operator is denoted by $n_j := c_j^\dagger c_j$.

Let $|0\rangle$ denote a reference state in which (in spin language) all the spins point downward or (in fermionic language) all the fermionic orbitals are empty. This $|0\rangle$ is not necessarily the ground state. In this section, we will focus, for concreteness, on the properties of single-spin, or single-fermion, excitations relative to $|0\rangle$. The $\ell^{\rm th}$ excitation is represented, in fermionic notation, as $\sum_x \psi_\ell(x) c_{x_\ell}^\dagger |0\rangle$. The single-excitation wave functions $\psi_\ell(x)$ are localized: x_ℓ denotes the point at which the probability density $|\psi_\ell(x)|^2$ peaks. The wave function decays exponentially with the distance $|x - x_\ell|$ from the peak:

$$\psi_\ell(x) \approx \sqrt{\frac{2}{\xi_{\rm And}}} \, e^{-|x-x_\ell|/\xi_{\rm And}} \, . \tag{H3}$$

The localization length is denoted by $\xi_{\rm And}$.

H 2 Single-particle localization length $\xi_{\rm And}$

The localization length varies with the microscopic Hamiltonian parameters as

$$\xi_{\rm And} \sim \frac{1}{\ln h} \, . \tag{H4}$$

Equation (H4) follows from a simple physical argument.

Consider measuring whether a particle occupies the position $x = x_\ell$. The probability density $|\psi_\ell(x)|^2$ peaks sharply at $x = x_\ell$. The measurement therefore has a high probability of yielding "yes."

Consider measuring, instead, whether a particle sits m sites rightward, at $x = x_{\ell+m}$. Loosely, the measurement is of whether the particle has hopped to $x_{\ell+m}$. Let P denote the probability that the measurement yields "yes." We construct two expressions for P. One expression contains $\xi_{\rm And}$; and the other, h. We equate the expressions, then solve for $\xi_{\rm And}$.

The first expression stems from the localization length's definition:

$$P \sim e^{-2m/\xi_{\rm And}} \, . \tag{H5}$$

The two comes from the probability's equaling the probability amplitude's *square* modulus. To construct the second expression, we construct the probability p that a particle hops from site ℓ to site $\ell + 1$. p grows as the hopping frequency $\mathcal{E}$ grows and as the potential $\sim h\mathcal{E}$ weakens. Hence $p \sim \frac{\mathcal{E}}{\mathcal{E}h} = \frac{1}{h}$. The probability that the particle hops m sites rightward of ℓ is

$$P \sim p^{2m} \sim \left(\frac{1}{h} \right)^{2m} \, . \tag{H6}$$

Equating (H5) with (H6), then solving for $\xi_{\rm And}$, yields (H4).

H 3 Local level repulsion in Anderson insulators

We begin with the infinitely localized limit $h \to \infty$. We take $\mathcal{E} \to 0$ to keep the Hamiltonian's energy scale finite. The hopping terms can be neglected, and particles on different sites do not repel. Single-particle excitations are localized on single sites. The site-i excitation corresponds to an energy $2\mathcal{E}hh_i$. Since the on-site potentials $h \cdot h_i$ are uncorrelated, neighboring-site excitations' energies are uncorrelated.

Let us turn to large but finite h. Recall that $h \cdot h_i$ is drawn uniformly at random from $[-h, h]$. The uniform distribution has a standard deviation of $\frac{h}{\sqrt{3}} \gg 1$. Therefore, $h|h_i - h_{i+1}| \gg 1$ for most pairs of neighboring sites. The hopping affects these sites' wave functions and energies weakly. But with a probability $\sim \frac{1}{h}$, neighboring sites have local fields $h \cdot h_i$ and $h \cdot h_{i+1}$ such that $h|h_i - h_{i+1}| \lesssim 1$. The hopping hybridizes such sites. The hybridization splits the sites' eigenvalues by an amount $\sim \sqrt{h^2(h_i - h_{i+1})^2 + \mathcal{E}^2} \geq \mathcal{E}$.

Consider, more generally, two sites separated by a distance L. Suppose that the sites' disorder-field strengths are separated by $< 1/h^L$. (The upper bound approximates the probability amplitude associated with a particle's hopping the L intervening sites). The sites' excitation energies and energy eigenfunctions are estimated perturbatively. The expansion parameter is $1/h$. To zeroth order, the energies are uncorrelated and (because $h|h_i - h_{i+L}| < 1/h^L$) are split by $< \mathcal{E}/h^L$. The eigenfunctions are hybridized at order L. The perturbed energies are split by $\geq \mathcal{E}/h^L \sim \mathcal{E}e^{-L/\xi_{\rm And}}$. [Recall that $\xi_{\rm And} \sim 1/\ln h$, by Eq. (H4).]

Hence eigenstates localized on nearby sites have correlated energies: *The closer together sites lie in real space, the lower the probability that they correspond to similar energies.* This conclusion agrees with global Poisson statistics: Consider a large system of $N \gg 1$ sites. Two randomly chosen single-particle excitations are typically localized a distance $\sim N$ apart. The argument above implies only that the energies are at least $\sim \mathcal{E}e^{-N/\xi_{\rm And}}$ apart. This scale is exponentially smaller (in system size) than the average level spacing $\sim \frac{\mathcal{E}h}{N}$ between single-particle excitations.[18]

We can quantify more formally the influence of hybridization on two energies separated by ω and associated with eigenfunctions localized a distance L apart. The *level correlation function* is defined as

$$R(L, \omega) := \frac{1}{N^2} \sum_{i,n,n'} |\langle 0|\sigma_i^+|n\rangle|^2 \, |\langle 0|\sigma_{i+L}^+|n'\rangle|^2 \, \delta(E_n - E_{n'} - \omega) - \tilde{\mu}(\omega)^2 \, . \tag{H7}$$

The spatially averaged density of states at frequency ω is denoted by $\tilde{\mu}(\omega) := \frac{1}{N} \sum_n |\langle 0|\sigma_i^+|n\rangle|^2 \, \delta(E_n - \omega)$. $|n\rangle$ and $|n'\rangle$ denote eigenstates, corresponding to single-particle excitations relative to $|0\rangle$, associated with energies E_n and $E_{n'}$. In the Anderson insulator, $R(L, \omega) \approx 0$ when $\omega \gg \mathcal{E}e^{-L/\xi_{\rm And}}$: Levels are uncorrelated when far apart in space and/or energy. When energies are close ($\omega \lesssim \mathcal{E}e^{-L/\xi_{\rm And}}$), $R(L, \omega)$ is negative. These levels repel (in energy space).

H 4 Generalization to many-body localization

The estimates above can be extended from single-particle Anderson-localized systems to MBL systems initialized in arbitrary energy eigenstates (or in position-basis product states). We formulated the level correlator $R(L, \omega)$ in terms of matrix elements $\langle 0|\sigma_i^+|n\rangle$ of local operators σ_i^+, rather than in terms of eigenfunctions. Whereas Anderson energy eigenfunctions differ from MBL energy eigenfunctions, the local operators relevant to Anderson insulators have the forms of the local operators relevant to MBL systems. Therefore, $R(L, \omega)$ is defined for MBL systems as for Anderson insulators, as in Eq. (H7). However, $|0\rangle$ now denotes a generic many-body state.

Let us estimate the scale $\mathcal{J}_L$ of the level repulsion between MBL energies. $\mathcal{J}_L$ will depend on the distance L between the energies' eigenfunctions. We focus on exponential behaviors, neglecting (1) numerical constants and (2) factors of (length)$^{(\text{finite } \#)}$. The MBL energy eigenstates result from perturbative expansions about Anderson energy eigenstates. Consider representing the Hamiltonian as a matrix $\mathcal{M}$ with respect to the true MBL energy eigenbasis. Off-diagonal matrix elements couple together unperturbed states. These couplings hybridize the unperturbed states, forming corrections. The couplings may be envisioned as rearranging particles throughout a distance L.

MBL dynamics is unlikely to rearrange particles across considerable distances, since MBL systems are localized. Such a rearrangement—a transition between states—is encoded in an off-diagonal element $\mathcal{M}_{ij}$ of $\mathcal{M}$. This $\mathcal{M}_{ij}$ must

---

[18] The average level spacing between single-particle excitations scales as $\sim 1/N$ for the following reason. The reference state $|0\rangle$ consists of N downward-pointing spins. Flipping one spin upward yields a single-particle excitation. N single-particle-excitation states exist, as the chain contains N sites. Each site has an energy $\sim \pm\mathcal{E}h$, to zeroth order, as explained three paragraphs ago. The excitation energies therefore fill a band of width $\sim \mathcal{E}h$. An interval $\sim \frac{\mathcal{E}h}{N}$ therefore separates single-particle-excitation energies, on average.

be small—suppressed exponentially in L. $\mathcal{M}_{ij}$ also forces the eigenstates' energies apart (App. F), contributing to level repulsion. Hence the level-repulsion scale is suppressed exponentially in L:

$$\mathcal{J}_L \sim \mathcal{E} e^{-L/\zeta} \, , \tag{H8}$$

for some constant ζ. At infinite temperature, ζ must $< \frac{1}{\ln 2}$ for the MBL phase to remain stable [103]. Substituting into Eq. (H8) yields $\mathcal{J}_L < \frac{\mathcal{E}}{2^L}$. The level-repulsion scale is smaller than the average gap.

The size and significance of $\mathcal{J}_L$ depend on the rearrangement distance L. Distances L fall into two regimes: small and large. At the crossover distance $L_{\rm Cross} \equiv \xi$, the repulsion $\mathcal{J}_L$ (between energy eigenfunctions localized a distance ξ apart) becomes comparable to the average gap $\sim \frac{\mathcal{E}}{2^\xi}$ between the eigenfunctions in the same length-ξ interval: $\mathcal{E} e^{-\xi/\zeta} \sim \frac{1}{e} \frac{\mathcal{E}}{2^\xi}$. Solving for the crossover distance yields

$$\xi \sim \frac{1}{\frac{1}{\zeta} - \ln 2} \, . \tag{H9}$$

Relation (H9) provides a definition of the MBL localization length ξ. (This ξ differs from the Anderson localization length $\xi_{\rm And}$, introduced in App. H 2.) Solving (H9) for ζ yields

$$\zeta \sim \frac{1}{\frac{1}{\xi} + \ln 2} \, . \tag{H10}$$

The MBL Otto cycle involves two localization lengths in the thermodynamic limit. In the shallowly localized (ETH-like) regime, $\xi = \xi_>$. Each eigenfunction has significant weight on $\xi_> \sim 12$ sites, in an illustrative example. (The choice of 12 is motivated by the 12-site numerics in Sec. III.) In the very localized regime, $\xi = \xi_<$. Eigenfunctions peak tightly, e.g., about single sites: $\xi_< \sim 1$. Shallowly localized eigenfunctions are spread across more sites than deeply localized eigenfunctions: $\xi_> > \xi_<$.

Suppose that the particles are rearranged across a large distance $L \gg \xi$. The level-repulsion scale is much smaller than the average gap, $\langle \delta \rangle$. The level-repulsion scale

$$\boxed{\mathcal{J}_{L \gg \xi}} \sim \mathcal{E} e^{-L/\zeta} \boxed{\sim \mathcal{E} e^{-L/\xi} \, 2^{-L}} \tag{H11}$$

is the minimum width reasonably attributable to any gap between MBL energies. In the MBL Otto engine's very localized regime, wherein $\xi = \xi_<$, if $L = \xi_>$ equals one subengine's length, $\mathcal{J}_{L \gg \xi} = \delta_-$.

Now, suppose that the particles are rearranged across a short distance $L \lesssim \xi$. Random-matrix theory approximates this scenario reasonably (while slightly overestimating the level repulsion). We can approximate the repulsion between nearby-eigenfunction energies with the average gap $\langle \delta \rangle^{(L)}$ in the energy spectrum of a length-L system:

$$\boxed{\mathcal{J}_{L \leq \xi} \sim \langle \delta \rangle^{(L)} \sim \frac{\mathcal{E}}{2^L}} \, . \tag{H12}$$

H 5 Application of local level repulsion to the MBL Otto engine in the thermodynamic limit

Consider perturbing an MBL system with a local operator. One might expect particles to be rearranged over just a short distance. But in the Heisenberg picture, a local operator spreads across a distance $L(t) \sim \zeta \ln(\mathcal{E} t)$ [3]. The longer the time t over which the system is perturbed, the farther the influence spreads. (A related discussion appears in [64].)

For example, the Hamiltonian consists of spatially local terms. Consider tuning the Hamiltonian infinitely slowly, to preclude diabatic transitions. The tuning lasts an infinitely long time: $t \to \infty$. The perturbation applied to spin 1 has time to propagate across the lattice and affect spin N. The global system cannot be subdivided into mostly independent subengines, if the Hamiltonian is tuned infinitely slowly.[19] The global system's average gap vanishes in

[19] Granted, subengines are coupled together even if the Hamiltonian is quenched infinitely quickly: $H_{\rm sim}(t)$ encodes a nearest-neighbor interaction, for example. That interaction might be regarded as coupling the edge of subengine k with the edge of subengine $k+1$. But subengines' edges may be regarded as ill-defined. The sites definitively in subengine k, near subengine k's center, should not couple to the sites near subengine ℓ's center, for any $\ell \neq k$, if the subengines are to function mostly independently. Alternatively, one may separate subenegines with "fallow" buffer zones.

the thermodynamic limit: $\langle\delta\rangle \to 0$. The average gap sets the scale of one engine's per-cycle power, $\langle W_{\rm tot}\rangle$. Hence the per-cycle power seems to vanish in the thermodynamic limit: $\langle W_{\rm tot}\rangle < \langle\delta\rangle \sim 0$.

But consider tuning the Hamiltonian at a finite speed v. Dimensional analysis suggests that the relevant time scale is $t \sim \frac{\mathcal{E}}{v}$. Local perturbations affect a region of length $\sim L(\mathcal{E}/v) \sim \zeta \ln(\mathcal{E}^2/v)$. On a length scale $L(\mathcal{E}/v)$, global many-body level correlations govern the engine's performance less than local level correlations do, i.e., less than $R\big(L(\mathcal{E}/v), \omega\big)$ does. This correlator registers level repulsion at a scale independent of the system size N. Finite-speed tuning enables local level repulsion to "wedge open" the average gap accessible to a set of independent subengines, the $\langle\delta\rangle$ that would otherwise close in the thermodynamic limit. Each mesoscale subengine therefore outputs $\langle W_{\rm tot}\rangle > 0$.

We can explain this "wedging open" of gaps differently: Suppose that the engine's state starts some trial with weight on the $j^{\rm th}$ energy level. The eigenenergies wiggle up and down in energy space during stroke 1. The $j^{\rm th}$ energy may approach the $(j-1)^{\rm th}$ energy. Such close-together energies likely correspond to far-apart subengines. If the levels narrowly avoided crossing, particles would be rearranged across a large distance. Particles must not be rearranged across such a large distance, as subengines must function independently. Therefore, the engine must undergo a diabatic transition: The engine's state must retain its configuration. The engine must behave as though the approaching energy level did not exist. Effectively removing the approaching level from available spectrum creates a gap in the spectrum. One can create such a gap, i.e., effectively remove the approaching level from the spectrum, i.e., promote diabatic transitions, by tuning the Hamiltonian at a finite speed v. This strategy is discussed further in App. J 1.

Appendix I MODEL FOR COLD THERMALIZATION

The engine thermalizes with a temperature-$T_{\rm C}$ bath during stroke 2. We quantify cold thermalization with four parameters. Then, we present an example form for the interaction Hamiltonian. We derive an expression for the thermalization time, $\tau_{\rm th}$, from Fermi's Golden Rule. Two constraints bound $\tau_{\rm th}$: (1) Markovianity and (2) the suppression of high-order-in-the-coupling-strength energy exchanges.

We neglect numerical constants, focusing on scaling behaviors. Exceptions include the 10 in $W_{\rm b} \sim \frac{\langle\delta\rangle}{10}$, used to express quantities in terms of correlation lengths ξ.

Recall that δ_- denotes the minimal level-repulsion scale, or the least size reasonably attributable to any gap, in the energy spectrum accessible to a set of independent subengines. Since each subengine has length ξ, we set $L = \xi_>$ in Eq. (H11). We set ξ to $\xi_<$ because the engine thermalizes with the cold bath when deeply localized:

$$\boxed{\delta_- \sim \mathcal{J}_{\xi_<} \sim \mathcal{E} e^{-\xi_>/\xi_<} 2^{-\xi_>}} \, . \tag{I1}$$

I 1 Parameterization of cold thermalization

Four parameters characterize cold thermalization:

1. The bath's bandwidth, $W_{\rm b}$. The bandwidth must be small, as explained in Sec. II B: $W_{\rm b} \ll \langle\delta\rangle$.

2. The strength g of the subengine-bath coupling. The coupling must be weak, as quantified in Apps. I 4 and I 5.

3. The number $L_{\rm bath}$ of sites coupled together by the cold bath. $L_{\rm bath}$ is small for two reasons. First, many physically realizable couplings are local. Second, suppose that $L_{\rm bath} \sim N_{\rm macro}$, that the bath directly coupled most of the sites in the engine. The bath would couple subengines together. Subengines should operate mostly independently. Therefore, the bath should interact with the engine only locally. We suppose, for concreteness, that $L_{\rm bath} = 2$: The bath directly couples together only nearest neighbors.

4. The amount $\tau_{\rm th}$ of time for which the subengine thermalizes with the cold bath.

I 2 Example form for the interaction between the engine and the cold bath

An interaction Hamiltonian $H_{\rm int}$ couples the engine to the cold bath. $H_{\rm int}$ has a form such as

$$H_{\rm int} = g \int_{-W_{\rm b}/\xi_>}^{W_{\rm b}/\xi_>} d\omega \sum_{j=1}^{N_{\rm macro}} \Big(c_j^\dagger c_{j+1} + {\rm h.c.} \Big) \big(b_\omega + b_\omega^\dagger \big) \, \delta\big(\langle 0 | c_j H_{\rm macro}(\tau) c_{j+1}^\dagger | 0 \rangle - \omega \big) \, . \tag{I2}$$

The annihilation and creation of a fermion at site j are denoted by c_j and $c_j^\dagger$. $H_{\rm macro}(t)$ denotes the Hamiltonian that would govern the engine at time t in the bath's absence. Cold thermalization lasts from $t = \tau$ to $t = \tau'$ (Fig. 6). b_ω and $b_\omega^\dagger$ represent the annihilation and creation of a frequency-ω boson in the bath.

What evolution does $H_{\rm int}$ generate? The interaction shifts a fermion from site j to site $j+1$. This shift likely changes the engine's energy. That energy enters the bath, manifesting as a boson $b_\omega^\dagger$. [What if the fermion shift expels an amount $E > W_{\rm b}$ of energy from a subengine? The bath can absorb part of the energy. Part of the energy manifests as a virtual particle. Meanwhile, and shortly thereafter, $H(t)$ will rearrange fermions elsewhere in the subengine. This rearrangement will require energy, annihilating the virtual particle.]

The frequency integral in Eq. (I2) is capped at $\pm\frac{W_{\rm b}}{\xi_>}$: The bath effectively can absorb only energy $|E| \leq \frac{W_{\rm b}}{\xi_>}$ from a pair of engine sites. Each length-$\xi_>$ subengine consists of $\xi_> - 1 \sim \xi_>$ pairs of nearest-neighbor sites. Hence the bath effectively can absorb only energy $|E| \leq W_{\rm b}$ from any subengine: Absorption of much larger quanta of energy is negligible [104] on the timescales relevant for cold thermalization. The frequency cap roughly equals the bath's speed of sound, c [65]. c is bounded by microscopic parameters in the bath Hamiltonian [66]. By tuning the parameters, one can cap the integral in Eq. (I2) at $\pm\frac{W_{\rm b}}{\xi_>}$.

I 3 Deriving an expression for the thermalization time $\tau_{\rm th}$

We construct an expression for $\tau_{\rm th}$ using Fermi's Golden Rule,

$$\Gamma_{fi} = |\langle f|V|i\rangle|^2 \, \mu_{\rm bath}(E_{if}) \, . \tag{I3}$$

As usual, $\hbar = 1$. $|i\rangle$ denotes the initial state of the system of interest. $|f\rangle$ denotes the state to which the coupling maps $|i\rangle$. The operator V encodes the mapping. Γ_{fi} denotes the rate of state interconversion. Transitioning from $|i\rangle$ to $|f\rangle$ expels an amount E_{if} of energy from the system. $\mu_{\rm bath}(E_{if})$ denotes the density of the bath's states at E_{if}.

Let us construct expressions for these factors. Cold thermalization transfers $E_{if} \sim W_{\rm b}$ from the subengine to the bath. $W_{\rm b}$ is very small. A change of the subengine's energy by $W_{\rm b}$ therefore rearranges particles across a large distance L, due to local level correlations (App. H). V acts nontrivially on just a few subengine sites. Such a local operator rearranges particles across a large distance L at a rate that scales as $\mathcal{J}_{L \gg \xi} = \delta_- \sim \mathcal{E} e^{-L/\xi} \, 2^{-L}$ [Eq. (H11)]. Whereas $\mathcal{E}$ sets the scale of the level repulsion δ_-, g sets the scale of $|\langle f|V|i\rangle|$. The correlation length $\xi = \xi_<$ during cold thermalization. We approximate L with the subengine length $\xi_>$. Hence

$$|\langle f|V|i\rangle| \sim \frac{g\delta_-}{\mathcal{E}} \sim g e^{-\xi_>/\xi_<} \, 2^{-\xi_>} \, . \tag{I4}$$

The left-hand side of Fermi's Golden Rule is $\Gamma_{fi} = 1/\tau_{\rm th}$. The bath DOS is approximated with $1/W_{\rm b}$. We substitute into Eq. (I3), then solve for $\tau_{\rm th}$:

$$\boxed{\tau_{\rm th} \sim W_{\rm b} \left(\frac{\mathcal{E}}{g\delta_-} \right)^2} \, . \tag{I5}$$

I 4 Constraint 1 on cold thermalization: Markovianity

Cold thermalization is assumed to satisfy Markovianity. Any information leaving the subengine dissipates into the bath. The information is assumed to disperse quickly, "spreading out" amongst many degrees of freedom. The information is assumed never to recollect and influence the subengine: The subengine's past cannot affect its future. The bath "lacks a memory."

Let us quantify Markovianity. Bath correlation functions must decay much more quickly than the coupling transfers energy. If $\tau_{\rm bath}$ denotes the correlation-decay time,

$$\tau_{\rm bath} < \frac{1}{g} \, . \tag{I6}$$

The small-bandwidth bath's $\tau_{\rm bath} \sim 1/W_{\rm b}$. Hence

$$g < W_{\rm b} \, . \tag{I7}$$

Inequality (I7), with Ineq. (I5), implies a lower bound on $\tau_{\rm th}$:

$$\boxed{\tau_{\rm th} > \frac{\mathcal{E}^2}{W_{\rm b}(\delta_-)^2}}. \tag{I8}$$

Let us express the right-hand side in terms of correlation lengths. We approximate $W_{\rm b} \sim \frac{1}{10}\langle\delta\rangle$, as in Sec. IV. We substitute in for $\langle\delta\rangle = \langle\delta\rangle^{\xi_>}$ from Eq. (H12):

$$\boxed{\langle\delta\rangle \sim \frac{\mathcal{E}}{2^{\xi_>}}}. \tag{I9}$$

Equation (I1) shows the form of δ_-. Substituting into Ineq. (I8) yields

$$\boxed{\tau_{\rm th} > \frac{10}{\mathcal{E}}\, e^{2\xi_>/\xi_<}\, 2^{3\xi_>}}. \tag{I10}$$

If $\xi_> = 12$ and $\xi_< = 1$, $\tau_{\rm th} > 10^{22}/\mathcal{E}$.

The thermalization time is exponentially large in the localization lengths. This largeness is expected, as MBL systems do not thermalize easily. A nonlocal bath coupling might decrease $\tau_{\rm th}$ while preserving the smallness of $W_{\rm b}$. We leave the coupling's optimization as an opportunity for further research.

$\tau_{\rm th}$ should not exceed the bound too far: Each subengine should thermalize internally, not with its neighbors. Suppose that the bath interacts with the center of subengine ℓ. Effects of the interaction should not have time to propagate to the far end of subengine $\ell + 1$. The time required for this undesirable interaction results roughly from replacing the δ_- in Eq. (I5) with $\mathcal{J}_{L\sim 1.5\xi_>}$, using Eq. (H11).

I 5 Constraint 2 on cold thermalization: Suppression of high-order-in-the-coupling energy exchanges

Appendix I 2 details the dominant mechanism by which the bath changes a subengine's energy. The subengine energy change by an amount $\sim W_{\rm b}$, at a rate $\sim g$. Higher-order processes can change the subengine energy by amounts $> W_{\rm b}$ and operate at rates $O(g^\ell)$, wherein $\ell \geq 2$. The subengine should thermalize across just small gaps. Hence the rate-g^ℓ processes must operate much more slowly than the rate-g processes: g must be small. We describe the higher-order processes, upper-bound g, and lower-bound $\tau_{\rm th}$.

The higher-order processes can be understood as follows. Let $H_{\rm tot} = H_{\rm macro}(\tau) + H_{\rm bath} + H_{\rm int}$ denote the Hamiltonian that governs the engine-and-bath composite. $H_{\rm tot}$ generates the time-evolution operator $U(t) := e^{-iH_{\rm tot}t}$. Consider Taylor-expanding $U(t)$. The $\ell^{\rm th}$ term is suppressed in g^ℓ; contains 2ℓ fermion operators c_j and $c_{j'}^\dagger$; and contains ℓ boson operators b_ω and $b_{\omega'}^\dagger$. This term encodes the absorption, by the bath, of ℓ energy quanta of sizes $\leq W_{\rm b}$. The subengine gives the bath a total amount $\sim \ell W_{\rm b}$ of heat. The subengine should not lose so much heat. Hence higher-order processes should occur much more slowly than the rate-g processes:

$$\tau_{\rm high-ord.} \gg \tau_{\rm th}\,. \tag{I11}$$

Let us construct an expression for the left-hand side. Which processes most urgently require suppressing? Processes that change the subengine's energy by $\gtrsim \langle\delta\rangle$. Figure 2 illustrates why. If the right-hand leg has length $\gtrsim \langle\delta\rangle$, the right-hand leg might be longer than the left-hand leg. If the right-hand leg is longer, the trial yields net negative work, $W_{\rm tot} < 0$. The bath would absorb energy $\langle\delta\rangle$ from a subengine by absorbing $\sim \frac{\langle\delta\rangle}{W_{\rm b}}$ packets of energy $\sim W_{\rm b}$ each. Hence the bath would appear to need to flip $\sim L = \frac{\langle\delta\rangle}{W_{\rm b}}$ spins to absorb energy $\sim \langle\delta\rangle$. (We switch from fermion language to spin language for convenience.) However, the length-L spin subchain has a discrete effective energy spectrum. The spectrum might lack a level associated with the amount (initial energy) $- \langle\delta\rangle$ of energy. If so, the bath must flip more than $\frac{\langle\delta\rangle}{W_{\rm b}}$ spins. Local level correlations suggest that the bath must flip $\sim \xi_>$ spins (App. H). Hence $L = \max\left\{\frac{\langle\delta\rangle}{W_{\rm b}}, \xi_>\right\}$. Energy is rearranged across the distance L at a rate $\propto g^L$.

Having described the undesirable system-bath interactions, we will bound g via Fermi's Golden Rule [Eq. (I3)]. Let $\Gamma_{fi} \sim 1/\tau_{\rm high-ord.}$ now denote the rate at which order-g^L interactions occur. The bath DOS remains $\mu_{\rm bath}(E_{if}) \sim \frac{1}{W_{\rm b}}$. Let us estimate the matrix-element size $|\langle f|V|i\rangle|$. The bath flips each spin at a rate g (modulo a contribution from the bath's DOS). Flipping one spin costs an amount $\sim \mathcal{E}$ of energy, on average. [$\mathcal{E}$ denotes the per-site energy density,

as illustrated in Eq. (24).] Hence L spins are flipped at a rate $\sim \mathcal{E} \left(\frac{g}{\mathcal{E}}\right)^L$. The initial $\mathcal{E}$ is included for dimensionality. We substitute into Fermi's Golden Rule [Eq. (I3)], then solve for the time:

$$\tau_{\rm high-ord.} \sim \frac{W_{\rm b}\, \mathcal{E}^{2(L-1)}}{g^{2L}} \quad \text{wherein} \quad L = \max\left\{ \frac{\langle \delta \rangle}{W_{\rm b}},\, \xi_> \right\} . \tag{I12}$$

We substitute from Eqs. (I12) and (I5) into Ineq. (I11). Solving for the coupling yields

$$g \ll \mathcal{E}^{(L-2)/(L-1)}\, \delta_-^{1/(L-1)} , \quad \text{wherein} \quad L = \max\left\{ \frac{\langle \delta \rangle}{W_{\rm b}},\, \xi_> \right\} . \tag{I13}$$

Substituting back into Eq. (I5) yields a second bound on $\tau_{\rm th}$:

$$\boxed{\tau_{\rm th} \gg W_{\rm b} \left(\frac{\mathcal{E}}{(\delta_-)^L} \right)^{2/(L-1)} , \quad \text{wherein} \quad L = \max\left\{ \frac{\langle \delta \rangle}{W_{\rm b}},\, \xi_> \right\}} . \tag{I14}$$

Let us express the bound in terms of localization lengths. We set $W_{\rm b} \sim \frac{\langle \delta \rangle}{10}$, as usual. We approximate $L \pm 1 \sim L \sim \xi_>$. We substitute in for $\langle \delta \rangle$ from Eq. (I9) and for δ_- from Eq. (I1):

$$\boxed{\tau_{\rm th} \gg \frac{1}{10\mathcal{E}}\, e^{2\xi_>/\xi_<}\, 2^{2\xi_>}} . \tag{I15}$$

The right-hand side is smaller than the right-hand side of Ineq. (I10). The no-higher-order-processes condition lower-bounds the thermalization time less stringently than Markovianity does.

Appendix J OPTIMIZATION OF THE MBL OTTO ENGINE

Consider the length-$N_{\rm macro}$ MBL Otto engine that consists of parallel subengines. Implementing the MBL Otto cycle involves four practicalities: At which speed v should the Hamiltonian be tuned? For what time $\tau_{\rm th}$ should the engine thermalize with the cold bath? For what time $\tau_{\rm cycle}$ must each cycle last? Which bandwidth $W_{\rm b}$ should the cold bath have?

We answer these questions in this appendix. We upper-bound v to suppress the probability of unwanted diabatic transitions. We lower-bound v to suppress interactions between subengines. We bounded $\tau_{\rm th}$, in App. I, such that cold thermalization is Markovian. The bounds on v and $\tau_{\rm th}$ imply a bound on $\tau_{\rm cycle}$. We bound $W_{\rm b}$ from both sides such that local energy-level correlations enhance the cycle. The MBL phenomenology in App. H informs several of these bounds.

Let us review some notation. $H_{\rm macro}(t)$ denotes the thermodynamically large MBL engine's Hamiltonian. If $H_{\rm macro}(t)$ is shallowly localized (ETH-like), the localization length is $\xi = \xi_>$. If $H_{\rm macro}(t)$ is deeply localized, $\xi = \xi_< \ll \xi_>$. Each subengine has length $N = \xi_>$.

As in App. H, we focus on order-of-magnitude estimates and on exponential scaling behaviors. We neglect numerical constants and factors of $(\text{length})^{(\text{finite \#})}$. The quantities $W_{\rm b}$ and $\beta_{\rm H}$ necessitate exceptions. These quantities do not inherently scale in any particular ways, unlike $\langle \delta \rangle$ and δ_-. Rather, we choose values or expressions for $W_{\rm b}$ and $\beta_{\rm H}$. We choose $W_{\rm b} \sim \frac{1}{10} \langle \delta \rangle$, in the spirit of Sec. IV. We do not neglect this factor of 10, which impacts order-of-magnitude estimates by definition. We assume that $\beta_{\rm H} \ll \frac{1}{\mathcal{E}\sqrt{N}}$, in accordance with App. G 2.

The analytic calculations in App. G (of $\langle Q_2 \rangle$, $\langle Q_4 \rangle$, $\langle W_{\rm tot} \rangle$, $\eta_{\rm MBL}$, and $\langle W_{\rm diab} \rangle$) describe one length-$N$ mesoscale engine. Those results can be translated approximately into the thermodynamic limit: The N in App. G is equated with $\xi_>$. Each energy quantity (e.g., $\langle W_{\rm tot} \rangle$) is multiplied by the number of subengines, which $\propto N_{\rm macro}$. Greater precision would require corrections, as shallowly-localized-MBL energy spectra do not obey the GOE distribution $P^{(E)}_{\rm GOE}(\delta)$. This distribution may be replaced with, e.g., the Rosenzweig-Porter random-matrix-theory distribution [105]. However, $P^{(E)}_{\rm GOE}(\delta)$ captures the crucial physics, some nontrivial degree of level repulsion.

J 1 Bounds on the Hamiltonian-tuning speed v

As $H_{\rm macro}(t)$ is tuned, the time-t energy eigenstates become linear combinations of the old eigenstates. Levels narrowly avoid crossing. To optimize the MBL Otto protocol, we must ensure that the engine likely (i) transitions

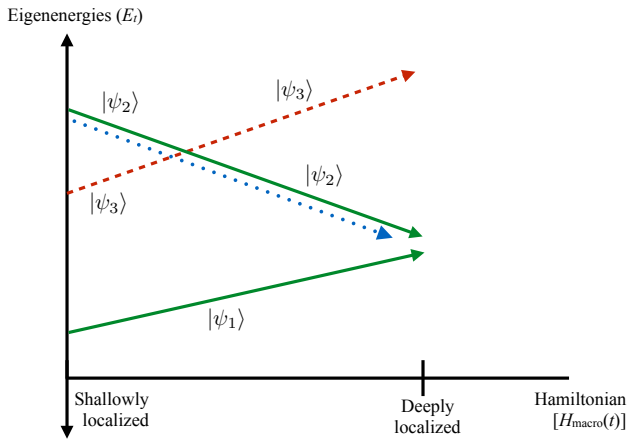

FIG. 16: Desirable diabatic transition between energy levels whose real-space eigenfunctions are localized in different subengines: The green, sloping solid lines represent elements $|\psi_1\rangle$ and $|\psi_2\rangle$ of the diabatic basis. The red, dashed line represents an energy eigenstate $|\psi_3\rangle$ that may be converted into $|\psi_2\rangle$ via long-range rearrangements of much energy (due to local level correlations; see App. H). The eigenstates' energies change as the Hamiltonian, $H_{\text{macro}}(t)$, is tuned. The blue, dotted line represents the state occupied by the engine in some trial. The engine should remain in $|\psi_2\rangle$ throughout the crossing. The transition must have a high probability of proceeding diabatically. This diabaticity requirement implies a lower bound on the Hamiltonian-tuning speed v.

diabatically between energy eigenstates $|\psi_1\rangle$ and $|\psi_2\rangle$ coupled weakly by local operators and (ii) transitions adiabatically between $|\psi_1\rangle$ and $|\psi_2\rangle$ coupled strongly by local operators. Requirements (i) and (ii) imply lower and upper bounds on the tuning speed v.

Lower bound on the Hamiltonian-tuning speed v: The lower bound stems from the requirement that subengines interact little. The engine must transition diabatically between energy levels interchanged via the rearrangement of much energy across a wide distance $L \gg \xi$.

Figure 16 illustrates three energy eigenstates whose energies change with the Hamiltonian parameter α_t. The green, sloping solid lines represent elements $|\psi_1\rangle$ and $|\psi_2\rangle$ of the *diabatic basis*. The functional forms of the $|\psi_\ell\rangle$'s remain constant. (Suppose that, at some instant t, $|\psi_1\rangle$ equals some linear combination $c_1|\uparrow \ldots \uparrow\rangle + \ldots c_{2^N}|\downarrow \ldots \downarrow\rangle$ of tensor products of σ_j^z eigenstates. $|\psi_1\rangle$ equals that combination at all times.) Where a $|\psi_\ell\rangle$ sits in the energy-level hierarchy can change with α_t.

Suppose that the engine begins in $|\psi_2\rangle$ (the top green, sloping solid line). The blue, dotted line represents the engine's state. The $|\psi_2\rangle$ line crosses a red, dashed line. The dashed line represents an energy eigenstate $|\psi_3\rangle$ coupled weakly to $|\psi_2\rangle$ by local operators. Let L denote the scale of the distance over which energy is rearranged during a transition between $|\psi_2\rangle$ and $|\psi_3\rangle$. If $L \geq 1.5\xi_>$, energy is transferred between subengines.[20] Subengines should evolve independently. Hence the engine must have a low probability of transitioning from $|\psi_2\rangle$ to $|\psi_3\rangle$. The crossing must have a high probability of being diabatic.

This demand can be rephrased in terms of work. Let $\langle W_{\text{adiab}}^{\text{cost}} \rangle$ denote the total work cost of undesirable adiabatic transitions incurred, on average, per subengine per cycle. Let $\langle W_{\text{tot}} \rangle$ denote the total average work outputted by one ideal subengine per cycle. The work cost must be much less than the ideally extracted work:

$$\left\langle W_{\text{adiab}}^{\text{cost}} \right\rangle \ll \langle W_{\text{tot}} \rangle \ . \tag{J1}$$

The right-hand side $\sim W_{\text{b}}$, to lowest order, by Eq. (9).

Let us estimate the left-hand side. We label as a "close encounter" an approach, of two levels, that might result in

[20] One may separate neighboring subengines with "fallow" buffer zones. Buffers would loosen the condition under which subengines interact, to $L \gg 1.5\xi_> +$ (length of buffer).

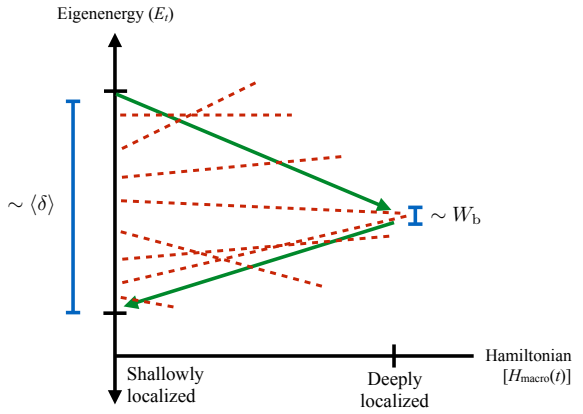

FIG. 17: "Close encounters" that might result in undesirable adiabatic transitions: The sloping, green solid lines represent the top and bottom of a "working gap." Suppose that the engine follows the top green line during stroke 1 and the bottom green line during stroke 2. The engine outputs net positive work $\langle W_{\rm tot}\rangle > 0$. The red, dashed lines represent other energy levels. Some cross (or anticross with) the working levels. Each such "close encounter" should proceed diabatically; the engine should remain on a green line, such that subengines do not interact. The work cost of an undesirable adiabatic transition $\sim \langle\delta\rangle$, the average gap in the spectrum accessible to an ideal subengine. The number of close counters $\sim \langle\delta\rangle \times \mu(E)$, wherein $\mu(E)$ denotes the density of states.

an undesirable adiabatic transition. The left-hand side of Ineq. (J1) has the form

$$\langle W^{\rm cost}_{\rm adiab}\rangle \approx \left(\frac{\text{Work cost}}{\text{1 undesirable adiab. transition}}\right)\left(\frac{\text{Prob. of undesirable adiab. transition}}{\text{1 close encounter}}\right) \times \left(\frac{\text{\# close encounters}}{\text{1 tuning stroke}}\right)\left(\frac{\text{Avg. \# strokes during which can lose work to adiab. transitions}}{\text{1 cycle}}\right). \tag{J2}$$

We estimate the factors individually.

We begin with the first factor, assisted by Fig. 17. Suppose that the engine starts a tuning stroke just above or below a working gap (on a solid green line). The engine might undesirably transition adiabatically to a red, dashed line. $\langle\delta\rangle$ denotes the average gap in the part of the spectrum accessible to an ideal mesoscale subengine (App. H). The average gap's form appears in Eq. (I9). Consider a red line that crosses a green line. The red line likely originated, in the shallowly-MBL regime, a distance $\sim$ (const.) $\langle\delta\rangle$ away. Hence the work cost of one undesirable adiabatic transition $\sim \langle\delta\rangle$.

Let us estimate the second factor in Eq. (J2), the probability that any given close encounter results in an undesirable adiabatic transition. The Landau-Zener formula encodes the probability that a close encounter proceeds diabatically [60]:

$$P_{\rm diab} = e^{-2\pi\mathcal{J}^2/v} \approx 1 - 2\pi\frac{\mathcal{J}^2}{v}. \tag{J3}$$

The $\mathcal{J}$ denotes the magnitude of the transition matrix element: Tuning $H_{\rm macro}(t)$ is equivalent to ramping up some perturbation V. V couples together elements $|E_n\rangle$ and $|E_m\rangle$ of the eigenbasis of the earlier Hamiltonian, $H_{\rm macro}(t_-)$. Some matrix represents V relative to the $H_{\rm macro}(t_-)$ eigenbasis. A matrix element $\mathcal{J}_{nm}$ represents the coupling of $|E_n\rangle$ to $|E_m\rangle$. This matrix element's size, $\mathcal{J}$, approximately equals the least width to which the gap narrows. Here, $\mathcal{J}$ roughly equals the least size $\mathcal{J}_{L\sim 1.5\xi_>}$ reasonably attributable to any gap accessible to a subsystem of length $L \sim 1.5\xi_>$ (App. II C). The condition $L \sim 1.5\xi_>$ ensures that the lefthand end of subengine ℓ fails to interact with the middle of subengine $\ell \pm 1$.[21] Figure 18 illustrates this condition. According to Eq. (H11),

$$\boxed{\mathcal{J}_{1.5\xi_>} \sim \mathcal{E} e^{-1.5\xi_>/\xi(t)}\, 2^{-1.5\xi_>}}. \tag{J4}$$

[21] If buffers separate the subengines, the condition becomes $L > 1.5\xi_>$. The lower bound on v weakens.

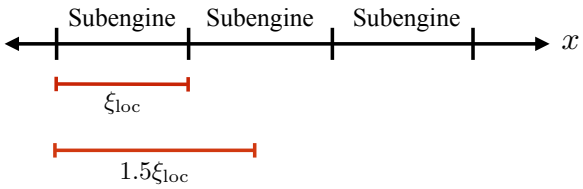

FIG. 18: Condition forbidding subengines from interacting: The long black line represents the composite engine. Each subengine has size $\xi_>$, the Hamiltonian's localization length in the shallow-localization regime. Subengines must not interact: Consider particles on one subengine's left-hand side. Those particles must not shift to the middle of any neighboring subengine, across a distance $1.5\xi_>$.

The $\xi(t)$ denotes the time-t localization length. We substitute into Eq. (J3). Subtracting $P_{\rm diab}$ from one yields a transition's probability of proceeding adiabatically:

$$P_{\rm adiab} = 1 - P_{\rm diab} \sim \frac{(\mathcal{J}_{1.5\xi_>})^2}{v} \sim e^{-3\xi_>/\xi(t)} \, 2^{-3\xi_>} \, \frac{\mathcal{E}^2}{v} \, . \tag{J5}$$

Let us estimate the third factor in Eq. (J2), the number of "close encounters" undergone by a subengine per tuning stroke. Consider, again, Fig. 17. How many dashed, red lines cross the bottom green line? Roughly

$$\begin{aligned} &\frac{1}{2}[(\#\text{ red lines inside the working gap in the shallow-localization regime}) \\ &\quad - (\#\text{ red lines inside the working gap in the deep-localization regime})] \, . \end{aligned} \tag{J6}$$

The $\frac{1}{2}$ comes from roughly half the red lines' exiting the working gap through the top green line and roughly half the red lines' exiting through the bottom green line. Let us estimate the first term in (J6). When $H_{\rm macro}(t)$ is shallowly localized, the working gap is of size $\sim \langle\delta\rangle \sim \mathcal{E}2^{-\xi_>}$ [Eq. (I9)]. The density of states accessible to a size-$(1.5\xi_>)$ subsystem is $\mu_{(1.5\xi_>)}(E) \sim \frac{1}{\langle\delta\rangle^{(1.5\xi_>)}} \sim \frac{2^{1.5\xi_>}}{\mathcal{E}}$. Hence roughly $\langle\delta\rangle \times \mu_{(1.5\xi_>)}(E) \sim 2^{\xi_>/2}$ red lines begin inside the working gap, on the left-hand side of Fig. 17.

Having estimated the first term in (J6), we consider the second. This second term $\lesssim W_{\rm b} \times \mu_{(1.5\xi_>)}(E)$, as shown in Fig. 17. By design, $W_{\rm b} \ll \langle\delta\rangle$ (App. G 2). Hence the second term in (J6) is much less than the first and can be neglected. Therefore, a subengine suffers about

$$\frac{1}{2} \, \langle\delta\rangle \times \mu_{1.5\xi_>}(E) \sim \frac{\langle\delta\rangle}{\langle\delta\rangle^{(1.5\xi_>)}} \sim 2^{\xi_>/2} \tag{J7}$$

close encounters per stroke.

Finally, we consider the last factor in Eq. (J2), the number of strokes during which the engine can undesirably transition adiabatically, on average, per trial. Adiabatic transitions cost net positive work on average, $\langle W^{\rm cost}_{\rm adiab}\rangle > 0$, only during otherwise successful trials—trials in which the subengine of interest would have outputted $W_{\rm tot} > 0$, in the absence of undesirable adiabatic transitions. Why only otherwise successful trials? For clarity, we suppose that $T_{\rm C} = 0$. Consider again Fig. 17.

First, we argue that inter-subengine adiabatic transitions cost positive average work, $\langle W\rangle > 0$, during otherwise successful trials. Suppose first that the engine starts a trial on the downward-sloping solid, green line. During stroke 1, inter-subengine adiabatic hops tend to lift the engine to upward-sloping red, dashed lines. Such upward hops raise the engine's energy, costing $W > 0$. During stroke 3, the hops tend to lift the engine to red lines that slope upward from right to left. Hence the engine's energy rises; such hops cost $W > 0$. Therefore, cross-engine adiabatic hops during otherwise successful trials cost, on average, positive total work $\langle W\rangle > 0$.

Now, we argue that inter-subengine adiabatic hops incurred during no-ops cost $\langle W\rangle = 0$. By "no-op," we mean a trial during which, in the absence of undesirable hops, the subengine of interest would output $W_{\rm tot} = 0$. Suppose that the engine starts some trial on the bottom green line in Fig. 17. Suppose that, in the very localized regime, a gap $\delta' > W_{\rm b}$ separates that bottom line from the next-lowest energy level accessible via rearrangements of energy within just one subengine. The engine would slide up the bottom green line during stroke 1, then slide downward during stroke 3: $W_{\rm tot} = 0$. Inter-engine adiabatic hops during stroke 1 tend to drop the engine to a red, dashed line, costing $W < 0$. The hops during stroke 3 tend to raise the engine to a red, dashed line, costing $W > 0$. The two costs cancel

each other, on average, by symmetry. An analogous argument concern no-ops begun on a downward-sloping green line. Therefore, inter-engine adiabatic hops during no-ops cost zero average work: $\langle W \rangle = 0$.

We can now assemble the final factor in Eq. (J2):

$$\frac{\text{Avg. \# strokes during which can lose work to adiab. transitions}}{\text{1 cycle}} \tag{J8}$$

$$\approx \left(\frac{\text{2 strokes}}{\text{1 otherwise successful trial}} \right) \left(\frac{\text{Prob. of success}}{\text{1 hop-free trial}} \right) \tag{J9}$$

$$\approx 2 \, \frac{W_{\rm b}}{\langle \delta \rangle} \sim \frac{W_{\rm b}}{\langle \delta \rangle} \, . \tag{J10}$$

The final factor is estimated in App. G.

We have estimated all the factors in Eq. (J2). Substituting in from Eqs. (I9), (J5), (J7), and (J10) yields

$$\left\langle W_{\rm adiab}^{\rm cost} \right\rangle \sim \langle \delta \rangle \cdot \frac{(\mathcal{J}_{1.5\xi_>})^2}{v} \cdot \frac{\langle \delta \rangle}{\langle \delta \rangle^{(1.5\xi_>)}} \cdot \frac{W_{\rm b}}{\langle \delta \rangle} \tag{J11}$$

$$= \frac{(\mathcal{J}_{1.5\xi_>})^2 \, W_{\rm b}}{v} \, \frac{\langle \delta \rangle}{\langle \delta \rangle^{(1.5\xi_>)}} \, . \tag{J12}$$

This average work cost must be much smaller than the ideally extracted work, $\langle W_{\rm tot} \rangle \sim W_{\rm b}$. We substitute into Ineq. (J1), then solve for v:

$$\boxed{v \gg (\mathcal{J}_{1.5\xi_>})^2 \, \frac{\langle \delta \rangle}{\langle \delta \rangle^{(1.5\xi_>)}} \sim e^{-3\xi_>/\xi(t)} \, 2^{-2.5\xi_>} \, \mathcal{E}^2} \, . \tag{J13}$$

The bound is twofold small in $\mathcal{J}_{1.5\xi_>} \ll \mathcal{E}$ and onefold large in $\frac{\langle \delta \rangle}{\langle \delta \rangle^{(1.5\xi_>)}} > 1$.

Let us evaluate the bound in the very localized regime, in which $\xi(t) \sim \xi_<$, and in the shallowly localized regime, in which $\xi(t) \sim \xi_>$. We choose $\xi_> = 12$, inspired by the numerical simulations in Sec. III, and $\xi_< = 1$. The bound becomes

$$\boxed{v \gg \begin{cases} 10^{-25} \, \mathcal{E}^2 \, , & \text{very localized} \\ 10^{-11} \, \mathcal{E}^2 \, , & \text{shallowly localized} \end{cases}} \, . \tag{J14}$$

We will compare these values with upper bounds on v.

Upper bound on the Hamiltonian-tuning speed v: We have discussed undesirable adiabatic transitions. Undesirable diabatic transitions are analyzed in App. G 8. These transitions' total average work cost, $\langle W_{\rm diab}^{\rm cost} \rangle$,[22] is small in parameters including $\frac{\sqrt{v}}{\langle \delta \rangle} \ll 1$. Let $\langle W_{\rm tot} \rangle \sim W_{\rm b}$ denote the work outputted, on average, by one ideal, adiabatically tuned subengine. The requirement

$$\left\langle W_{\rm diab}^{\rm cost} \right\rangle \ll \langle W_{\rm tot} \rangle \tag{J15}$$

implies an upper bound on v.

We estimated six contributions to $\langle W_{\rm diab}^{\rm cost} \rangle$ in App. G 8. Which contribution dominates the left-hand side of Ineq. (J15)? APT transitions dominate in the shallowly localized regime; and fractional-Landau-Zener transitions, in the very localized regime.

Upper bound on v in the shallowly localized regime: We estimated $\langle W_{\rm APT} \rangle$ in Eq. (G139). Substituting into Ineq. (J15) yields

$$\frac{1}{\sqrt{N}} \, \frac{v^2 \beta_{\rm H}}{\mathcal{E} \, \langle \delta \rangle} \, \log \left(\frac{\langle \delta \rangle^2}{v} \right) e^{-N(\beta_{\rm H} \mathcal{E})^2/4} \ll W_{\rm b} \, . \tag{J16}$$

---

[22] The average diabatic work cost was denoted by $\langle W_{\rm diab}^{\rm cost} \rangle$ earlier. The subscript is added here for emphasis and clarity.

The $\frac{1}{\sqrt{N}}$ and the log contribute subdominant (nonexponential) factors. The explicit exponential ≈ 1, since $\sqrt{N}\,\beta_{\rm H}\mathcal{E} \ll 1$ by assumption. Inequality (J16) simplifies to

$$\frac{v^2 \beta_{\rm H}}{\mathcal{E}\,\langle\delta\rangle} \ll W_{\rm b} \qquad \Rightarrow \qquad v \ll \sqrt{\frac{\langle\delta\rangle\, W_{\rm b} \mathcal{E}}{\beta_{\rm H}}}\,. \tag{J17}$$

In the spirit of Sec. IV, we approximate $W_{\rm b} \sim \frac{\langle\delta\rangle}{10}$. Since $\sqrt{N}\beta_{\rm H}\mathcal{E} \ll 1$ by assumption, $\frac{1}{\beta_{\rm H}} \gg \sqrt{N}\mathcal{E}$. We approximate $\frac{1}{\beta_{\rm H}} \sim N\mathcal{E}$. We substitute into Ineq. (J17) and ignore subdominant factors:

$$v \ll \langle\delta\rangle\,\mathcal{E}\,. \tag{J18}$$

This bound is looser than the small-parameter assumption

$$v \ll \langle\delta\rangle^2 \sim \frac{\mathcal{E}^2}{\mathcal{N}^2} \sim 2^{-2\xi_>}\,\mathcal{E}^2\,. \tag{J19}$$

in App. G 2. APT transitions do not upper-bound the tuning speed painfully.

Equation (G139) follows from the $\sim \frac{1}{\sqrt{\mathcal{N}}}$ scaling of a matrix element in the ETH phase. The ETH phase features in the mesoscale-MBL-engine cycle where shallowly localized MBL features in the thermodynamically-large-MBL-engine cycle. In the MBL phase, the matrix element $\sim \frac{1}{\mathcal{N}}$ (footnote 12). Introducing the extra $\frac{1}{\sqrt{\mathcal{N}}}$ would loosen the bound (J18) by a factor of $\sqrt{\mathcal{N}}$.

The upper bound (J19) lies above the lower bound (J13). The upper bound is suppressed only in $2^{-2\xi_>}$; the lower bound, in $e^{-3\xi_>/\xi(t)}\ 2^{-2.5\xi_>}$. The lower bound $\sim 10^{-7}\,\mathcal{E}^2$, if $\xi_> = 12$. The upper bound $\sim 10^{-11}\,\mathcal{E}^2$ [Ineq. (J14)]. Therefore, the bounds are consistent with each other.

Upper bound on v in the deeply localized regime from fractional-LZ transitions: We focus on the largest term in $\langle W_{\text{frac-LZ}}\rangle$. We have already substituted into Ineq. (J15), in App. G 8 iii. Solving for the speed yielded Ineq. (G153),

$$\boxed{v \ll \frac{(W_{\rm b})^3}{\delta_-}}, \tag{J20}$$

if the tolerance parameter $\epsilon = \frac{1}{3}$.

We assess the bound's size by expressing the right-hand side in terms of small parameters: $v \ll \left(\frac{W_{\rm b}}{\langle\delta\rangle}\right)^3 \frac{\langle\delta\rangle}{\delta_-}\ \langle\delta\rangle^2$. The right-hand side is threefold suppressed in $\frac{W_{\rm b}}{\langle\delta\rangle} \ll 1$ and is large in $\frac{\langle\delta\rangle}{\delta_-} \gg \frac{\langle\delta\rangle}{W_{\rm b}} \gg 1$.

We can express the bound in terms of localization lengths. Suppose that $W_{\rm b} \sim \frac{1}{10}\,\langle\delta\rangle$, in accordance with Sec. IV. We substitute in for $\langle\delta\rangle$ from Eq. (I9) and for δ_- from Eq. (I1). Inequality (J20) yields

$$\boxed{v \ll \frac{1}{10^3}\ e^{\xi_>/\xi_<}\ 2^{-2\xi_>}\mathcal{E}^2}. \tag{J21}$$

Let us check that this upper bound lies above the lower bound, Ineq. (J13). The lower bound is suppressed in $e^{-3\xi_>/\xi_<}\ 2^{-2.5\xi_>}$. The upper bound is suppressed only in $2^{-2\xi_>}$. Additionally, the upper bound is large in $e^{\xi_>/\xi_<}$. Hence (lower bound) $\ll$ (upper bound), by scaling.

We can compare more concretely by substituting values into Ineq. (J20). Setting $\xi_> = 12$ and $\xi_< = 1$ yields

$$\boxed{v \ll 10^{-5}\,\mathcal{E}^2}. \tag{J22}$$

This upper bound above below the lower bound, $v \gg 10^{-25}\,\mathcal{E}^2$ [Ineq. (J14)]. Hence the lower and upper bounds are consistent. Moreover, several orders of magnitude separate the bounds. At a range of speeds v, the work costs of undesirable adiabatic and undesirable diabatic fractional-Landau-Zener transitions are suppressed.

J 2 Time $\tau_{\rm cycle}$ required to implement a cycle

For how long a time interval $\tau_{\rm cycle}$ must one engine cycle last? The answer depends on the times required to implement parts of the cycle. These times follow from three bounds we derived:

1. To suppress undesirable fractional-Landau-Zener transitions, the tuning speed must satisfy $v \ll \frac{(W_{\rm b})^3}{\delta_-} \sim \frac{1}{10^3}\, e^{\xi_>/\xi_<}\, 2^{-2\xi_>} \mathcal{E}^2$ [Ineqs. (J20) and (J21)].

   Let us infer, from this bound on v, a bound on a time scale. The speed is defined as $v := \mathcal{E} \left| \frac{d\alpha_t}{dt} \right|$. Hence $\left| \frac{dt}{d\alpha_t} \right| = \frac{\mathcal{E}}{v}$. Fear of fractional-LZ transitions limits v during some part of stroke 3. We extend that part so it becomes all of stroke 3, for simplicity. During stroke 3, α_t runs from 1 to 0. Therefore, stroke 3 lasts for a time

$$\tau_{\text{frac-LZ}} = \int_1^0 \frac{dt}{d\alpha_t}\, d\alpha_t = \int_1^0 \left(-\frac{\mathcal{E}}{v} \right) d\alpha_t = \frac{\mathcal{E}}{v} \tag{J23}$$

$$\gg \frac{\delta_- \mathcal{E}}{(W_{\rm b})^3} \sim 10^3\, e^{-\xi_>/\xi_<}\, 2^{2\xi_>}/\mathcal{E}\,. \tag{J24}$$

   If $\xi_> = 12$ and $\xi_< = 1$, $\tau_{\text{frac-LZ}} \sim 10^5/\mathcal{E}$.

2. Satisfying $v \leq \langle \delta \rangle^2 \sim 2^{-2\xi_>}\, \mathcal{E}^2$ [Ineq. (J19)] suppresses crosstalk between subengines. Let $\tau_{\rm APT}$ denote the time for which fear of APT transitions governs v. $\tau_{\rm APT}$ includes stroke 1. Hence $\tau_{\rm APT} \sim \frac{\mathcal{E}}{v} \sim 2^{2\xi_>}\, \mathcal{E} \sim 10^7/\mathcal{E}$. The final expression follows from $\xi_> = 12$. This time scale is much larger than $\tau_{\text{frac-LZ}}$. Hence the APT bound on v affects the cycle time more than the fractional-LZ bound does.

3. The engine thermalizes with the cold bath for a time $\tau_{\rm th} > \frac{\mathcal{E}^2}{W_{\rm b}(\delta_-)^2} \sim \frac{10}{\mathcal{E}}\, e^{2\xi_>/\xi_<}\, 2^{3\xi_>}$ [Ineqs. (I8) and (I10)]. If $\xi_> = 12$ and $\xi_< = 1$, $\tau_{\rm th} > 10^{22}/\mathcal{E}$. Hence cold thermalization lasts much longer than the Hamiltonian tunings. (The time required for hot thermalization is much less than $\tau_{\rm th}$, as the hot bath does not need a small bandwidth $W_{\rm b}$.)

Cold thermalization dominates the cycle time:

$$\boxed{\tau_{\rm cycle} \sim \tau_{\rm th} > \frac{\mathcal{E}^2}{W_{\rm b}(\delta_-)^2} \sim \frac{10}{\mathcal{E}}\, e^{2\xi_>/\xi_<}\, 2^{3\xi_>}}\,. \tag{J25}$$

J 3 Bounds on the cold-bath bandwidth $W_{\rm b}$

Bounding $W_{\rm b}$ enables us to take advantage of local level correlations, which mimic the discrepancy between GOE and MBL level statistics. $W_{\rm b}$ must be great enough to couple nearby energies, deep in the MBL phase, accessible to a subengine The smallest gap reasonably attributable to a subengine follows from Eq. (H11): $\delta_- = \mathcal{J}_{\xi_>} \sim \mathcal{E} e^{-\xi_>/\xi_<}\, 2^{-\xi_>}$.

$W_{\rm b}$ must be small enough to couple only levels whose energies likely separate during stroke 3. That is, the engine must traverse trapezoids as in Fig. 2 clockwise. $W_{\rm b}$ must be less than the average level spacing $\langle \delta \rangle$ accessible to a subengine. (If $W_{\rm b}$ were greater, the engine could, with nonnegligible frequency, traverse trapezoids whose leftmost legs were shorter than their rightmost legs. Each such cycle would output $W_{\rm tot} < 0$.) We substitute the subengine length $\xi_>$ for N in Eq. (D4): $\langle \delta \rangle \approx \frac{\mathcal{E}}{2^{\xi_>}}$.

The lower and upper bounds on $W_{\rm b}$ are combined into $\boxed{\delta_- < W_{\rm b} \ll \langle \delta \rangle}$, approximated with

$$\boxed{\mathcal{E} e^{-\xi_>/\xi_<}\, 2^{-\xi_>} < W_{\rm b} \ll \frac{\mathcal{E}}{2^{\xi_>}}}\,. \tag{J26}$$

Appendix K NUMERICAL SIMULATIONS OF THE MBL OTTO ENGINE

We simulated one mesoscale engine, a chain of $N = 12$ sites. (We also studied other system sizes, to gauge finite-size effects.) The random-field Heisenberg Hamiltonian (24) governed the system. We drop the subscript from $H_{\rm sim}(t)$ in this appendix, for conciseness.

We worked at half-filling, for two reasons. First, at half-filling, the ETH system's level spacing obeys the GOE distribution (D5). Second, half-filling neutralizes a subtle accordion-like effect. If one considers all the energy eigenstates in all the particle-number sectors, the Hamiltonian's bond term causes a slight asymmetry in the DOS $\mu(E)$. If the onsite-field strength is small, the mean of $\mu(E)$ lies above the median $\text{Tr}\big(H(t)\big) = 0$. As one increases $h(\alpha_t)$,

the mean slowly decreases towards the median. The asymmetry therefore breaks our assumption, in App. G, that the ETH DOS has the form of the MBL DOS. In the language of Sec. II B, the DOS's variation squeezes the bottom of the accordion, while pulling apart the top. How does this variation impact the calculation of the per-trial power, $\langle W_{\rm tot} \rangle$? The variation generates $\beta_{\rm H}$ corrections irrelevant to the physics we seek to explore, the effects of level-spacing statisticson thermodynamic engines.

Call the times at which the strokes end $t = \tau, \tau', \tau''$, and τ''', as in Fig. 6. For each of $N_{\rm reals} \sim 1,000$ disorder realizations, we computed the whole density matrix $\rho(t)$ at $t = 0, \tau, \tau', \tau'', \tau'''$. (See App. K 3 and K 4 for an explanation of how.) The engine's time-t internal energy is

$$E(t) = \mathrm{Tr}\big(H(t)\rho(t)\big) \,. \tag{K1}$$

The quantities of interest are straightforwardly

$$\langle W_1 \rangle = E(0) - E(\tau) \,, \tag{K2}$$
$$\langle W_3 \rangle = E(\tau''') - E(\tau'') \,, \tag{K3}$$
$$\langle Q_2 \rangle = E(\tau'') - E(\tau') \,, \qquad \text{and} \tag{K4}$$
$$\langle Q_4 \rangle = E(0) - E(\tau''') \,. \tag{K5}$$

We disorder-average these quantities before dividing to compute the efficiency, $\eta_{\rm MBL} = 1 - \frac{\langle W_1 \rangle + \langle W_3 \rangle}{\langle Q_4 \rangle}$.

K 1 Scaling factor

We wish to keep the DOS constant through the cycle. To fix $\mu(E)$, we rescale the Hamiltonian by a factor $Q\big(h(\alpha_t)\big)$. We define $Q^2\big(h(\alpha_t)\big)$ as the disorder average of the variance of the unrescaled DOS:

$$Q^2\big(h(\alpha_t)\big) := \left\langle \left(\frac{1}{\mathcal{N}} \sum_{j=1}^{\mathcal{N}} E_j^2 \right) - \left(\frac{1}{\mathcal{N}} \sum_{j=1}^{\mathcal{N}} E_j \right)^2 \right\rangle_{\rm disorder} \tag{K6}$$

$$= \left\langle \frac{1}{\mathcal{N}} \mathrm{Tr}\big(\tilde{H}^2(t)\big) - \left(\frac{1}{\mathcal{N}} \mathrm{Tr}\big(\tilde{H}(t)\big) \right)^2 \right\rangle_{\rm disorder} \,. \tag{K7}$$

$$\tag{K8}$$

The $\tilde{H}(t)$ denotes an unrescaled variation on the random-field Heisenberg Hamiltonian $H(t)$ of Eq. (24):

$$\tilde{H}(t) := \mathcal{E} \left[\sum_{j=1}^{N-1} \boldsymbol{\sigma}_j \cdot \boldsymbol{\sigma}_{j+1} + h(\alpha_t) \sum_{j=1}^{N} h_j \sigma_j^z \right] \,. \tag{K9}$$

To compute $Q^2\big(h(\alpha_t)\big)$, we rewrite the unrescaled Hamiltonian as

$$\tilde{H}(t) = \mathcal{E} \left[2 \sum_{j=1}^{N-1} \left(\sigma_j^+ \sigma_{j+1}^- + \text{h.c.} \right) + \sum_{j=1}^{N-1} \sigma_j^z \sigma_{j+1}^z + h(\alpha_t) \sum_{j=1}^{N} h_j \sigma_j^z \right] \,. \tag{K10}$$

We assume that N is even, and we work at half-filling. The $\frac{N}{2}$-particle subspace has dimensionality

$$\mathcal{N} = \binom{N}{N/2} \,. \tag{K11}$$

Let us calculate some operator traces that we will invoke later. Let $X := \prod_{j=1}^{N} \sigma^x$ denote the global spin-flip operator. For any operator A such that $X^\dagger A X = -A$,

$$\mathrm{Tr}(A) = \mathrm{Tr}\left(X^\dagger A X \right) = -\mathrm{Tr}(A) \,. \tag{K12}$$

We have used the evenness of N, which implies the invariance of the half-filling subspace under X. Also,

$$\mathrm{Tr}(A) = 0 \,. \tag{K13}$$

In particular,

$$0 = \mathrm{Tr}(\sigma_j^z) = \mathrm{Tr}(\sigma_j^z \sigma_{j'}^z \sigma_{j''}^z)\,, \tag{K14}$$

if $j \neq j' \neq j''$.

Traces of products of even numbers of σ^z factors require more thought:

$$\begin{aligned}\mathrm{Tr}(\sigma_j^z \sigma_{j+1}^z) &= (\#\text{ states } j, j+1 = \uparrow\uparrow) + (\#\text{ states } j, j+1 = \downarrow\downarrow) - 2(\#\text{ states } j, j+1 = \uparrow\downarrow) \\ &= \binom{N-2}{N/2-2} + \binom{N-2}{N/2} - 2\binom{N-2}{N/2-1} \\ &= -\mathcal{N}\frac{1}{N-1}\,. \end{aligned} \tag{K15}$$

Similarly,

$$\mathrm{Tr}\left([\sigma_j^+\sigma_j^-][\sigma_{j+1}^-\sigma_{j+1}^+]\right) = \mathrm{Tr}\left([\sigma_j^-\sigma_j^+][\sigma_{j+1}^+\sigma_{j+1}^-]\right) = (\#\text{ states } j, j+1 = \uparrow\downarrow) = \binom{N-2}{N/2-1} \tag{K16}$$

$$= \mathcal{N}\frac{N}{4(L-1)}\,, \tag{K17}$$

and

$$\begin{aligned}\mathrm{Tr}\left(\sigma_j^z \sigma_{j+1}^z \sigma_{j'}^z \sigma_{j'+1}^z\right) &= (\#\text{ states } j, j+1, j', j'+1 = \uparrow\uparrow\uparrow\uparrow) + \binom{4}{2}(\#\text{ states } j, j+1, j', j'+1 = \uparrow\uparrow\downarrow\downarrow) \\ &\quad + (\#\text{ states } j, j+1, j', j'+1 = \downarrow\downarrow\downarrow\downarrow) \\ &\quad - \binom{4}{1}(\#\text{ states } j, j+1, j', j'+1 = \uparrow\uparrow\uparrow\downarrow) - \binom{4}{1}(\#\text{ states } j, j+1, j', j'+1 = \uparrow\downarrow\downarrow\downarrow) \\ &= \binom{N-4}{N/2-4} + 6\binom{N-4}{N/2-2} + \binom{N-4}{N/2} - 6\binom{N-4}{N/2-3} - 6\binom{N-4}{N/2-1} \\ &= \mathcal{N}\frac{3}{(N-1)(N-3)}\,, \end{aligned} \tag{K18}$$

wherein the first equality's combinatorial factors come from permutations on sites j, $j+1$, j', and $j'+1$.

Assembling these pieces, we find

$$\mathrm{Tr}(\tilde{H}(t)) = \mathcal{E}\sum_{j=1}^{N-1}\mathrm{Tr}\left(\sigma_j^z\sigma_j^z\right) = -\mathcal{E}\mathcal{N}. \tag{K19}$$

Next, we compute $\mathrm{Tr}(\tilde{H}^2(t))$:

$$\begin{aligned}\tilde{H}^2(t) = \mathcal{E}^2\Bigg[&4\sum_j^{N-1}(\sigma_j^+\sigma_j^-)(\sigma_{j+1}^-\sigma_{j+1}^+) + 4\sum_j^{N-1}(\sigma_j^-\sigma_j^+)(\sigma_{j+1}^+\sigma_{j+1}^-) + \sum_{j,j'=1}^{N-1}\sigma_j^z\sigma_{j+1}^z\sigma_{j'}^z\sigma_{j'+1}^z + h^2(\alpha_t)\sum_{j=1}^N h_j^2 \\ &+ (\text{traceless terms})\Bigg] \end{aligned} \tag{K20}$$

$$\begin{aligned}= \mathcal{E}^2\Bigg[&4\sum_j^{N-1}(\sigma_j^+\sigma_j^-)(\sigma_{j+1}^-\sigma_{j+1}^+) + 4\sum_j^{N-1}(\sigma_j^-\sigma_j^+)(\sigma_{j+1}^+\sigma_{j+1}^-) + \sum_{j=1}^{N-1}\mathbb{1} + \sum_{j=1}^{N-2}\sigma_j^z\sigma_{j+2}^z \\ &+ \sum_{j=1}^{N-3}\sum_{j'=j+2}^{N-1}\sigma_j^z\sigma_{j+1}^z\sigma_{j'}^z\sigma_{j'+1}^z + h(\alpha_t)^2(\alpha_t)\sum_{j=1}^N h_j^2 + (\text{traceless terms})\Bigg]. \end{aligned} \tag{K21}$$

We take the trace, using Eqs. (K15), (K16), and (K18):

$$\mathrm{Tr}(\tilde{H}^2(t)) = \mathcal{N}\left[3N - 1 + \frac{N-2}{N-1} + h^2\sum_{j=1}^N h_j^2\right]. \tag{K22}$$

We disorder-average by taking $h_j^2 \mapsto \int_0^1 dh_j h_j^2 = \frac{1}{3}$:

$$\Big\langle \mathrm{Tr}(H^2(t)) \Big\rangle_{\mathrm{disorder}} = \mathcal{N}\left[3N - 1 + \frac{N-2}{N-1} + N\frac{h^2}{3}\right]. \tag{K23}$$

Substituting into Eq. (K6), we infer the rescaling factor's square:

$$Q^2\big(h(\alpha_t)\big) = 3N - 2 + \frac{N-2}{N-1} + N\frac{h^2}{3}\,. \tag{K24}$$

Our results are insensitive to the details of Q. The width of the DOS in one disorder realization will differ from the disorder average (K24). Moreover, that difference will vary as we tune $h(\alpha_t)$, because the disorder affects only one term. The agreement between the analytics, in which $\mu(E)$ is assumed to remain constant in t, and the numerics is therefore comforting: The engine is robust against small variations in the rescaling.

K 2 Representing states and Hamiltonians

We structured our software to facilitate two possible extensions. First, the Hamiltonian tuning may be generalized to arbitrary speeds. Second, the cold bath might be modeled more realistically, as coupling to the engine only locally.

We represent the state of one mesoscopic MBL Otto engine with a density matrix

$$\rho \in \mathbb{C}^{\mathcal{N}\times\mathcal{N}}\,, \tag{K25}$$

and the Hamiltonian with a matrix

$$H \in \mathbb{C}^{\mathcal{N}\times\mathcal{N}}\,, \tag{K26}$$

relative to the basis $\{|s_1\rangle, \ldots, |s_{\mathcal{N}}\rangle\} = \{|\uparrow \ldots \uparrow\rangle, \ldots, |\downarrow \ldots \downarrow\rangle\}$ of products of σ^z eigenstates. We track the whole density matrix, rather than just the energy-diagonal elements, with an eye toward the coherent superpositions that diabatic corrections create. Because we work on an N-site chain at half-filling,

$$\mathcal{N} = \binom{N}{N/2} \simeq \sqrt{\frac{2}{\pi N}}\, 2^N\,. \tag{K27}$$

K 3 Strokes 1 and 3: Adiabatic evolution

The (l, m) entry of the initial-state density matrix is

$$\rho(0)_{lm} = \langle s_l | \frac{1}{Z} e^{-\beta_{\mathrm{H}} H(0)} | s_m \rangle = \frac{1}{Z}\sum_j e^{-\beta_{\mathrm{H}} E_j(0)} \langle s_l | E_j(0)\rangle\langle E_j(0) | s_m\rangle\,. \tag{K28}$$

The j^{th} eigenstate of $H(0)$, associated with energy $E_j(0)$, is denoted by $|E_j(0)\rangle$. We approximate the time evolution from 0 to τ (during stroke 1) as adiabatic. The evolution therefore does not move weight between levels:

$$\rho(\tau)_{lm} = \frac{1}{Z}\sum_j e^{-\beta_{\mathrm{H}} E_j(0)} \langle s_l | E_j(\tau)\rangle\langle E_j(\tau) | s_m\rangle\,. \tag{K29}$$

If we represented our density matrix relative to an instantaneous energy eigenbasis, simulating the time evolution would be trivial: We would reinterpret the diagonal matrix ρ as being diagonal with the same elements in a new basis. However, we wish to represent $\rho(t)$ relative to the σ_j^z product basis. This representation enhances the code's flexibility, facilitating future inclusion of diabatic evolutions and a more detailed model of cold thermalization. To represent $\rho(t)$ relative to the σ_j^z product basis, we note that

$$\rho(\tau)_{lm} = \sum_j \langle s_l | E_j(\tau)\rangle\langle E_j(0) | \rho(0) | E_j(0)\rangle\langle E_j(\tau) | s_m\rangle = [U(\tau,0)\rho(0)U(\tau,0)^\dagger]_{lm}\,. \tag{K30}$$

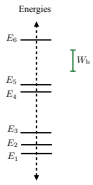

FIG. 19: Energies of a cold-thermalized system: We illustrate our implementation of cold thermalization with this example chain of six energies. The cold bath has a bandwidth of size W_b, depicted in green.

We have defined a time-evolution matrix $U(\tau, 0) \in \mathbf{C}^{\mathcal{N}\times\mathcal{N}}$ by

$$U(\tau, 0)_{lm} = \sum_j \langle s_l | E_j(\tau)\rangle\langle E_j(0) | s_m\rangle \,. \tag{K31}$$

This matrix is easily computed via exact diagonalization of $H(0)$ and $H(\tau)$.

We can compute the density matrix $\rho(\tau'')$ at the end of stroke 3 (the tuning from MBL to GOE) from the density matrix $\rho(\tau')$ at the end of stroke 2 (the cold-bath thermalization) similarly:

$$\rho(\tau'') = U(\tau'', \tau')\rho(\tau')U(\tau'', \tau')^\dagger \,. \tag{K32}$$

The time-evolution matrix $U(\tau'', \tau') \in \mathbf{C}^{\mathcal{N}\times\mathcal{N}}$ is given by

$$U(\tau'', \tau')_{lm} = \sum_j \langle s_l | E_j(0)\rangle\langle E_j(\tau) | s_m\rangle \,. \tag{K33}$$

[Recall that $H(\tau'') = H(0)$ and $H(\tau') = H(\tau)$.]

K 4 Stroke 2: Thermalization with the cold bath

During stroke 2, the system thermalizes with a cold bath that has a small bandwidth W_b. We make three assumptions. First, the bandwidth cutoff at W_b is hard: The bath can transfer only amounts of energy less than W_b at a time. Therefore, the cold bath cannot move probability mass between adjacent levels separated by just one gap of size $\delta' > W_\mathrm{b}$. Second, we assume that the bath is Markovian. Third, we assume that the system thermalizes with the bath for a long time. The bath has time to move weight across sequences of small gaps $\delta'_j, \delta'_{j+1}, \ldots < W_\mathrm{b}$.

Consequently, we can implement the effect of thermalization as follows. First, we identify sequences of levels connected by small gaps. Second, we reapportion weight amongst the levels according to a Gibbs distribution.

Suppose, for example, that the MBL Hamiltonian $H(\tau)$ contains the following chain of six energies, $E_1, \ldots, E_6$, separated from its surrounding levels by large gaps (Fig. 19):

$$\begin{aligned} &(E_2 - E_1), (E_3 - E_2) < W_\mathrm{b} \\ &(E_5 - E_4) < W_\mathrm{b} \,, \quad \text{and} \\ &(E_4 - E_3), (E_6 - E_5) > W_\mathrm{b} \,. \end{aligned}$$

We suppress the time arguments to simplify notation. Before thermalization, the density operator is diagonal with respect to the energy basis:

$$\rho(\tau) = \sum_j \rho_j |E_j\rangle\langle E_j| \,. \tag{K34}$$

The weight on level j is denoted by ρ_j. Thermalization maps

$$\begin{aligned} \rho(\tau) \mapsto \rho(\tau') = &\frac{\rho_1 + \rho_2 + \rho_3}{e^{-\beta_\mathrm{C} E_1} + e^{-\beta_\mathrm{C} E_2} + e^{-\beta_\mathrm{C} E_3}} \Big(e^{-\beta_\mathrm{C} E_1} |E_1\rangle\langle E_1| + e^{-\beta_\mathrm{C} E_2} |E_2\rangle\langle E_2| + e^{-\beta_\mathrm{C} E_3} |E_3\rangle\langle E_3| \Big) \\ &+ \frac{\rho_4 + \rho_5}{e^{-\beta_\mathrm{C} E_4} + e^{-\beta_\mathrm{C} E_5}} \Big(e^{-\beta_\mathrm{C} E_4} |E_4\rangle\langle E_4| + e^{-\beta_\mathrm{C} E_5} |E_5\rangle\langle E_5| \Big) + \rho_6 |E_6\rangle\langle E_6| \,. \end{aligned} \tag{K35}$$

Appendix L COMPARISON WITH COMPETITOR OTTO ENGINES: DETAILS AND EXTENSIONS

Otto cycles can be implemented with many media. Why implement this paper's MBL engine? We compare our engine with six competitors. Three rely on mechanisms other than the "athermality" of MBL level statistics. First, the conventional thermodynamic Otto engine consists of an ideal gas (Sec. V A). Second, one could attempt to prepare noninteracting bits and to modulate their gaps in parallel, such as with quantumdots (Sec. V B). Third, one could form a "bandwidth engine": The energy band, not just the gaps near the band's center, could be compressed and expanded. The final three competitors result from relaxing restrictions on our cycle. Fourth, we consider tuning $H_{\rm macro}(t)$ between two disorder realizations whose disorder strengths equal each other, rather than between shallow and deep localization (Sec. V D). Fifth, we consider increasing the cold-bath bandwidth $W_{\rm b}$. Sixth, we consider replacing MBL with single-particle (Anderson) localization.

Below, we detail two arguments summarized in the main text: We discuss the bandwidth engine, then the MBL engine tuned between same-strength disorder realizations. Next, we introduce the ordinary-$W_{\rm b}$ engine and the Anderson-localized engine.

L 1 Details: Comparison with a bandwidth engine

We analyzed an accordion-like "bandwidth engine" in Sec. V C. To work reasonably, we claimed, the bandwidth engine must not undergo diabatic transitions. Stringently limiting the diabatic-hop probability might seem unfair to the bandwidth engine: Whereas the MBL engine depends on fine spectral properties, the bandwidth engine depends on just the gross variation of the spectrum's width. Surely the bandwidth engine could withstand several diabatic jumps—say, jumps through $0.02\mathcal{N}_{\rm macro}$ levels?

The answer turns out to be no. The reason is that the ground state pulls away from the rest of the spectrum as the system size $N_{\rm macro}$ grows. Suppose, for simplicity, that $T_{\rm C} = 0$ and $T_{\rm H} = \infty$. The bandwidth engine starts stroke 1 with zero energy, in the maximally mixed state $\rho(0) = \mathbb{1}/\mathcal{N}_{\rm macro}$, on average. Diabatic hops fail to affect the engine state $\rho(t)$ during stroke 1, on average: The engine as likely drops downward as hops upward. Cold thermalization drops the bandwidth engine to the ground state (plus an exponentially small dusting of higher-level states), since $T_{\rm C} = 0$. The ground-state energy is generically extensive. Hence the bandwidth engine absorbs $\langle Q_2 \rangle_{\rm macro} \sim -N_{\rm macro}$, on average. Suppose that, during stroke 3, the bandwidth engine jumps upward through 2% of the levels. The bandwidth engine ends about two standard deviations below the spectrum's center, with average energy $\sim \sqrt{N_{\rm macro}}$. While returning to $T_{\rm H} = 0$ during the average stroke 4, the bandwidth engine absorbs $\langle Q_4 \rangle_{\rm macro} \sim \sqrt{N_{\rm macro}}$. The average outputted work $\langle W_{\rm tot} \rangle_{\rm macro} = \langle Q_4 \rangle_{\rm macro} + \langle Q_2 \rangle_{\rm macro} \sim \sqrt{N_{\rm macro}} - N_{\rm macro}$. As the system size $N_{\rm macro}$ grows, $\langle W_{\rm tot} \rangle_{\rm macro}$ shrinks, then goes negative. Few diabatic jumps do threaten the bandwidth engine's ability to output positive work.

The bandwidth cycle's speed must decline as $N_{\rm macro}$ grows for another reason: As $N_{\rm macro}$ grows, the typical whole-system gap $\langle \delta \rangle_{\rm macro} \sim \frac{\mathcal{E}}{\mathcal{N}_{\rm macro}}$ shrinks. The smaller the gaps, the greater the likelihood that a given speed v induces diabatic jumps. In the thermodynamic limit, as $\langle \delta \rangle_{\rm macro} \to 0$, v must $\to 0$. The MBL Otto cycle proceeds more quickly: The composite engine's division into subengines renders certain diabatic transitions beneficial, lower-bounding the ideal speed (see App. J 1).

L 2 Details: Comparison with an MBL engine tuned between same-strength disorder realizations

Consider tuning the Hamiltonian between MBL Hamiltonians whose disorder strengths $h(\alpha_t)$ equaled each other. Let $\tilde{S}$ denote one subengine in this composite engine. We denote by S one subengine in the MBL engine introduced in the main text. The smallness of $W_{\rm b}$ would ensure that cold thermalization drops $\tilde{S}$ across just small gaps. The average successful trial would manifest as a trapezoid as in Fig. 2. The average successful $\tilde{S}$ trial would resemble the average successful S trial. But $\tilde{S}$ suffers more worst-case trials and from less reliability.

In worst-case trials, a subengine outputs a negative amount $W_{\rm tot} < 0$ of work. $W_{\rm tot} < 0$ if a subengine traverses, clockwise, a trapezoid whose shorter vertical leg lies leftward of its longer vertical leg. S and $\tilde{S}$ have equal probabilities of traversing trapezoids whose right-hand legs are short. $\tilde{S}$ has a greater probability than S of traversing a trapezoid whose left-hand leg is short: The left-hand $\tilde{S}$ leg represents a gap in a Hamiltonian as localized as the right-hand Hamiltonian. The left-hand and right-hand $\tilde{S}$ Hamiltonians have the same gap statistics. Hence $\tilde{S}$ has a nontrivial probability of starting any given trial atop a small gap $\Delta < W_{\rm b}$ that widens to $\Delta' \in (\Delta, W_{\rm b})$. $\tilde{S}$ has a higher probability of traversing a worst-case trapezoid.

Let us estimate the S and $\tilde{S}$ worst-case probabilities. Again, we suppose that $T_{\rm H} = \infty$ and $T_{\rm C} = 0$ for simplicity. The probability that any given S trial outputs $W_{\rm tot} < 0$ is

$$\begin{aligned} p_{\rm worst} \approx & \text{ (Prob. that the left-hand gap} < \text{the right-hand gap)} \\ & \times \text{ (Prob. that the right-hand gap is small enough to be cold-thermalized)} \end{aligned} \tag{L1}$$

$$\approx \text{(Prob. that the left-hand gap} < W_{\rm b}) \times \frac{W_{\rm b}}{\langle \delta \rangle} \, . \tag{L2}$$

The initial factor is modeled by the area of a region under the $P^{(E)}_{\rm GOE}(\delta)$ curve. The region stretches from $\delta = 0$ to $\delta = W_{\rm b}$. We approximate the region as a triangle of length $W_{\rm b}$ and height $\frac{\pi}{2} \frac{W_{\rm b}}{\langle \delta \rangle^2} e^{-\frac{\pi}{4} (W_{\rm b})^2 / \langle \delta \rangle^2} \sim \frac{W_{\rm b}}{\langle \delta \rangle^2}$. [We have substituted $\delta = W_{\rm b}$ into Eq. (D5) and invoked $\frac{W_{\rm b}}{\langle \delta \rangle} \ll 1$.] The triangle has an area of $\frac{1}{2} \cdot W_{\rm b} \cdot \frac{\pi}{2} \frac{W_{\rm b}}{\langle \delta \rangle^2} \sim \left(\frac{W_{\rm b}}{\langle \delta \rangle} \right)^2$. Substituting into Eq. (L2) yields

$$p_{\rm worst} \sim \left(\frac{W_{\rm b}}{\langle \delta \rangle} \right)^3 . \tag{L3}$$

Let $\tilde{p}_{\rm worst}$ denote the probability that any given $\tilde{S}$ trial outputs $W_{\rm tot} < 0$. $\tilde{p}_{\rm worst}$ has the form of Eq. (L2). We approximate the initial factor with the area of a region under the $P^{(E)}_{\rm MBL}(\delta)$ curve. The region extends from $\delta = 0$ to $\delta = W_{\rm b}$. The region resembles a rectangle of height $P^{(E)}_{\rm MBL}(0) \approx \frac{1}{\langle \delta \rangle}$. Substituting the rectangle's area, $\frac{W_{\rm b}}{\langle \delta \rangle}$, into the right-hand side of Eq. (L2) yields

$$\tilde{p}_{\rm worst} \sim \left(\frac{W_{\rm b}}{\langle \delta \rangle} \right)^2 . \tag{L4}$$

Let us compare Eqs. (L3) and (L4). Recall that $\frac{W_{\rm b}}{\langle \delta \rangle} \ll 1$. The small-bandwidth cycle has a much lesser chance of undergoing a worst-case trial: $p_{\rm worst} \ll \tilde{p}_{\rm worst}$. The discrepancy is exaggerated if the exponent in Eq. (L3) rises. The exponent rises if the left-hand S Hamiltonian is modeled with a Gaussian ensemble other than the GOE. The Gaussian Unitary Ensemble (GUE) corresponds to an exponent of 4; the Gaussian Symplectic Ensemble (GSE), to an exponent of 6. Different Gaussian ensembles model different symmetries.

$\tilde{S}$ not only undergoes more worst-case trials than S. The $W_{\rm tot}$ extracted from $\tilde{S}$ fluctuates more, from trial to trial, than the $W_{\rm tot}$ extracted from S. Whereas the left-hand S gap distribution is GOE, the left-hand $\tilde{S}$ gap distribution is Poisson. A Poisson-distributed gap is more likely small than a GOE-distributed gap. So, too, is a Poisson-distributed gap more likely large [45]. $\tilde{S}$ has a greater chance of starting any given trial just above an extreme-size left-hand gap. Hence $\tilde{S}$ has higher chances of outputting extreme $W_{\rm tot}$ values.

Such unreliability poses a disadvantage in one-shot information theory. One-shot information theory has been applied to thermodynamic tasks including work extraction [8, 9, 11, 12, 14, 15, 76–81]. An agent is modeled as having an error tolerance ϵ, a greatest acceptable probability that any given trial's $W_{\rm tot}$ will be undesirable. Risk-averse agents will prefer S to $\tilde{S}$. Fluctuations in the composite engine's work statistics, one might object, decay in the thermodynamic limit. But each subengine's work statistics vary from trial to trial; and work statistics vary, within a trial, spatially across the composite engine. Also, realistic engines lie outside the thermodynamic limit. Finite-size engines are studied in one-shot information theory, called also "finite-size information theory".

L 3 Comparison with an MBL Otto engine whose cold bath has an ordinary bandwidth

Small-bandwidth baths feature in condensed matter [56–58] and in applications of quantum information theory to thermodynamics. Baths are modeled with qubits, for example, in [23, 106]. Yet restricting certain platforms' bandwidths might be difficult. Practicality motivates the question "How would the MBL-to-MBL engine perform if $\frac{W_{\rm b}}{\langle \delta \rangle}$ were not $\ll 1$?" Let $\tilde{S}$ denote the ordinary-bandwidth MBL subengine, while S denotes our small-$W_{\rm b}$ subengine. The probability that $\tilde{S}$ traverses a quadrilateral, as in Fig. 2, in any given trial exceeds the probability that S traverses a quadrilateral. During the average quadrilateral traversal, S outputs more work than $\tilde{S}$.

$\tilde{S}$ more often traverses quadrilaterals than S. An engine can output work only during a quadrilateral traversal, in the adiabatic approximation. An engine fails to traverse a quadrilateral if cold thermalization fails to change the engine's energy. Cold thermalization fails if $W_{\rm b}$ is less than the gap just below the level occupied by the engine at the end of stroke 1. The larger the $W_{\rm b}$, the more likely the cold bath is to shift the engine to another level.

Let us estimate the engines' quadrilateral-traversal probabilities. Ignoring higher-order corrections, we suppose that $T_{\rm H} = \infty$ and $T_{\rm C} = 0$. S has a probability $\approx \frac{W_{\rm b}}{\langle \delta \rangle}$ of starting a trial on one side of a gap Δ that changes to a gap $\Delta' < W_{\rm b}$ that the cold bath can thermalize. The $T_{\rm C} = 0$ bath has a probability 1 of dropping the subengine's energy. Hence S's probability of traversing a quadrilateral $\approx \frac{W_{\rm b}}{\langle \delta \rangle}$. $\tilde{S}$ has a probability ≈ 1 of starting a trial just above a gap Δ that changes to a gap Δ' that the cold bath can thermalize. Hence the probability that $\tilde{S}$ traverses a quadrilateral far exceeds the S probability: $1 \gg \frac{W_{\rm b}}{\langle \delta \rangle}$.

Though $\tilde{S}$ traverses more quadrilaterals than S, $\tilde{S}$ outputs less work per average quadrilateral traversal. Cold thermalization likely shifts S one level downward. Neighboring levels (near the band's center) tend to lie closer together in the deeply localized spectrum than in the shallowly localized spectrum. During strokes 1 and 3, S's energy likely declines more than it rises, as shown in Fig. 2. S likely outputs $W_{\rm tot} > 0$. The average work outputted, as explained in the main text, approximately equals $W_{\rm b}$.

In contrast, cold thermalization can shift $\tilde{S}$ to any energy level. The energies less likely splay out as $H_{\rm macro}(t)$ is tuned from deeply localized to shallowly. If $\tilde{S}$ traverses a quadrilateral, it outputs the work (average right-hand gap) - (average left-hand gap) $\approx \langle \delta \rangle - \langle \delta \rangle = 0$, on average. As $0 < W_{\rm b}$, $\tilde{S}$ outputs less work than S during the average trapezoid traversal.

L 4 Comparison with an Anderson-localized engine

Anderson localization resembles MBL. Anderson-localized particles, however, fail to interact (App. H). Having been discovered before MBL, Anderson insulators enjoy less of an aura of exoticism. Would an Anderson insulator suffice for the less-localized $H_{\rm macro}(t)$ in our level-statistics cycle? Yes. In fact, our order-of-magnitude estimates (Sec. IV) concern phosphorus-doped silicon. Anderson localization, rather than MBL, have been realized in such semiconductors. However, using MBL requires less control than using an Anderson insulator. Also, MBL is, in fact, less exotic, or more generic.

One could implement our Otto cycle with an Anderson insulator because Anderson Hamiltonians exhibit Poissonian level statistics. But tuning between Anderson-localized and ETH Hamiltonians requires the switching off and on of interactions. Tuning the interaction, as well as the disorder-to-interaction ratio, requires more effort than tuning just the latter. [One might object that the $Q\big(h(\alpha_t)\big)$ in Eq. (24) requires not only the MBL engine's disorder strength, but also its interaction strength, to be tuned. But $Q\big(h(\alpha_t)\big)$ appears in Eq. (24) for theoretical purposes: We wished to distinguish between the work extracted from level correlations and the work extracted from bandwidth compression and expansion (App. L 1). An agent operating an MBL Otto engine need not care about the distinction.]

Particles typically interact in many-body systems. Interactions' ubiquitousness plagues builders of quantum computers, for example. MBL particles interact; Anderson-localized particles do not. Hence one might expect less difficulty in engineering MBL engines than in engineering Anderson-localized engines.

REFERENCES

[1] J. A. Kjäll, J. H. Bardarson, and F. Pollmann, Phys. Rev. Lett. **113**, 107204 (2014).
[2] M. Schreiber *et al.*, Science **349**, 842 (2015), http://science.sciencemag.org/content/349/6250/842.full.pdf.
[3] R. Nandkishore and D. A. Huse, Annual Review of Condensed Matter Physics **6**, 15 (2015), 1404.0686.
[4] J. M. Deutsch, Phys. Rev. A **43**, 2046 (1991).
[5] M. Srednicki, Phys. Rev. E **50**, 888 (1994).
[6] M. Rigol, V. Dunjko, V. Yurovsky, and M. Olshanii, Phys. Rev. Lett. **98**, 050405 (2007).
[7] D. Janzing, P. Wocjan, R. Zeier, R. Geiss, and T. Beth, Int. J. Theor. Phys. **39**, 2717 (2000).
[8] O. C. O. Dahlsten, R. Renner, E. Rieper, and V. Vedral, New J. Phys. **13**, 053015 (2011).
[9] J. Åberg, Nat. Commun. **4**, 1925 (2013).
[10] F. G. S. L. Brandão, M. Horodecki, J. Oppenheim, J. M. Renes, and R. W. Spekkens, Physical Review Letters **111**, 250404 (2013).
[11] M. Horodecki and J. Oppenheim, Nat. Commun. **4**, 1 (2013).
[12] D. Egloff, O. C. O. Dahlsten, R. Renner, and V. Vedral, New Journal of Physics **17**, 073001 (2015).
[13] J. Goold, M. Huber, A. Riera, L. del Río, and P. Skrzypczyk, Journal of Physics A: Mathematical and Theoretical **49**, 143001 (2016).
[14] G. Gour, M. P. Müller, V. Narasimhachar, R. W. Spekkens, and N. Yunger Halpern, Physics Reports **583**, 1 (2015), The resource theory of informational nonequilibrium in thermodynamics.
[15] N. Yunger Halpern and J. M. Renes, Phys. Rev. E **93**, 022126 (2016).
[16] N. Yunger Halpern, ArXiv e-prints (2014), 1409.7845.
[17] S. Deffner, J. P. Paz, and W. H. Zurek, Phys. Rev. E **94**, 010103 (2016).

[18] H. Wilming and R. Gallego, ArXiv e-prints (2017), 1701.07478.
[19] J. E. Geusic, E. O. Schulz-DuBios, and H. E. D. Scovil, Phys. Rev. **156**, 343 (1967).
[20] A. del Campo, J. Goold, and M. Paternostro, Scientific Reports **4** (2014).
[21] N. Brunner *et al.*, Phys. Rev. E **89**, 032115 (2014).
[22] F. C. Binder, S. Vinjanampathy, K. Modi, and J. Goold, New Journal of Physics **17**, 075015 (2015).
[23] M. P. Woods, N. Ng, and S. Wehner, ArXiv e-prints (2015), 1506.02322.
[24] D. Gelbwaser-Klimovsky and A. Aspuru-Guzik, The Journal of Physical Chemistry Letters **6**, 3477 (2015), http://dx.doi.org/10.1021/acs.jpclett.5b01404, PMID: 26291720.
[25] Q. Song, S. Singh, K. Zhang, W. Zhang, and P. Meystre, ArXiv e-prints (2016), 1607.00119.
[26] H. Terças, S. Ribeiro, M. Pezzutto, and Y. Omar, ArXiv e-prints (2016), 1604.08732.
[27] M. Perarnau-Llobet, A. Riera, R. Gallego, H. Wilming, and J. Eisert, ArXiv e-prints (2015), 1512.03823.
[28] R. Kosloff and Y. Rezek, Entropy **19**, 136 (2017).
[29] J. Lekscha, H. Wilming, J. Eisert, and R. Gallego, ArXiv e-prints (2016), 1612.00029.
[30] J. Jaramillo, M. Beau, and A. del Campo, New Journal of Physics **18**, 075019 (2016).
[31] D. Basko, I. Aleiner, and B. Altshuler, Annals of Physics **321**, 1126 (2006).
[32] V. Oganesyan and D. A. Huse, Phys. Rev. B **75**, 155111 (2007).
[33] A. Pal and D. A. Huse, Phys. Rev. B **82**, 174411 (2010).
[34] D. A. Huse, R. Nandkishore, and V. Oganesyan, Phys. Rev. B **90**, 174202 (2014).
[35] M. Serbyn and J. E. Moore, Phys. Rev. B **93**, 041424 (2016).
[36] S. S. Kondov, W. R. McGehee, W. Xu, and B. DeMarco, Phys. Rev. Lett. **114**, 083002 (2015).
[37] M. Ovadia *et al.*, Scientific Reports **5**, 13503 EP (2015), Article.
[38] J.-y. Choi *et al.*, Science **352**, 1547 (2016).
[39] H. P. Lüschen *et al.*, Phys. Rev. X **7**, 011034 (2017).
[40] G. Kucsko *et al.*, ArXiv e-prints (2016), 1609.08216.
[41] J. Smith *et al.*, Nat Phys **12**, 907 (2016), Letter.
[42] P. Bordia *et al.*, ArXiv e-prints (2017), 1704.03063.
[43] B. Kramer and A. MacKinnon, Reports on Progress in Physics **56**, 1469 (1993).
[44] U. Sivan and Y. Imry, Phys. Rev. B **35**, 6074 (1987).
[45] L. D'Alessio, Y. Kafri, A. Polkovnikov, and M. Rigol, Advances in Physics **65**, 239 (2016), http://dx.doi.org/10.1080/00018732.2016.1198134.
[46] S. Vinjanampathy and J. Anders, Contemporary Physics **0**, 1 (0), http://dx.doi.org/10.1080/00107514.2016.1201896.
[47] D. Quattrochi, The internal combustion engine (otto cycle), 2006.
[48] M. O. Scully, Phys. Rev. Lett. **88**, 050602 (2002).
[49] O. Abah *et al.*, Phys. Rev. Lett. **109**, 203006 (2012).
[50] J. Deng, Q.-h. Wang, Z. Liu, P. Hänggi, and J. Gong, Phys. Rev. E **88**, 062122 (2013).
[51] Y. Zheng and D. Poletti, Phys. Rev. E **90**, 012145 (2014).
[52] B. Karimi and J. P. Pekola, Phys. Rev. B**94**, 184503 (2016), 1610.02776.
[53] S.-Z. Lin and S. Hayami, Phys. Rev. B **93**, 064430 (2016).
[54] P. Corboz, Phys. Rev. B **94**, 035133 (2016).
[55] S. Gopalakrishnan, M. Knap, and E. Demler, Phys. Rev. B **94**, 094201 (2016).
[56] A. V. Khaetskii, D. Loss, and L. Glazman, Phys. Rev. Lett. **88**, 186802 (2002).
[57] S. Gopalakrishnan and R. Nandkishore, Phys. Rev. B **90**, 224203 (2014).
[58] S. A. Parameswaran and S. Gopalakrishnan, Phys. Rev. B **95**, 024201 (2017).
[59] C. De Grandi and A. Polkovnikov, Adiabatic Perturbation Theory: From Landau-Zener Problem to Quenching Through a Quantum Critical Point, in *Lecture Notes in Physics, Berlin Springer Verlag*, edited by A. K. K. Chandra, A. Das, and B. K. K. Chakrabarti, , Lecture Notes in Physics, Berlin Springer Verlag Vol. 802, p. 75, 2010, 0910.2236.
[60] S. Shevchenko, S. Ashhab, and F. Nori, Physics Reports **492**, 1 (2010).
[61] Y. Imry and S.-k. Ma, Phys. Rev. Lett. **35**, 1399 (1975).
[62] S. V. Syzranov, A. V. Gorshkov, and V. Galitski, ArXiv e-prints (2017), 1704.08442.
[63] P. W. Anderson, Phys. Rev. **109**, 1492 (1958).
[64] V. Khemani, R. Nandkishore, and S. L. Sondhi, Nature Physics **11**, 560 (2015), 1411.2616.
[65] H. Kim and D. A. Huse, Phys. Rev. Lett. **111**, 127205 (2013).
[66] E. Lieb and D. Robinson, Commun. Math. Phys. **28**, 251257 (1972).
[67] M. T. Brown, Bacterial flagellar motor: Biophysical studies, in *Encyclopedia of Biophysics*, edited by G. C. K. Roberts, pp. 155–155, Springer Berlin Heidelberg, Berlin, Heidelberg, 2013.
[68] E. Geva and R. Kosloff, The Journal of Chemical Physics **96**, 3054 (1992), http://dx.doi.org/10.1063/1.461951.
[69] E. Geva and R. Kosloff, The Journal of Chemical Physics **97**, 4398 (1992), http://dx.doi.org/10.1063/1.463909.
[70] T. Feldmann, E. Geva, R. Kosloff, and P. Salamon, American Journal of Physics **64**, 485 (1996), http://dx.doi.org/10.1119/1.18197.
[71] J. He, J. Chen, and B. Hua, Phys. Rev. E **65**, 036145 (2002).
[72] G. Alvarado Barrios, F. Albarrán-Arriagada, F. A. Cárdenas-López, G. Romero, and J. C. Retamal, ArXiv e-prints (2017), 1707.05827.
[73] J. R. Petta *et al.*, Science **309**, 2180 (2005), http://science.sciencemag.org/content/309/5744/2180.full.pdf.
[74] J. Petta *et al.*, Physica E: Low-dimensional Systems and Nanostructures **34**, 42 (2006), Proceedings of the 16th Interna-

tional Conference on Electronic Properties of Two-Dimensional Systems (EP2DS-16).
[75] A. Chandran, I. H. Kim, G. Vidal, and D. A. Abanin, Phys. Rev. B**91**, 085425 (2015).
[76] L. del Río, J. Aberg, R. Renner, O. Dahlsten, and V. Vedral, Nature **474**, 61 (2011).
[77] O. C. O. Dahlsten, Entropy **15**, 5346 (2013).
[78] F. Brandão, M. Horodecki, Woods, N. Ng, J. Oppenheim, and S. Wehner, **112**, 3275 (2015).
[79] G. Gour, Phys. Rev. A **95**, 062314 (2017).
[80] K. Ito and M. Hayashi, ArXiv e-prints (2016), 1612.04047.
[81] R. van der Meer, N. H. Y. Ng, and S. Wehner, ArXiv e-prints (2017), 1706.03193.
[82] R. Modak and M. Rigol, ArXiv e-prints (2017), 1704.05474.
[83] W. Verstraelen, D. Sels, and M. Wouters, ArXiv e-prints (2017), 1702.07654.
[84] D. Ferraro, M. Campisi, V. Pellegrini, and M. Polini, ArXiv e-prints (2017), 1707.04930.
[85] P. Skrzypczyk, A. J. Short, and S. Popescu, ArXiv e-prints (2013), 1302.2811.
[86] M. Lostaglio, D. Jennings, and T. Rudolph, Nature Communications **6**, 6383 (2015), 1405.2188.
[87] M. Lostaglio, D. Jennings, and T. Rudolph, New Journal of Physics **19**, 043008 (2017).
[88] N. Yunger Halpern, P. Faist, J. Oppenheim, and A. Winter, Nature Communications **7**, 12051 (2016), 1512.01189.
[89] Y. Guryanova, S. Popescu, A. J. Short, R. Silva, and P. Skrzypczyk, Nature Communications **7**, 12049 (2016), 1512.01190.
[90] X. Chen *et al.*, Phys. Rev. Lett. **104**, 063002 (2010).
[91] E. Torrontegui *et al.*, Advances in Atomic Molecular and Optical Physics **62**, 117 (2013), 1212.6343.
[92] O. Abah and E. Lutz, ArXiv e-prints (2016), 1611.09045.
[93] K. Maruyama, F. Nori, and V. Vedral, Rev. Mod. Phys. **81**, 1 (2009).
[94] H. Tasaki, arXiv e-print (2000), cond-mat/0009244.
[95] J. Kurchan, ArXiv e-prints (2000), cond-mat/0007360.
[96] M. Ziman *et al.*, eprint arXiv:quant-ph/0110164 (2001), quant-ph/0110164.
[97] V. Scarani, M. Ziman, P. Štelmachovič, N. Gisin, and V. Bužek, Phys. Rev. Lett. **88**, 097905 (2002).
[98] N. Yunger Halpern, A. J. P. Garner, O. C. O. Dahlsten, and V. Vedral, New Journal of Physics **17**, 095003 (2015).
[99] G. E. Crooks, Journal of Statistical Physics **90**, 1481 (1998).
[100] N. W. Ashcroft and N. D. Mermin, *Solid State Physics*, 1 ed. (Brooks Cole, 1976).
[101] E. W. Weisstein, Polylogarithm, Wolfram MathWorld.
[102] M. Serbyn, Z. Papić, and D. A. Abanin, Phys. Rev. X **5**, 041047 (2015).
[103] S. Gopalakrishnan *et al.*, Phys. Rev. B **92**, 104202 (2015).
[104] D. A. Abanin, W. De Roeck, W. W. Ho, and F. Huveneers, Phys. Rev. B **95**, 014112 (2017), 1510.03405.
[105] A. Altland, M. Janssen, and B. Shapiro, Phys. Rev. E **56**, 1471 (1997).
[106] C. Perry, P. Ćwikliński, J. Anders, M. Horodecki, and J. Oppenheim, ArXiv e-prints (2015), 1511.06553.